Doping-dependent superconducting properties of two-dimensional metals with different types of interparticle coupling (Review)

V. M. Loktev*

Bogolyubov Institute for Theoretical Physics, Metrologichna St. 14-b, Kiev 03143, Ukraine

V. M. Turkowski**

CFIF, Instituto Superior Tecnico, Av. Rovisto Pais, 1049-001 Lisbon, Portugal
(Submitted June 27, 2003; revised September 30, 2003)
Fiz. Nizk. Temp. **30**, 247–260 (March 2004)

The superconducting properties of a two-dimensional metallic system with arbitrary carrier density and both local and various types of attractive indirect boson-exchange interaction in the cases of s- and d-wave pairing are analyzed and reviewed at $T=0$. In particular, the possibility of a crossover from the Bose–Einstein condensation regime to Bardeen–Cooper–Schrieffer-like superconductivity with growing carrier density and changing coupling in the case of different pairing channels is discussed. Gaussian fluctuations of the order parameter are taken into account, and the carrier density dependence of the gap magnitude is studied. The role of the form of the interparticle attractive interaction in the physical behavior of the system is also considered. © *2004 American Institute of Physics.*
[DOI: 10.1063/1.1645175]

1. INTRODUCTION

The doping dependence of the various properties of superconductors (including high-temperature ones, called HTSCs below) raises many theoretical questions—in particular, the question of the consistent description of such a dependence, which has a long history. Probably the first attempt to solve this problem self-consistently was made by Eagles in Ref. 1, in which the author tried to employ for HTSCs his results for the description of the superconducting properties of Zr-doped $SrTiO_3$ (Ref. 2; see also Ref. 3, where some experimental data were interpreted as the observation of Bose–Einstein condensation (BEC) of electronic pairs in this compound at low itinerant carrier densities, and Refs. 4 and 5, where it was theoretically demonstrated that there were reasons for such an interpretation). More precisely, the author studied the dependence of the superconducting gap at $T=0$ and of the mean-field critical temperature on the free charge carrier densities in two-dimensional (2D) and three-dimensional (3D) systems with a phonon-like indirect attraction at low densities. The set of coupled equations for the gap (gap equation) and the Fermi energy, or chemical potential (number equation), for these cases was obtained and analyzed. It was estimated that at such densities the diameter of the electronic pairs is smaller than the distance between them, and therefore in fact the superconductivity has to correspond to superfluidity of spatially separated (and in this sense small, or so-called local) pairs. It is important that if one can change the distance between the particles (for instance, by doping), the transition from one regime to another (with strongly overlapped pairs) becomes in principle possible. Now this phenomenon is well known as the crossover from BEC to Bardeen–Cooper–Schrieffer (BCS) superconductivity with changing carrier density.

In Ref. 1 it was also shown that in 3D systems there exists a critical value of the attraction below which there are no local pairs, so that BEC–BCS crossover is impossible. It is noteworthy that the possibility of a superfluidity scenario for superconductivity was proposed by Ogg[6] and Schafroth[7–9] long before Eagles's paper was published.

Later on the problem of the BEC–BCS crossover was considered by Leggett,[10] who studied systems with short-range repulsion and finite-range attraction, analyzing the dependence of the superconducting properties of the system on the dimensionless parameter $1/(ak_F)$ (a is the scattering length and $\mathbf{k}_F$ is the Fermi momentum), which defines the itinerant particle number in the crystal. It was shown that in the limiting cases the metallic system consists of bound "bielectronic molecules" in real space if $1/(ak_F)=\infty$ and of Cooper pairs in $\mathbf{k}$ space when $1/(ak_F)=-\infty$. Nozières and Schmitt-Rink[11] generalized these results to the case of finite temperatures and the lattice model with a separable interparticle nonretarded attractive potential V. They have demonstrated that the BEC–BCS crossover is smooth with changing k_F and V when V is larger than the corresponding critical value for the two-particle (two-fermion) bound state formation. The aforementioned results were obtained for the case of s-wave pairing.

The real and unprecedented boom of interest in crossover phenomena started in the second half of the 1980s after the discovery of copper oxide HTSCs, materials with an evident and rather unusual dependence of the superconducting properties on the carrier density. It should be stressed that practically all physical (and observable) properties of the HTSC compounds are doping dependent, but below we shall concentrate on the description of the superconductivity and superconducting properties only.

Development of a consistent theory of HTSCs still remains one of the most difficult and one of the most important problems of modern condensed matter physics. Due to the

complicated (multicomponent) crystal structure, lowered dimensionality, magnetism, strong electron correlations, inevitable presence of disorder, etc., a generally accepted theory of these compounds has not yet been completed.

During the last decade many models (see, for example, the review[12]) which take into account some (not all) cuprate peculiarities have been proposed to describe various properties of HTSCs, among them the doping dependence of the superconducting gap and the critical temperature. For instance, the BEC–BCS crossover in the s-wave pairing channel was studied in Refs. 12–19 for the model with local (so-called four-fermion, or 4F) attraction, and in Ref. 20 for the model of a nonlocal although separable attractive potential. In Ref. 12 an additional example with on-site repulsion and intersite attraction was also considered. The role of the order parameter fluctuations at $T=0$ was analyzed in Ref. 21 (3D case) and in Ref. 22 (both 2D and 3D cases). A quasi-2D model with s pairing at zero temperature was also studied in Ref. 23. It can be also noticed that the role of the number equation in connection with the HTSC problem was emphasized in Refs. 24.

For a pure 2D system the problem of the crossover in the isotropic s-wave pairing channel was discussed at zero T (when real long-range superconducting order is certainly possible—the Mermin–Wagner–Hohenberg–Coleman–Bogolyubov theorem[25]) in Refs. 12, 15, 18, 20 and 26–31 and at finite T (when this order is characterized by the weak algebraic decay of correlations) in Refs. 12, 15, 18–20, 28–30, 32, and 33.

The metal–superconductor phase boundaries on the n_f-U phase diagram (n_f is the number of fermionic particles, and U is the on-site attraction in the ''negative-U'' Hubbard model) was investigated in Ref. 34 for $T=0$ by means of the dynamical mean-field theory. The retarded indirect, phonon-mediated interfermion attraction and the features of the corresponding BEC–BCS crossover at $T=0$ were studied for the first time in Refs. 35 and 36

The 2D crossover for the anisotropic d-wave pair symmetry is more important because just such a pairing is usually considered to be observed in HTSCs. The models which lead to this phenomenon were considered in Refs. 18, 32 and 37 at $T=0$. The case of finite temperatures was studied in Ref. 38, where an effective (Ginzburg–Landau) potential with carrier-density-dependent coefficients was also derived. The doping dependence of the critical temperature T_c in the strongly correlated electron model with electron–phonon interaction was studied in Refs. 39 and 40. It was found that the vertex corrections to the electron–phonon coupling in this model lead to strengthening of the d-wave superconductivity. In Ref. 29 the cases with different pairing symmetries, s, s_{ext}, d_{xy} and $d_{x^2-y^2}$, in the 2D system with nearest-neighbor (n.n.) and next-nearest-neighbor (n.n.n.) attraction in the square lattice were studied at zero and finite temperatures in order to describe the doping dependence of the superconducting gap and critical temperature (see also Ref. 41). The possibility of the BEC–BCS crossover at zero temperature for s, d and mixed $s+id$ pairings in the 2D system as a function of coupling constant was considered in Ref. 42. The same problem in the quasi-2D Hubbard model with n.n. attraction at finite T was studied in Ref. 43, where the doping dependence of the superconducting properties was also analyzed.

The 2D model with n.n. attraction and also with n.n. and n.n.n. hopping at $T=0$ was studied in Ref. 44. It was shown that for some relation between n.n. and n.n.n. hopping parameters the system proves always to be in the BEC regime and that there is no pairing at low carrier densities when the coupling is weak (see also Ref. 37). However, as was stressed in Refs. 31 and 45, such a statement cannot be correct. A more general model with on-site repulsion and n.n. attraction at $T=0$ in the s- and d-wave channels was investigated in Ref. 46, where the role of n.n.n. hoping was also studied. The s- and d-wave crossover at zero temperature in the model with a doping-dependent attractive interaction was considered in Ref. 47. It is interesting to note that the boson–fermion model with electrons and holes and different kinds of fermion–boson coupling was proposed in Ref. 48 to unify the Bose–Einstein and BCS collective phenomena. It was shown that the regime of superfluidity with local pairs and the regime of superconductivity with Cooper pairs take place in different sectors of the model parameters.

Even though the d-wave pairing symmetry is now considered as the typical and almost imprescriptible property of the HTSC cuprate compounds,[49] there is experimental evidence that mixed $s+id$- or even pure s-wave pairing can exist in some of these materials at certain doping values. Indeed, it has been observed that optimally doped $Pr_{1.855}Ce_{0.145}CuO_{4y}$ at low enough temperatures demonstrates a nodeless gap inconsistent with pure d-wave symmetry,[50] and the superconducting compound $Sr_{0.9}La_{0.1}CuO_2$ reveals s-wave pairing near the optimal doping.[51] The analysis shows[52] that the dominant bulk symmetry of the order parameter in some cuprates is the extended (or anisotropic) s-wave one. It was also observed that the crossover from the d-wave pairing in the underdoped and optimally doped regime to the $s+id$-wave pairing in the overdoped regime takes place in $YBa_2Cu_3O_7$ (Ref. 53). A crossover from d-wave to s-wave pairing with doping near optimal x was found for the electron-doped $Pr_{2x}Ce_xCuO_4$ (Ref. 54) amd $Pr_{2x}Ce_xCuO_{4y}$ and $La_{2x}Ce_xCuO_{4y}$ (Ref. 55). However, the s-wave pairing is not always present in underdoped and overdoped cuprates, but the d-wave order parameter symmetry in overdoped $TlBa_2Cu_3O_{6+\delta}$ was found in Ref. 56.

The results cited above evidently show that the investigation of the doping dependence of the physical properties of superconductors is now an important field in solid state physics. The corresponding questions have not yet been reviewed in the literature and demand some generalization. Below an attempt will be made to analyze the behavior of properties of superconducting systems with different interparticle potentials in the s- and d-wave pairing channels as functions of particle densities and interaction strength. For the sake of simplicity we restrict our discussion here to the case $T=0$. We briefly survey the main superconducting properties of different systems. We should kindly apologize because the results of many authors could not be included in our paper, since it is very difficult and in fact impossible to cover all of them in such a wide and rapidly growing field as high-

temperature superconductivity, even within a separate, special and rather narrow topic.

2. THE MODEL AND THE MAIN EQUATIONS

The most general and, at the same time, the simplest Hamiltonian, which is usually studied in the theory of superconductivity, can be written as

$$
\begin{aligned}
H = &- \sum_{\mathrm{n,m},\sigma} t_{\mathrm{nm}} c^{\dagger}_{\mathrm{n}\sigma} c_{\mathrm{m}\sigma} - \mu \sum_{\mathrm{n},\sigma} c^{\dagger}_{\mathrm{n}\sigma} c_{\mathrm{n}\sigma} \\
&- V_0 \sum_{\mathrm{n}} c^{\dagger}_{\mathrm{n}\uparrow} c^{\dagger}_{\mathrm{n}\downarrow} c_{\mathrm{n}\downarrow} c_{\mathrm{n}\uparrow} - \sum_{\mathrm{n,m}} V_{\mathrm{nm}} c^{\dagger}_{\mathrm{n}\uparrow} c^{\dagger}_{\mathrm{m}\downarrow} c_{\mathrm{m}\downarrow} c_{\mathrm{n}\uparrow} \\
&+ \sum_{\mathrm{n,q}} g_{\mathrm{n}}(\mathbf{q}) c^{\dagger}_{\mathrm{n}\sigma} c_{\mathrm{n}\sigma} X_{\mathrm{n}}(\mathbf{q}) \\
&+ \frac{1}{2} \sum_{\mathrm{n,q}} \left[\frac{\mathrm{p_n}^2(\mathbf{q})}{m(\mathbf{q})} + m(\mathbf{q}) \omega^2_{\mathrm{n}}(\mathbf{q}) X^2_{\mathrm{n}}(\mathbf{q}) \right],
\end{aligned}
\tag{1}
$$

where $c_{\mathbf{n}\sigma} \equiv c_{\sigma}(\mathbf{n},\tau)$ is the fermionic field operator with spin $\sigma = \uparrow, \downarrow$ at the lattice site $\mathbf{n}$ and at the time τ, $t_{\mathbf{nm}}$ describes the n.n., n.n.n., and other hopping processes; μ is the chemical potential of the system; the nonretarded interparticle interaction is modeled by the terms proportional to V_0 (the on-site attraction if $V_0 > 0$ and repulsion otherwise) and $V_{\mathbf{nm}}$ (n.n. or n.n.n. interaction). The last two terms in (1) describe an additional retarded fermion–boson interaction and the free boson parts of the Hamiltonian, where $\mathbf{q}$ is a boson mode with the coordinate $X_{\mathbf{n}}(\mathbf{q})$, momentum $\mathbf{p_n}(\mathbf{q})$, and frequency $\omega_{\mathbf{n}}(\mathbf{q})$ and $g_{\mathbf{n}}(\mathbf{q})$ is the fermion–boson coupling. One can easily pass to the continuum version of this Hamiltonian by replacing the n.n. hopping operator $t_{\mathbf{nm}}$ by $t_{\mathbf{nm}} \to \delta_{\mathbf{nm}} t(1 - (a^2/(2d))\nabla^2)$ (here a is the intersite distance, $d(=2,3)$ is the dimensionality of the system), introducing a cutoff radius in the interaction terms, etc.

In the case of the d-dimensional square lattice, the free fermion dispersion relation in momentum space has the following form, when the n.n. hopping takes place:

$$
\xi(\mathbf{k}) = -2t \sum_{j=1}^{d} \cos a k_j - \mu, \tag{2}
$$

where $\mathbf{k}$ is a d-dimensional wave vector.

As is well known, it is convenient to calculate the thermodynamic potential by using the path integral approach for studying the properties of a quantum many-particle system. This method is not necessary in the case of the mean-field solution, but it is extremely useful (see below) when the fluctuations are studied. Probably one of the first to apply the path integral methodics for the description of superconductivity was Svidzinsky.[57]

The partition function of the system is

$$
Z = \int D\psi^{\dagger} D\psi \; \mathrm{e}^{-S} \tag{3}
$$

with the action

$$
S = \int_0^{\beta} d\tau \left[\sum_{\mathrm{n},\sigma} \psi^{\dagger}_{\mathrm{n}\sigma}(\tau) \partial_{\tau} \psi_{\mathrm{n}\sigma}(\tau) + H(\tau) \right], \quad \beta = 1/T. \tag{4}
$$

To study the superconducting properties of the system, one should make the Hubbard–Stratonovich transformation with so-called bilocal fields $\Phi_{\mathbf{nm}}(\tau_1,\tau_2)$ and $\Phi^{\dagger}_{\mathbf{nm}}(\tau_1,\tau_2)$ (Ref. 57; it must be noted that in the textbook[57] the functional integration was developed for the situation when the spatially inhomogeneous order parameter of the system depends upon one space variable only, which excluded a d-wave symmetry):

$$
\begin{aligned}
&\exp\left[\psi^{\dagger}_{\mathbf{n}\uparrow}(\tau_1)\psi^{\dagger}_{\mathbf{m}\downarrow}(\tau_2) V_{\mathrm{nm}}(\tau_1,\tau_2)\psi_{\mathrm{m}\downarrow}(\tau_2)\psi_{\mathrm{n}\uparrow}(\tau_1)\right] \\
&= \int D\Phi^{\dagger} D\Phi \exp\left[-\int_0^{\beta} d\tau_1 \int_0^{\beta} d\tau_2 \left(\frac{|\Phi_{\mathrm{nm}}(\tau_1,\tau_2)|^2}{V_{\mathrm{nm}}(\tau_1,\tau_2)} \right.\right. \\
&- \Phi^{\dagger}_{\mathrm{nm}}(\tau_1,\tau_2)\psi_{\mathrm{n}\downarrow}(\tau_1)\psi_{\mathrm{m}\uparrow}(\tau_2) \\
&\left.\left. - \psi^{\dagger}_{\mathrm{n}\uparrow}(\tau_1)\psi^{\dagger}_{\mathrm{m}\downarrow}(\tau_2)\Phi_{\mathrm{nm}}(\tau_1,\tau_2) \right) \right],
\end{aligned}
\tag{5}
$$

where $V_{\mathbf{nm}}(\tau_1,\tau_2)$ includes the effective interparticle attraction due to boson coupling after integrations over the boson fields $X_{\mathbf{n}}(\mathbf{q})$.

Let us introduce the Nambu spinor

$$
\Psi_{\mathbf{n}}(\tau) = \begin{pmatrix} \psi_{\mathbf{n}\uparrow}(\tau) \\ \psi^{\dagger}_{\mathbf{n}\downarrow}(\tau) \end{pmatrix},
$$

$$
\Psi^{\dagger}_{\mathbf{n}}(\tau) = (\psi^{\dagger}_{\mathbf{n}\uparrow}(\tau), \psi_{\mathbf{n}\downarrow}(\tau)).
$$

In these terms the partition function can be formally written as

$$
Z = \int D\Psi^{\dagger} D\Psi D\Phi^{\dagger} D\Phi \, \mathrm{e}^{-S(\Psi^{\dagger},\Psi,\Phi^{\dagger},\Phi)},
$$

where

$$
\begin{aligned}
&S(\Psi,\Psi^{\dagger},\Phi,\Phi^{\dagger}) \\
&= \int_0^{\beta} d\tau_1 \int_0^{\beta} d\tau_2 \sum_{\mathrm{n,m}} \left\{ \frac{|\Phi_{\mathrm{nm}}(\tau_1,\tau_2)|^2}{V_{\mathrm{nm}}(\tau_1,\tau_2)} - \delta(\tau_1 - \tau_2)\Psi^{\dagger}_{\mathrm{n}}(\tau_1) \right. \\
&\times [-\delta_{\mathrm{nm}}\partial_{\tau_2} - \hat{\tau}_z(t_{\mathrm{nm}} - \delta_{\mathrm{nm}}\mu)]\Psi_{\mathrm{m}}(\tau_2) \\
&- \Phi^{\dagger}_{\mathrm{nm}}(\tau_1,\tau_2)\Psi^{\dagger}_{\mathrm{n}}(\tau_1)\hat{\tau}_{-}\Psi_{\mathrm{m}}(\tau_2) \\
&\left. - \Psi^{\dagger}_{\mathrm{n}}(\tau_1)\hat{\tau}_{+}\Psi_{\mathrm{m}}(\tau_2)\Phi_{\mathrm{nm}}(\tau_1,\tau_2) \right\},
\end{aligned}
\tag{7}
$$

and $\hat{\tau}_{\pm} = 1/2(\hat{\tau}_x \pm \hat{\tau}_y)$ and $\hat{\tau}_z$ are the Pauli matrices.

The latter action is diagonal over the fermionic fields, and therefore the integration over $\Psi^{\dagger}$ and Ψ can be performed exactly. In this case the partition function becomes

$$
Z = \int D\Phi D\Phi^{*} \exp(-\beta\Omega[G]),
$$

where $\Omega[G]$ is the thermodynamic potential, which in the "leading order" is

$$
\begin{aligned}
\beta\Omega[G] = &\int_0^{\beta} d\tau_1 \int_0^{\beta} d\tau_2 \sum_{\mathbf{n,m}} \frac{|\Phi_{\mathbf{nm}}(\tau_1,\tau_2)|^2}{V_{\mathbf{nm}}(\tau_1,\tau_2)} \\
&- \mathrm{Tr}\,\mathrm{Ln}G^{-1} + \mathrm{Tr}\,\mathrm{Ln}G_0^{-1}.
\end{aligned}
\tag{8}
$$

The Nambu spinor Green function G satisfies the following equation:

$$[-\delta(\tau_1-\tau_3)\delta_{\mathbf{nl}}\partial_{\tau_3}\hat{I}+\delta(\tau_1-\tau_3)(t_{\mathbf{nl}}-\delta_{\mathbf{nl}}\mu)\hat{\tau}_z + \hat{\tau}_+\Phi_{\mathbf{nl}}(\tau_1,\tau_3)+\hat{\tau}_-\Phi^*_{\mathbf{nl}}(\tau_1,\tau_3)]G_{\mathbf{lm}}(\tau_3,\tau_2) = \delta(\tau_1-\tau_2)\delta_{\mathbf{nm}} \tag{9}$$

with anti-periodic boundary conditions for fermions,

$$G_{\mathbf{nm}}(\tau_1-\tau_2+\beta)=-G_{\mathbf{nm}}(\tau_1-\tau_2).$$

The thermodynamic potential (8) is the most general form of the superconducting effective action, or Ginzburg–Landau potential, with a nonlocal retarded interparticle interaction. As was already mentioned, it will be used below to study fluctuation effects.

The minimization of the thermodynamic potential with respect to the order parameter and the chemical potential leads to the following system of coupled equations:

$$\frac{\delta\Omega}{\delta\Phi_{\mathbf{nm}}(\tau_1,\tau_2)}=0; \tag{10}$$

$$\frac{\partial\Omega}{\partial\mu}=-N_f, \tag{11}$$

or

$$\Phi_{\mathbf{nm}}(\tau_1,\tau_2)=V_{\mathbf{nl}}(\tau_1,\tau_3)\mathrm{Tr}\,\hat{\tau}_+G_{\mathbf{lm}}(\tau_3;\tau_2); \tag{12}$$

$$n_f=-\mathrm{Tr}\,\hat{\tau}_zG_{\mathbf{nn}}(\tau,\tau). \tag{13}$$

where $n_f=N_f/v$ is the free fermion density in the system (v is the volume of the system).

In general, it is very difficult to find the Green's function $G_{\mathbf{lm}}(\tau_1,\tau_2)$, and therefore some simplifications must be applied. In particular, we shall consider the case of the space and time invariance, $V_{\mathbf{nm}}(\tau_1,\tau_2)=V_{\mathbf{n-m}}(\tau_1-\tau_2)$. In this case the Green's function has the following form in momentum space:

$$G(i\omega_n,\mathbf{k}) = -\frac{i\omega_n+\hat{\tau}_z\xi(\mathbf{k})-\Phi(i\omega_n,\mathbf{k})\hat{\tau}_+-\Phi^*(i\omega_n,\mathbf{k})\hat{\tau}_-}{\omega_n^2+\xi^2(\mathbf{k})+|\Phi(i\omega_n,\mathbf{k})|^2},$$

and the system of equations (12), (13) acquires the following form:

$$\Phi(i\omega_n,\mathbf{k})=\int\frac{d^dp}{(2\pi)^d}\sum_m\frac{\Phi(\omega_m,\mathbf{p})}{\omega_m^2-\xi^2(\mathbf{p})-|\Phi(\omega_m,\mathbf{p})|^2} \times\left[V(\mathbf{p},\mathbf{k})+g_{f-b}^2 \times\int\frac{d^dk}{(2\pi)^d}\frac{\omega^2(\mathbf{p}-\mathbf{k})}{(\omega_m-\omega_n)^2-\omega^2(\mathbf{p}-\mathbf{k})}\right]; \tag{14}$$

$$n_f=\int\frac{d^dp}{(2\pi)^d}\left[1-\sum_m\frac{\xi(\mathbf{p})}{\omega_m^2-\xi^2(\mathbf{p})-|\Phi(\omega_m,\mathbf{p})|^2}\right]. \tag{15}$$

In Eq. (14) $V(\mathbf{p},\mathbf{k})$ is the Fourier transform of the nonretarded interaction, and the term proportional to g_{f-b} corresponds to the interparticle attraction through the boson field; $\omega_n=\pi T(2n+1)$ is the Matsubara frequency. The interaction term in (14) is written in general form; it describes, for example, a local nonretarded interaction, when $V(\mathbf{p}-\mathbf{k})=\mathrm{const}$, $g_{f-b}=0$; a nonlocal (nonretarded) interaction, when $V(\mathbf{p}-\mathbf{k})\neq\mathrm{const}$, but $g_{f-b}=0$; a local retarded interaction, when $V(\mathbf{p}-\mathbf{k})=\mathrm{const}$, $g_{f-b}\neq0$, and $\omega(\mathbf{p}-\mathbf{k})=\mathrm{const}$, etc. The system (14), (15) will be analyzed in the next Section for various forms of the interparticle potential $V(\mathbf{p},\mathbf{k})$ and boson spectrum $\omega(\mathbf{k})$.

3. THE SOLUTIONS

3.1. Model with local nonretarded attraction

The problem of the crossover from small to large fermion density in the model with local attraction was considered in Refs. 1 and 12–19 for the 3D case and in Refs. 1, 12, 18, 26 and 31 for the 2D case. The corresponding results can be reduced to the following.

For the simplest case of local nonretarded attraction, the interaction parameters in equations (14), (15) have the following form: $V(\mathbf{p},\mathbf{k})\equiv V=\mathrm{const}$, $g_{f-b}=0$. Therefore, the gap in this case is momentum- and frequency-independent:

$$\Phi(\omega_n,\mathbf{k})=\Delta=\mathrm{const}.$$

The summation over frequency in (14), (15) can be easily performed, and one gets the standard system of equations:

$$1=V\int\frac{d^dk}{(2\pi)^d}\frac{1}{2\sqrt{\xi^2(\mathbf{k})+\Delta^2}}\tanh\left(\frac{\sqrt{\xi^2(\mathbf{k})+\Delta^2}}{2T}\right); \tag{16}$$

$$n_f=\int\frac{d^dk}{(2\pi)^d}\left[1-\frac{\xi(\mathbf{k})}{\sqrt{\xi^2(\mathbf{k})+\Delta^2}}\tanh\left(\frac{\sqrt{\xi^2(\mathbf{k})+\Delta^2}}{2T}\right)\right], \tag{17}$$

which at $T=0$ have a simple form:

$$1=V\int\frac{d^dk}{(2\pi)^d}\frac{1}{2\sqrt{\xi^2(\mathbf{k})+\Delta^2}}; \tag{18}$$

$$n_f=\int\frac{d^dk}{(2\pi)^d}\left[1-\frac{\xi(\mathbf{k})}{\sqrt{\xi^2(\mathbf{k})+\Delta^2}}\right]. \tag{19}$$

Since the gap is momentum-independent, only the isotropic s-wave pairing regime is possible in the model with the on-site attraction. Equation (19) is crucial if one wants to investigate the doping dependence of superconducting properties. As a rule, it is not taken into account in the standard theory of superconductivity (or the BCS theory).

The s-wave pairing regime in the case of a quadratic dispersion law

$$\xi(\mathbf{k})=\frac{\mathbf{k}^2}{2m}-\mu$$

and an indirect pairing with boson (''Debye'') energy cutoff $\theta(\omega_D-|\xi(\mathbf{k})-\mu|)$ was considered in the mean-field approximation for the 2D and 3D cases and at low carrier densities in Ref. 1 (see also Refs. 4 and 5). In fact, in such a situation the integration over momentum $\int d^dk/(2\pi)^d$ can be replaced by the integration over energy $\int\rho(\epsilon)d\epsilon$, where $\rho(\epsilon)$ is the density of states (DOS); it is constant in the case $d=2$ and $\sim\sqrt{\epsilon}$ in the case $d=3$.

It is very easy to solve the system (18), (19) in the 2D case. When $\varepsilon_F \ll W$ (W is the free fermion bandwidth), the solution has a simple form:

$$\Delta \simeq \sqrt{2W\epsilon_F}\mathrm{e}^{-2\pi/mV} = \sqrt{2|\varepsilon_b|\varepsilon_F};$$

$$\mu \simeq \epsilon_F - |\varepsilon_b|/2,$$

where $\varepsilon_b = -2W\mathrm{e}^{-4\pi/mV}$ is the two-fermion bound state energy. Obviously, the crossover from superfluidity to superconductivity with doping occurs in the 2D case at any coupling constant; then there exists the value of ϵ_F when $\mu = 0$ for any V.

This is not true in the 3D case, when the BEC–BCS crossover takes place only when the coupling constant is larger than some critical value V_{cr}. This distinction follows from the above-mentioned difference in the DOS in the gap equation. In the 2D case, when $\rho(\epsilon) = \mathrm{const}$, the gap equation has the solution $\Delta = \sqrt{2W|\varepsilon_b|}$ at $\mu = 0$ and any coupling constant.

For the 3D system the gap equation has the following form:

$$1 = V\int \frac{k^2 dk}{2\pi^2}\frac{1}{2\sqrt{k^4+\Delta^2}} \tag{20}$$

at $\mu = 0$. The integral over k on the right-hand side has the maximal value $\sqrt{2mW}/(4\pi^2)$ at $\Delta = 0$. Therefore, a simple estimate for V_{cr} is given by the relation $1 \simeq V_{\mathrm{cr}}\sqrt{2mW}/(4\pi^2)$ or $V_{\mathrm{cr}} \simeq 4\pi^2/\sqrt{2mW}$.

In the case of the momentum cutoff

$$\int \frac{d^d k}{(2\pi)^d}\theta(\omega_D - |\xi(\mathbf{k}) - \mu|),$$

the approximate solution can also be easily obtained in the 2D case:

$$\Delta \simeq \sqrt{2|\varepsilon_b|\Delta_{BCS}}\theta(\omega_D - \epsilon_F) + \Delta_{BCS}\theta(\epsilon_F - \omega_D);$$

$$\mu = \epsilon_F - \frac{|\varepsilon_b|}{2},$$

where $\Delta_{BCS} = 2\omega_D \mathrm{e}^{-2\pi/(mV_{\mathrm{eff}})}$ is the BCS expression for the gap, and the bound state energy in this case also exists: $\varepsilon_b = -2\omega_D \mathrm{e}^{-4\pi/(mV_{\mathrm{eff}})}$, where V_{eff} is proportional to the fermion–boson coupling constant g_{f-b}. The gap is an increasing function of doping in this case, and it asymptotically approaches its maximal value Δ_{BCS} when $\epsilon_F \gg \omega_D$. In other words, the dependence of the gap value on the carrier density has no maximum, which evidently means that such a dependence with saturation is not identical to the "increasing–decreasing" dependence of the gap upon the effective coupling constant V_{eff}.

In the 3D case, the DOS in equations (18) and (19) can be substituted by the DOS at the Fermi level, and the solution can be obtained from the 2D result with substitution $mV/(2\pi) \to k_F mV/(4\pi^2)$. It is possible to estimate the critical value of the coupling constant when the crossover takes place: $V_{\mathrm{cr}} = 2\pi^2/\sqrt{m\omega_D}$. In both cases, with and without momentum cutoff, the BEC–BCS transition from superfluidity to superconductivity is smooth and is not a phase transition; the gap value grows continuously with doping.

3.2. Models with nonlocal nonretarded interaction

It is important to study the more realistic case of nonlocal attraction in the presence of a short-range Coulomb repulsion. In order to study the superconducting properties of such a model in channels with different pair angular momentum l, it is convenient (see, for example, Refs. 32, 33, and 46) to approximate the interaction potential by a separable function:

$$V_l(\mathbf{k}_1, \mathbf{k}_2) = -\lambda_l w_l(\mathbf{k}_1) w_1(\mathbf{k}_2), \tag{21}$$

where λ_l is an effective coupling constant, and

$$w_l(\mathbf{k}) = h_l(\mathbf{k})\cos l\varphi_{\mathbf{k}}; \tag{22}$$

$$h_l(\mathbf{k}) = \frac{(k/k_1)^l}{(1+k/k_0)^{l+1/2}}; \tag{23}$$

$k = |\mathbf{k}|$ is the momentum modulus and $\varphi_{\mathbf{k}}$ is the momentum angle in polar coordinates $\mathbf{k} = k(\cos\varphi_{\mathbf{k}}, \sin\varphi_{\mathbf{k}})$. The parameters k_0 and k_1 put the momentum range in the proper region—the potential is attractive at $r_0 < r < r_1$ and repulsive at $r < r_0$, where $k_0 \sim 1/r_0$ and $k_1 \sim 1/r_1$. The separable form of the interparticle potential (21) is based on the group theory decomposition of an arbitrary potential into spherical harmonics, for example, and the restriction to the relevant terms only, which in our case correspond to the order-parameter symmetry under consideration.

It is easy to see that the interaction potential (21) has the correct asymptotic behavior at small and large momenta: $V_l(\mathbf{k}_1, \mathbf{k}_2) \sim k_1^l k_2^l$ and $V_l(\mathbf{k}_1, \mathbf{k}_2) \sim 1/\sqrt{k_1 k_2}$, respectively. Since the region of low carrier concentrations, where the crossover can take place, is the most interesting, the correct behavior of the interaction potential at small momenta should be most important. These momenta give the main contribution to the integrals in the case of low carrier concentrations (see equations below). We shall study the s- and d-wave channels with $l = 0$ and 2 separately, so we assume that the parameters λ_l for the two channels are independent.

In this case the equations for the gap and for the chemical potential have the following form:

$$\Delta_l(\mathbf{k}) = -\lambda_l \int \frac{d\mathbf{p}}{(2\pi)^2}\frac{\Delta_l(\mathbf{p})}{2\sqrt{\varepsilon^2(\mathbf{p}) + \Delta_l^2(\mathbf{p})}} V_l(\mathbf{p}, \mathbf{k}); \tag{24}$$

$$n_f = \int \frac{d\mathbf{k}}{(2\pi)^2}\left[1 - \frac{\varepsilon(\mathbf{k})}{\sqrt{\varepsilon^2(\mathbf{k}) + \Delta_l^2(\mathbf{k})}}\right]. \tag{25}$$

The solution of equation (24) has the following form:

$$\Delta_l(\mathbf{k}) = \Delta_l^{(0)} w_l(\mathbf{k}), \tag{26}$$

where $\Delta_l^{(0)}$ does not depend on the momentum $\mathbf{k}$.

As was shown in Refs. 32 and 33, the BEC–BCS crossover from superfluidity to superconductivity with increasing doping is smooth (see Figs. 1 and 2 below). However, in the d-wave paring channel there exists a critical value of the interaction potential, below which this crossover is impossible. This circumstance makes the cases of isotropic s- and anisotropic d-wave pairing essentially different.

The more realistic case in connection with HTSCs was considered in Ref. 47, where the correlation length r_0 was studied at small carrier densities as $r_0 \sim a/\sqrt{n_f}$. This depen-

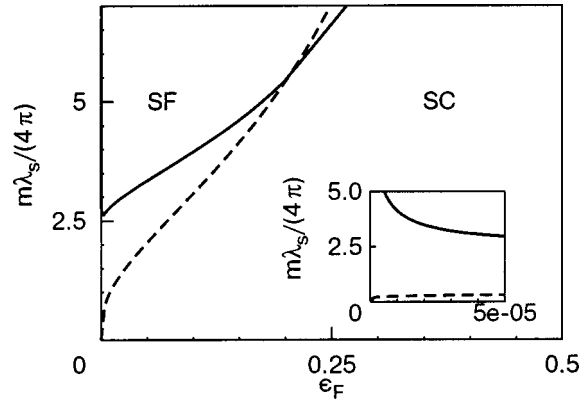

FIG. 1. Coupling–carrier density crossover line for the s-pairing channel (solid line). The dotted curve represents the corresponding line for the case $r_0(n_f)=\text{const}$ at $r_0=a_0$. The inset shows the doping dependence of the crossover value for coupling at very low charge carrier densities.[47] Here and below all parameters are expressed in units of the bandwidth W.

dence for the spin–spin correlation length at small carrier densities was found in $La_{2-x}Sr_xCuO_4$, for example. The magnetic correlation length decreases with carrier density per cell in this material as 3.8 Å$/\sqrt{n_f}$ (Ref. 59). The value of a was considered to be $a=\sqrt{2/\pi}a_0$, where a_0 is the simple square lattice constant. The value of a can be estimated from the relation $(\pi/2)r_0^2N_f=a_0^2N_{\text{cell}}$, where in the left-hand side the volume of the 2D system is expressed as the volume (circle of radius $\sim r_0$) occupied by one particle, multiplied by the total number of particles N_f, and N_{cell} is the number of unit cells in the layered system. The free fermion bandwidth W is related to a_0 as $W=\pi^2/(ma_0^2)$. It should be noted that the relation $r_0\sim a\sqrt{n_f}$ at $a=\sqrt{2/\pi}a_0$ is in good agreement with the experimental data for $La_{2-x}Sr_xCuO_4$ (Ref. 59), where the magnetically ordered (orthorhombic) plane lattice parameters are equal to 5.354 Å and 5.401 Å, and the corresponding parameter a is $\simeq$3.8 Å.

It was shown that the critical value of the coupling constant exists even in the s-wave pairing channel for this case (see Figs. 1 and 2).

Let us consider different versions of the previous model. Namely, the correlation radius $r_0(n_f)=a_0\sqrt{2/(\pi n_f)}$ can be introduced in a model with an exponential decay of the attraction:

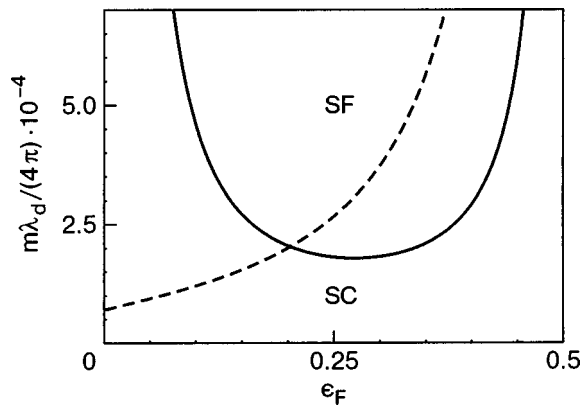

FIG. 2. Coupling–carrier density crossover line for the d-wave case (solid line). The dotted curve is the crossover line for the case $r_0(n_f)=\text{const}$ at $r_0=a_0$ (Ref. 47).

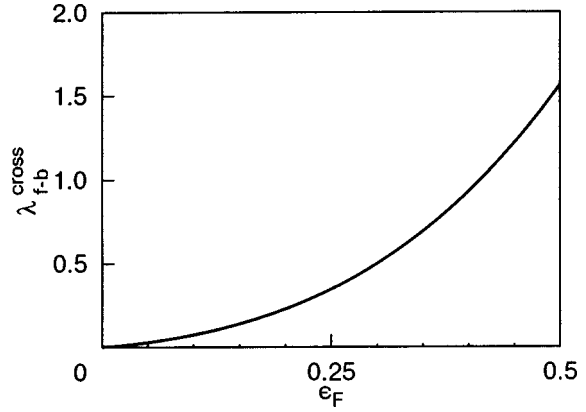

FIG. 3. The crossover interaction value $\lambda_{f-b}^{\text{cross}}$ (defined by the condition $\mu=0$) as a function of ϵ_F at $\lambda_{f-f}=0$.

$$V_b(\mathbf{r},t)=g_{f-b}\frac{e^{-r/r_0}}{r}. \tag{27}$$

Its Fourier transform has the following form:

$$D_b(\mathbf{q})=\frac{g_{f-b}r_0}{(2\pi)^2\sqrt{1+r_0^2\mathbf{q}^2}}. \tag{28}$$

In addition, a similar kind of short-range fermion–fermion repulsion should be taken into account. It is easy to see that in the 2D case this potential has the following form (see, for example, Ref. 60):

$$D_f(\mathbf{q})=\frac{g_{f-f}}{q+q_{TF}g(q/2k_F)}, \tag{29}$$

where $g_{f-f}\equiv2\pi e^2$, $q_{TF}=4e^2m/\pi=4/\pi a_B$ is the Thomas–Fermi momentum, and $a_B=1/(e^2m)\simeq0.529$ Å is the Bohr radius. The function $g(x)$ is defined as

$$g(x)=1-\theta(x-1)\sqrt{1-1/x^2}. \tag{30}$$

This model of the s-wave pairing channel demonstrates the crossover from superfluidity to superconductivity at any value of the coupling constant, contrary to the previous case (see Fig. 3). The doping dependence of the gap and of the chemical potential at different values of the dimensionless interaction parameters $\lambda_{f-b}=g_{f-b}^2mr_0/(8\pi^2)$, $\lambda_{f-f}=g_{f-f}^2mr_0/(4\pi)$ is presented in Figs. 4 and 5. As follows from these figures, the gap decreases with increasing doping at large ϵ_F. This situation is in qualitative agreement with the experiments for the cuprates. One can also consider the interesting situation of a combined local+nonlocal attraction, when the local (on-site) attraction will tend to transform the Cooper pairs into local pairs.

The "mixed" case with $h_l(\mathbf{k})=1$ and $\lambda=\lambda_s+\lambda_d\cos2\varphi_{\mathbf{k}}$ was considered in Refs. 41 and 42. In particular, it was shown in Ref. 41 that the crossover from d-wave to s-wave superconductivity with doping takes place with an intermediate $s+d$ symmetry, in full agreement with the experiments on some cuprate materials.[53–55]

The d-wave case, when $w_d(\mathbf{k})=\cos k_x-\cos k_y$ was considered in Refs. 37, 44 and 45. For example, the effect of the n.n.n. hopping $t_{n.n.n.}$ on the pairing was studied in Refs. 44

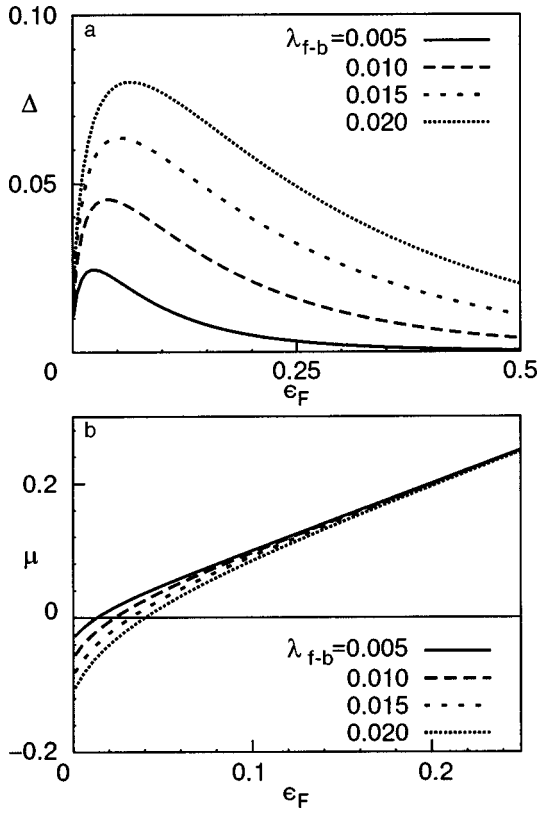

FIG. 4. The gap (a) and the chemical potential (b) as functions of ϵ_F at different λ_{f-b} and $\lambda_{f-f}=0$.

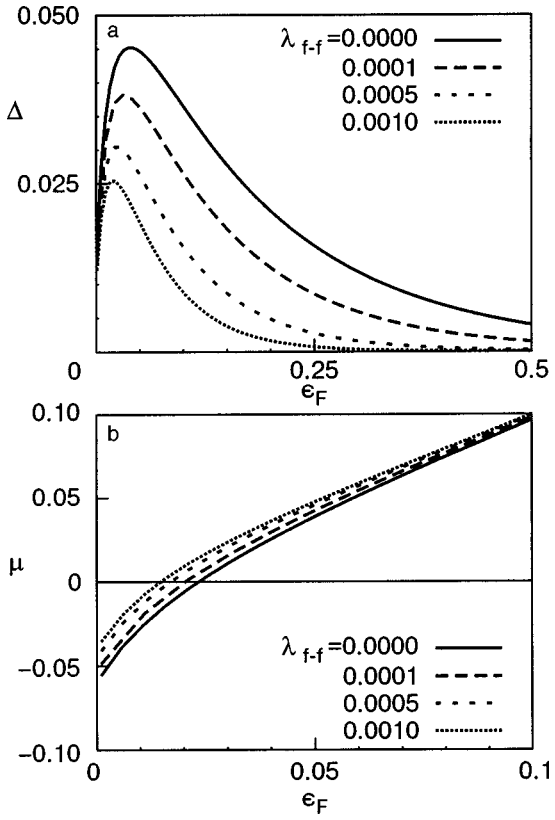

FIG. 5. The gap (a) and the chemical potential (b) as functions of ϵ_F at different λ_{f-f} and $\lambda_{f-b}=0.01$.

and 45. It was shown in the latter paper that the crossover with doping takes place at any value of $t_{n.n.n.}$ when the coupling constant is larger than $V_{\rm cr}$.

Finally, it was stated in Ref. 29 that the model with small on-site repulsion and n.n. $V_{n.n.}$ and n.n.n. $V_{n.n.n.}$ attraction with $V_{n.n.n.}\sim 60-80$ meV and $V_{n.n.n.}/V_{n.n.}\simeq 1.3-1.5$ can describe well the experimental data for the hole-doped oxides.

3.3. Models with retarded interaction

As is well-known, retardation effects in the interaction can play a very important role in the superconducting properties of a system. For instance, let us consider a boson propagator with dispersion $\omega=\omega(\mathbf{k})$ [cf. Eq. (14)]:

$$D(\omega,\mathbf{k})=\frac{\omega^2(\mathbf{k})}{\omega^2-\omega^2(\mathbf{k})+i\delta}. \tag{31}$$

It can be noted that in the general case of phonon dispersion one has $\omega(\mathbf{k})=\sqrt{\omega_0^2+c_{\rm ph}^2\mathbf{k}^2}$. We shall describe this rather general case below with the following approximation: $D(\omega,\mathbf{k})\simeq D(\omega,\mathbf{k}_F)$, so the effective propagator can be written as

$$D(\omega,\mathbf{k})=\frac{\omega_0^2}{\omega^2-\omega_0^2+i\delta}, \tag{32}$$

where $\sqrt{\omega_0^2+c_{\rm ph}^2\mathbf{k}_F^2}$ is replaced by a new effective frequency ω_0. This approximation corresponds to the case of the optical phonon attraction (in the case when $\omega_0\neq 0$). Generally speaking, the gap is frequency dependent in this model. The problem of the crossover in the model with a frequency-dependent gap was investigated in Ref. 36.

The set of equations for the gap and for the chemical potential in this case is:

$$\Phi(\omega)=-ig_{f-b}^2 \times\int\frac{d^2kd\nu}{(2\pi)^2}\frac{\Phi(\nu)}{\nu^2-\xi(\mathbf{k})^2-|\Phi(\nu)|^2+i\delta}\frac{\omega_0^2}{(\omega-\nu)^2-\omega_0^2+i\delta}; \tag{33}$$

$$2\epsilon_F=\mathrm{Re}\int_0^\infty d\omega\left[\left(\frac{\omega}{\sqrt{\omega^2-|\Phi(\omega)|^2}}-1\right)\times\theta(\mu+\sqrt{\omega^2-|\Phi(\omega)|^2})+\left(\frac{\omega}{\sqrt{\omega^2-|\Phi(\omega)|^2}}+1\right)\times\theta(\mu-\sqrt{\omega^2-|\Phi(\omega)|^2})\right]. \tag{34}$$

Let us consider briefly how this system of equations can be analyzed analytically. First of all, it is possible to show that the approximation $\Phi(\omega)=\Delta=\mathrm{const}$ in (34) is rather good. Then, this equation results in

$$\mu=\epsilon_F-\frac{\Delta^2}{2\epsilon_F}\simeq\epsilon_F-\frac{|\varepsilon_b|}{2},$$

where the two-particle bound state energy ε_b depends on the coupling parameter in this case (see below).

After the Wick rotation $\omega \to i\omega$ the gap equation reads:

$$\Phi(\omega) = g_{f-b}^2 \omega_0^2 \times \int \frac{d^2k d\nu}{(2\pi)^3} \frac{\Phi(\nu)}{\nu^2 + (\mathbf{k}^2/2m - \mu)^2 + \Phi^2(\nu)} \frac{1}{(\omega - \nu)^2 + \omega_0^2}. \quad (35)$$

In polar coordinates, after integration over the angle we come to:

$$\Phi(\omega) = \frac{g_{f-b}^2 \omega_0^2}{(2\pi)^2} \int_{-\infty}^{+\infty} d\nu \frac{\Phi(\nu)}{(\omega - \nu)^2 + \omega_0^2} \times \int_0^{\infty} \frac{k dk}{(\mathbf{k}^2/2m - \mu)^2 + \nu^2 + \Phi^2(\nu)}.$$

Since $\Phi(\omega)$ is an even function of ω, it can depend only on ω^2, and we restrict the integration over ν to positive values:

$$\Phi(\omega) = \frac{\lambda \omega_0^2}{2} \int_0^{\infty} \frac{d\nu \Phi(\nu)}{\sqrt{\nu^2 + \Phi^2(\nu)}} \frac{1}{(\omega - \nu)^2 + \omega_0^2} \times \left[\frac{\pi}{2} + \arctan \frac{\mu}{\sqrt{\nu^2 + \Phi^2(\nu)}} \right], \quad (36)$$

where the dimensionless coupling constant $\lambda = g_{f-b}^2 m/(2\pi)$ is introduced. The asymptotic behavior for $\Phi(\omega)$ is

$$\Phi(\omega)|_{\omega \to 0} \to \text{const}, \quad \Phi(\omega)|_{\omega \to \infty} \sim \frac{1}{\omega^2}. \quad (37)$$

As the next step we use the following approximation in the interaction potential:[61,62]

$$\frac{1}{(\omega - \nu)^2 + \omega_0^2} = \frac{1}{\omega^2 + \omega_0^2} \theta(\omega - \nu) + \frac{1}{\nu^2 + \omega_0^2} \theta(\nu - \omega). \quad (38)$$

Then differentiation with respect to ω gives

$$\Phi'(\omega) = -\frac{\lambda \omega_0^2 \nu}{(\nu^2 + \omega_0^2)^2} \int_0^{\omega} \frac{d\nu \Phi(\nu)}{\sqrt{\nu^2 + \Phi^2(\nu)}} \times \left[1 + \frac{2}{\pi} \arctan \frac{\mu}{\sqrt{\nu^2 + \Phi^2(\nu)}} \right]. \quad (39)$$

It is evident that $\Phi' < 0$, i.e., $\Phi_{\max} = \Phi(0) \equiv \Delta$.

After one more differentiation and the introduction of a new variable: $x = \nu^2/\omega_0^2$, one gets the following differential equation:

$$\Phi''(x) + \frac{2}{x+1} \Phi'(x) + \frac{\lambda}{4\sqrt{x}(x+1)^2 \sqrt{x + [\Phi(x)/\omega_0]^2}} \times \left[1 + \frac{2}{\pi} \arctan \frac{\mu/\omega_0}{\sqrt{x + [\Phi(x)/\omega_0]^2}} \right] \Phi(x) = 0 \quad (40)$$

with the boundary conditions

$$\Phi'(x)|_{x=0} = 0; \quad [\Phi(x) + (x+1)\Phi'(x)]|_{x=\infty} = 0, \quad (41)$$

which follow directly from expressions (36), (38), and (39).

Analysis of Eq. (40) shows that the approximate solution for the gap in both the weak and strong coupling regimes is (see Ref. 36 for details): $\Delta(\omega) \simeq \Delta\, \theta(\omega_0^2 - \omega^2)$, where Δ is a parameter that depends on the coupling constant and, what is very important, on the carrier density. In the weak coupling regime the parameter Δ has the following coupling and carrier-density dependence:

$$\Delta = \sqrt{2|\varepsilon_b|\omega_0}\, \theta(\omega_0 - \epsilon_F) + \Delta_{BCS} \theta(\epsilon_F - \omega_0),$$

where $\Delta_{BCS} = 2\omega_0 e^{-1/\lambda}$ is in fact the BCS expression for the gap, and the bound (Cooper) state energy in this case is $\varepsilon_b = -2\omega_0 e^{-2/\lambda}$. In the strong coupling regime $\varepsilon_b \simeq \lambda$ and $\Delta_{BCS} \to (4/3)\lambda\omega_0$ at large carrier densities.[35,36]

To summarize, the BEC–BCS crossover with changing carrier density and coupling constant in this effective model with retarded interaction is also smooth, and the gap is not small when the pair frequency is smaller than the boson frequency. Such an approach can be used for studying the crossover in cases of different symmetries of the order parameter.

It is important to mention that the case considered here can be easily generalized to the case when one takes into account the vertex correction to the electron–phonon interaction. This correction is usually small when $\epsilon_F \gg \omega_0$ (the Migdal theorem). As was shown in Ref. 63, this correction is rather small even when $\epsilon_F \ll \omega_0$. However, in some cases the vertex correction can lead to rather strong enhancement of the superconductivity.[40,64,65] It is also necessary to note that this correction leads to enhancement of the *d*-wave superconductivity even in a strongly correlated electron system,[39,40] in spite of the fact that the phonon interaction due to the symmetry does not allow *d*-wave pairing in the case when the short-range electron repulsion is not taken into consideration.

4. THE ROLE OF THE ORDER PARAMETER FLUCTUATIONS

The fluctuations of the order parameter in the 2D and even in the 3D case at $T = 0$ should be essential. As is shown in Ref. 22, the Gaussian fluctuation corrections to the *s*-wave order parameter is non-negligible even in the weak coupling case. On the other hand, the fluctuations of the order parameter phase can lead to increasing of the gap.

In this Section we shall consider how simultaneous order parameter modulus and phase fluctuations in the model with 4F attraction result in a strong increase of the order parameter when the carrier densities are small and to a weak decrease of the order parameter when the carrier densities are large.

At zero temperature, as follows from (8), the thermodynamic potential of the system with local attraction has the following form:

$$\Omega = v \left[\frac{|\Phi|^2}{V} - \int \frac{d^2k}{(2\pi)^2} \left[\sqrt{\xi^2(\mathbf{k}) + |\Phi|^2} - \xi(\mathbf{k}) \right] \right].$$

In other words, it depends on the sum of its real and imaginary parts: $|\Phi|^2 = (\mathrm{Re}\,\Phi)^2 + (\mathrm{Im}\,\Phi)^2$. For studying fluctuations of the order parameter, it is convenient to use new real variables:

$$\overline{\Phi}(x) = \begin{pmatrix} \phi_1(x) \\ \phi_2(x) \end{pmatrix},$$

such that $\overline{\Phi}^2(x)=\phi_1^2(x)+\phi_2^2(x)=|\Phi(x)|^2$. Another possibility is to use the decomposition of the order parameter into its phase and modulus: $\Phi(x)=\Delta(x)\exp[i\theta(x)]$. However, it leads to some difficulties, since one needs to keep the order parameter modulus positive in the functional integration over the fluctuations; we therefore follow another way. The ''old'' order parameter variables are connected with the new ones as

$$\Phi(x)=\phi_1(x)+i\phi_2(x),\quad \Phi^*(x)=\phi_1(x)-i\phi_2(x).$$

We assume that the mean-field value of the field $\overline{\Phi}$ is chosen as

$$\overline{\Phi}_0(x)=\begin{pmatrix}\Delta\\0\end{pmatrix}.$$

The order parameter $\overline{\Phi}$ can be written as

$$\overline{\Phi}(x)=\overline{\Phi}_0+\delta\overline{\Phi}(x)\equiv\begin{pmatrix}\Delta+\delta\phi_1(x)\\ \delta\phi_2(x)\end{pmatrix} \tag{42}$$

in the case when its fluctuations are considered. We neglect the fluctuations of the carrier density $n_f(\mathbf{r})$, and consider a homogeneous constant value of n_f over the lattice: $n_f(\mathbf{r})=n_f=\text{const}$.

Substitution of (42) into the expression for the thermodynamic potential gives the following correction to the thermodynamic potential to the second order in fluctuations:[66]

$$\delta\Omega=-\int_{-\infty}^{\infty}\frac{d\nu}{2\pi}\int\frac{d^2k}{(2\pi)^2}\,\delta\overline{\Phi}(i\nu,\mathbf{k})\hat{A}(i\nu,\mathbf{k})\delta\overline{\Phi}(-i\nu,-\mathbf{k}), \tag{43}$$

where $\hat{A}(i\nu,\mathbf{k})=1/V+\hat{\chi}(i\nu,\mathbf{k})$ is the 2×2 matrix with the susceptibility components

$$\chi_{jk}(i\nu,\mathbf{k})=\frac{1}{2}\mathrm{Tr}\int_{-\infty}^{\infty}\frac{d\omega}{2\pi}\int\frac{d^2q}{(2\pi)^2}$$
$$(-1)^{j+k}G(i\omega_+,\mathbf{q}_+)\hat{\tau}_jG(i\omega_-,\mathbf{q}_+)\hat{\tau}_k,$$

where $\omega_\pm=\omega\pm\nu/2$, $\mathbf{q}_\pm=\mathbf{k}\pm\mathbf{q}/2$, and $j,k\equiv x,y$. The integration over ω can be easily performed:

$$\chi_{11}(i\nu,\mathbf{k})=-\int\frac{d^2q}{(2\pi)^2}\frac{1}{2}\frac{E_++E_-}{\nu^2+(E_++E_-)^2}\times\left[1+\frac{\xi_+\xi_--\Delta^2}{E_+E_-}\right];$$

$$\chi_{12}(i\nu,\mathbf{k})=-\chi_{21}(i\nu,\mathbf{k})=-\int\frac{d^2q}{(2\pi)^2}\frac{1}{2}\frac{E_+\xi_-+E_-\xi_+}{[\nu^2+(E_++E_-)^2]E_+E_-};$$

$$\chi_{22}(i\nu,\mathbf{k})=-\int\frac{d^2q}{(2\pi)^2}\frac{1}{2}\frac{E_++E_-}{\nu^2+(E_++E_-)^2}\times\left[1+\frac{\xi_+\xi_-+\Delta^2}{E_+E_-}\right],$$

where $E_\pm=\sqrt{\xi_\pm^2+\Delta^2}$ and $\xi_\pm=(\mathbf{k}\pm\mathbf{q}/2)^2/(2m)-\mu$ is the free fermion dispersion relation. After the integrating out of the fluctuation field $\overline{\Phi}$, the correction to the thermodynamic potential has the following form:

$$\delta\Omega=\frac{1}{2}\int_{-\infty}^{\infty}\frac{d\nu}{2\pi}\int\frac{d^2k}{(2\pi)^2}\ln\left[\left\{\frac{1}{V}+\chi_{11}(i\nu,\mathbf{k})\right\}\times\left\{\frac{1}{V}+\chi_{22}(i\nu,\mathbf{k})\right\}-\chi_{12}(i\nu,\mathbf{k})\chi_{21}(i\nu,\mathbf{k})\right].$$

The factor $\sim\Delta$ which appears in the measure of the functional integration over Δ in Z due to the taking into account of the symmetry of the thermodynamic potential with respect to the transformation $\overline{\Phi}\to e^{i\alpha}\overline{\Phi}$ (see, for example, Ref. 66) is omitted in the last expression. This factor can be absorbed in the measure of the functional integral over Δ in the partition function, where the functional integration can be actually performed over the variable Δ^2. Let us note that only the first component $(1/V+\chi_{11}(i\nu,\mathbf{k}))$ under the logarithm in $\delta\Omega$ (see below) will be present if one considers the particular case of the order parameter phase fluctuations.

It is useful to diagonalize the matrix $\hat{A}(i\nu,\mathbf{k})$ in order to find the contributions which come from both the phase and the modulus fluctuations of the order parameter. Obviously, the first component will correspond to the phase fluctuations and the second, to the modulus fluctuations, as follows from the definitions of the field $\overline{\Phi}$ [see Eq. (42)]. So, one can easily arrive at the following representation:

$$\delta\Omega=\frac{1}{2}\int_{-\infty}^{\infty}\frac{d\nu}{2\pi}\int\frac{d^2k}{(2\pi)^2}\ln\left[\left\{\frac{1}{V}+\chi_\theta(i\nu,\mathbf{k})\right\}\times\left\{\frac{1}{V}+\chi_\Delta(i\nu,\mathbf{k})\right\}\right],$$

where

$$\chi_\theta(i\nu,\mathbf{k})=\frac{1}{2}[\chi_{11}(i\nu,\mathbf{k})+\chi_{22}(i\nu,\mathbf{k})]$$
$$-\sqrt{\frac{1}{4}[\chi_{11}(i\nu,\mathbf{k})-\chi_{22}(i\nu,\mathbf{k})]^2-\chi_{12}(i\nu,\mathbf{k})\chi_{21}(i\nu,\mathbf{k})}$$

and

$$\chi_\Delta(i\nu,\mathbf{k})=\frac{1}{2}[\chi_{11}(i\nu,\mathbf{k})+\chi_{22}(i\nu,\mathbf{k})]$$
$$+\sqrt{\frac{1}{4}[\chi_{11}(i\nu,\mathbf{k})-\chi_{22}(i\nu,\mathbf{k})]^2-\chi_{12}(i\nu,\mathbf{k})\chi_{21}(i\nu,\mathbf{k})}$$

are the effective contributions to the thermodynamic potential from the fluctuations of the order parameter phase and modulus, respectively.

The equations for the gap and for the chemical potential (10) and (11) have the following form in the case of a Gaussian correction to the thermodynamic potential due to the order parameter fluctuations:

$$\frac{\Delta}{V}=\int\frac{d^2k}{(2\pi)^2}\frac{\Delta}{2\sqrt{\xi^2(\mathbf{k})+\Delta^2}}+\frac{1}{2}\int_{-\infty}^{\infty}\frac{d\nu}{2\pi}\int\frac{d^2k}{(2\pi)^2}\left[\frac{\partial\chi_\theta(i\nu,\mathbf{k})/\partial\Delta}{1/V+\chi_\theta(i\nu,\mathbf{k})}+\frac{\partial\chi_\Delta(i\nu,\mathbf{k})/\partial\Delta}{1/V+\chi_\Delta(i\nu,\mathbf{k})}\right];$$

$$n_f=\int\frac{d^2k}{(2\pi)^2}\left[1-\frac{\xi(\mathbf{k})}{\sqrt{\xi^2(\mathbf{k})+\Delta^2}}\right]+\int_{-\infty}^{\infty}\frac{d\nu}{2\pi}\int\frac{d^2k}{(2\pi)^2}\left[\frac{\partial\chi_\theta(i\nu,\mathbf{k})/\partial\mu}{1/V+\chi_\theta(i\nu,\mathbf{k})}+\frac{\partial\chi_\Delta(i\nu,\mathbf{k})/\partial\mu}{1/V+\chi_\Delta(i\nu,\mathbf{k})}\right].$$

In considering the limit of a weak coupling, the functions χ_θ and χ_Δ in the denominators can be neglected, and then the integration over ν can be performed; after some trivial manipulations, the following rather simple equation can be obtained [compare with (18) and (19)]:

$$\frac{1}{V}=\int\frac{d^2k}{(2\pi)^2}\frac{1}{2\sqrt{\xi^2(\mathbf{k})+\Delta^2}}+\frac{V}{2}\int\frac{d^2q}{(2\pi)^2}\int\frac{d^2k}{(2\pi)^2}\frac{\xi_+\xi_-}{E_+^3E_-};\tag{44}$$

$$n_f=\int\frac{d^2k}{(2\pi)^2}\left[1-\frac{\xi(\mathbf{k})}{\sqrt{\xi^2(\mathbf{k})+\Delta^2}}\right]+V\int\frac{d^2q}{(2\pi)^2}\int\frac{d^2k}{(2\pi)^2}\frac{\Delta^2(\xi_+-\xi_-)}{E_+^3E_-}.\tag{45}$$

The substitution $\mathbf{k}\rightarrow-\mathbf{k}$ in a part of the terms was made in deriving Eqs. (44) and (45). It is interesting to note that in the case of the phase fluctuations, the numerator in the last term under the integral in the gap equation will be $\frac{1}{2}\xi_+(\xi_--\xi_+)$, and the last term in the number equation will be multiplied by 1/2. It is also a good approximation to put $\mu=\epsilon_F$, since in the weak coupling regime, μ is different from ϵ_F only at extremely low carrier densities. The solution of the equation (44) for the gap parameter as a function of ϵ_F at $\mu=\epsilon_F$ and different values of the coupling constant is presented in Fig. 6. An estimate of the order parameter in the case of phase fluctuation is also presented. As was shown in Ref. 22, in the 2D case the phase fluctuations lead to an effective increase of the coupling constant: $V\rightarrow V(1+2/\pi^2)$. The gap can be calculated from the standard mean-field BCS equation. A comparison of the different cases shows that the phase fluctuations lead to increasing of the gap, while the total fluctuations lead to a much stronger increasing of the gap at low carrier densities and to decreasing of the gap when the carrier density is large. The last result is familiar, but the first one is very surprising. The dependence of the gap on coupling at a low value of the carrier density is presented in Fig. 7. These results suggest that corrections of higher order in the fluctuations should be studied for better understanding of the behavior of the system.

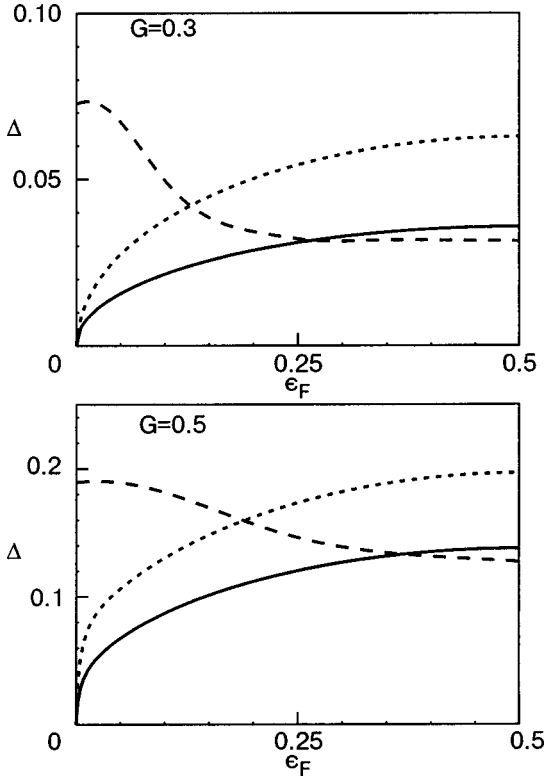

FIG. 6. The dependence of Δ on ϵ_F for the case of the mean-field solution (solid curve) and for the order parameter fluctuations case (dashed curve) at different values of the dimensionless coupling parameter $G=mV/(2\pi)$. The dotted curve is the estimate from Ref. 22 for the case of order parameter phase fluctuations.

It should be mentioned that the role of the disorder due to the dopants in the fluctuations of the inhomogeneous order parameter was recently studied by Yu. G. Pogorelov and the present authors in Refs. 67–69. However, we have not discussed this important issue here, since it deserves a special detailed review.

5. CONCLUSIONS

In this paper the BEC–BCS crossover from superfluidity to superconductivity with increasing doping at $T=0$ in the cases of the s-wave and d-wave pairing was briefly re-

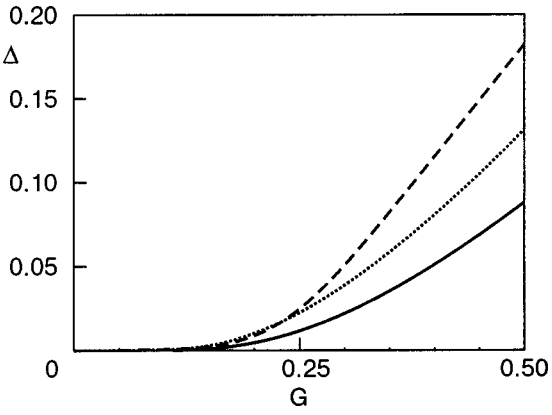

FIG. 7. The dependence of Δ on G for the case of the mean-field solution (solid curve) and for the case of order parameter fluctuations (dashed curve) at $\epsilon_F=0.1$. The dotted curve is the estimate from Ref. 22 for the order parameter phase fluctuations.

viewed. In the 3D case this crossover does not take place at weak coupling constants, and the same situation takes place in the d-wave pairing case in two-dimensions, when the interaction does not depend on the doping. When the correlation radius depends on the doping, a minimal value of the coupling for the two-particle bound state exists even in the s-wave channel. Also the gap can decrease with doping in this case.

It was also shown that the fluctuations of the order parameter play an important role even at $T=0$. The fluctuations of the order parameter phase in the weak coupling limit in the case of the s-wave pairing regime lead to enhancement of superconductivity at any physical carrier density, while the modulus fluctuations lead to much stronger enhancement of superconductivity at low carrier densities. At high carrier densities they lead to suppression of the order parameter; as a result, the gap decreases in the BCS regime when both the modulus and the phase fluctuations are taken into account.

This means that higher-order fluctuation corrections should be investigated in order to develop a self-consistent theory of superconductivity (which can be similar to superfluidity) at low carrier densities.

We would like to mention some topics that may be interesting for future investigations. The problem of the crossover with realistic dispersion relations has not been studied even on the mean-field level in many interesting cases. Another important problem is the interplay between disorder and superconductivity and between strong correlations and superconductivity in so-called bad metals. The fluctuations in the d-wave pairing channel and in other nonisotropic pairing channels have not yet been studied carefully even in the case of Gaussian fluctuations. It is also important to go beyond the Gaussian fluctuations, since the pair susceptibility is divergent in the 2D and in the 3D cases, as was mentioned in Ref. 22. The role of the interlayer coupling is another problem which has not solved in general at present. The solution of the problems mentioned above will lead to better understanding of the superconducting properties of systems with arbitrary carrier density and pairing potential.

First of all, we would like to thank Prof. D. M. Eagles who called our attention to Refs. 3–5 and kindly sent them to us. We also express our gratitude to the referee of this review, whose constructive scientific and editorial (mainly linguistic) remarks helped us to improve it. One of us (V.M.L.) acknowledges support by SCOPES-project 7UKPJ062150.00/1 of the Swiss National Science Foundation.

*E-mail: vloktev@bitp.kiev.ua
**E-mail: turk@physics.georgetown.edu. Present address: Department of Physics, Georgetown University, Washington DC, 20057 USA

[1] D. M. Eagles, Phys. Rev. **186**, 456 (1969).
[2] H. P. R. Frederikse, Phys. Rev. Lett. **16**, 579 (1966).
[3] R. J. Tainsh and C. Andrikidis, Solid State Commun. **60**, 519 (1986).
[4] D. M. Eagles, Solid State Commun. **60**, 521 (1986).
[5] D. M. Eagles, R. J. Tainsh, and C. Andrikidis, Physica C **157**, 48 (1989).
[6] R. A. Ogg Jr., Phys. Rev. **69**, 243 (1946).
[7] M. R. Schafroth, Phys. Rev. **96**, 1149 (1954).
[8] M. R. Schafroth, Phys. Rev. **96**, 1442 (1954).
[9] M. R. Schafroth, Phys. Rev. **100**, 463 (1955).
[10] A. J. Leggett, in *Modern Trends in the Theory of Condensed Matter*, Springer-Verlag (1980), p. 13.
[11] P. Nozières and P. Schmitt-Rink, J. Low Temp. Phys. **59**, 195 (1985).
[12] R. Micnas, J. Ranninger, and S. Robaszkiewicz, Rev. Mod. Phys. **62**, 113 (1990).
[13] C. A. R. Sá de Melo, M. Randeria, and J. R. Engelbrecht, Phys. Rev. Lett. **71**, 3202 (1993).
[14] R. Haussmann, Phys. Rev. B **49**, 12975 (1994).
[15] M. Randeria, in *Bose-Einstein Condensation*, A. Griffin, D. W. Snoke, and S. Stringari (eds.), Cambridge University Press, New York (1995), p. 355.
[16] J. R. Engelbrecht, M. Randeria, and C. A. R. Sá de Melo, Phys. Rev. B **55**, 15153 (1997).
[17] M. Marini, F. Pistolesi, and G. C. Strinati, Eur. Phys. J. B **1**, 151 (1998).
[18] N. Andrenacci, A. Perali, P. Pieri, and G. C. Strinati, Phys. Rev. B **60**, 12410 (1999).
[19] E. Babaev, Phys. Rev. B **63**, 184514 (2000).
[20] F. Pistolesi and G. C. Strinati, Phys. Rev. B **53**, 15168 (1996).
[21] I. J. R. Aitchison, P. Ao, D. J. Thouless, and X.-M. Zhu, Phys. Rev. B **51**, 6531 (1995).
[22] S. Koš and A. J. Millis, Preprint cond-mat/0207190 (2002).
[23] E. V. Gorbar, V. M. Loktev, and S. G. Sharapov, Physica C **257**, 355 (1996).
[24] V. P. Galaiko, Fiz. Nizk. Temp. **13**, 1102 (1987) [Sov. J. Low Temp. Phys. **13**, 627 (1987)]; I. O. Kulik, Fiz. Nizk. Temp. **13**, 879 (1987) [Sov. J. Low Temp. Phys. **13**, 505 (1987)].
[25] N. D. Mermin and H. Wagner, Phys. Rev. Lett. **17**, 1113 (1966); P. C. Hohenberg, Phys. Rev. **158**, 383 (1967); S. Coleman, Commun. Math. Phys. **31**, 259 (1973).
[26] M. Randeria, J.-M. Duan, and L. Y. Sheih, Phys. Rev. Lett. **62**, 981 (1989).
[27] M. Randeria, J.-M. Duan, and L. Y. Sheih, Phys. Rev. B **41**, 327 (1990).
[28] F. Pistolesi and G. C. Strinati, Phys. Rev. B **49**, 6356 (1994).
[29] R. Fehrenbacher and M. R. Norman, Phys. Rev. Lett. **74**, 3884 (1995).
[30] P. Nozières and F. Pistolesi, Eur. Phys. J. B **10**, 649 (1999).
[31] E. V. Gorbar, V. P. Gusynin, and V. M. Loktev, Fiz. Nizk. Temp. **19**, 1171 (1993) [Low Temp. Phys. **19**, 832 (1993)].
[32] L. S. Borkowski and C. A. R. Sá de Melo, Preprint cond-mat/9810370 (1998).
[33] R. D. Duncan and C. A. R. Sá de Melo, Phys. Rev. B **62**, 9675 (2000).
[34] M. Capone, C. Castellani, and M. Grilli, Phys. Rev. Lett. **88**, 126403 (2002).
[35] V. M. Loktev, V. M. Turkowski, and S. G. Sharapov, J. Phys. Stud. **1**, 431 (1997) [in Ukrainian].
[36] V. M. Loktev, V. M. Turkowski, and S. G. Sharapov, Teor. Mat. Fiz. **115**, 419 (1998) [Theor. Math. Phys. **115**, 694 (1998)].
[37] B. C. den Hertog, Phys. Rev. B **60**, 559 (1999).
[38] S. Stintzing and W. Zwerger, Phys. Rev. B **56**, 9004 (1997).
[39] M. Mierzejewski, J. Zieli'nski, and P. Entel, Phys. Rev. B **57**, 590 (1998).
[40] P. Paci, C. Grimaldi, and L. Pietronero, Eur. Phys. J. B **17**, 235 (1999).
[41] K. A. Musaelian, J. Betouras, A. V. Chubukov, and R. Joynt, Phys. Rev. B **53**, 3598 (1996).
[42] E. V. Gorbar, V. M. Loktev, and V. S. Nikolaev, Supercond., Phys. Chem. Technol. **7**, 1 (1994).
[43] J. P. Wallington and J. F. Annett, Phys. Rev. B **61**, 1433 (2000).
[44] M. B. Soares, F. Kokubun, J. J. Rodríguez-Núñez, and O. Rendun, Phys. Rev. **65**, 174506 (2002).
[45] A. Perali, P. Pieri, and G. C. Strinati, Preprint cond-mat/0211132 (2002).
[46] F. Pistolesi and Ph. Noziéres, Phys. Rev. B **66**, 054501 (2002).
[47] V. M. Loktev and V. Turkowski, Physica C **383**, 256 (2002).
[48] J. Batle, M. Casas, M. Fortes *et al.*, Preprint cond-mat/0211456 (2002).
[49] C. C. Tsuei and J. R. Kirtley, Rev. Mod. Phys. **72**, 969 (2000).
[50] J. A. Skinta, T. R. Lemberger, T. Greibe, and M. Naito, Phys. Rev. Lett. **87**, 207003 (2002).
[51] C.-T. Chen, P. Seneor, N.-C. Yeh, R. P. Vasquez, L. D. Bell, C. U. Jung, J. Y. Kim, Min-Seok Park, Heon-Jung Kim, and Sung-Ik Lee, Phys. Rev. Lett. **88**, 227002 (2002).
[52] G.-M. Zhao, Phys. Rev. B **64**, 024503 (2002).
[53] N.-C. Yeh, C.-T. Chen, G. Hammerl, J. Mannhart, A. Schmehl, C. W. Schneider, R. R. Schultz, S. Tajima, K. Yoshida, D. Garrigus, and M. Strasik, Phys. Rev. Lett. **87**, 087003 (2001).
[54] A. Biswas, P. Fournier, M. M. Qazilbash, V. N. Smolyaninova, H. Balci, and R. L. Greene, Phys. Rev. Lett. **88**, 207004 (2002).
[55] J. A. Skinta, M.-S. Kim, T. R. Lemberger, T. Greibe, and M. Naito, Phys. Rev. Lett. **88**, 207005 (2002).
[56] C. Proust, E. Boaknin, R. W. Hill, L. Taillefer, and A. P. Mackenzie, Phys. Rev. Lett. **89**, 147003 (2002).

[57] A. V. Svidzinsky, *Spatially Inhomogeneous Problems of Superconductivity* [in Russian], Nauka, Moscow (1982).
[58] H. Kleinert, Fortschr. Phys. **26**, 565 (1978).
[59] T. R. Thurston, R. J. Birgeneau, M. A. Kastner, N. W. Preyer, G. Shirane, Y. Fujii, K. Yamada, Y. Endoh, K. Kakurai, M. Matsuda, Y. Hidaka, and T. Murakami, Phys. Rev. B **40**, 4585 (1989).
[60] A. L. Fetter and J. D. Walecka, *Quantum Theory of Many-Particle Systems*, McGraw-Hill, New York (1971).
[61] T. Appelquist, M. J. Bowick, D. Karabali, and L. C. R. Wijewardhana, Phys. Rev. B **33**, 3774 (1986).
[62] V. P. Gusynin, V. A. Miransky, and I. A. Shovkovy, Nucl. Phys. B **462**, 249 (1996).
[63] M. A. Ikeda, A. Ogasawara, and M. Sugihara, Phys. Lett. A **170**, 319 (1992).
[64] L. Pietronero and S. Strassler, Europhys. Lett. **18**, 627 (1992).
[65] C. Grimaldi, L. Pietronero, and S. Strassler, Phys. Rev. Lett. **75**, 1158 (1995).
[66] J. Negele and H. Orland, *Quantum Many-Particle Systems*, Addison-Wesley (1987).
[67] V. M. Loktev and Yu. G. Pogorelov, Physica C **272**, 151 (1996).
[68] V. M. Loktev and Yu. G. Pogorelov, Fiz. Nizk. Temp. **27**, 1039 (2001) [Low Temp. Phys. **27**, 767 (2001)].
[69] V. M. Loktev, Yu. G. Pogorelov, and V. M. Turkowski, Int. J. Mod. Phys. B **17**, 3607 (2003).

This article was published in English in the original Russian journal. Reproduced here with stylistic changes by AIP.

QUANTUM LIQUIDS AND QUANTUM CRYSTALS

On the possibility of simultaneous spiral and superfluid ordering in a Fermi liquid

S. V. Peletminskii,* A. A. Yatsenko, and S. N. Shul'ga

National Science Center, Kharkov Institute of Physics and Technology, ul. Akademicheskaya 1, Kharkov 61108, Ukraine

(Submitted July 28, 2003; revised November 10, 2003)
Fiz. Nizk. Temp. **30**, 261–270 (March 2004)

A study is made of one of the possible forms of ordering of Fermi systems—superfluid spiral ordering, wherein not only the phase invariance of the state is broken but so are the translational invariance and the invariance with respect to spin rotations. A general method of studying superfluid spiral ordering is formulated on the basis of the Fermi-liquid approach to the consideration of superfluid states. For a one-component Fermi system we obtain the self-consistency equations for four order parameters and the temperature of the simultaneous phase transition to the superfluid and spiral states. The system of equations is investigated in the case of two nonzero order parameters. The transition temperature and the energy gap in the spectrum of elementary fermionic excitations are obtained as functions of the parameter of the spiral. The region of values of the spiral parameter in which the spiral superfluid ordering can exist is determined. The correlation function of the spins in the presence of spiral ordering is investigated. [DOI: 10.1063/1.1645176]

1. INTRODUCTION

In this paper we investigate a superfluid spirally ordered state of a Fermi liquid.

The state of statistical equilibrium of the superfluid liquid with spiral ordering of the spins is investigated using the Fermi liquid approach to the theory of superfluidity. This means that the energy functional of the Fermi liquid is invariant with respect to arbitrary spatial translations in arbitrary spin rotations. However, the state of statistical equilibrium of a Fermi liquid is invariant only with respect to the simultaneous displacement by an arbitrary vector **a** and rotation of the spins by an angle $2\mathbf{a}\cdot\mathbf{q}$ ($2\mathbf{q}$ is the vector of the spiral).

The possibility of magnetic ordering was considered, e.g., in Ref. 1, where the question of the existence of ferromagnetic and superconducting states as a consequence of electrons exchanging a magnon (rather than a phonon, as in the BCS theory) was studied for the first time. Such an exchange can also lead to an attraction between electrons.

Superfluid spiral ordering has been considered in many papers. For example, it was shown in a study[2] of the coexistence of superfluid and magnetic ordering that a superconducting phase with a spiral ordering of the magnetic moments can form in a magnetic superconductor. The question of the coexistence of superconductivity and antiferromagnetism, or of the influence of antiferromagnetic ordering of localized spins on the superconducting state, was examined in a review article.[3] Spiral spin ordering in magnetic superconductors due to an interaction between the photon field, persistent current, and a localized spin moment was investigated in Ref. 4. An expression for the spin susceptibility of such a system was obtained, and the dynamical properties due to spiral spin ordering were investigated. It was shown in a review[5] that the temperature of the transition to the magnetic superfluid state in high-T_c superconductors is significantly lower than the temperature of the transition from the normal to the superconducting state.

Unlike the aforementioned studies and many others, in the present paper the phase transition to the superfluid state arises simultaneously with a spiral ordering of the spins.

The Fermi-liquid approach to the theory of superfluidity is based on the introduction of a nonequilibrium statistical operator for an ideal gas of quasiparticles and the construction of a nonequilibrium entropy on the basis of it.

For studying the kinetics and equilibrium state of a superfluid Fermi liquid it is necessary to introduce an energy functional which is a functional of the normal f and anomalous g matrix distribution functions. In the semiphenomenological theory this energy functional replaces the Hamiltonian of the system in the rigorous microscopic theory.

An expression for the entropy of the system, together with the energy functional of the system, allows one to find the normal f and anomalous g distribution functions in a state of statistical equilibrium on the basis of a variational principle.

A spirally ordered state of statistical equilibrium is spatially nonuniform.

An important point here is that it is possible to go over, as a result of a unitary transformation, from a spatially nonuniform state to a state which is effectively spatially uniform as a result of a unitary transformation; this substantially simplifies the treatment of spiral studying of a superfluid liquid.

In this paper we derive general equations determining the order parameter $\Delta=(\Delta_0+\vec{\Delta}\vec{\sigma})\sigma_2$. Here the solution of the problem reduces to finding the roots of a bicubic equation and then performing some rather awkward calculations.

For this reason we shall consider only the particular case $\Delta_0+\Delta_3\sigma_3=0$.

Analytical expressions are obtained for the order parameter $\Delta_2\pm i\Delta_1$ and transition temperature as functions of the spiral vector **q**. The three-dimensional surface describing the dependence of the spiral vector on temperature and the order parameter is found numerically.

It is shown that in the state under consideration the mean value of the spin is nonzero and independent of the coordinates, while the spin correlation function $\langle\hat{\sigma}_m(\mathbf{x})\hat{\sigma}_n(\mathbf{y})\rangle$ is periodic in the variable $(\mathbf{x}+\mathbf{y})/2$ and decaying in the variable $\mathbf{x}-\mathbf{y}$.

2. BASIC EQUATIONS OF A FERMI LIQUID WITH SPIRAL ORDERING

The state of a superfluid Fermi liquid is characterized by a normal $f_{\kappa\kappa'}$ and an anomalous $g_{\kappa\kappa'}$ distribution function,

$$f_{\kappa\kappa'}=\mathrm{Tr}\ \rho\ a^{\dagger}_{\kappa'}a_{\kappa},\quad g_{\kappa\kappa'}=\mathrm{Tr}\ \rho\ a_{\kappa'}a_{\kappa}, \tag{1}$$

where ρ is the statistical operator of the Fermi liquid, $a^{\dagger}_{\kappa}$ and a_{κ} are the creation and annihilation operators for particles in state κ ($\kappa\equiv\mathbf{p},\alpha$; $\mathbf{p}$ is the momentum and α the spin projection of the particle). The energy of a superfluid Fermi liquid is specified by a functional of the normal and anomalous distribution functions f and g:

$$E=E(f,g). \tag{2}$$

In a state of statistical equilibrium the normal and anomalous distribution functions are determined from the condition of maximum entropy S at a fixed energy E of the system and total number of particles N (the momentum of the system is assumed to be zero). For solving this variational problem it is convenient to introduce a block density matrix (supermatrix)

$$\hat{f}=\begin{pmatrix} f & g \\ g^{\dagger} & \widetilde{1-f}\end{pmatrix} \tag{3}$$

(the elements of this matrix are expressed in terms of the single-particle distribution functions $f_{\kappa\kappa'}$ and $g_{\kappa\kappa'}$).

Then the equilibrium single-particle density matrix $\hat{f}$ is found from the nonlinear integral equation[6]

$$\hat{f}=\{\exp\beta\,[\hat{\varepsilon}(\hat{f})-\hat{\mu}]+1\}^{-1}, \tag{4}$$

where

$$\hat{\varepsilon}(\hat{f})=\begin{pmatrix}\varepsilon & \Delta\\ \Delta^{\dagger} & -\widetilde{\varepsilon}\end{pmatrix},\qquad \hat{\mu}=\mu\begin{pmatrix}1 & 0\\ 0 & -1\end{pmatrix}, \tag{5}$$

$$\varepsilon_{\kappa\kappa'}=\frac{\partial E}{\partial f_{\kappa'\kappa}},\qquad \Delta_{\kappa\kappa'}=2\frac{\partial E}{\partial g^{\dagger}_{\kappa'\kappa}}, \tag{6}$$

where μ is the chemical potential, $\beta=1/T$ is the inverse temperature, and $g^{\dagger}_{\kappa'\kappa}=(g_{\kappa\kappa'})^{*}$. We note that the matrix f is Hermitian, $f^{\dagger}_{\kappa\kappa'}=f_{\kappa\kappa'}$, and that the matrix g, by virtue of the Fermi statistics, is antisymmetric: $g_{\kappa\kappa'}=-g_{\kappa'\kappa}$.

We assume that the energy functional $E(f,g)$ is invariant with respect to spatial translations and spin rotations and has the following structure:

$$E(f,g)=E_0(f)+E_f(f)+E_g(g), \tag{7}$$

where

$$E_0(f)=\frac{1}{V}\sum_{\kappa,\kappa'}\varepsilon^{0}_{\kappa\kappa'}f_{\kappa'\kappa}, \tag{8}$$

and the interaction between particles is determined by functionals which are quadratic with respect to the normal and anomalous distribution functions:

$$E_f(f)=\frac{1}{2V}\sum_{\kappa_1\ldots\kappa_4}v(\kappa_1\kappa_2\kappa_3\kappa_4)(f_{\kappa_3\kappa_1}f_{\kappa_4\kappa_2}-f_{\kappa_3\kappa_2}f_{\kappa_4\kappa_1}), \tag{9}$$

$$E_g(g)=\frac{1}{2V}\sum_{\kappa_1\ldots\kappa_4}v(\kappa_1\kappa_2\kappa_3\kappa_4)g^{\dagger}_{\kappa_2\kappa_1}g_{\kappa_3\kappa_4} \tag{10}$$

(the Hartree–Fock approximation), where

$$v(\kappa_1\kappa_2\kappa_3\kappa_4)=v_0(\mathbf{p}_1\mathbf{p}_2\mathbf{p}_3\mathbf{p}_4)\delta_{\alpha_1\alpha_3}\delta_{\alpha_2\alpha_4}+v_1(\mathbf{p}_1\mathbf{p}_2\mathbf{p}_3\mathbf{p}_4)\overline{\sigma}_{\alpha_1\alpha_3}\overline{\sigma}_{\alpha_2\alpha_4}. \tag{11}$$

We assume[7] that the interaction amplitudes v_0 and v_1, which contain the Kronecker delta $\delta_{\mathbf{p}_1+\mathbf{p}_2,-\mathbf{p}_3-\mathbf{p}_4}$, are independent of the total momentum $\mathbf{p}_1+\mathbf{p}_2$. Then v_0 and v_1 can be written in the form

$$v_0(\mathbf{p}_1\mathbf{p}_2\mathbf{p}_3\mathbf{p}_4)=v_0(\mathbf{k},-\mathbf{k};\mathbf{k}',-\mathbf{k}')\equiv v_0(\mathbf{k},\mathbf{k}'),$$
$$v_1(\mathbf{p}_1\mathbf{p}_2\mathbf{p}_3\mathbf{p}_4)=v_1(\mathbf{k},-\mathbf{k};\mathbf{k}',-\mathbf{k}')\equiv v_1(\mathbf{k},\mathbf{k}')$$
$$(\mathbf{p}_1+\mathbf{p}_2=\mathbf{p}_3+\mathbf{p}_4), \tag{12}$$

where

$$\mathbf{k}=\frac{\mathbf{p}_1-\mathbf{p}_2}{2}\qquad \mathbf{k}'=\frac{\mathbf{p}_3-\mathbf{p}_4}{2}.$$

It follows from the Hermitianity of the Hamiltonian that $v_{0,1}(\mathbf{k},\mathbf{k}')=v^{*}_{0,1}(\mathbf{k}',\mathbf{k})$. Furthermore, we assume that the kinetic energy of free quasiparticles has the form

$$\varepsilon^{0}_{\kappa_1\kappa_2}=\frac{\mathbf{p}_1^2}{2m}\delta_{\kappa_1\kappa_2}. \tag{13}$$

It follows from formulas (6), (9), and (10) that the matrices $\varepsilon_{\kappa\kappa'}$ and $\Delta_{\kappa\kappa'}$ are related to the normal f and anomalous g distribution functions by the relations

$$\varepsilon_{\kappa_1\kappa_2}=\frac{1}{2V}\sum_{\kappa_3,\kappa_4}[v(\kappa_4\kappa_1\kappa_3\kappa_2)+v(\kappa_1\kappa_4\kappa_2\kappa_3)-v(\kappa_1\kappa_4\kappa_3\kappa_2)-v(\kappa_4\kappa_1\kappa_2\kappa_3)]f_{\kappa_3\kappa_4}, \tag{14}$$

$$\Delta_{\kappa_1\kappa_2}=\frac{1}{V}\sum_{\kappa_3,\kappa_4}v(\kappa_1\kappa_2\kappa_3\kappa_4)g_{\kappa_3\kappa_4}. \tag{15}$$

Relation (15) establishes a connection between the order parameter Δ, the interaction amplitudes v, and the anomalous distribution function g.

We have proposed a model description of the spiral ordering with respect to the spins of a superfluid Fermi liquid. Spiral ordering means that the state of the system is invariant with respect to an arbitrary displacement by a vector **a** and a simultaneous rotation of the spins around the z axis by an angle $2\mathbf{a}\cdot\mathbf{q}$. This means that the density matrix $\hat{f}$ satisfies the symmetry relation

$$\hat{V}\,\hat{f}\,\hat{V}^{\dagger}=\hat{f},\quad [f,\hat{\mathbf{p}}-\mathbf{q}\hat{\sigma}_3]=0, \tag{16}$$

where $\hat{V}$ is the unitary operator

$$\hat{V}=\exp i\mathbf{a}\cdot(\hat{\mathbf{p}}-\mathbf{q}\hat{\sigma}_3). \tag{17}$$

Here

$$\hat{\sigma}_3=\begin{pmatrix}\sigma_3 & 0\\ 0 & -\sigma_3\end{pmatrix},\quad \hat{\mathbf{p}}=\begin{pmatrix}\mathbf{p} & 0\\ 0 & -\tilde{\mathbf{p}}\end{pmatrix},$$

σ_3 is the Pauli matrix, and $\hat{\mathbf{p}}$ is the Fermi-particle momentum operator generalized to a superfluid Fermi liquid.[6]

Such states of a superfluid Fermi liquid are analogous to the spiral ordering of magnets and exist owing to the spin and translational invariance of the energy functional; they may possibly be realized in some phase of superfluid ^{3}He (Ref. 8).

It follows from formulas (3) and (16) that the unitary transformation

$$\hat{U}=\exp i\mathbf{q}\cdot\hat{\mathbf{x}}\sigma_3, \tag{18}$$

where $\begin{pmatrix}\mathbf{x} & 0\\ 0 & \hat{\mathbf{x}}\end{pmatrix}$ takes the state $\hat{f}$ to the state

$$\hat{f}_{\mathbf{q}}=\hat{U}\,\hat{f}\,\hat{U}^{\dagger}, \tag{19}$$

which is spatially uniform, i.e.,

$$[\hat{f}_{\mathbf{q}},\hat{\mathbf{p}}]=0, \tag{20}$$

and at the same time it preserves the structure of the supermatrix $\hat{f}$:

$$\hat{f}_{\mathbf{q}}=\begin{pmatrix}f_{\mathbf{q}} & g_{\mathbf{q}}\\ g_{\mathbf{q}}^{\dagger} & 1-\tilde{f}_{\mathbf{q}}\end{pmatrix}. \tag{21}$$

The normal and anomalous spatially uniform distribution functions $f_{\mathbf{q}}$ and $g_{\mathbf{q}}$ that determine the supermatrix $\hat{f}_{\mathbf{q}}$ are related to f and g by the following relations:

$$f_{\mathbf{q}}=e^{-i\mathbf{q}\mathbf{x}\sigma_3}\,f e^{i\mathbf{q}\mathbf{x}\sigma_3},\quad g_{\mathbf{q}}=e^{-i\mathbf{q}\mathbf{x}\sigma_3}\,g e^{-i\mathbf{q}\tilde{\mathbf{x}}\sigma_3}. \tag{22}$$

The uniform distribution functions $f_{\mathbf{q}}$ and $g_{\mathbf{q}}$, or the supermatrix $\hat{f}_{\mathbf{q}}$, satisfy a self-consistency equation that follows from (4):

$$\hat{f}_{\mathbf{q}}=\{\exp\beta[\hat{\varepsilon}_{\mathbf{q}}(f_{\mathbf{q}},g_{\mathbf{q}})-\hat{\mu}]+1\}^{-1}, \tag{23}$$

where

$$\hat{\varepsilon}_{\mathbf{q}}=\hat{U}\hat{\varepsilon}\hat{U}=\begin{pmatrix}\varepsilon_q & \Delta_q\\ \Delta_{\mathbf{q}}^{\dagger} & -\tilde{\varepsilon}_{\mathbf{q}}\end{pmatrix}.$$

For finding the solutions of this nonlinear self-consistency equation for a spatially uniform matrix $f_{\mathbf{q}}$ one can use the theory developed in Ref. 6.

3. SPIRAL SUPERFLUID STATE IN A HOMOGENEOUS REPRESENTATION

It follows from formulas (22) that the normal and anomalous distribution functions f and g are related to the spatially uniform distribution functions $f_{\mathbf{q}\kappa\kappa'}=f_{\mathbf{q}}(\mathbf{p})_{\alpha\alpha'}\delta_{\mathbf{p}\mathbf{p}'}$ and $g_{\mathbf{p}\kappa\kappa'}=g_{\mathbf{q}}(\mathbf{p})_{\alpha\alpha'}\delta_{\mathbf{p},-\mathbf{p}'}$ by the formulas

$$f_{\mathbf{p}\mathbf{p}'}=\sum_{\alpha,\beta=\pm1}P_{\alpha}\,f_{\mathbf{q}}(\mathbf{p}-\alpha\mathbf{q})P_{\beta}\,\delta_{\mathbf{p}-\alpha\mathbf{q},\mathbf{p}'-\beta\mathbf{q}}, \tag{24}$$

$$g_{\mathbf{p}\mathbf{p}'}=\sum_{\alpha,\beta=\pm1}P_{\alpha}\,g_{\mathbf{q}}(\mathbf{p}-\alpha\mathbf{q})P_{\beta}\,\delta_{\mathbf{p}-\alpha\mathbf{q},-\mathbf{p}'+\beta\mathbf{q}}. \tag{25}$$

In these relations the matrices $f_{\mathbf{p}\mathbf{p}'}$, $g_{\mathbf{p}\mathbf{p}'}$, $f_{\mathbf{q}}(\mathbf{p})$, and $g_{\mathbf{q}}(\mathbf{p})$ act only in spin space. Analogous formulas are valid for $\varepsilon_{\mathbf{p}\mathbf{p}'}$ and $\Delta_{\mathbf{p}\mathbf{p}'}$ as well. These formulas were obtained with the use of the relation

$$\langle\mathbf{p}|e^{i\mathbf{q}\cdot\mathbf{x}\sigma_3}|\mathbf{p}'\rangle=\sum_{\alpha=\pm1}\delta_{\mathbf{p},\mathbf{p}'+\alpha\mathbf{q}}P_{\alpha},$$

with $P_{\alpha}=1+\alpha\sigma_3/2$, where $\alpha=\pm1$ is the projection operator on a state with spin projection $\alpha/2$.

The inverse formulas expressing $f_{\mathbf{q}}$ and $g_{\mathbf{q}}$ in terms of f and g are also valid:

$$f_{\mathbf{q}}(\mathbf{p})\,\delta_{\mathbf{p},\mathbf{p}'}=\sum_{\alpha,\beta=\pm1}P_{\alpha}\,f(\mathbf{p}+\alpha\mathbf{q},\ \mathbf{p}'+\beta\mathbf{q})p_{\beta}, \tag{26}$$

$$g_{\mathbf{q}}(\mathbf{p})\,\delta_{\mathbf{p},-\mathbf{p}'}=\sum_{\alpha,\beta=\pm1}P_{\alpha}g(\mathbf{p}+\alpha\mathbf{q},\ \mathbf{p}'+\beta\mathbf{q})P_{\beta}, \tag{27}$$

and also the analogous relations linking $\varepsilon_{\mathbf{q}}$ and $\Delta_{\mathbf{q}}$ with ε and Δ:

$$\varepsilon_{\mathbf{q}}(\mathbf{p})\,\delta_{\mathbf{p},\mathbf{p}'}=\sum_{\alpha,\beta=\pm1}P_{\alpha}\,\varepsilon(\mathbf{p}+\alpha\mathbf{q},\mathbf{p}'+\beta\mathbf{q})P_{\beta}, \tag{28}$$

$$\Delta_{\mathbf{q}}(\mathbf{p})\,\delta_{\mathbf{p},-\mathbf{p}'}=\sum_{\alpha,\beta=\pm1}P_{\alpha}\,\Delta(\mathbf{p}+\alpha\mathbf{q},\mathbf{p}'+\beta\mathbf{q})P_{\beta}. \tag{29}$$

The matrix $g_{\mathbf{q}}(\mathbf{p})=(g_0(\mathbf{p})+\vec{g}(\mathbf{p})\vec{\sigma})\sigma_2$ is conveniently expressed in terms of the diagonal matrices $g_{\parallel}(\mathbf{p})$ and $g_{\perp}(\mathbf{p})$:

$$g_{\mathbf{q}}(\mathbf{p})=g_{\parallel}(\mathbf{p})\sigma_2+g_{\perp}(\mathbf{p}), \tag{30}$$

where

$$\begin{aligned}g_{\parallel}(\mathbf{p})&\equiv g_0(\mathbf{p})+g_3(\mathbf{p})\sigma_3,\\ g_{\perp}(\mathbf{p})&\equiv g_2(\mathbf{p})+ig_1(\mathbf{p})\sigma_3.\end{aligned} \tag{31}$$

The matrix $\Delta_{\mathbf{q}}(\mathbf{p})=(\Delta_0(\mathbf{p})+\vec{\Delta}(\mathbf{p})\vec{\sigma})\sigma_2$ can also be represented in the form

$$\Delta_{\mathbf{q}}(\mathbf{p})=\Delta_{\|}(\mathbf{p})\sigma_2+\Delta_{\perp}(\mathbf{p}), \tag{32}$$

where

$$\begin{aligned}\Delta_{\|}(\mathbf{p}) &\equiv \Delta_0(\mathbf{p})+\Delta_3(\mathbf{p})\sigma_3,\\ \Delta_{\perp}(\mathbf{p}) &\equiv \Delta_2(\mathbf{p})+i\Delta_1(\mathbf{p})\sigma_3.\end{aligned} \tag{33}$$

In an analogous way the matrices $f_{\mathbf{q}}(\mathbf{p})=f_0(\mathbf{p})+\vec{f}(\mathbf{p})\vec{\sigma}$ and $\varepsilon_{\mathbf{q}}(\mathbf{p})=\varepsilon_0(\mathbf{p})+\vec{\varepsilon}(\mathbf{p})\vec{\sigma}$ are represented as

$$f_{\mathbf{q}}(\mathbf{p})=f_{\|}(\mathbf{p})+f_{\perp}(\mathbf{p})\sigma_2,\ \ \varepsilon_{\mathbf{q}}(\mathbf{p})=\varepsilon_{\|}(\mathbf{p})+\varepsilon_{\perp}(\mathbf{p})\sigma_2,$$

where the diagonal matrices $f_{\|}$, $f_{\perp}$, $\varepsilon_{\|}$, and $\varepsilon_{\perp}$ are given by the formulas

$$f_{\|}(\mathbf{p})=f_0(\mathbf{p})+f_3(\mathbf{p})\sigma_3,\ \ f_{\perp}(\mathbf{p})=f_2(\mathbf{p})+if_1(\mathbf{p})\sigma_3,$$

$$\varepsilon_{\|}(\mathbf{p})=\varepsilon_0(\mathbf{p})+\varepsilon_3(\mathbf{p})\sigma_3,\ \ \varepsilon_{\perp}(\mathbf{p})=\varepsilon_2(\mathbf{p})+i\varepsilon_1(\mathbf{p})\sigma_3.$$

According to (13), $\varepsilon^0_{\mathbf{q}}(\mathbf{p})$ is equal to

$$\varepsilon^0_{\mathbf{q}}(\mathbf{p})=\frac{(\mathbf{p}+\mathbf{q}\sigma_3)^2}{2m}=\varepsilon_0(\mathbf{p})+\varepsilon_3(\mathbf{p})\sigma_3, \tag{34}$$

where

$$\varepsilon_0(\mathbf{p})=\frac{\mathbf{p}^2+\mathbf{q}^2}{2m},\varepsilon_3(\mathbf{p})=\frac{\mathbf{p}\cdot\mathbf{q}}{m}.$$

Using these designations, we transform Eq. (15) to

$$\begin{aligned}\Delta^{\alpha}_{\|}(\mathbf{p})=\sum_{\mathbf{p}'}\{&[v_0(\mathbf{p}+\alpha\mathbf{q},\mathbf{p}'+\alpha\mathbf{q})-v_1(\mathbf{p}+\alpha\mathbf{q},\mathbf{p}'\\ &+\alpha\mathbf{q})]g^{\alpha}_{\|}(\mathbf{p}')-2v_1(\mathbf{p}+\alpha\mathbf{q},\mathbf{p}'\\ &-\alpha\mathbf{q})g^{-\alpha}_{\|}(\mathbf{p}')\},\end{aligned} \tag{35}$$

$$\Delta^{\alpha}_{\perp}(\mathbf{p})=\sum_{\mathbf{p}'}[v_0(\mathbf{p},\mathbf{p}')+v_1(\mathbf{p},\mathbf{p}')]g^{\alpha}_{\perp}(\mathbf{p}'). \tag{36}$$

Here

$$\Delta^{\alpha}_{\|}(\mathbf{p})\equiv\Delta_0(\mathbf{p})+\alpha\Delta_3(\mathbf{p}),\ \ g^{\alpha}_{\|}(\mathbf{p})\equiv g_0(\mathbf{p})+\alpha g_3(\mathbf{p}),$$

$$\Delta^{\alpha}_{\perp}(\mathbf{p})\equiv\Delta_2(\mathbf{p})+i\alpha\Delta_1(\mathbf{p}),$$

$$g^{\alpha}_{\perp}(\mathbf{p})\equiv g_2(\mathbf{p})+i\alpha g_1(\mathbf{p}).$$

In the general case Eqs. (35), (36) comprise a coupled system of equations for determining the four order parameters $\Delta_0(\mathbf{p})$ and $\vec{\Delta}(\mathbf{p})$ (or $\Delta_{\|}(\mathbf{p})$ and $\Delta_{\perp}(\mathbf{p})$), since $g_{\|}(\mathbf{p})$ and $g_{\perp}(\mathbf{p})$ depend on these four order parameters.

For $\mathbf{q}=0$ these equations go over to common equations for the order parameters $\Delta_{\mathbf{q}}(\mathbf{p})=(\Delta_0(\mathbf{p})+\vec{\Delta}(\mathbf{p})\vec{\sigma})\sigma_2$, which correspond to a superposition of a singlet and a triplet pairing ($\vec{\Delta}\neq 0$).[9]

We note that it follows from the definitions (33) that $g_{\perp}$ and $\Delta_{\perp}$ are odd with respect to momenta and describe a triplet state with $S=1$, $S_z=\pm 1$, while the functions $g_{\|}$ and $\Delta_{\|}$ describe a superposition of a singlet ($S=0$) and a triplet ($S=1$) state with $S_z=0$, and they therefore do not have a definite parity with respect to the momenta $\mathbf{p}$.

4. DIAGONALIZATION

We express the normal and anomalous "uniform" distribution functions $f_{\mathbf{q}}$ and $g_{\mathbf{q}}$ in terms of the four order parameters Δ_0 and $\vec{\Delta}$ (or $\Delta_{\|}$ and $\Delta_{\perp}$). With this goal we turn to a procedure developed in Ref. 6 for block diagonalization of the self-consistency equation (4).

The matrix $\hat{\xi}=\left(\begin{smallmatrix}\xi & \Delta\\ \Delta^{\dagger} & -\tilde{\xi}\end{smallmatrix}\right)$ is reduced to the block diagonal form $\left(\begin{smallmatrix}\xi' & 0\\ 0 & -\tilde{\xi}'\end{smallmatrix}\right)$ by means of the Bogolyubov unitary transformation

$$\hat{\xi}'=\hat{U}^{\dagger}\hat{\xi}\hat{U}=\begin{pmatrix}\xi' & 0\\ 0 & -\tilde{\xi}'\end{pmatrix}, \tag{37}$$

where the unitary operator $\hat{U}$ has the form

$$\hat{U}\equiv\begin{pmatrix}u & v\\ v^* & u^*\end{pmatrix}. \tag{38}$$

The main role in the diagonalization process is played by the matrix X relating the blocks v and u by the formula $v=Xu^*$. This matrix satisfies the equation

$$X\Delta^{\dagger}X-\xi X+X\tilde{\xi}-\Delta=0,\ \xi=\varepsilon-\mu. \tag{39}$$

After solving this nonlinear matrix equation, one can determine the spatially uniform normal and anomalous matrix distribution functions by means of the formulas

$$f=Kn+X(1-\tilde{n})X^{\dagger}K, \tag{40}$$

$$g=K(1-n)X-X\tilde{n}_{-\mathbf{p}}\tilde{K}_{-\mathbf{p}}, \tag{41}$$

where

$$K=(1+XX^{\dagger})^{-1},\quad n=\left[\exp\left(\frac{\xi-X\Delta^{\dagger}}{T}\right)+1\right]^{-1}. \tag{42}$$

The eigenvalues of the matrix $\xi-X\Delta^{\dagger}=\mathscr{E}$ determine the spectrum of elementary fermionic excitations. This spectrum is real, since the matrix $\mathscr{E}$ is Hermitian in the positive-definite scalar product $\langle\varphi,\psi\rangle=(\varphi,K\psi)$. Indeed, we note in this regard that the following identities hold:

$$(\xi-X\Delta^{\dagger})(1+XX^{\dagger})=(\xi X-X\Delta^{\dagger}X+\Delta)X^{\dagger}+\xi,$$

$$(1+XX^{\dagger})(\xi-\Delta X^{\dagger})=X(\Delta^{\dagger}+X^{\dagger}\xi-X^{\dagger}\Delta X^{\dagger})+\xi.$$

Therefore, by virtue of (42) and the fact that $\xi=\xi^{\dagger}$, we have $K(\xi-X\Delta^{\dagger})=(\xi-\Delta X^{\dagger})K$ or $K\mathscr{E}=\mathscr{E}^{\dagger}K$. In the new scalar product $(\varphi,K\psi)$ (where $(\varphi,\psi)\equiv\varphi^*_{\alpha}\psi_{\alpha}$ is the ordinary scalar product) the operation of Hermitian conjugation is defined in the standard way: $\langle\varphi,A\psi\rangle=\langle A^{\varphi}\varphi,\psi\rangle$, i.e., $A^{\varphi}=K^{-1}A^{\dagger}K$. It follows that in such a scalar product the operator $\mathscr{E}$ is Hermitian, $\mathscr{E}^{\varphi}=\mathscr{E}$, and, consequently, the eigenvalues of $\mathscr{E}$ are real.

Noting that

$$X = (\xi - \mathscr{E})(\Delta^\dagger)^{-1}, \tag{43}$$

we obtain from (39) an equation for $\mathscr{E}$:

$$\mathscr{E}^2 + 2\mathscr{E}\vec{b}\vec{\sigma} = \mathscr{E}_0^2, \tag{44}$$

where

$$2\vec{b}\vec{\sigma} = \xi_3\sigma_3 - (\Delta^\dagger)^{-1}\xi_3\sigma_3\,\Delta^\dagger,$$
$$\mathscr{E}_0^2 = \xi^2 - 2\xi\vec{b}\vec{\sigma} + \Delta\Delta^\dagger. \tag{45}$$

Writing the matrix $\mathscr{E}$ in the form

$$\mathscr{E} \equiv \zeta + \vec{y}\vec{\sigma}, \tag{46}$$

we obtain from equation (44) after some transformations a bicubic equation for ζ:

$$\zeta^6 - e_0^2\zeta^4 + (\vec{b}^2 e_0^2 + \vec{e}^2 - \vec{b}^2\vec{b}^2)\zeta^2 - (\vec{e}\vec{b})^2 = 0 \tag{47}$$

and a linear algebraic equation for the vector $\vec{y}$, the solution of which has the form

$$\vec{y} = \frac{1}{\zeta^2 - \vec{b}^2}\left(\zeta\vec{e} - i[\vec{e},\vec{b}] - \vec{b}\,\frac{\vec{e}\vec{b}}{\zeta}\right) - \vec{b}. \tag{48}$$

It follows from formulas (43) and (45) that

$$e_0^2 = \xi_0^2 + \vec{\xi}^2 + \Delta_0\Delta_0^* + \vec{\Delta}\vec{\Delta}^*, \tag{49}$$

$$\vec{e} = \xi_0(\vec{\xi} - \vec{b}) - i[\vec{\xi},\vec{b}] + \frac{1}{2}(\Delta_0\vec{\Delta}^* + \Delta_0^*\vec{\Delta} + i[\vec{\Delta}\vec{\Delta}^*]), \tag{50}$$

$$\vec{b} = \frac{1}{D^*}(i\Delta_0^*[\vec{\xi},\vec{\Delta}^*] - (\vec{\Delta}\vec{\xi})\vec{\Delta}^* + \xi\vec{\Delta}^*\vec{\Delta}^*). \tag{51}$$

The quantity D^* in these formulas is equal to $\vec{\Delta}^*\vec{\Delta}^* - \Delta_0^*\Delta_0^*$.

From these formulas and the definition (46) we obtain the following expression for the spectrum of elementary excitations (the eigenvalues of the matrix $\mathscr{E}$):

$$\mathscr{E}_\pm = \zeta \pm |\vec{y}|, \qquad |\vec{y}| = \sqrt{e_0^2 - \zeta^2 - 2(\vec{e}\vec{b}/\zeta)}. \tag{52}$$

Thus formulas (49)–(51) determine the spectrum of elementary fermionic excitations (52) in terms of the initial quantities ξ and Δ and the solution ζ of the bicubic equation (47).

As a result of solution of the equation for ζ^2, the quantity X is determined by the formulas

$$X = (X_0 + \vec{X}\vec{\sigma})\sigma_2 \equiv X_\parallel\sigma_2 + X_\perp, \tag{53}$$

$$X_0 = \frac{1}{D^*}\{(\vec{y} + \vec{\xi},\vec{\Delta}^*) - (\zeta + \xi_0)\Delta_0^*\}, \tag{54}$$

$$\vec{X} = \frac{1}{D^*}\{i[\vec{y} + \vec{\xi},\vec{\Delta}^*] + \vec{\Delta}^*(\zeta + \xi_0) - \Delta_0^*(\vec{y} + \vec{\xi})\}. \tag{55}$$

Further, using formulas (40) and (41) we can, in principle, find explicit expressions for $f_\mathbf{q}$ and $g_\mathbf{q}$ in terms of ξ and Δ. Substituting the expression for g into formulas (35) and (36), we obtain an equation that determines the order parameter Δ.

We note here that formulas (53)–(55) and (47) give a concrete solution of the quadratic matrix equation $X^2 - 2pX + q = 0$ and generalize the well-known Sylvester formula.[10]

However, for solution of this problem when Δ_0 and $\Delta_1, \Delta_2, \Delta_3 \neq 0$, we run up against some rather awkward algebraic expressions and formulas. Therefore, in this paper we restrict consideration to two particular cases, when in the representation $\Delta = \Delta_\parallel\sigma_2 + \Delta_\perp$ one of two variants is realized: $\Delta_\parallel = 0$, $\Delta_\perp \neq 0$ or $\Delta_\parallel \neq 0$, $\Delta_\perp = 0$.

5. ANALYSIS OF THE SOLUTION OF THE SELF-CONSISTENCY EQUATIONS FOR SUPERFLUID SPIRAL ORDERING

In both variants Eq. (47) for ζ reduces to a biquadratic equation. Since we are interested not only in the roots of equation (47) but also in the whole matrix X and the distribution functions f and g, we note that in these particular cases the matrices $\Delta_\perp$ for $\Delta_\parallel = 0$ or $\Delta_\parallel$ for $\Delta_\perp = 0$ are diagonal, and therefore it is simpler to start directly from Eq. (39) for X, in which only diagonal matrices appear as unknown coefficients.

Consider the case $\Delta_\parallel = 0$, when the solution of equation (39) for X has the form

$$X = X_\perp = \frac{\xi_0 + \alpha E_\perp}{\Delta_\perp^\dagger}, \tag{56}$$

where $\alpha = \pm 1$, $\xi_0 = [\mathbf{p}^2 + \mathbf{q}^2/2m] - \mu$, $E_\perp \equiv \sqrt{\xi_0^2 + \Delta_\perp\Delta_\perp^\dagger}$.

The spatially uniform normal and anomalous distribution functions then have the form

$$g_\mathbf{q} = g_\perp = -\frac{\Delta_\perp}{2E_\perp}[1 - n(E_\perp - \xi_3) - n(E_\perp + \xi_3)],$$
$$g_\parallel = 0; \tag{57}$$

$$f_\mathbf{q} = f_\parallel = \frac{1}{2}\left\{1 + n(E_\perp + \xi_3) - n(E_\perp - \xi_3) - \frac{\xi_0}{E_\perp}[1 - n(E_\perp + \xi_3) - n(E_\perp - \xi_3)]\right\}, \quad f_\perp = 0, \tag{58}$$

where

$$n(A) \equiv [\exp(A/T) + 1]^{-1}. \tag{59}$$

In the case $\Delta_\perp = 0$ we have

$$X = X_\parallel = \frac{\xi + \alpha E_\parallel}{\Delta_\parallel} \quad (\alpha = \pm 1), \tag{60}$$

$$E_\parallel \equiv \sqrt{\xi^2 + |\Delta_\parallel|^2}, \tag{61}$$

and

$$g_{\mathbf{q}} = -\frac{\Delta_\parallel}{2E_\parallel}[1 - 2n(E_\parallel)]\sigma_2 = g_\parallel \sigma_2, \quad g_\perp = 0, \tag{62}$$

$$f_{\mathbf{q}} = f_\parallel = \frac{1}{2}\left\{1 - \frac{\xi}{E_\parallel}[1 - 2n(E_\parallel)]\right\}, \quad f_\perp = 0. \tag{63}$$

Using these formulas and equations (36), we obtain the following self-consistency equation for determining $\Delta_\perp$ in the case $\Delta_\parallel = 0$:

$$\Delta_\perp(\mathbf{p}) = -\frac{1}{4V}\sum_{\mathbf{p}'} \Psi(\mathbf{p},\mathbf{p}')\frac{\Delta_\perp(\mathbf{p}')}{E_\perp(\mathbf{p}')}\left\{\tanh\frac{\beta}{2}\left[E_\perp(\mathbf{p}') + \frac{\mathbf{p}'\cdot\mathbf{q}}{m}\right] + \tanh\frac{\beta}{2}\left[E_\perp(\mathbf{p}') - \frac{\mathbf{p}'\cdot\mathbf{q}}{m}\right]\right\}, \tag{64}$$

where

$$\Psi(\mathbf{p},\mathbf{p}') \equiv v_0(\mathbf{p},\mathbf{p}') + v_1(\mathbf{p},\mathbf{p}'). \tag{65}$$

In an analogous way in the case $\Delta_\perp = 0$ we have

$$\Delta_\parallel^\alpha(\mathbf{p}) = -\frac{1}{2V}\sum_{\mathbf{p}'}\left\{[v_0(\mathbf{p}+\alpha\mathbf{q},\mathbf{p}'+\alpha\mathbf{q}) - v_1(\mathbf{p}+\alpha\mathbf{q},\mathbf{p}'+\alpha\mathbf{q})]\frac{\Delta_\parallel^\alpha(\mathbf{p}')}{E_\parallel^\alpha(\mathbf{p}')}\tanh\frac{E_\parallel^\alpha(\mathbf{p}')}{2T} - 2v_1(\mathbf{p}+\alpha\mathbf{q},\mathbf{p}'-\alpha\mathbf{q})\frac{\Delta_\parallel^{-\alpha}(\mathbf{p}')}{E_\parallel^{-\alpha}(\mathbf{p}')}\tanh\frac{E_\parallel^{-\alpha}(\mathbf{p}')}{2T}\right\}. \tag{66}$$

It follows from this equation that its solution reduces to the BCS equation for a superposition of a singlet and a triplet order parameter if $S_z = 0$. We shall therefore not consider it further but instead turn to an analysis of Eq. (64) for $\Delta_\perp$, which corresponds only to triplet pairing with $S = 1$ and $l = 1$ and a superposition of wave functions of Cooper pairs with $S_z = 1$ and $S_z = -1$. In this case $\Delta = \Delta_2 + i\Delta_1\sigma_3 = (\Delta_2\sigma_2 + \Delta_1\sigma_1)\sigma_2$.

By virtue of the definition of the function $\Psi(\mathbf{p}_1,\mathbf{p}_2)$, it should be antisymmetric with respect to both its arguments $\mathbf{p}_1$ and $\mathbf{p}_2$. Therefore, the expansion of the function $\Psi(\mathbf{p}_1,\mathbf{p}_2)$ in Legendre polynomials $P_l(\cos\widehat{\mathbf{p}_1\mathbf{p}_2})$ will contain only odd polynomials. For simplicity we consider only the first Legendre polynomial in the expansion. Thus, we shall assume that

$$\Psi(\mathbf{p}_1,\mathbf{p}_2) = V(p_1,p_2)\cos\theta, \theta = \widehat{\mathbf{p}_1\cdot\mathbf{p}_2}.$$

In this case

$$\Delta_\perp(\mathbf{p}) \equiv \Delta_\perp(p)\cos\theta, \quad \theta = \widehat{\mathbf{p}\cdot\mathbf{q}}. \tag{67}$$

Furthermore, we shall assume that $V(p_1,p_2)$ is nonzero in a narrow energy layer with respect to the arguments p_1 and p_2 (as is assumed in the BCS theory):

$$V(p_1,p_2) = -V\begin{cases} 1, & \left|\frac{p_1^2}{2m} - \mu\right| \leqslant \Theta, \quad \left|\frac{p_2^2}{2m} - \mu\right| \leqslant \Theta \\ 0 & \text{otherwise} \end{cases} \tag{68}$$

Here 2Θ is the width of the energy layer near the Fermi surface. In this case $\Delta_\perp(p) = 0$ if p lies outside the narrow energy layer and $\Delta_\perp(p) = \text{const}$ if p lies inside that layer. Thus equation (64) becomes

$$1 = \frac{v}{8}\int_{-1}^{1} dx\, x^2 \int_{-\vartheta}^{\vartheta} \frac{d\xi(1+\xi)^{3/2}}{\sqrt{(\xi+\underline{q}^2)^2 + \delta^2 x^2(1+\xi)}} \times[\tanh u^+ + \tanh u^-], \tag{69}$$

where

$$u^\pm \equiv \frac{1}{2t}[\sqrt{(\xi+\underline{q}^2)^2 + \delta^2x^2(1+\xi)} \pm 2\underline{q}x\sqrt{1+\xi}].$$

The dimensionless parameters δ, $\underline{q}$, and t are related to $\Delta_\perp$, q, and T by the formulas

$$\delta \equiv \frac{\Delta_\perp}{\varepsilon_f}, \quad t \equiv \frac{T}{\varepsilon_f}, \quad \underline{q} \equiv \frac{q}{p_f}. \tag{70}$$

The dimensionless energies characterizing the interaction potential are expressed by the formulas

$$v = -\frac{k_f^3}{4\pi^2\varepsilon_f}V(p_f,p_f), \quad \vartheta = \frac{\Theta}{\varepsilon_f},$$

and the dimensionless integration parameters ξ and x are given by

$$\xi = \frac{1}{\varepsilon_f}\left(\frac{p^2}{2m} - \mu\right), \quad x = \cos\widehat{\mathbf{p}\cdot\mathbf{q}}.$$

In solving Eq. (69) we shall assume that $v \ll 1$. Then $\delta \ll 1$, $t_c \ll 1$. The layer width ϑ is taken such that $\delta \ll \vartheta$, $t_c \ll \vartheta$, and $\underline{q} \ll \vartheta$. In that case we can assume $1 + \xi \approx 1$ and $\xi + \underline{q}^2 \approx \xi$. Then Eq. (69) becomes

$$1 = \frac{v}{2}\int_0^1 dx\, x^2 \int_0^\vartheta \frac{d\xi}{\sqrt{\xi^2+\delta^2x^2}}\left[\tanh\frac{1}{2t}(\sqrt{\xi^2+\delta^2x^2} + 2\underline{q}x) + \tanh\frac{1}{2t}(\sqrt{\xi^2+\delta^2x^2} - 2\underline{q}x)\right]. \tag{71}$$

In the limiting cases $\delta = 0$ or $t = 0$ this equation can be simplified substantially.

Let us find the transition temperature t_c of the spirally ordered state as a function of the spiral parameter $\underline{q}$. This temperature is determined by Eq. (71) with $\delta = 0$:

$$1 = \frac{v}{2}\int_0^1 dx\, x^2 \int_0^\vartheta \frac{d\xi}{\xi}\left\{\tanh\frac{1}{2t}(\xi + 2\underline{q}x) + \tanh\frac{1}{2t}(\xi - 2\underline{q}x)\right\}. \tag{72}$$

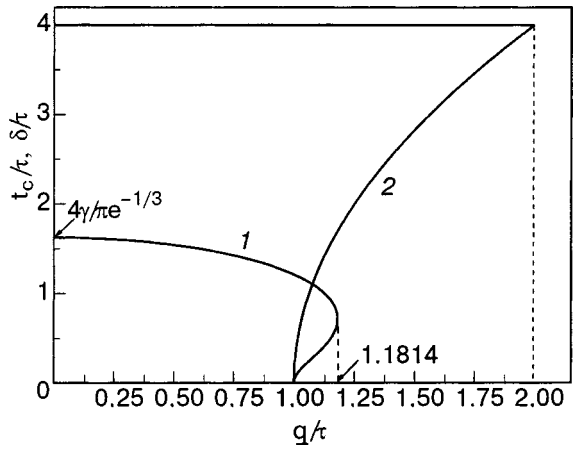

FIG. 1. Transition temperature t_c (*1*) and order parameter δ (*2*) at $T=0$ versus the spiral parameter.

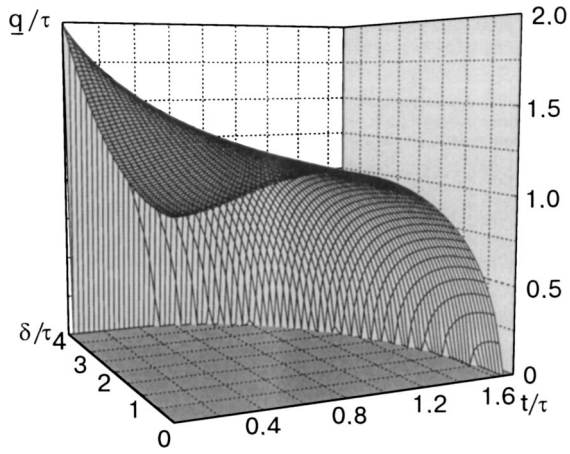

FIG. 2. Spiral parameter q as a function of the temperature t and order parameter δ.

Integrating over ξ using integration by parts and then evaluating the integral over x, we obtain the following equation in the logarithmic approximation ($\vartheta/tc \gg 1$):

$$2\ln\frac{t_c}{\tau}-\frac{\pi^2}{6a^2}+\int_{-\infty}^{\infty}\frac{ds}{\cosh^2 s}\left(1+\frac{s^3}{a^3}\right)\ln|a+s|=0, \quad (73)$$

where $a\equiv q/t_c$ and we have introduced the parameter τ:

$$\tau\equiv\frac{\vartheta}{2}\exp\left(\frac{1}{3}-\frac{3}{v}\right). \quad (74)$$

For $q=0$ we have $t_c=4\tau\gamma\exp(-1/3)/\pi$, where $\gamma=\exp(0.577\ldots)$ is the Euler constant.

For $q=\tau$ the transition temperature t_c goes to zero, and in the vicinity of that point it has the asymptotics

$$t_c\approx\frac{1}{\pi}\sqrt{8\tau(q-\tau)}. \quad (75)$$

For $q>\tau$ the function $t_c(q)$ is two-valued, and $q(t_c)$ has a maximum given by the condition

$$\int_{-\infty}^{\infty}\frac{ds\,s^3}{\cosh^2 s}\ln|a-s|+\frac{a\pi^2}{6}=0, \quad (76)$$

from which we get $a\approx 1.644$ and $q\approx 1.181\tau$. The dependence of the transition temperature t_c on q is shown in Fig. 1.

We now determine the dependence of δ on the spiral vector q at $t=0$. According to Eq. (71), we have

$$1=v\int_0^{\vartheta}d\xi\int_0^1\frac{dx\,x^2}{\sqrt{\xi^2+\delta^2x^2}}\Theta\left(\sqrt{\xi^2+\delta^2x^2}-2qx\right), \quad (77)$$

where $\Theta(x)$ is the Heaviside step function. This equation has two solutions. The first satisfies the condition $\delta>2q$, and the second satisfies $\delta<2q$. For $\delta>2q$ we have $\delta=4\tau$ or $\delta=2\vartheta\exp(1/3-3/v)$. This is the formula of BCS theory for triplet pairing. For $\delta<2q$ we have

$$\delta=4\sqrt{\tau(q-\tau)}. \quad (78)$$

In the region $\tau<q<2\tau$ we have a double-valued behavior of the gap as a function of the spiral vector. A graph of the curve $\delta(q)$ at $t=0$ is shown in Fig. 1 in the same scale as $t_c(q)$.

The general solution of equation (71) is obtained by numerical methods and is shown in Fig. 2. It is seen from this graph that $q=2\tau$ is the maximum possible value of the spiral parameter, which is reached at $t=0$ and $\delta=4\tau$. Thus for $q>2\tau$ the spiral superfluid state does not exist. Figure 3 shows sections of solution (71) by planes with different values of q.

6. CORRELATION OF SPINS

The matrix distribution functions f and g determine the various physical quantities in a state of statistical equilibrium. For example, it follows from the formulas for f that the mean value of the spin in the case $\Delta_{\|}=0$ is constant:

$$\langle\sigma_m\rangle=\delta_{3m}\langle\sigma_3\rangle,\quad \langle\sigma_3\rangle=\mathrm{Tr}\,f_{\|}\sigma_3=\frac{1}{V}\sum_{\mathbf{p}}f_3(\mathbf{p}). \quad (79)$$

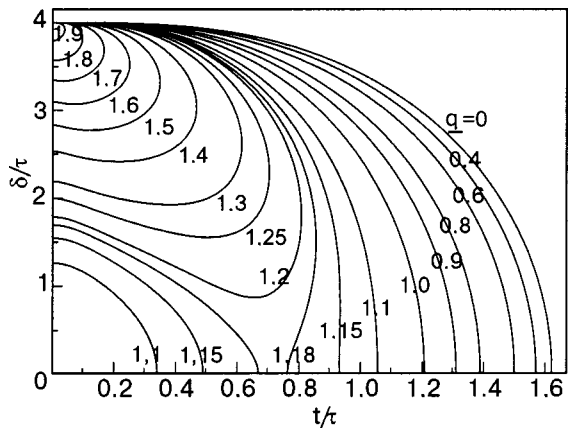

FIG. 3. Order parameter versus temperature for different values of the spiral parameter q.

In this connection let us determine the correlation of the spins $\hat{\sigma}^m(\mathbf{x}) \equiv \psi^\dagger_\alpha(\mathbf{x})\hat{\sigma}^m_{\alpha\beta}\psi_\beta(\mathbf{x})$ in a superfluid Fermi liquid with spiral ordering. Since

$$\psi_\alpha(\mathbf{x}) \equiv \frac{1}{\sqrt{V}}\sum_{\mathbf{p}} \exp(i\mathbf{p}\cdot\mathbf{x})a_{\alpha\mathbf{p}},$$

we have

$$\begin{aligned}\langle \hat{\sigma}_m(\mathbf{x})\hat{\sigma}_n(\mathbf{y})\rangle = \frac{1}{V^2}\sum_{\mathbf{p}_1,\ldots,\mathbf{p}_4} \{&\mathrm{tr}\sigma_m f_{\mathbf{p}_2\mathbf{p}_1}\cdot \mathrm{tr}\sigma_n f_{\mathbf{p}_4\mathbf{p}_3} \\ &+ \mathrm{tr}\sigma_m(\delta_{\mathbf{p}_2\mathbf{p}_3} - f_{\mathbf{p}_2\mathbf{p}_3})\sigma_n f_{\mathbf{p}_4\mathbf{p}_1} \\ &- \mathrm{tr}\sigma_m \vec{g}_{\mathbf{p}_4\mathbf{p}_2}\tilde{\sigma}_n g^\dagger_{\mathbf{p}_3\mathbf{p}_1}\}\exp i[\mathbf{x}\cdot(\mathbf{p}_2-\mathbf{p}_1) \\ &+ \mathbf{y}\cdot(\mathbf{p}_4-\mathbf{p}_3)].\end{aligned}$$

Here the transposition is done only in spin space. Hence we obtain the desired formula:

$$\begin{aligned}\langle \hat{\sigma}_m(\mathbf{x})\hat{\sigma}_n(\mathbf{y})\rangle - \langle\sigma_3\rangle^2\delta_{3m}\delta_{3n} = &\sum_{\beta=\pm1}(\delta_{mn} + i\beta\varepsilon_{mn3}) \\ &\times f^\beta_{\|}(0)\delta(\mathbf{r}) + \frac{1}{V^2}\sum_{\alpha,\beta=\pm1} T(m,\alpha,n,\beta)\{-f^\alpha_{\|}(\mathbf{r})f^\beta_{\|}(-\mathbf{r}) \\ &\times \exp[i(\alpha-\beta)\mathbf{r}\cdot\mathbf{q}] + (2\delta_{2n}-1)g^\alpha_\perp(-\mathbf{r})g^{*\beta}_\perp(-\mathbf{r}) \\ &\times \exp[-i(\alpha+\beta)\mathbf{r}\cdot\mathbf{q}]\exp[i(\alpha-\beta)(2\mathbf{R}-\mathbf{r})\cdot\mathbf{q}]\},\end{aligned} \tag{80}$$

where $\mathbf{r}\equiv\mathbf{x}-\mathbf{y}$, $\mathbf{R}\equiv(\mathbf{x}+\mathbf{y})/2$,

$$f^\pm_{\|}(\mathbf{r}) \equiv \sum_{\mathbf{p}} f^\pm_{\|}(\mathbf{p})e^{i\mathbf{p}\cdot\mathbf{r}}, \quad g^\pm_\perp(\mathbf{r}) \equiv \sum_{\mathbf{p}} g^\pm_\perp(\mathbf{p})e^{i\mathbf{p}\cdot\mathbf{r}}, \tag{81}$$

$$f^\alpha_{\|}(\mathbf{p}) \equiv f_0(\mathbf{p}) + \alpha f_3(\mathbf{p}), \quad g^\alpha_\perp(\mathbf{p}) \equiv g_2(\mathbf{p}) + i\alpha g_1(\mathbf{p}) \tag{82}$$

and

$$\begin{aligned}T(m,\alpha,n,\beta) &\equiv \mathrm{tr}\ \sigma_m P_\alpha \sigma_n P_\beta \\ &= \frac{1}{2}[\delta_{mn}(1-\alpha\beta+2\alpha\beta\delta_{3m}) - i(\alpha-\beta)\varepsilon_{mn3}].\end{aligned} \tag{83}$$

As we see, in this case the spiral ordering is manifested in the circumstance that the correlation functions $\langle\sigma_m(\mathbf{x})\sigma_n(\mathbf{y})\rangle - \langle\sigma_3\rangle^2\delta_{3m}\delta_{3n}$ are periodic functions of the variable $(\mathbf{x}+\mathbf{y})/2$. By virtue of the principle of spatial decay of correlations the correlation functions of the spins with respect to the variable $\mathbf{x}-\mathbf{y}$ tend toward zero. Therefore the spiral ordering is manifested directly only in the correlation function of the spins.

We note in conclusion that superfluid liquids of the ^{3}He type, with a tensor order parameter, admit the existence of a large number of diverse phase states, many of which have not yet been found.[8] Nonuniform spiral states of superfluid phases can be encountered in the study of crystals with overlapping energy bands and also in the study of heavy nuclei (nuclear matter) and astrophysical objects such as neutron stars.

The spin spiral ordering studied here arises simultaneously with superfluid ordering and constitutes a state of an antiferromagnetic type in which the spatial nonuniformity is manifested in the anomalous distribution function and in the spin correlation function, which can be measured experimentally. Although such a nonuniform spiral superfluid state has not been found, it is of interest as an object of study in both low-temperature physics and in the physics of ultradense states of matter.

*E-mail: spelet@kipt.kharkov.ua

[1] A. I. Akhiezer and I. Ya. Pomeranchuk, Zh. Éksp. Teor. Fiz. **36**, 859 (1959) [Sov. Phys. JETP **9**, 605 (1959)].
[2] Yu. A. Izyumov and Yu. N. Skryabin, Fiz. Met. Metalloved. **49**, 903 (1980).
[3] Yu. A. Izumov and V. M. Laptev, Int. J. Mod. Phys. B **5**, 563 (1991).
[4] M. Tachiki, A. Kotani, H. Matsumoto, and H. Umezawa, Solid State Commun. **31**, 927 (1979).
[5] K. H. Mueller and V. N. Narozhnyi, Rep. Prog. Phys. **64**, 943 (2001).
[6] A. I. Akhiezer, V. V. Krasil'nikov, S. V. Peletminskii, and A. A. Yatsenko, Phys. Rep. **245**, 1 (1994).
[7] B. I. Barts, Yu. A. Bolotin, E. V. Inopin, and V. Yu. Gonchar, *Hartree–Fock Method in the Theory of the Nucleus* [in Russian], Naukova Dumka, Kiev (1982).
[8] M. Yu. Kovalevskii, S. V. Peletminsky, and N. N. Chekanova, Fiz. Nizk. Temp. **28**, 327 (2002) [Low Temp. Phys. **28**, 227 (2002)].
[9] A. I. Akhiezer, A. A. Isaev, S. V. Peletminsky, and A. A. Yatsenko, Teor. Mat. Fiz. **118**, 459 (1998).
[10] R. Bellman, *Introduction to Matrix Analysis*, McGraw-Hill, New York (1960), Nauka, Moscow (1969).

Translated by Steve Torstveit

Variational approach to the problem of the energy spectrum of surface electrons over a liquid helium film

S. S. Sokolov*

B. Verkin Institute for Low Temperature Physics and Engineering of the National Academy of Sciences of Ukraine, 47 Lenin Ave., Kharkov 61103, Ukraine
(Submitted July 25, 2003)
Fiz. Nizk. Temp. **30**, 271–275 (March 2004)

The energies of the first two subbands are calculated, within a variational approach, for electrons localized over the surface of a liquid helium film covering a solid substrate. The results are obtained for arbitrary value of the dielectric constant of the solid substrate, covering both the limit of a substrate with a dielectric constant close to unity (such as a rare gas solid) and a metal. The results for the subband energies in the case of a metallic substrate are compared with those obtained previously by a different method by Gabovich, Ilchenko, and Pashitskiĭ. The agreement is rather good, supporting the applicability of the variational method for calculating the energy spectrum of surface electrons in a wide range of substrate parameters. © *2004 American Institute of Physics.* [DOI: 10.1063/1.1645177]

1. INTRODUCTION

The properties of surface electrons (SE) localized over a liquid helium film are substantially more complicated than those over bulk helium. As is known, the potential energy of SE in the point z over bulk liquid occupying the semispace with $z \leqslant 0$ can be written as[1]

$$U_b(z) = -\frac{\Lambda_0}{z+z_0} + eE_\perp z \tag{1}$$

where $\Lambda_0 = e^2(\varepsilon_{\mathrm{He}}-1)/[4(\varepsilon_{\mathrm{He}}+1)]$, $E_\perp$ is the holding electric field oriented normally to helium surface, e is the electron charge, and $\varepsilon_{\mathrm{He}} \simeq 1.0572$ is the dielectric constant of liquid helium. The parameter $z_0 \simeq 1.01$ Å is introduced in Eq. (1) to take into account the finiteness of the potential barrier $V_0 \simeq 1$ eV on the liquid helium surface, which is an obstacle to electron penetration inside the liquid phase, and to avoid divergence of the first term of Eq. (1) at $z \to 0$. The value of z_0 is estimated by comparison of the experimental data on the frequencies of spectroscopic transitions between the SE surface states and theoretical calculation based on Eq. (1) in the limit of small holding field. One should note that in the limit $V_0 \to \infty$ ($z_0 = 0$) one obtains a SE energy spectrum very close to that really observed,[2] and for that reason this limit is widely used in calculations. The applicability of the limit $V_0 \to \infty$ is based on the strong inequality $|\Delta_l| \ll V_0$, where Δ_l is the energy of SE states numbered by $l = 1,2,\ldots$. For a liquid helium film located at $-d < z < 0$ over a solid substrate with dielectric constant ε_s the SE potential energy can be written as[3]

$$U_f(z) = U_b(z) + U_s(z), \tag{2}$$

where

$$U_s(z) = -\Lambda_1 \sum_{n=1}^{\infty} \frac{(-a)^{n-1}}{z+nd},$$

$\Lambda_1 = e^2\varepsilon_{\mathrm{He}}(\varepsilon_s - \varepsilon_{\mathrm{He}})/[(\varepsilon_{\mathrm{He}}+1)^2(\varepsilon_s+\varepsilon_{\mathrm{He}})]$, and $a = (\varepsilon_{\mathrm{He}}-1)(\varepsilon_s-\varepsilon_{\mathrm{He}})/[(\varepsilon_{\mathrm{He}}+1)(\varepsilon_s+\varepsilon_{\mathrm{He}})]$. Because of the small difference between $\varepsilon_{\mathrm{He}}$ and unity one can disregard, in the sum of $U_s(z)$, the terms with $n \geqslant 2$ and write, to a very good accuracy, $U_s(z) = \Lambda_1/(z+d)$.

The additional contribution $U_s(z)$ to the equation for the SE potential energy, in comparison with that over the bulk liquid, is connected with the polarization interaction between the SEs and image forces in the solid substrate at $z < -d$. This energy influences strongly the properties of SEs over film changing not only the structure of the SE energy states, which were first considered by Shikin and Monarkha,[3] but also the Hamiltonian of electron–ripplon scattering, which determines the kinetic properties of the SEs under their motion in the plane of the vapor–liquid phase boundary.[3] Furthermore, one more scattering mechanism by substrate surface defects can appear which contributes to the SE transport properties.[4]

The role of $U_s(z)$ is especially well pronounced for substrates with $\varepsilon_s \gg 1$, such as, for example, some types of glass, where $\varepsilon_s \gtrsim 7$, to say nothing of metals, where $\varepsilon_s \to \infty$. For a metallic substrate one has $\Lambda_1 = e^2\varepsilon_{\mathrm{He}}/(\varepsilon_{\mathrm{He}}+1)^2 \simeq e^2/4$, and the contribution of $U_s(z)$ dominates in $U_f(z)$ of Eq. (2). The Schrödinger equation for the SE wave functions and energy spectrum has been solved, in that approximation, by Gabovich, Ilchenko, and Pashitskiĭ,[5] and the final expression for the spectrum at $E_\perp = 0$, in the limit $V_0 \to \infty$, can be written as

$$\Delta_l \simeq -\frac{e^2}{32a_0}\left[l - \frac{3}{4} + \frac{1}{\pi}\sqrt{\frac{2d}{a_0}}\right]^{-2} \tag{3}$$

which differs essentially from the hydrogenlike spectrum $\Delta_l = -\Delta_0/l^2$ of SEs over bulk helium.[3] Here $a_0 = \hbar^2/me^2$ is the Bohr radius, $\Delta_0 = \hbar^2\gamma_0^2/2m$, $\gamma_0 = m\Lambda_0/\hbar^2$, and m is the free electron mass. Equation (3) is valid for $1 \ll (e^2/4\hbar)\sqrt{m/2|\Delta_l|} \ll d/a_0$, which is well satisfied for $d \geqslant 5 \times 10^{-7}$ cm.

For the substrates with relatively small ($\varepsilon_s \gtrsim 1$) or intermediate values of ε_s the contribution of $U_b(z)$ to $U_f(z)$ can be comparable with that of $U_s(z)$. In such a situation the only possible way to estimate analytically the SE spectrum

over a helium film is to apply the variational approach. The aim of the present work is to obtain the variational solution for the energies of two lowest SE subbands $l=1$ and $l=2$. For the sake of generality, the calculation is carried out for a substrate with an arbitrary value of ε_s, and the effect of the holding field is also included. The result for a metallic substrate is obtained under the limiting transition $\varepsilon_s \to \infty$ and is compared with that given by Eq. (3). Such a comparison can make clearer the possibilities of applying the different approaches in the problem of description of the SE spectrum. In view of the rising interest in investigating both quasi-two-dimensional and quasi-one-dimensional SE properties over helium film in recent years, the present study seems timely.[7–13]

2. MAIN RELATIONS

To calculate the energies Δ_1 and Δ_2 one applies the orthonormalized trial wave functions[14,15]

$$f_1(z)=2\gamma_1^{3/2} z \exp(-\gamma_1 z), \tag{4}$$

$$f_2=\frac{2\sqrt{3}\,\gamma_2^{5/2} z}{(\gamma_1^2-\gamma_1\gamma_2+\gamma_2^2)^{1/2}}\left[1-\left(\frac{\gamma_1+\gamma_2}{3}\right)z\right]\exp(-\gamma_2 z), \tag{5}$$

where γ_1 and γ_2 are variational parameters. The energy of the lth subband is calculated as

$$\Delta_l=\left\langle l\left|-\frac{\hbar^2}{2m}\frac{d}{dz}+U_f(z)\right|l\right\rangle.$$

The method of calculation is a generalization of that developed in Ref. 15 for the microstratified liquid solution ^{3}He–^{4}He, and the final expressions for the energies are

$$\Delta_1=\frac{\hbar^2\gamma_1^2}{2m}-\Lambda_0\gamma_1-\Lambda_1\gamma_1[1-2\gamma_1 d - 4(\gamma_1 d)^2\exp(2\gamma_1 d)\mathrm{Ei}(-2\gamma_1 d)]+\frac{3eE_\perp}{2\gamma_1} \tag{6}$$

and

$$\Delta_2=\frac{\hbar^2\gamma_1^2}{6m}\left(\frac{\gamma_1^2-\gamma_1\gamma_2+7\gamma_2^2}{\gamma_1^2-\gamma_1\gamma_2+\gamma_2^2}\right)-\frac{\Lambda_0\gamma_2}{2}\left(\frac{\gamma_1^2-2\gamma_1\gamma_2+3\gamma_2^2}{\gamma_1^2-\gamma_1\gamma_2+\gamma_2^2}\right)-\frac{\Lambda_1\gamma_2}{2(\gamma_1^2-\gamma_1\gamma_2+\gamma_2^2)}$$
$$\times\{\gamma_1^2-2\gamma_1\gamma_2+3\gamma_2^2-\frac{2}{3}(\gamma_2 d)(\gamma_1+\gamma_2)^2+\frac{2}{3}\gamma_2^2[3+(\gamma_1+\gamma_2)d]^2[1-2\gamma_2 d-4(\gamma_2 d)^2\exp(2\gamma_2 d)\mathrm{Ei}(-2\gamma_2 d)]\}$$
$$+\frac{eE_\perp}{2\gamma_2}\left(\frac{5\gamma_1^2-2\gamma_1\gamma_2+2\gamma_2^2}{\gamma_1^2-\gamma_1\gamma_2+\gamma_2^2}\right), \tag{7}$$

where $\mathrm{Ei}(x)$ is the exponential integral. In the limiting case $d\to\infty$ the terms depending on d in Eqs. (6) and (7) disappear, and we reproduce the values of γ_l obtained in Refs. 14 and 15 for the bulk liquid. It is interesting to note that for $d\to 0$ the terms depending on d also disappear in Eqs. (6) and (7), which are formally the same as those for $d\to\infty$ but now depend on $\Lambda_0^*=\Lambda_0+\Lambda_1$. It is easy to see that in this limit, where $\varepsilon_{\mathrm{He}}$ is replaced by unity in the expression for Λ_0, one obtains the energies of an electron localized over a semi-infinite medium at $z\leqslant 0$ with a dielectric constant ε_s and without a helium blanket.

The values of γ_1 and γ_2 are calculated numerically by cumbersome transcedental equations $\partial\Delta_1/\partial\gamma_1=0$ and $\partial\Delta_2/\partial\gamma_2=0$. By determining the roots of these equations and replacing the values of γ_1 and γ_2 in Eqs. (6) and (7) by them one calculates the energies Δ_1 and Δ_2.

3. RESULTS AND DISCUSSION

Here we restrict ourselves to the limit of zero holding field $E_\perp=0$, where the influence of film effects on the SE energy spectrum is especially pronounced. The corrections due to finite value of $E_\perp$ can be included in a straightforward way.[5,6]

We start our consideration by calculating the mean electron distance from the helium surface. Based on the SE wave functions of Eqs. (4) and (5) one can easily obtain

$$\langle z\rangle_1=\frac{3}{2}\gamma_1^{-1} \quad \text{and} \quad \langle z\rangle_2=\frac{5\gamma_1^2-2\gamma_1\gamma_2+2\gamma_2^2}{2\gamma_2(\gamma_1^2-\gamma_1\gamma_2+\gamma_2^2)}. \tag{8}$$

The dependences of $\langle z\rangle_1$ and $\langle z\rangle_2$ on d for a metallic substrate are plotted in Fig. 1. As is seen from Fig. 1 the values of $\langle z\rangle_l$ increase with d. For a small film thickness of 5×10^{-7} cm one has $\langle z\rangle_1\simeq 29$ Å and $\langle z\rangle_2\simeq 72.5$ Å. At smaller values of d the mean electron distance, calculated by Eq. (8), tends to the microscopic range, where the above-mentioned approach to the description of the SE states over a helium film is no longer applicable. Note that, for the same d, the values of $\langle z\rangle_1$ and $\langle z\rangle_2$ are substantially larger for the substrate with $\varepsilon_s\gtrsim 1$. For example, for solid neon ($\varepsilon_s\gtrsim 1.20$) we estimate $\langle z\rangle_1\simeq 89$ Å and $\langle z\rangle_2\simeq 288$ Å (for comparison, $\langle z_1\rangle\simeq 144$ Å and $\langle z\rangle_2\simeq 456$ Å for SEs over bulk helium[3]). One concludes that the characteristic values of the mean electron distance from the liquid surface satisfy the inequality $\langle z\rangle_l \gg z_0$, being substantially larger than atomic scale $\sim 10^{-8}$ cm. For this reason the microscopic nature of the helium surface, leading, in particular, to a small incertainty of the position of the potential barrier V_0, cannot influence appreciably the SE energy properties; this supports the applicability of the limit $V_0\to\infty$ with the boundary condition for the SE wave function $f_l(z)=0$ at $z=0$.[3]

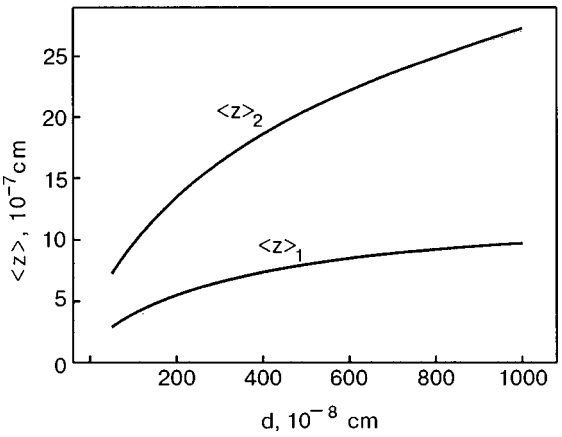

FIG. 1. The mean electron distance from the helium surface for the subbands 1 and 2 as a function of film thickness d for a metallic substrate.

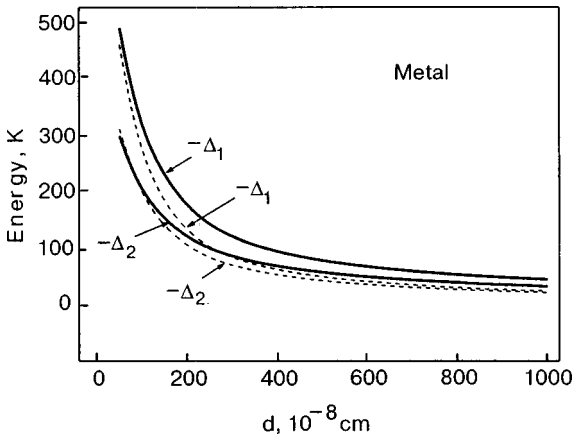

FIG. 3. The same as in Fig. 2 but for a metallic substrate. The solid curves are the results of the present work, and the dashed curves the results of Ref. 5.

The dependences of the SE energies Δ_1 and Δ_2 on d for a solid neon substrate, calculated numerically by Eqs. (6) and (7), are presented in Fig. 2. One observes the increase of the energies with d (the decrease of the absolute values of Δ_1 and Δ_2), which is a natural consequence of the decreasing contribution of $-\Lambda_1/(z+d)$ with increasing d. As a result, the absolute values of the surface energy levels decrease, and the distance between them also decreases, tending, for zero holding field, to the hydrogenlike values of SE energies over bulk helium, $\Delta_l=-\Delta_0/l^2$, whereas the roots of the minimization equations $\partial\Delta_1/\partial\gamma_1$ and $\partial\Delta_2/\partial\gamma_2$ tend to the values $\gamma_1=\gamma_0$ and $\gamma_2=\gamma_0/2$, coinciding with the exact result of solving the Schrödinger equation in the limit $d\to\infty$ and $E_\perp=0$.[3] For solid neon this asymptotic limit is achieved for $d\gtrsim 10^{-5}$ cm. At the same time, for a metallic substrate, where the value of Λ_1 is much larger than that over solid neon, the region in which Δ_1 and Δ_2 practically coincide with those of the hydrogenlike spectrum starts at significantly larger values $d\gtrsim 10^{-4}$ cm.

Figure 3 shows the dependences of Δ_1 and Δ_2 on d for a metallic substrate (solid lines). For comparison the values of the level energies calculated by Eq. (3) are also plotted by the dashed lines. It is seen that the agreement between the energies calculated in different ways is reasonable, especially for relatively small values of d. At the same time, the agreement becomes less satisfactory under increase of d. Note that in the derivation of our Eq. (3) in Ref. 5, the contribution $-\Lambda_0/(z+z_0)$ of the polarization of the liquid helium to the SE potential energy was omitted. Obviously, with increasing d and a decreasing contribution $-\Lambda/(z+d)$ of the polarization of the solid substrate to Eq. (2), the role of $-\Lambda_0/z$ becomes more essential, which can explain some divergence of the results calculated by Eqs. (3), (6), and (7) at $d>10^{-6}$ cm. To make this point clearer we have plotted, in Fig. 4, the values of Δ_1 and Δ_2 calculated by Eqs. (6) and (7), where we put $\Lambda_0=0$. One can see the substantially better agreement with the results of Eq. (3) than that in Fig. 3, especially for the level $l=2$ with the larger value of $\langle z\rangle_2$ and, consequently, with the larger distance from the helium free surface; for this reason the contribution to the structure of the $l=2$ subband from the SE potential energy due to polarization of the medium is smaller than the contribution to the ground subband. As a result, the choice of approach to describe the SE potential energy becomes less essential for $l=2$ than for $l=1$.

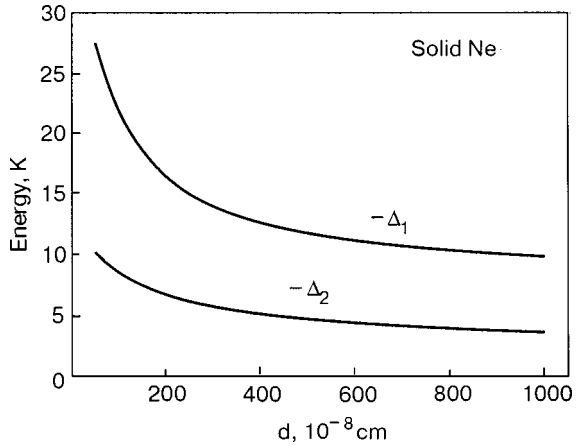

FIG. 2. The energies of the subbands 1 and 2 versus film thickness for a solid neon substrate.

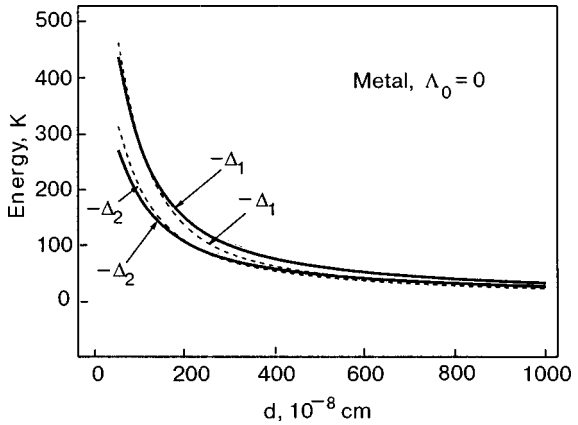

FIG. 4. The same as in Fig. 3 but for $\Lambda_0=0$.

4. CONCLUSIONS

In the present work the energies of the ground and first excited SE subbands over helium film are estimated within a variational approach. The expressions for the level energies are estimated for arbitrary value of substrate dielectric constant ε_s. The values of the mean electron distance from the helium surface are estimated in the macroscopic range, supporting the applicability of the approach $V_0 \to \infty$ where the potential barrier is supposed to be exactly at the free helium surface. The SE energies are calculated, as functions of film thickness, for substrates of solid neon and a metal. The results for the metallic substrate are compared with those obtained analytically in Ref. 5. The agreement between the results of the present work and those of Ref. 5 seems rather good, being especially satisfactory for thin helium films with $d < 10^{-6}$ cm, in spite of the different methods of calculations in the present work and in Ref. 5. One should note the application of the variational approach to obtain the energies of subbands with $l > 2$ leads to overcumbersome calculations with practically intractable results. In such a situation the results of Ref. 5 (Eq. (3)) are especially important, giving the only way to describe analytically the energy spectrum for subbands with $l \geqslant 3$ of SEs localized over a helium film covering a metal.

In closing, the author is highly indebted to V.E. Sivokon and Ye. V. Syrnikov for assistance in the numerical calculations.

*E-mail: sokolov@ilt.kharkov.ua

[1] O. Hipólito, J. R. D. de Felício, and G. A. Farias, Solid State Commun. **28**, 635 (1978).
[2] L. Zipfel, T. R. Brown, and C. C. Grimes, Phys. Rev. Lett. **37**, 1760 (1976).
[3] V. B. Shikin and Yu. P. Monarkha, J. Low Temp. Phys. **16**, 193 (1974).
[4] S. S. Sokolov and N. Studart, Phys. Rev. B **67**, 132510 (2003).
[5] A. M. Gabovich, L. G. Ilchenko, and E. A. Pashitskiĭ, Zh. Éksp. Teor. Fiz. **81**, 2063 (1981) [Sov. Phys. JETP **54**, 1089 (1981)].
[6] S. S. Sokolov and N. Studart, J. Phys.: Condens. Matter **12**, 9563 (2000).
[7] H. Etz, W. Gombert, W. Idstein, and, P. Leiderer, Phys. Rev. Lett. **53**, 2567 (1984).
[8] X. L. Hu and A. J. Dahm, Phys. Rev. B **42**, 2010 (1990).
[9] T. Günzler, B. Bitnar, G. Mistura, S. Neser, and P. Leiderer, Surf. Sci. **341/342**, 831 (1996).
[10] G. Mistura, T. Günzler, S. Neser, and P. Leiderer, Phys. Rev. B **56**, 8360 (1997).
[11] R. J. F. van Haren, G. Acres, P. Fozooni, A. Kristensen, M. J. Lea, P. J. Richardson, A. M. C. Valkering, and R. W. van der Heijden, Physica B **249–251**, 656 (1998).
[12] S. P. Gladchenko, V. A. Nikolaenko, Yu. Z. Kovdrya, and S. S. Sokolov, Fiz. Nizk. Temp. **27**, 3 (2000) [Low Temp. Phys. **27**, 3 (2000)].
[13] P. Glasson, V. Dotsenko, P. Fozooni, M. J. Lea, W. Bailey, G. Papageorgiou, S. E. Andersen, and A. Kristensen, Phys. Rev. Lett. **87**, 176802 (2001).
[14] Yu. P. Monarkha, S. S. Sokolov, and V. B. Shikin, Solid State Commun. **38**, 611 (1981).
[15] S. S. Sokolov, Fiz. Nizk. Temp. **11**, 875 (1985) [Sov. J. Low Temp. Phys. **11**, 481 (1985)].

This article was published in English in the original Russian journal. Reproduced here with stylistic changes by AIP.

SUPERCONDUCTIVITY, INCLUDING HIGH-TEMPERATURE SUPERCONDUCTIVITY

Depairing critical currents and self-magnetic field effects in submicron $YBa_2Cu_3O_{7-\delta}$ microbridges and bicrystal junctions

Z. G. Ivanov†

Department of Physics, Chalmers University of Technology and University of Göteborg, S-412 96 Göteborg, Sweden

N. Ya. Fogel*

Solid State Institute, Technion 32100, Haifa, Israel; Department of Physics, Chalmers University of Technology and University of Göteborg, S-412 96 Göteborg, Sweden

O. I. Yuzephovich**

B. Verkin Institute for Low Temperature Physics and Engineering National Academy of Sciences of Ukraine, 47 Lenin Ave., Kharkov 61103, Ukraine

E. A. Stepantsov and A. Ya. Tzalenchuk

Institute of Crystallography, Russian Academy of Sciences, Moscow 117333, Russia; Department of Physics, Chalmers University of Technology and University of Göteborg, S-412 96 Göteborg, Sweden

(Submitted February 24, 2003; revised July 30, 2003)
Fiz. Nizk. Temp. **30**, 276–281 (March 2004)

We report on depairing critical currents in submicron $YBa_2Cu_3O_{7-\delta}$ microbridges. A small-angle bicrystal grain boundary junction is used as a tool to study the entrance of vortices induced by a transport current and their influence on the $I-V$ curves. The interplay between the depairing and the vortex motion determines a crossover in the temperature dependence of the critical current. The high entrance field of vortices in very narrow superconducting channels creates the possibility of carrying a critical current close to the depairing limit determined by the $S-S'-S$ nature of the small-angle grain boundary junction. © *2004 American Institute of Physics.* [DOI: 10.1063/1.1645178]

1. INTRODUCTION

An understanding of the limitations of supercurrent transport in high-T_c superconductors (HTS) is important from both the fundamental and applied points of view. The upper limit for the critical current density, j_{cp}, in these superconductors is determined by the mechanism of Cooper pair breaking. High nondissipative currents of the order of j_{cp}, however, can only be attained in some special cases. One of the main mechanisms responsible for the reduced values observed is the motion of vortices, which leads to energy dissipation. The critical current density, j_c, in such a case is determined by vortex pinning. Pinning in an HTS is weak because of the small coherence length, ξ, and to hinder the vortex motion a special approach is needed. This may be achieved by employing narrow superconducting channels. In such a channel the penetration of magnetic field and the vortex motion can be blocked by a surface barrier, which may be an effective additional pinning source in the case of a large surface-to-volume ratio. Experiments on narrow $YBa_2Cu_3O_{7-\delta}$ (YBCO) microbridges with widths W of 2–13 μm showed a tendency for j_c to increase while W decreased.[1] It was suggested that in the limit of very narrow microbridges with $W<\lambda_{\text{eff}}$ the value j_{cp} may be attained due to the increasing role of the surface barrier.[1] Here $\lambda_{\text{eff}}=2\lambda_L^2/d$ is the effective magnetic field penetration depth for the superconducting film, λ_L is the London penetration depth, and d is the film thickness. Experimentally, such behavior has until now been confirmed in only one experiment.[2] It was reported that a j_c value of 10^9 A/cm^2 was measured at 77 K in a 50 nm wide YBCO microbridge. Similar microbridges prepared on the same chip showed a critical current density two orders of magnitude lower. Although a submicron processing may give a random structural degradation, the reason for such a spread in j_c values is not completely understood. Thus the limitation of critical current densities in high-T_c oxides, especially in the case of narrow filaments, continues to be an unresolved issue and requires further investigation. In particular, large vortex entrance fields for narrow superconducting channels[3] and the influence of inhomogeneities in the case of a restricted geometry have not been investigated.

In this paper we report on supercurrent transport in submicron YBCO microbridges, with and without a predetermined grain boundary. An asymmetric 4° grain boundary is exploited as a tool to study the entrance of vortices and their influence on j_c and the $I-V$ curves. A self-magnetic field, which is due to the transport current, serves as a source of vortices in the grain boundary, and therefore one can determine the value of the current at which the self-induced vor-

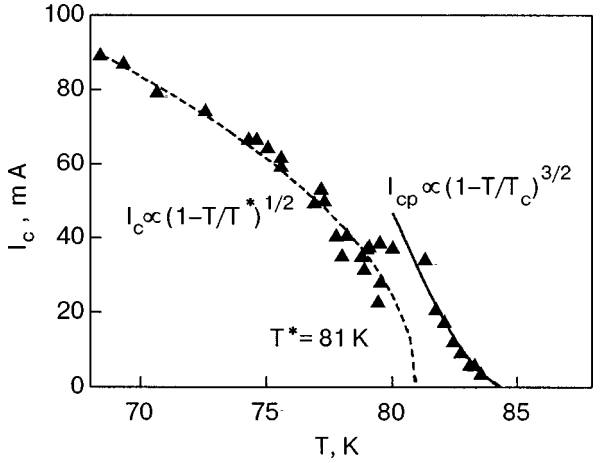

FIG. 1. $I_c(T)$ dependence for a YBCO microbridge ($W=500$ nm) with a 4° bicrystal grain boundary junction. The solid line corresponds to the dependence $j_c \propto (1-T/T_c)^{3/2}$ and the dotted one to $j_c \propto (1-T/T^*)^{1/2}$. Note the large spread in I_c within the crossover region.

tices start to contribute to dissipation. This characteristic current separates two different regimes, where depairing and flux flow effects are the dominating mechanisms limiting the magnitude of the supercurrent. The interplay of these two mechanisms determines the unusual temperature dependence of j_c observed in our experiments.

2. EXPERIMENTAL DETAILS

We investigated YBCO microbridges 0.5–1 μm wide and 10 μm long. *C*-axis oriented YBCO thin films with a thickness d of 120 nm were grown by laser deposition on Y-ZrO_2 bicrystal substrates. The films had a superconducting transition temperature T_c of 89–90 K with ΔT_c of 1 K before patterning. Three microbridges were patterned across the bicrystal boundary and two microbridges on each side of the boundary. A mask of SAL601 *e*-beam resist and Ar ion milling were used to pattern microbridges and electrodes for four-point measurements. The samples were ion milled at $-20\,^{\circ}$C and the T_c of the microbridges decreased by 3–5 K in comparison to the as-deposited films. The submicron bridges had a well-defined trapezoid geometry with a slope of the edges of about 55°, and according to SEM investigations no YBCO "foot" was observed around them.

Standard four-point probe measurements were performed on all the microbridges. The critical current I_c was determined from the current-voltage characteristics at the voltage level of 1 μV, and its density j_c was calculated using the geometrical cross-sectional area without taking into account the real current distribution.

3. RESULTS AND DISCUSSIONS

Current-voltage characteristics were measured at different temperatures. The I_c versus T dependence for a microbridge with a 4° bicrystal grain boundary junction (GBJ) is shown in Fig. 1. Two well-defined regions with different temperature dependences can be distinguished. Close to T_c the $I_c(T)$ dependence is described by a relation $I_c \propto (1-T/T_c)^{3/2}$. This behavior is further illustrated in Fig. 2a using the coordinates $j_c^{2/3}$ and reduced temperature T/T_c. Such

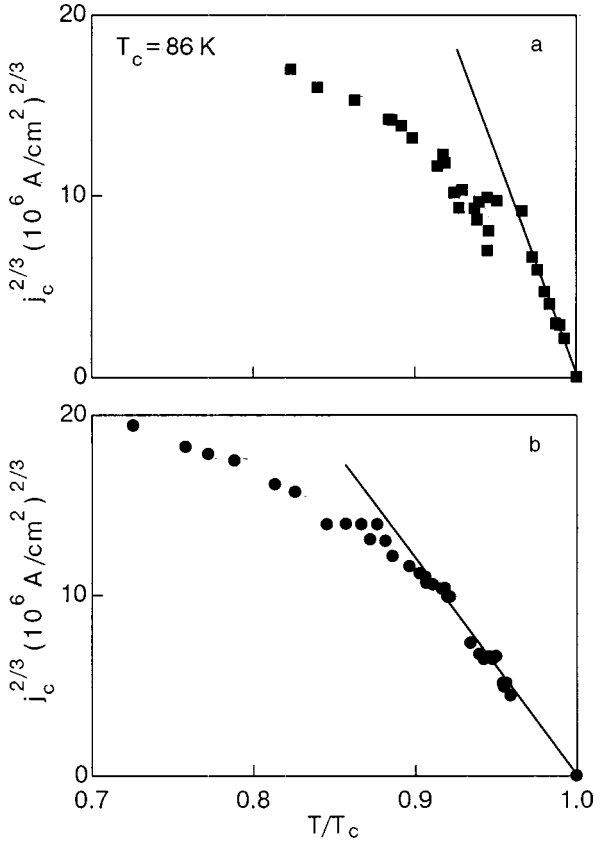

FIG. 2. $j_c^{2/3}$ versus T/T_c dependences for a microbridge with a 4° grain boundary junction (a) and for a uniform microbridge (b). The microbridges were 500 nm wide, 120 nm thick, and 10 μm long.

behavior is similar to that expected for the depairing critical current, but it was observed only in a limited temperature range. At temperatures around $T^*=81$ K, I_c becomes unstable. Below T^* the temperature dependence of I_c changes radically. Simultaneously, a change of $I-V$ characteristics takes place. Above T^* the $I-V$ curves are smooth, but at $T<T^*$ regular steps appear in the $I-V$ curves which are periodic in current (Fig. 3). These steps are only observed in

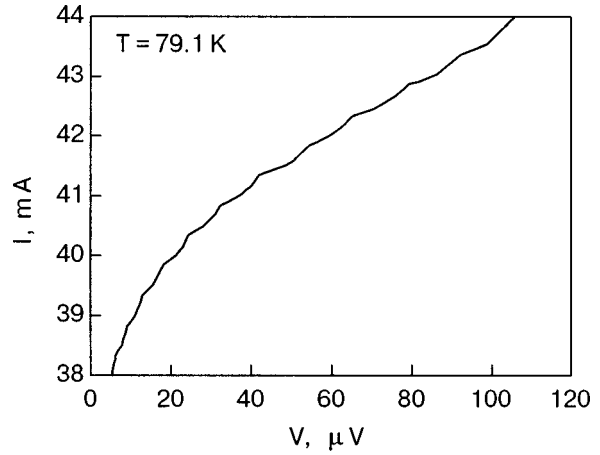

FIG. 3. $I-V$ curve plotted for currents larger than the critical value in a 500 nm wide microbridge crossing a 4° grain boundary. $T=79.1$ K. Note the periodic structure ($\Delta I \approx 0.5$ mA) and that the slope (resistance) in the intermediate regions is proportional to the step number.

a limited temperature range of 2–4 K, where a large spread in j_c values was also noted. At lower temperatures, the $I-V$ characteristics are of the flux flow type with $V\propto(I-I_c)^2$.

The maximum value of I_c at $T\approx T^*$ corresponds to a high current density of 3×10^7 A/cm^2. We will show below that the critical current densities in the temperature range between T^* and T_c are very close to the depairing critical current not only qualitatively but quantitatively as well. As shown in Fig. 2b, the critical current densities of the microbridge in the body of the grain are close to the j_c of the GBJ at the same reduced temperatures.

To explain the $I_c(T)$ dependence measured for microbridges with GBJ in the whole temperature range and the high values of j_c, two assumptions were made. First, the barrier of the small-angle GBJ may be described as a ''weak'' superconductor (S'), with a T_c lower than in the electrodes. Values of j_c approaching the depairing limit can be reached only in weak links with large transparency, and the $S-S'-S$ model may then explain the high j_c values in our experiments in the vicinity of T_c. Another important assumption concerns the absence of vortices in the microbridge at $T>T^*$. As was shown by Likharev,[3] the vortex entrance field, H_V, becomes width dependent when the microbridge width is comparable to λ_{eff} and it may attain large values exceeding the first critical field H_{c1} even in bulk superconductors. For a narrow microbridge[3]

$$H_V=\begin{cases}(2\Phi_0/\pi W^2)\ln(W/4\xi) & \text{at } W\ll\lambda_{\text{eff}}\\ (\Phi_0/\pi W\lambda_{\text{eff}})\ln(\lambda_{\text{eff}}/\xi) & \text{at } WL\gg\lambda_{\text{eff}}\end{cases}. \tag{1}$$

Here Φ_0 is the magnetic flux quantum. The $H_V\propto W^{-2}$ dependence was observed for narrow microbridges of conventional superconductors.[4] If the microbridge edges are smooth, the entrance field may even exceed the calculated H_V values due to the surface barrier.[3] Large entrance fields governed by the surface barrier and exceeding H_V have also been observed experimentally.[5]

The properties of $S-S'-S$ weak links have been investigated theoretically.[6] The authors considered a model of a weak link, S', which only differed in its properties relative to those of the bulk electrodes, S, in having a shorter electron mean free path l. The weakness of the link was defined by a parameter $\gamma=\chi_{Wl}/\chi_{el}$, where χ is a Gorkov universal function of the impurity parameter l/ξ_0 (ξ_0 is the BCS coherence length). The subscripts Wl and el denote the weak-link region and electrode regions, respectively. It was shown that the critical current density of the weak link exceeds its intrinsic value due to the proximity effect, especially in close vicinity to T_c (the coherence length diverges as $(1-T/T_c)^{-1/2}$). If the condition $L/2\xi_{Wl}<\gamma^{1/2}$ is met (L is the geometrical length of the weak link and $L/2\xi_{Wl}$ is its normalized length), then the critical current density of the weak region is only slightly below the value in the electrodes, i.e., it can be close to the pair-breaking current density $j_{cp}(T)$. Nevertheless, since the order parameter in such a contact is depressed in the middle of the weak link, the current-phase relation is close to the Josephson one, and one can expect a Josephson-like behavior.[6] This assumption explains the $(T_c-T)^{3/2}$ dependence of j_c and its large value near T_c. Now let us try to understand the $I_c(T)$ dependence of the microbridges with GBJ obtained in the range $T<T^*$. Near T^*, the j_c of the junction attains values exceeding 10^7 A/cm^2. At such current densities and small cross sections of the microbridge, the self-magnetic field of the critical current, H_{Ic}, at the outer edge of the microbridge, with thickness d, is given by the expression:

$$H_{Ic}=2\pi j_c d/c. \tag{2}$$

The field H_{Ic} is quite large and may play an essential role in determining the GBJ behavior. As long as this field is lower than H_V determined by formula (1), there are no vortices inside the sample, and the critical current is determined by pair-breaking. Estimates using (1) and (2) show that H_{Ic} is equal to H_V at $T=81$ K for the microbridge in Fig. 1.

Penetration of vortices begins at the weakest spot, i.e., in the Josephson contact. We believe that the instability that appears at $T\approx T^*$ is connected to the penetration of vortices into the weak link. The critical magnetic field H_{c1J} for penetration of a single vortex into a tunnel junction is[7]

$$H_{c1J}=2\Phi_0/(\pi^2\lambda_J L_{\text{eff}}). \tag{3}$$

Here $\lambda_J=(c\Phi_0/8\pi^2 j_c L_{\text{eff}})^{1/2}$ is the Josephson penetration length, and $L_{\text{eff}}=2\lambda_L+L$. Formula (3) is obtained for a tunnel junction, but one can assume that it is valid for an $S-S'-S$ junction as well, since the area occupied by a flux quantum is about $\lambda_J L_{\text{eff}}$. Assuming $L\ll\lambda_L$ and substituting for λ_J in (3), we obtain the following expression:

$$H_{c1J}=(4/\pi)(\Phi_0 j_c/c\lambda_L)^{1/2}. \tag{4}$$

Near T_c, where $H_{Ic}<H_{c1J}$, the critical current of the weak link is close to the pair-breaking critical current $j_{cp}(T)$ for the bulk material. As the two fields become equal, the mechanism leading to disappearance of superconductivity changes. Starting with the assumption that at $T<T^*$ the critical current density may be defined by the condition $H_{Ic}=H_{c1J}$, one can find the critical current density connected to the vortex mechanism. Using formulas (2) and (4), we obtain

$$j_c(T)=4c\Phi_0/\pi^4 d^2\lambda_L(T). \tag{5}$$

Relation (5), with the temperature dependence $\lambda_L(T)\propto(1-T/T^*)^{-1/2}$ near T^* taken into account, is shown by the dashed curve in Fig. 1 (T^* is assumed to be the transition temperature of the S' superconductor). The agreement of this approximation with the experimental data is good. $\lambda_L(0)$ in the GBJ region was the only fitting parameter. The value obtained, 62 nm, is less than the values of $\lambda_L(0)$ for YBCO known from the literature ($\lambda_L(0)=100-140$ nm; see Ref. 8 and references therein). In view of the approximateness of our approach the agreement is quite reasonable. In particular, a numerical coefficient may appear in (5) to take into account the nonuniform distribution of the self-magnetic field of the transport current.

There is additional confirmation that crossover in the j_c temperature dependence is associated with the beginning of self-field vortex penetration into the microbridge. The cross-

over takes place at practically the same critical current density on different microbridges with equal widths (see Fig. 2).

As always, the critical current connected with vortex motion should be smaller than the pair-breaking one. Indeed, we found not only a drastically changed temperature dependence of j_c below T^*, but relatively small values of j_c in comparison with values extrapolated from the $(1-T/T_c)^{3/2}$ dependence. The suppression of j_c may also be considered as evidence for the validity of our model.

The data for a uniform microbridge cut in the body of a single grain (see Fig. 2b) also demonstrate a $j_c \propto (1-T/T_c)^{3/2}$ dependence near T_c. For a uniform microbridge with $W=0.8$ μm, the deviation of the experimental points from a $(1-T/T_c)^{3/2}$ dependence takes place at a lower T/T_c than for a microbridge with a GBJ, but the phenomenon determining this deviation from the $j_{cp}(T)$ dependence is of the same type as in the case of the microbridge with a GBJ, although it is less pronounced. In the uniform microbridge, features similar to those of the GBJ have been observed: instability of j_c around T^*, steps in the $I-V$ curves (although irregular), and a change of the $j_c(T)$ dependence below T^*. These data can be reasonably explained with the assumption that the uniform microbridge contains some random, uncontrolled $S-S'-S$ weak links which are not as clearly defined as the specially introduced GBJ, but which influence the j_c and $I-V$ curves in a similar way. One may conclude that only if such weak links are not present can the depairing critical current be observed to low temperatures.

It is also easy to estimate the temperature T^* below which the inequality $H_{Ic}<H_{c1J}$ is violated. Using the experimental temperature dependence of j_c obtained near T_c, one can rewrite this condition as follows:

$$1-T^*/T_c = 4c\Phi_0/\pi^4 d^2 j_c(0)\lambda_L(0). \tag{6}$$

Here $j_c(0)$ is the coefficient in the experimental dependence $j_c(T)=j_c(0)(1-T/T_c)^{3/2}$. The resulting value $T^*=79.4$ K is rather close to that observed in the experiment (see Fig. 1) when the value $\lambda_L(0)=62$ nm obtained above is used.

A comparison of the experimental $j_c(T)$ dependence at $T>T^*$ with the formula for the depairing critical current,[9]

$$j_{cp}=c\Phi_0/[12\sqrt{3}\pi^2\xi(T)\lambda_L^2(T)], \tag{7}$$

may also be used to estimate the value of $\lambda_L(0)$. It should be pointed out that there is some uncertainty in such an estimate because of the substantial discrepancy in the values of $\xi(0)$ obtained by different authors ($\xi_{ab}(0)=1-3$ nm; see Ref. 8 and references therein). Another source of error is connected with a coefficient $j_{cWl}/j_{cel}<1$ which should be introduced in (7) to take into account the reduced value of j_c in a junction in comparison with that of the "bulk." Using formula (7) with $\lambda_L(0)=62$ nm defined in the range $T<T^*$, one obtains $\xi(0)=3.3$ nm. This value is in the range of those from other measurements. Therefore, the parameter $\alpha=j_{cWl}/j_{cel}$ is close to unity. This is expected due to the proximity effect between S and S'.

Thus all the experimental numerical values and the temperature dependence of j_c in the whole temperature range may be described self-consistently in terms of an $S-S'-S$ weak-link model using only one fitting parameter, $\lambda_L(0)=62$ nm. The distinction of this parameter from the values of $\lambda_L(0)$ known from the literature may be explained by the uncertainty in the numerical factors in formulas (5) and (7). This implies that the measurements of $j_c(T)$ in microbridges cannot be used for precise $\lambda_L(0)$ determination.

It is worthwhile also to mention here that a theory[10] considering the critical current of wide HTS epitaxial films with small-angle misorientation between grains predicts that the $j_c(T)$ dependence is governed by the temperature dependence $(1-T/T_c)^{3/2}$ of the depairing current if the distance between edge dislocations r_d on the bicrystal grain boundary is less than the coherence length $\xi(T)$. For a 4° grain boundary the value of r_d is equal to 5.7 nm. This means that such a dependence should be observed to temperatures very close to T_c ($T/T_c=0.997$).

The most remarkable feature of Fig. 1 is the crossover in the temperature dependence of I_c and the large spread in the values of the critical current around the crossover temperature. This I_c instability is not understood in detail, but most probably such a behavior is connected with the dynamics of vortex nucleation and motion under conditions when magnetic field of the transport current attains the threshold for the vortex pair penetration in the GBJ.

Besides the nontrivial $j_c(T)$ dependence, another remarkable feature that is characteristic for a small-angle GBJ is the presence of steps in the $I-V$ curves. The steps are periodic with current and they appear within a limited temperature interval. At first sight, the origin of regular periodic steps in $I-V$ appearing in the temperature range where the critical current is governed by the penetration of Josephson vortices in the weak link can be connected with the oscillatory behavior predicted in Ref. 11. It would then reflect the entrance of the second, third and further vortex-antivortex pairs into the Josephson junction.

However, the periodicity of the steps in terms of the self-field of the current is found to be several Oe, while the expected periodicity for the entrance of the next vortices,[11] $\Delta H=\Phi_0/2W\lambda_L(T)$, is more than an order of magnitude larger than the values obtained experimentally.

The interaction of moving vortices with the periodic inhomogeneities in the bicrystal boundary (regular misfit dislocation grid) may be considered as a possible explanation of the step structure in the $I-V$ curve.[12] The commensurability of the dislocation grid and the vortex spacing, which is determined by the magnetic field (i.e., transport current), may play the key role in this scenario.

In the case of the "uniform" microbridge, the steps are not periodic with current. This may be explained by the presence of a number of low-angle grain boundaries in the microbridge due to YBCO island growth.

The question of the origin of the step-like behavior requires a closer investigation. The transition at lower temperatures to the usual flux flow behavior may be explained by a penetration of Abrikosov vortices along the whole length of the microbridge and their motion.

In summary, we have shown that near T_c the critical current density of a submicron microbridge is governed by the pair-breaking mechanism. This is also true for a microbridge containing a controlled weak link of the grain bound-

ary type if the misorientation angle is small. The possibility of carrying a critical current close to the depairing limit is due, in particular, to the absence of vortices in the microbridge. This is caused by the high vortex entrance field for narrow superconducting channels. The properties of such small-angle junctions may be described in a model of an $S-S'-S$ Josephson contact with a high current density. The value of j_c in such a contact differs only slightly from j_{cp} in the electrodes due to the influence of the proximity effect. At lower temperatures, when j_c becomes controlled by Josephson vortex penetration into the weak link, the $j_c(T)$ dependence changes radically and the j_c values become lower. The same is true for ''uniform'' microbridges that often contain low-angle grain boundaries. The crossover to the vortex-motion mechanism of dissipation is accompanied by the appearance of steps in the $I-V$ curves. These disappear again when the whole microbridge enters the vortex state. The steps may be connected with the dynamics of vortex pair motion and annihilation.

Discussions with R. I. Shekhter and L. Yu. Gorelik are gratefully acknowledged. This project utilized the Swedish Nanometer Laboratory and was supported by the Materials Consortium on Superconductivity.

†Deceased
*E-mail: nfogel@techunix.technion.ac.il
**E-mail: yuzephovich@ilt.kharkov.ua

[1] S. Tahara, S. M. Anlage, J. Halbbritter, C. B. Eom, D. K. Fork, T. H. Geballe, and M. R. Beasley, Phys. Rev. B **41**, 11203 (1990).
[2] H. Jiang, Y. Huang, H. How, S. Zhang, C. Vittoria, A. Widom, D. B. Chrisey, J. S. Horwitz, and R. Lee, Phys. Rev. Lett. **66**, 1785 (1991).
[3] K. K. Likharev, Izv. Vyssh. Uchebn. Zaved., Radiofiz. **14**, 919 (1971).
[4] R. D. Parks and J. M. Mochel, Rev. Mod. Phys. **36**, 284 (1964).
[5] V. G. Cherkasova and N. Ya. Fogel, Fiz. Nizk. Temp. **15**, 383 (1989) [Sov. J. Low Temp. Phys. **15**, 216 (1989)].
[6] A. Baratoff, J. A. Blackburn, and B. B. Schwartz, Phys. Rev. Lett. **25**, 1096 (1970).
[7] I. O. Kulik and I. K. Yanson, *The Josephson Effect in Superconducting Tunnel Structures*, Keter Press, Jerusalem (1972), Nauka, Moscow, (1970).
[8] D. M. Ginsberg, in *Physical Properties of High Temperature Superconductors*, D. M. Ginsberg (ed.), World Scientific, Singapore (1989).
[9] J. Bardeen, Rev. Mod. Phys. **34**, 667 (1962).
[10] E. A. Pashitskii, V. I. Vakaryuk, S. M. Ryabchenko, and Yu. V. Fedotov, Fiz. Nizk. Temp. **27**, 131 (2001) [Low Temp. Phys. **27**, 96 (2001)].
[11] R. Fehrenbacher, V. B. Geshkenbein, and G. Blatter, Phys. Rev. B **45**, 5450 (1992).
[12] X. Y. Cai, A. Gurevich, I-Fei Tsu, D. L. Kaiser, S. E. Babcock, and D. C. Larbalestier, Phys. Rev. B **57**, 10951 (1998).

This article was published in English in the original Russian journal. Reproduced here with stylistic changes by AIP.

Order parameter phase locking as a cause of a zero bias peak in the differential tunneling conductance of bilayers with electron–hole pairing

A. I. Bezuglyj[a)]

National Science Center "Kharkov Institute of Physics and Technology," 1 Academicheskaya St., Kharkov 61108, Ukraine

S. I. Shevchenko[b)]

B. Verkin Institute for Low Temperature Physics and Engineering of the National Academy of Sciences of Ukraine, 47 Lenin Ave., Kharkov 61103, Ukraine

(Submitted June 13, 2003; revised October 2, 2003)
Fiz. Nizk. Temp. **30**, 282–287 (March 2004)

In $n-p$ bilayer systems an exotic phase-coherent state emerges due to Coulomb pairing of n-layer electrons with p-layer holes. Unlike Josephson junctions, the order parameter phase may be locked by matrix elements of interlayer tunneling in $n-p$ bilayers. Here we show how the phase locking phenomenon specifies the response of the electron–hole condensate to interlayer voltages. In the absence of an applied magnetic field, the phase is steady-state (locked) at low interlayer voltages, $V<V_c$, but the phase increases monotonically with time (is unlocked) at $V>V_c$. The change in the system dynamics at $V=V_c$ gives rise to a peak in the differential tunneling conductance. The peak width V_c is proportional to the absolute value of the tunneling matrix element $|T_{12}|$, but its height does not depend on $|T_{12}|$; thus the peak is sharp for small $|T_{12}|$. An in-plane magnetic field reduces the peak height considerably. The present results are in qualitative agreement with the zero-bias peak behavior that has recently been observed in bilayer quantum Hall pseudoferromagnets with spontaneous interlayer phase coherence. © *2004 American Institute of Physics.* [DOI: 10.1063/1.1645179]

The idea that in bilayer $n-p$ structures consisting of an electron-conductivity layer (n-layer) and a hole-conductivity layer (p-layer) the Coulomb attraction of electrons and holes may lead to the formation of electron–hole pairs with spatially separated components was put forward rather long ago.[1,2] As a result of Bose–Einstein condensation of these pairs, there arises a peculiar superfluid (phase-coherent) state, in which a nondissipative motion of pairs gives rise to equal-in-magnitude and oppositely directed supercurrents in the n and p layers. At present, two variants of the systems have been realized experimentally, where an excitonic condensate with spatially separated components is formed. In both cases, these are closely lying GaAs/AlGaAs double quantum wells, where either interwell excitons are excited by a laser pulse[3,4] or two-dimensional electron layers are formed due to doping. In the latter case, the electron layers must be placed in a strong magnetic field, normal to the layers, such that the total filling factor should be $\nu_T=\nu_1+\nu_2=1$.[5] Since all these systems have one and the same exciton mechanism for the interlayer phase coherence,[6] the physical properties of these systems in the coherent state must be qualitatively similar.

The present paper has mainly been stimulated by recent impressive experiments of Spielman *et al.*,[7,8] who have found that if a bilayer electron system transitions into a phase-coherent state (in which the quantum Hall effect is observed at $\nu_T=1$), then this transition is accompanied by a sharp rise in the differential tunneling conductance G_T at low interlayer voltages V. As the temperature is lowered, this tunneling conductance peak remains of finite height and width, in contrast to the tunneling conductance peak of the Josephson junction. In a magnetic field H parallel to the layers the peak height decreases the more drastically the higher is the field, and at $H>0.6$ T the peak becomes practically indistinguishable.

A number of papers have been devoted to theoretical interpretation of the experimental results obtained by Spielman *et al.* For example, Fogler and Wilczek[9] have treated the tunneling conductance peak as a consequence of the Josephson effect in a long inhomogeneous junction. In Refs. 10 and 11, the interpretation of the peak is based on the notion of a finite time of phase coherence. Joglekar and MacDonald[12] have performed both phenomenological and microscopic calculations of the tunneling conductance G_T value at $V=0$. In Ref. 13, $G_T(V,H)$ was calculated using a phenomenological equation similar to the Landau–Lifshitz equation for the magnetic moment. Such a diversity of theoretical approaches in the interpretation of experiment[7,8] gives impetus to a consistent microscopic consideration of the dynamics of phase-coherent bilayer systems, this being the subject of the present paper. Though we consider the $n-p$ system in the absence of a perpendicular magnetic field, the exciton nature of the collective state in all the above-mentioned systems encourages us to believe that the present results provide a qualitative description of the experiments of Spielman *et al.*[7,8]

An important but still not completely resolved problem for the systems with electron–hole pairing is the problem of phase locking by interband transitions[1)] (Ref. 14), which coincide with interlayer tunneling transitions in the systems under consideration. The tunneling transitions lift the degen-

eracy in the phase of the order parameter, thereby locking the phase and making it equal to the phase of the tunneling matrix elements. The last statement is valid in the absence of a magnetic field parallel to the layers. Kulik and one of the present authors[15] have shown that in a magnetic field parallel to the layers the phase is locked only at fields $H<H_{c1}$. (The critical field $H_{c1}\propto|T_{12}|^{1/2}$, where $T_{12}=|T_{12}|e^{i\chi}$ is the matrix element of interlayer tunneling.) At $H>H_{c1}$ the phase locking is lifted and the phase changes monotonically in the direction normal to the field, this giving rise to spatial oscillations of the tunneling current (vortex state). The phase locking phenomenon appears to exert an essential effect not only on the thermodynamic properties of $n-p$ systems but also on their kinetics.

Relying on the microscopic approach, the present paper deals with the response of a phase-coherent $n-p$ system to the interlayer voltage V. We demonstrate that similarly to the existence of the critical field H_{c1}, in the case under consideration there exists a threshold voltage $V_c(\propto|T_{12}|)$ that quantitatively characterizes the degree of phase locking in the $n-p$ system. At low voltages, $V<V_c$, the order parameter phase is locked (steady-state), and the direct tunneling current is proportional to V. The Ohmic character of a spatially uniform tunneling current at $V<V_c$ means that in the phase-coherent $n-p$ system there is no dc Josephson effect.[16] (The absence of the dc Josephson effect in the two-layer electron system has been established by Joglekar and MacDonald.[12]) At voltages $V>V_c$, the phase changes monotonically with time, and this results in tunneling current oscillations with frequency $\omega=e\sqrt{V^2-V_c^2}$ (here e is the elementary charge, and $\hbar=1$). So, at $V>V_c$ the $n-p$ system retains the essential feature of the ac Josephson effect in superconductors, namely, the presence of tunneling current oscillations at a constant applied voltage. At the same time, the dissipative character of the oscillating tunneling current (see below), the nonuniversality of the voltage dependence of ω, and the presence of a threshold voltage V_c are specific to phase-coherent bilayer $n-p$ systems.

Further on, we show that the above-described ''liberation'' of the order parameter phase at $V=V_c$ results in a sharp peak of $G_T(V)$, the height of which is independent of $|T_{12}|$ and the width equal to $2V_c$, i.e., for small $|T_{12}|$ the peak will be high and sharp. Thus in our opinion the nature of the tunneling conductance peak observed in the experiments of Spielman *et al.* is closely connected with the phenomenon of order parameter phase locking by tunneling transitions. The experimentally observed suppression of the $G_T(V)$ peak with an increasing parallel magnetic field[8] also lends support in favor of this interpretation, because, as indicated above, a sufficiently strong in-plane magnetic field eliminates the phase locking.

We are now coming to the analysis of the dynamics of a phase-coherent $n-p$ system in the limit of a high pair density, when the average distance between the electron–hole pairs is small compared to the characteristic pair size. The advantage of the high-density limit lies in the possibility of considering the phase-coherent system dynamics in the gapless state, when the gap in the excitation spectrum becomes zero under the action of strong depairing, and the order parameter Δ is reduced but remains nonzero[2)] (Ref. 17). For the $n-p$ bilayer the order parameter is proportional to the average $\langle\psi_1(\mathbf{r},t)\psi_2^+(\mathbf{r},t)\rangle$, where ψ_i^+ (ψ_i) is the electron creation (annihilation) operator in the layer i. An essential simplification consists in the fact that the absence of the gap makes it possible to describe the dynamics of the phase-coherent system only in terms of the complex order parameter ($\Delta=|\Delta|e^{i\theta}$) without involving the dynamics of the quasiparticle distribution function.

The dynamical equation for the order parameter of the $n-p$ system was derived by the Green function technique in our previous paper[18] and has the following form:

$$-(\dot{\Delta}-ieV\Delta)+\left\{A-B|\Delta|^2+D\left[\frac{\partial}{\partial\mathbf{r}}+\frac{ie}{c}(\mathbf{A}_1-\mathbf{A}_2)\right]^2\right\}\times\Delta+\frac{T_{12}}{\zeta\tau}=0. \tag{1}$$

The equation obtained is in perfect agreement with the general theory of relaxation of an order parameter near the point of a second-order phase transition (see, for instance, Ref. 19). In accordance with this theory a state of a physical system under a second-order phase transition can be described by an order parameter, that is nonzero below the transition point and equal to zero above this point. An equilibrium value of the order parameter can be found from the condition that the variation of the corresponding thermodynamic potential is equal to zero. In the absence of interband hybridization the thermodynamic potential for a condensate of electron–hole pairs with spatially separated components can be presented in the form

$$F=\int\left\{D\left|\left[-i\frac{\partial}{\partial\mathbf{r}}+\frac{e}{c}(\mathbf{A}_1-\mathbf{A}_2)\right]\Delta\right|^2-A|\Delta|^2+\frac{1}{2}B|\Delta|^4\right\}d\mathbf{r}. \tag{2}$$

Expression (2) is similar to the thermodynamic potential for Cooper pairs in the Ginzburg–Landau theory, but here the term $2e\mathbf{A}$ is replaced by the term $e(\mathbf{A}_1-\mathbf{A}_2)$. Such a modification is quite natural. Indeed, for the case of electron–hole pairs with spatially separated components an electron in the layer 1 ''sees'' the vector potential $\mathbf{A}_1$, while a hole in the layer 2 ''sees'' the vector potential $\mathbf{A}_2$. Since the signs of the electron and hole charges are different, the vector potentials $\mathbf{A}_1$ and $\mathbf{A}_2$ are subtracted from each other in Eq. (2). In equilibrium the order parameter $\Delta(\mathbf{r})$ is found from the condition $\delta F/\delta\Delta^*(\mathbf{r})=0$. For a small deviation from equilibrium, when the derivative $\delta F/\delta\Delta^*(\mathbf{r})$ is nonzero but small, the order parameter relaxation rate (the derivative $\partial\Delta/\partial t$) is also small. In the mean field approximation these two derivatives should be proportional to each other. But it is necessary to take into account that due to the gauge invariance of the theory the derivative $\partial/\partial t$ must enter into the equation in combination with the term $ie(V_1-V_2)$, where V_1 and V_2 are the electrostatic potentials in layers 1 and 2, respectively. As a result, in the absence of interband hybridization one arrives at Eq. (1), where $T_{12}=0$.

In the presence of interband hybridization the Hamiltonian of the system contains terms linear in the order parameter Δ and in the matrix elements T_{12} and the corre-

sponding conjugate terms (and that means that the thermodynamic potential contains the same terms). These terms play the role of a source of electron–hole pairs. They are analogous to the terms that appear in the Hamiltonian of a ferromagnet in an external magnetic field. For the case of a magnet it results in the appearance of a term linear in the magnetic field in the equation for the order parameter. Since for the system considered the matrix element T_{12} is analogous to the magnetic field, a term linear in T_{12} should appear in the equation for the order parameter in the presence of interband hybridization. We see that Eq. (1) does in fact contain this term. The microscopic analysis shows that although the phenomenological arguments presented look quite general, in reality Eq. (1) is valid only in a rather narrow interval of impurity concentration, just in the case of the Gor'kov–Eliashberg equation for superconductors containing paramagnetic impurities.[20]

In the gapless situation under consideration, the coefficients of the dynamic Ginzburg–Landau equation (1) have the forms $A(T)=(2\pi^2/3)\tau(T_c^2-T^2)$, $B=4m\tau/3M$, $D=p_0^2\tau/M^2$ (Ref. 18). Here τ is the electron elastic scattering time (for simplicity, it is considered equal to the hole elastic scattering time), T is the temperature ($k_B=1$), T_c is the critical temperature, $M=m_1+m_2$ is the pair mass, $m=m_1m_2/M$ is the reduced mass of a pair, p_0 is the Fermi momentum of electrons and holes, and ζ is the dimensionless constant of the Coulomb interaction.[2] It should be noted that Eq. (1) is derived by expansion of the anomalous Green function as a power series in (Δ/T_c).[18] Since a term linear in the matrix element T_{12} appears in the expression for the order parameter, it is necessary that $|T_{12}|\ll T_c$ for validity of Eq. (1).

At low fields and currents, the modulus of the order parameter varies only slightly in space and time. Assuming $|\Delta|$ to be constant equal to Δ_0, the imaginary part of Eq. (1) can be written as follows:

$$\dot{\phi}-D\frac{\partial}{\partial\mathbf{r}}\left(\frac{\partial\phi}{\partial\mathbf{r}}-\frac{2\pi d}{\Phi_0}[\mathbf{H}\times\mathbf{n}]\right)-eV+eV_c\sin\phi=0. \quad (3)$$

Here the gradient-invariant phase $\phi=\theta-\chi-(2\pi d/\Phi_0)A_z$ is introduced, d is the interlayer distance, and $\Phi_0=hc/e$ is the magnetic flux. The unit vector $\mathbf{n}=(0,0,1)$ is normal to the layers and is directed from layer 1 (electron layer) to layer 2 (hole layer). The threshold voltage $V_c=|T_{12}|/(e\zeta\tau\Delta_0)$.

It is readily seen that in the uniform case Eq. (3) for the phase ϕ is different from the equation $\dot{\phi}=eV$ that appears in a number of papers and is treated as the Josephson relation for phase-coherent bilayer systems. The occurrence of the term proportional to $|T_{12}|$ in the dynamical equation for the phase radically changes the solutions of this equation. Thus, in the absence of external fields the stable steady-state and uniform solution of Eq. (3) is $\phi=0$, i.e., $\theta=\chi$, and this means that the interlayer tunneling transitions hold the order parameter phase locked. Below, we consider in detail how the phase locking phenomenon influences the dynamic properties of $n-p$ systems.

We start from an analysis of the dynamics of the $n-p$ system in the phase-coherent state for the spatially uniform case in the absence of magnetic field. Let the $n-p$ tunneling junction be incorporated into an electrical circuit having resistance R and a voltage source $\mathscr{E}$. The resulting voltage V across the $n-p$ tunnel junction determines the difference of electrochemical potentials of the layers and thereby dictates the carrier density in the n and p layers. If δn is the deviation of the electron density from equilibrium, then the equality $eV=-\delta n/N_*(0)$ is valid, where the renormalized density of states on the Fermi surface is

$$N_*(0)=N(0)\left(1+\frac{e^2m}{\pi C}\right)^{-1}$$

(C is the capacitance of the bilayer system per unit area; $N(0)=m/\pi$).

In the approximation linear in T_{12} the density of tunneling current from layer 1 to layer 2 is equal to $J=J_c\sin\phi$, where $J_c=4eN(0)|T_{12}|\Delta_0/\zeta$.[18] The charge balance equation for layer 1 can be written as

$$eS\delta\dot{n}+\frac{\mathscr{E}-V}{R}-I_c\sin\phi=0, \quad (4)$$

where S is the area of the $n-p$ junction, and $I_c=SJ_c$. Though below we assume $\mathscr{E}=$const, it should be noted that Eq. (4) also holds for a time-dependent voltage source.

Making use of the relationship between δn and V, from Eqs. (3) and (4) one can derive the equation for the phase ϕ. In terms of dimensionless variables, this equation takes on the following form, well known in the theory of Josephson junctions:

$$\ddot{\phi}+\frac{1}{\sqrt{\beta}}(1+\varepsilon\cos\phi)\dot{\phi}+\sin\phi=\rho. \quad (5)$$

Here the following dimensionless parameters are introduced: $\beta=e\mathscr{E}_ct_0$, $\varepsilon=eV_ct_0$, $\rho=\mathscr{E}/\mathscr{E}_c$, where $\mathscr{E}_c=V_c+I_cR$ and $t_0=e^2N_*(0)RS$. The time is measured in units of $1/\omega_0$, where $\omega_0=(e\mathscr{E}_c/t_0)^{1/2}$.

Despite the coincidence of Eq. (5) with the dynamical equation for the phase difference across the Josephson junction, the different meaning of the parameter ρ entering into these equations leads (as will be seen from what follows) to a substantially different behavior of $n-p$ systems and Josephson junctions.

A detailed analysis of the dynamic states of the system described by Eq. (5) was performed by Belykh *et al.*[21] Without going into the details of that analysis, we shall mention its main results. For each value of the parameter ε one can find the corresponding number β_1. At $\beta>\beta_1$ (large resistances R), the range of ρ values is split into three adjacent intervals: $0<\rho<\rho_c$, $\rho_c<\rho<1$, and $\rho>1$ [$\rho_c(\beta,\varepsilon)$ is the bifurcation value of the parameter ρ; Ref. 21]. In the first interval, there is only one stable solution, $\phi=\arcsin\rho$; in the third interval the only stable state is the limit cycle embracing the phase cylinder. In the intermediate (second) interval both solutions, $\phi=\arcsin\rho$ and the limit cycle, are stable. This nonuniqueness of the solution of Eq. (5) results in hysteresis of the current–voltage characteristic (CVC) at $\beta>\beta_1$. For $\beta<\beta_1$ (low resistances R) the stable solutions will be $\phi\arcsin\rho$ at $0<\rho<1$ and the limit cycle at $\rho>1$, while the interval of ρ with two stable states drops out. Correspondingly, at $\beta<\beta_1$ the CVCs have no hysteresis.

Further on, we find the CVC and the differential tunneling conductance of the $n-p$ system in the simple, but physically rather illustrative, case $R=0$. In this limit, no distinction may be made between V and $\mathscr{E}$, V_c and $\mathscr{E}_c$, and the dynamics of the system may be analyzed on the basis of Eq. (3) (without spatial derivatives). Since in the case considered we have $\beta<\beta_1$, hysteresis of the CVC is absent.

If the system is spatially uniform and the voltage V does not depend on time, Eq. (3) can be integrated. One can see that for $V<V_c$ Eq. (3) has the time-independent solution $\phi_0=\arcsin V/V_c$. In such a case the tunnel current, also independent of time, is equal to $I_c\sin\phi_0=I_cV/V_c\equiv V/R_c$. This current is proportional to the applied voltage V and it is an ordinary dissipative current.

The corresponding tunneling conductance is given by

$$G_T=\frac{dI}{dV}=R_c^{-1}=4e^2N(0)\tau\Delta_0^2S. \tag{6}$$

Note that at $V<V_c$ the tunneling conductance is constant and is independent of the value of the tunneling matrix element $|T_{12}|$. This independence of the tunneling conductance from $|T_{12}|$ and also its proportionality to $\Delta_0^2(T)$ are in agreement with the result of Joglekar and MacDonald[12] for G_T at $V=0$.

In case of $V>V_c$ the integration yields the tunnel current, equal to

$$I(t)=2I_c\frac{\tan\dfrac{\phi(t)}{2}}{1+\tan^2\dfrac{\phi(t)}{2}} \tag{7}$$

where

$$\tan\frac{\phi(t)}{2}=V_c/V+\sqrt{1-(V_c/V)^2}\times\tan\left[\frac{e}{2}(V^2-V_c^2)^{1/2}(t-t_0)\right]. \tag{8}$$

One can see that the interlayer current oscillates with the frequency $\omega=e(V^2-V_c^2)^{1/2}$ and that this current is not sinusoidal. Because of the nonsinusoidal character of the oscillations, the average value of the tunnel current is nonzero. The average current is a function of the voltage V:

$$I=(I_c/V_c)(V-\sqrt{V^2-V_c^2}). \tag{9}$$

The behavior of the system considered is similar to the behavior of a Josephson junction between two superconductors in a circuit in which the junction is connected in series with a resistor and a voltage generator. But in the former case the essential difference is that the resistor (with $R_c=V_c/I_c$) is embedded in the junction and cannot be deleted from the circuit. Thus there is no transverse superconductivity in the systems considered.

Since according to Eq. (9) the tunneling current decreases with increasing voltage, the differential tunneling conductance at $V>V_c$ is negative:

$$G_T(V)=-(I_c/V_c)[V(V^2-V_c^2)^{-1/2}-1]. \tag{10}$$

The conductance $G_T(V)$ has its maximum (constant) value at $|V|<V_c$ and points of discontinuity at $V=\pm V_c$. At $|V|>V_c$, as $|V|$ increases, the tunneling conductance tends monotonically to zero, remaining negative. If we take into account the fluctuation smoothing of the CVC, then the dependence of G_T on V will look like a smooth curve with a maximum at $V=0$ (approximately $2V_c$ in width) and two minima at $V\approx\pm V_c$. It is just this behavior of the $G_T(V)$ curve that was observed in experiment[8] in the absence of a magnetic field parallel to the layers.

It should be noted that both at $V>V_c$ and $V<V_c$ the spatially uniform tunneling current is dissipative. The reason for the dissipation lies in the fact that the uniform interlayer current causes the order parameter phase to deviate from its equilibrium value, and a continuous input of energy is required to maintain this nonequilibrium state.

Now let the bilayer $n-p$ structure be placed in a magnetic field $\mathbf{H}$ parallel to the layers and directed along the x axis. If $H>H_{c1}=(2\Phi_0/\pi^2d)(J_cM/en_s)^{1/2}$ (the two-dimensional density of pairs $n_s=4p_0^2N(0)(\tau\Delta_0)^2/M$), then the magnetic field between the layers has a nonuniform (vortex) component. We shall show that the CVCs of the $n-p$ system in the magnetic field differ strongly from the CVCs in zero field and are substantially different at both low and high resistances R. In the limiting case $R=0$ (and $H\gg H_{c1}$), the solution of Eq. (3) can be derived using perturbation theory. Putting $\phi=\phi_0+\phi_1$, where $\phi_0=ky+\omega t$ ($k=2\pi dH/\Phi_0$, $\omega=eV$) and taking into account the correction term ϕ_1 (proportional to a small T_{12} value) as a perturbation, we obtain the following expression for the average tunneling current density:

$$J=J_c\frac{eV_c}{2}\frac{\omega}{(Dk^2)^2+\omega^2}. \tag{11}$$

So, for $R=0$ the CVC has a wide diffusion maximum at $\omega=Dk^2$.

At high R values, the charge transport from one layer to the other over the electrical circuit is insignificant, and the electron density dynamics in layer 1 is determined by the continuity equation

$$e\,\delta\dot{n}=\mathrm{div}_2\,\mathbf{j}+J_c\sin\phi, \tag{12}$$

where $\mathrm{div}_2\,\mathbf{j}$ denotes the two-dimensional divergence of the intralayer current

$$\mathbf{j}=-\frac{en_s}{M}\left(\frac{\partial\phi}{\partial\mathbf{r}}-\frac{2\pi d}{\Phi_0}[\mathbf{H}\times\mathbf{n}]\right).$$

On the assumption that $eV\ll\tau\Delta_0^2$, the above-described perturbation-theory procedure yields the following equation for ϕ_1:

$$\ddot{\phi}_1-D\frac{\partial^2\dot{\phi}_1}{\partial^2\mathbf{r}}-u_0^2\frac{\partial^2\phi_1}{\partial^2\mathbf{r}}=-\frac{J_c}{eN_*(0)}\sin\phi_0, \tag{13}$$

where $u_0=(n_s/MN_*(0))^{1/2}$. Unlike the $R=0$ case, the left-hand side of Eq. (13) has a wave character rather than a diffusion character. Correspondingly, the expression for the average tunneling current density

$$J=J_c\frac{1}{2\lambda_J^2}\frac{\omega\alpha k^2}{(\omega^2/u_0^2-k^2)^2+(\omega\alpha k^2)^2} \tag{14}$$

has a resonance at $\omega = u_0 k$, the width of which is determined by the attenuation $\alpha = D/u_0^2$. This resonance results from the coincidence between the plasmon velocity u_0 in the bilayer structure and the velocity of the magnetic-field vortices. The parameter λ_J is equal to $(en_s/MJ_c)^{1/2}$.

From relations (11) and (14) it follows that at $H \gg H_{c1}$ the $G_T(0)$ value is proportional to a small $|T_{12}|^2$ value, i.e., the differential tunneling conductance peak (occurring at $H = 0$) is strongly suppressed. The reason for this suppression lies in the fact that at $H > H_{c1}$ the phase ϕ varies monotonically with the coordinate, and in this case Eq. (3) has no stationary solution at finite voltage, i.e., no phase locking arises.

Thus, the present work has demonstrated in the framework of a consistent microscopic approach that in phase-coherent bilayer $n-p$ systems the known phenomenon of order-parameter phase locking by tunneling matrix elements T_{12} leads to a sharp peak in the differential tunneling conductance $G_T(V)$ at $V = 0$. The peak height is independent of $|T_{12}|$ and its width is proportional to $|T_{12}|$, i.e., at weak tunneling the peak is high and sharp. These results are in qualitative agreement with the peculiarities of $G_T(V)$ observed in electron bilayer systems in the regime of the integral quantum Hall effect at the total filling factor $\nu_T = 1$. We stress once again that though the theory developed here describes the $n-p$ system without a transverse magnetic field, the present results are in qualitative agreement with the data from experiments on electron bilayer systems in a strong transverse magnetic field. This agreement does not seem to be accidental. The reason is that most likely the strong magnetic field does not affect the structure of the equation that defines the dynamics of the order parameter, but only changes the values of the coefficients entering into this equation.

This work was supported by the INTAS program, Grant No. 01-2344.

[a)]E-mail: bezugly@ic.kharkov.ua
[b)]E-mail: shevchenko@ilt.kharkov.ua

[1)]R. R. Gusejnov and L. V. Keldysh have first demonstrated that interband transitions lift the phase degeneracy of the wave function of the electron–hole condensate in the exciton dielectric.

[2)]Similarly to magnetic impurities in superconductors, the usual (nonmagnetic) impurities and crystal lattice distortions in the $n-p$ system suppress the order parameter and lead to the transition of the system to the gapless state in a narrow range of defect concentrations in the vicinity of the critical concentration.

[1] Yu. E. Lozovik and V. I. Yudson, Zh. Eksp. Teor. Fiz. **71**, 738 (1976) [Sov. Phys. JETP **44**, 389 (1976)].
[2] S. I. Shevchenko, Fiz. Nizk. Temp. **2**, 505 (1976) [Sov. J. Low Temp. Phys. **2**, 251 (1976)]; Phys. Rev. Lett. **72**, 3242 (1994).
[3] L. V. Butov, C. W. Lai, A. L. Ivanov, A. C. Gossard, and D. S. Chemia, Nature (London) **417**, 47 (2002); L. V. Butov, A. C. Gossard, and D. S. Chemia, Nature (London) **418**, 751 (2002).
[4] A. V. Larionov, V. B. Timofeyev, J. Hvam, and K. Soerensen, JETP Lett. **75**, 200 (2002); A. A. Dremin, V. B. Timofeyev, A. V. Larionov, J. Hvam, and K. Soerensen, *ibid.* **76**, 450 (2002).
[5] J. P. Eisenstein, in *Perspectives in Quantum Hall Effects*, S. Das Sarma and A. Pinczuk (eds.), Wiley, New York (1997).
[6] A. H. MacDonald and E. H. Rezayi, Phys. Rev. B **42**, 3224 (1990).
[7] I. B. Spielman, J. P. Eisenstein, L. N. Pfeiffer, and K. W. West, Phys. Rev. Lett. **84**, 5808 (2000).
[8] I. B. Spielman, J. P. Eisenstein, L. N. Pfeiffer, and K. W. West, Phys. Rev. Lett. **87**, 036803 (2001).
[9] M. M. Fogler and F. Wilczek, Phys. Rev. Lett. **86**, 1833 (2001).
[10] L. Balents and L. Radzikhovsky, Phys. Rev. Lett. **86**, 1825 (2001).
[11] A. Stern, S. M. Girvin, A. H. MacDonald, and N. Ma, Phys. Rev. Lett. **86**, 1829 (2001).
[12] G. N. Joglekar and A. H. MacDonald, Phys. Rev. Lett. **87**, 196802 (2001).
[13] M. Abolfath, R. Khomeriki, and K. Mullen, cond-mat/0208236.
[14] R. R. Gusejnov and L. V. Keldysh, Zh. Eksp. Teor. Fiz. **63**, 2255 (1972) [Sov. Phys. JETP **36**, 1193 (1972)].
[15] I. O. Kulik and S. I. Shevchenko, Fiz. Nizk. Temp. **2**, 1406 (1976) [Sov. J. Low Temp. Phys. **2**, 687 (1976)].
[16] S. I. Shevchenko, *Theory of Low-Dimensional Superfluidity in Bose and Fermi Systems* [in Russian], Thesis, Kharkov (1992) (unpublished).
[17] A. I. Bezuglyj and S. I. Shevchenko, Fiz. Nizk. Temp. **3**, 428 (1977) [Sov. J. Low Temp. Phys. **3**, 204 (1977)].
[18] A. I. Bezuglyj and S. I. Shevchenko, Fiz. Nizk. Temp. **4**, 454 (1978) [Sov. J. Low Temp. Phys. **4**, 222 (1978)].
[19] L. D. Landau and E. M. Lifshitz and L. P. Pitaevskiĭ, *Physical Kinetics*, Vol. 10 of Course in Theoretical Physics by L. D. Landau and E. M. Lifshitz, Pergamon Press, Oxford (1981), Nauka, Moscow (1979).
[20] L. P. Gor'kov and G. M. Eliashberg, Zh. Eksp. Teor. Fiz. **54**, 612 (1968) [Sov. Phys. JETP **27**, 328 (1968)].
[21] V. N. Belykh, N. F. Pedersen, and O. H. Soerensen, Phys. Rev. B **16**, 4853 (1977).

This article was published in English in the original Russian journal. Reproduced here with stylistic changes by AIP.

Josephson and spontaneous currents at the interface between two *d*-wave superconductors with transport current in the banks

Yu. A. Kolesnichenko, A. N. Omelyanchouk,* and S. N. Shevchenko

B. Verkin Institute for Low Temperature Physics and Engineering of the National Academy of Sciences of Ukraine, 47 Lenin Ave., 61103, Kharkov, Ukraine
(Submitted November 6, 2003)
Fiz. Nizk. Temp. **30**, 288–294 (March 2004)

A stationary Josephson effect in the ballistic contact of two *d*-wave superconductors with different orientation of the axes and with transport current in the banks is considered theoretically. The influence of the transport current on the current–phase relation of the Josephson and tangential currents at the interface is studied. It is demonstrated that the spontaneous surface current at the interface depends on the transport current in the banks due to the interference of the angle-dependent condensate wave functions of the two superconductors. © *2004 American Institute of Physics.* [DOI: 10.1063/1.1645180]

1. INTRODUCTION

It has been shown that in the ground state of the contact of two *d*-wave superconductors with different orientation of the axes there is a current tangential to the boundary.[1–8] For the particularly interesting case of $\pi/4$ misorientation the ground state is twofold degenerate: there are the tangential currents in opposite directions at $\varphi = \pm \pi/2$ in the absence of Josephson current. The probabilities of finding the contact in one of the two states are equal, and the corresponding tangential current is referred to as the spontaneous one. It has been proposed to use such two-state quantum systems for quantum computation.[9–11] It is of interest to study the possibility of controlling this system by the external transport current, which is the motivation for the present work.

In the above-described problem of the Josephson contact of two *d*-wave superconductors with transport current in the banks, the resulting tangential current is not a sum of the spontaneous and transport current. In Ref. 12 we studied the simpler case of the contact of two *s*-wave superconductors with a transport current flowing in the banks. It was shown that the presence of magnetic field,[13–16] of transport superconducting current,[12] or of current in the normal layer[17,18] in a mesoscopic Josephson junction can significantly influence the current–phase characteristics, current distribution, etc.

In the present problem the Josephson current is determined by the interference of the angle-dependent condensate wave functions of the two superconductors. There are two factors of anisotropy which determine the angle dependence of the order parameter: the pairing anisotropy and the transport current. Thus it is natural to expect that the resulting interference current (which has both normal and tangential components) is parametrized by the external phase difference φ and by the value of the transport current (or by the superfluid velocity v_s). The presence of these two controlling parameters can be useful in the applications of Josephson junctions of high-T_c superconductors.

In Sec. 2 we derive basic equations to describe a ballistic planar Josephson junction of two differently oriented *d*-wave superconductors with uniform current in the banks. These equations are solved analytically in Sec. 3. Then in Sec. 4 we study the influence of the transport current on the Josephson current and *vice versa* at the interface. In the Appendix the order parameter and the current density in the homogeneous situation are considered.

2. MODEL AND BASIC EQUATIONS

We consider a model of the Josephson junction as an ideal plane between two singlet (in particular, *d*-wave) superconductors with different orientation of the axes (see Fig. 1). The pair breaking and the scattering at the junction as well as the electron scattering in the bulk of the metals are ignored. We did not take into account the possibility of the generation of a subdominant order parameter, which results in decreasing of the current amplitude.[7] The *c* axes of both superconductors are parallel to the interface. The *c* axis direction is chosen as the *z* axis. The *a* and *b* axes are situated in the *xy* plane. In the banks of the contact a uniform current flows with a superconducting velocity $\mathbf{v}_s$. We consider the superfluid velocity $\mathbf{v}_s$ in the left (L) and right (R) superconducting half-spaces to be parallel to each other $\mathbf{v}_{sL} \| \mathbf{v}_{sR}$ and to

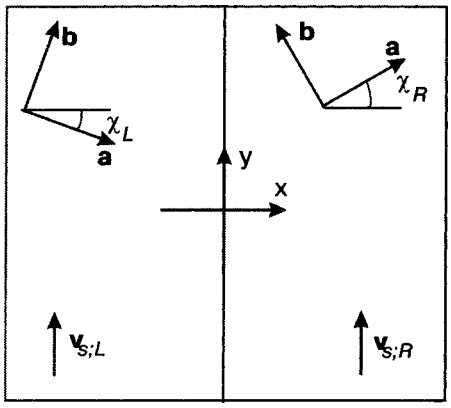

FIG. 1. Geometry of the contact of two superconductors with different orientation of the axes and different transport currents (superfluid velocities $\mathbf{v}_{s;L,R}$) in the banks.

the boundary; we choose the y axis along $\mathbf{v}_s$ and the x axis perpendicular to the boundary; $x=0$ is the boundary plane.

We describe the coherent current state in the superconducting ballistic structure in the quasiclassical approximation by the Eilenberger equation[19,20]

$$\mathbf{v}_F\frac{\partial}{\partial\mathbf{r}}\hat{G}+[\tilde{\omega}\hat{\tau}_3+\hat{\Delta},\hat{G}]=0, \tag{1}$$

where $\tilde{\omega}=\omega_n+i\mathbf{p}_F\cdot\mathbf{v}_s$, $\omega_n=\pi T(2n+1)$ are the Matsubara frequencies, $\hat{G}=\hat{G}_\omega(\mathbf{v}_F,\mathbf{r})=\begin{pmatrix} g & f \\ f^+ & -g\end{pmatrix}$ is the energy-integrated Green function, and $\hat{\Delta}=\begin{pmatrix} 0 & \Delta \\ \Delta^* & 0\end{pmatrix}$. Equation (1) should be supplemented by the equation for the order parameter (the self-consistency equation):

$$\Delta(\mathbf{v}_F,\mathbf{r})=\pi N_0 T\sum_\omega\langle V(\mathbf{v}_F,\mathbf{v}_F')f(\mathbf{v}_F',\mathbf{r})\rangle_{\mathbf{v}_F'}, \tag{2}$$

N_0 is the density of states at the Fermi level and $\langle\ldots\rangle_{\mathbf{v}_F}$ denotes averaging over directions of $\mathbf{v}_F$; $V(\mathbf{v}_F,\mathbf{v}_F')$ is a pairing attractive potential. For the bulk d-wave superconductor it is usually assumed that $\Delta(\theta)=\Delta_0(T,\mathbf{v}_s)\cos 2\theta$ and $V(\mathbf{v}_F,\mathbf{v}_F')=V_d\cos 2\theta\cos 2\theta'$, where the angle θ defines a direction of the velocity $\mathbf{v}_F$. Solutions of Eqs. (1), (2) must satisfy the conditions for the Green functions and gap function in the banks far from the interface:

$$g(\mp\infty)=\frac{\omega_{L,R}}{\Omega_{L,R}}, \tag{3}$$

$$f(\mp\infty)=\frac{\Delta(\mp\infty)}{\Omega_{L,R}}, \tag{4}$$

$$\Delta(\mp\infty)=\Delta_{L,R}\exp(\pm i\varphi/2). \tag{5}$$

Here $\omega_{L,R}=\omega_n+i\mathbf{p}_F\cdot\mathbf{v}_{s,L,R}$, $\Omega_{L,R}=\sqrt{\omega_{L,R}^2+\Delta_{L,R}^2}$; φ is the phase difference between the left and right superconductors, which parametrizes the Josephson current state. The angles $\chi_{L,R}$ define the orientation of the crystal axes **a** and **b** in the left and right half-spaces (see Fig. 1). The angle between the axes of the right and left superconductors (the misorientation angle) is $\delta\chi=\chi_R-\chi_L$.

Provided we know the Green function $\hat{G}$, we can calculate the current density:

$$\mathbf{j}(\mathbf{r})=-2\pi ieN_0T\sum_\omega\langle\mathbf{v}_F g(\mathbf{v}_F,\mathbf{r})\rangle_{\mathbf{v}_F}. \tag{6}$$

For singlet superconductors it is usually assumed that $\Delta(-\mathbf{v}_F)=\Delta(\mathbf{v}_F)$, and we therefore have:

$$f^+(\omega,-\mathbf{v}_F)=f^+(-\omega,\mathbf{v}_F)=f^*(\omega,\mathbf{v}_F), \tag{7}$$

$$g(\omega,-\mathbf{v}_F)=-g(-\omega,\mathbf{v}_F)=g^*(\omega,\mathbf{v}_F). \tag{8}$$

Making use of Eq. (8), we can rewrite Eq. (6) as

$$\mathbf{j}(\mathbf{r})=-j_0\frac{T}{T_c}\sum_{\omega>0}\langle\hat{\mathbf{v}}_F\,\mathrm{Im}\,g(\mathbf{r})\rangle_{\mathbf{v}_F},$$

$$j_0=4\pi|e|N(0)v_FT_c. \tag{9}$$

3. ANALYTICAL SOLUTION OF THE EILENBERGER EQUATION

In this paper we consider the problem non-self-consistently: we assume the superconducting velocity $\mathbf{v}_s$ is uniform and that the order parameter Δ is constant in the two half-spaces:

$$\mathbf{v}_s(\mathbf{r})=\begin{cases}\mathbf{v}_{s;L}, & x<0\\ \mathbf{v}_{s;R}, & x>0\end{cases},\quad \Delta(\mathbf{r})=\begin{cases}\Delta_L\exp(i\varphi/2), & x<0\\ \Delta_R\exp(-i\varphi/2), & x>0\end{cases}. \tag{10}$$

As was shown in Refs. 7, the self-consistent consideration of a Josephson junction of d-wave superconductors does not differ qualitatively from the non-self-consistent treatment. In Ref. 7 the self-consistent solution is compared numerically with the non-self-consistent one. The self-consistency of the solution allows one to take into account the suppression of the order parameter at the interface; the major effect of this is a reduction in the current.[7]

Equation (1), taken together with Eqs. (3)–(5) and (10), yields for the left and right superconductors:

$$g_{LR}(x)=\frac{\omega_{L,R}}{\Omega_{L,R}}+C_{L,R}\exp\left(-\frac{2|x|}{|v_x|}\Omega_{L,R}\right), \tag{11}$$

$$f_{L,R}(x)=\frac{\Delta_{L,R}}{\Omega_{L,R}}e^{-\mathrm{sgn}(x)i\varphi/2}-C_{L,R}\frac{\mathrm{sgn}(x)\,\eta\Omega_{L,R}+\omega_{L,R}}{\Delta_{L,R}}\times\exp\left(-\frac{2|x|}{|v_x|}\Omega_{L,R}\right)e^{-\mathrm{sgn}(x)i\varphi/2}, \tag{12}$$

where $\eta=\mathrm{sgn}(v_x)$. Making use of the continuity condition, we obtain the expression for the g function at the interface:

$$g(0)=\frac{\Omega_L\omega_R+\Omega_R\omega_L-i\,\eta\Delta_L\Delta_R\sin\varphi}{\Omega_L\Omega_R+\omega_L\omega_R+\Delta_L\Delta_R\cos\varphi}. \tag{13}$$

Equations (9) and (13) allow us to calculate the Josephson current $j_J=j_x(x=0)$ and the tangential current $j_y(x=0)$ at the interface. We emphasize that these equations are valid for describing the current at the interface of two singlet superconductors with different orientation of the axes and with different transport currents in the banks. The contact of conventional superconductors was considered in Ref. 12, and in the present paper we study the contact of d-wave superconductors, for which the order parameter is $\Delta_{L,R}\theta=\Delta_0(T,\mathbf{v}_{s;L,R})\cos 2(\theta-\chi_{L,R})$. The treatment presented here can be also used to consider the contact of g-wave superconductors or an s-wave/d-wave contact, etc.

As we restrict ourselves to the non-self-consistent model, we should calculate the order parameter $\Delta_0=\Delta_0(T,\mathbf{v}_s)$ in the bulk d-wave superconductor. That is the subject of the Appendix.

In the particular case considered in detail below, we have $\mathbf{v}_{s;L}=\mathbf{v}_{s;R}=\mathbf{v}_s$ and denote $\tilde{\omega}=\omega_n+i\mathbf{p}_F\cdot\mathbf{v}_s$, $\Omega_{L,R}=\sqrt{\tilde{\omega}^2+\Delta_{L,R}^2}$; in this case we obtain

$$g(0)=\frac{\tilde{\omega}(\Omega_L+\Omega_R)-i\,\eta\Delta_L\Delta_R\sin\varphi}{\Omega_L\Omega_R+\tilde{\omega}^2+\Delta_L\Delta_R\cos\varphi}. \tag{14}$$

In the absence of the transport current ($\mathbf{v}_s=0$) in this expression: $\tilde{\omega}=\omega_n$ (Ref. 7).

We should also clarify the sign of the square root in $\Omega_{L,R}$. To make the solution (11) convergent, we must re-

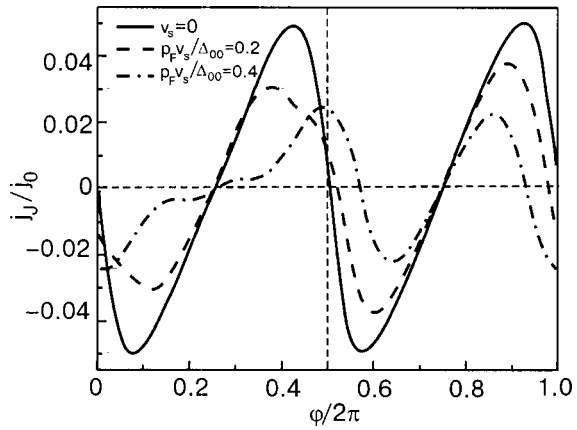

FIG. 2. Josephson current density through the interface j_J versus phase φ ($\chi_L=0, \chi_R=\pi/4, T=0.1T_c$); $\Delta_{00}=\Delta_0(T=0, v_s=0)=2.14T_c$.

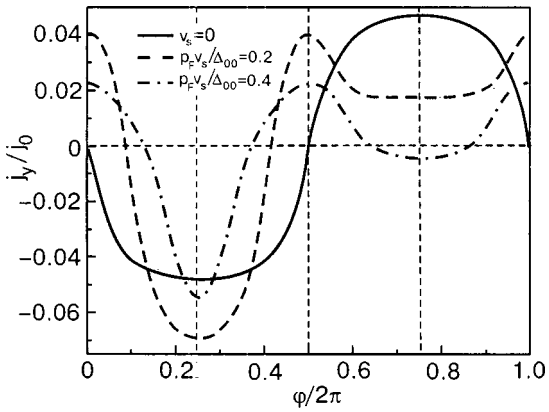

FIG. 3. Fig. 3. Tangential current density at the interface j_y versus phase φ ($\chi_L=0, \chi_R=\pi/4, T=0.1T_c$).

quire $\mathrm{Re}\,\Omega_{L,R}>0$, which fixes the sign of the square root in $\Omega_{L,R}$ to be $\mathrm{sgn}(\omega \mathbf{p}_F \cdot \mathbf{v}_{s;L,R})$. Moreover, this requirement, as can be shown, provides a supplementary condition on $\mathrm{Re}\,g$: $\mathrm{sgn}(\mathrm{Re}\,g)=\mathrm{sgn}(\omega)$.

4. INFLUENCE OF THE TRANSPORT CURRENT ON THE JOSEPHSON AND SPONTANEOUS CURRENTS AT THE INTERFACE

Below we study the Josephson contact for the particular case when $\mathbf{v}_{sL}=\mathbf{v}_{sR}=\mathbf{v}_s$ and $\chi_L=0$ and $\chi_R=\pi/4$.

For small values of v_s (in the approximation linear in $p_F v_s/T_c$) we can state the following approximate relations (which are valid for values of φ in the vicinity of $\pm\pi/2$):

$$j_J(-\mathbf{v}_s,\varphi)\simeq j_J(\mathbf{v}_s,\varphi),$$

$$j_y(-\mathbf{v}_s,\varphi)\simeq -j_y(\mathbf{v}_s,-\varphi),$$

and for the difference $\delta j \equiv j(\mathbf{v}_s)-j(\mathbf{v}_s=0)$:

$$\delta j_J(-\varphi)\simeq -\delta j_J(\varphi),\quad \delta j_y(-\varphi)\simeq \delta j_y(\varphi),$$

while at $\mathbf{v}_s=0$

$$j_J(-\varphi)=-j_J(\varphi),\quad j_y(-\varphi)=-j_y(\varphi).$$

In the linear approximation the shift current δj_y is an even function of φ, in contrast to $j_y(\mathbf{v}_s=0)$. For the spontaneous current (at $\varphi=\pm\pi/2$) the shift currents δj_y are equal:

$$j_y(\varphi=\pm\pi/2)=j_S+\delta j_y. \tag{15}$$

$$j_S(-\pi/2)=-j_S(\pi/2),\quad \delta j_y(-\pi/2)=\delta j_y(\pi/2).$$

In a nonlinear treatment these shift currents are different for the two cases and are discussed below.

In Figs. 2 and 3 we plot the normal (Josephson) and tangential components of the current densities at the plane of the interface as functions of the phase difference φ at low temperature. In the absence of the transport current: (i) $\mathbf{j}$ is an odd function of φ; (ii) the normal component of the current (Josephson current) is π-periodic; (iii) in the equilibrium state at $\varphi=\pm\pi/2$: $j_J=0$, $j_y(\pm\pi/2)=j_S=\mp|j_S|$. This being the case, the tangential current exists in the absence of the Josephson current; for that reason it is referred to as the spontaneous current. The presence of the transport current breaks the symmetry relations (i)–(iii). There is a nonzero Josephson current at $\varphi=0,\pi$. How the transport current influences the spontaneous current (i.e., the tangential current at $\varphi=\pi/2$ and $\varphi=-\pi/2$) is shown in Fig. 4. The shift of the two values of the current for small values of v_s (in the approximation linear in $p_F v_s/T_c$) is equal [see Eq. (15)]; however, at values $v_s\sim 0.2\Delta_{00}/p_F$ the shift current (i.e., the difference $j_y(\mathbf{v}_s)-j_S(\mathbf{v}_s=0)$) is of different sign for the two currents and in the directions opposite to j_S.

We also note the following relations for $\mathbf{v}_s\neq 0$: 1) $j_J(\varphi=\pi)=-j_J(\varphi=0)\neq 0$ (the presence of the transport current induces a nonzero Josephson current in the absence of an external phase difference); 2) $j_J(\varphi=\pm\pi/2)=0$, $dj_J/d\varphi\times(\varphi=\pm\pi/2)>0$ (the transport current does not change the values of the equilibrium phase difference, at $\varphi\pm\pi/2$); 3) $j_y(\varphi=\pi)=j_y(\varphi=0)\neq 0$. This last relation concerns the interesting phenomena studied in Ref. 12: for some values of the phase difference (here in the vicinity of $\varphi=0,\pi$) the interference of the angle-dependent condensate wave functions results in the appearance of an additional tangential current with the direction opposite to the transport current in the banks. We emphasize that the resulting tangential current is not the sum of the spontaneous current and the transport current.[12] Thus, the transport current drastically influences both the tangential (spontaneous) and Josephson currents.

We can write down explicitly an expression for the cur-

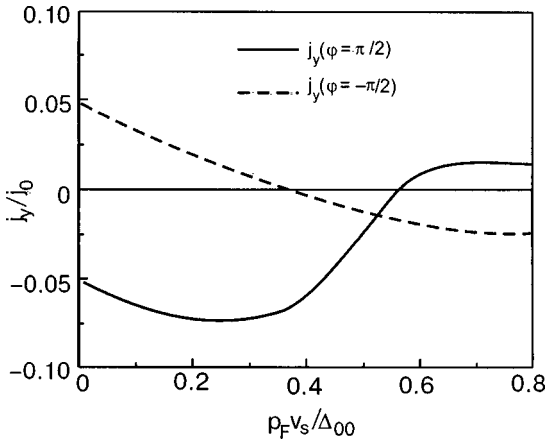

FIG. 4. Tangential current density at the interface j_y for two values of the phase difference (spontaneous current) versus superfluid velocity v_s ($\chi_L=0, \chi_R=\pi/4, T=0.1T_c$).

rent for temperatures close to the critical (so close that $\Delta_0, p_F v_s \ll T_c$). From Eq. (14) we have:

$$\mathrm{Im}\, g(0) \simeq \Delta_L \Delta_R \left[-\eta \frac{1}{2\omega_n^2} \sin\varphi + \frac{\mathbf{p}_F \mathbf{v}_s}{\omega_n^3} \cos\varphi + \eta \frac{3}{2} \frac{(\mathbf{p}_F \mathbf{v}_s)^2}{\omega_n^4} \sin\varphi + \eta \frac{\Delta_L \Delta_R}{8\omega_n^4} \sin 2\varphi \right]. \quad (16)$$

At $\chi_L = 0$ and $\chi_R = \pi/4$ this results in the following:

$$\mathbf{j} = \mathbf{j}_J + \mathbf{j}_S + \tilde{\mathbf{j}}, \quad (17)$$

$$\mathbf{j}_J = -\frac{1}{3024\pi} j_0 \frac{\Delta_0^4}{T_c^4} \sin 2\varphi \cdot \mathbf{e}_x, \quad (18)$$

$$\mathbf{j}_S = -\frac{1}{60\pi} j_0 \frac{\Delta_0^2}{T_c^2} \sin\varphi \cdot \mathbf{e}_y, \quad (19)$$

$$\tilde{\mathbf{j}} = \frac{3}{560\pi} j_0 \frac{\Delta_0^2}{T_c^2} \frac{(p_F v_s)^2}{T_c^2} \sin\varphi \cdot \mathbf{e}_y. \quad (20)$$

Here $\Delta_0 = \Delta_0(T, v_s)$ and is defined by Eq. (25). In particular, at $v_s = 0$ this gives:

$$j_J = -1.7 \times 10^{-2} j_0 \left(1 - \frac{T}{T_c}\right)^2 \sin 2\varphi, \quad (21)$$

$$j_S = -6.6 \times 10^{-2} j_0 \left(1 - \frac{T}{T_c}\right) \sin\varphi. \quad (22)$$

We note that $\tilde{\mathbf{j}} = -\frac{9}{28}[(p_F v_s)^2/T_c^2]\mathbf{j}_S$. It follows that the effect of transport current on the spontaneous tangential current at $T \sim T_c$ is to reduce its value by a small shift. It is remarkable that the current tangential to the boundary contains only corrections of the second order in the parameter $p_F v_s / T_c$.[1)] If $\chi_L = 0$ and $\chi_R = \delta\chi \neq \pi/4$, the integration of the second term in Eq. (16) would give us the factor $\pi \cos^2 \delta\chi - \pi/2$, which is zero for $\delta\chi = \pi/4$; this term at $\delta\chi = 0$ and $\varphi = 0$ gives the uniform current density (Eq. (26)).

The integration of the first term in Eq. (16) gives us the factor $\cos 2\delta\chi$ for the x component of the current and $\sin 2\delta\chi$ for the y component. In the case $\delta\chi = \pi/4$ this term gives only the tangential component. As a consequence $j_S \gg j_J$ [see Eqs. (21), (22)].

It was discussed above that the terms linear in $p_F v_s / T_c$ result in a uniform shift of j_S. We can see that nonlinear terms result in a shift of different sign, and in both cases in the direction opposite to j_S [see Eq. (20)]. This in part explains the nonmonotonic behavior of j_y (see Fig. 4). The fact that the presence of the transport current significantly changes the tangential (spontaneous) currents might be used for its control, which is important in view of their possible application for quantum computation.[9–11]

5. CONCLUSION

We have studied influence of the transport current, which flows in the banks, on the stationary Josephson effect in the contact of two d-wave superconductors. We have derived equations which allow general consideration of the contact of two singlet superconductors with different orientation of the axes and with different transport currents in the banks. In particular, we have studied the planar contact of two d-wave superconductors in the case of $\pi/4$ misorientation with equal transport currents in the banks. It was demonstrated that the current–phase relation depends drastically on the value of the transport current. The ground state degeneracy in the absence of transport current (at $\varphi = \pm\pi/2$) is lifted at $v_s \neq 0$. The dependence of the shift current (which is the difference of the tangential current and the spontaneous one) on v_s is shown to be nonlinear. It is proposed to use the transport current for the control of qubits based on the contact of two d-wave superconductors.

We acknowledge support from D-Wave Systems, Inc. (Vancouver).

Results of the present study were reported at the International Conferences: ''Applied Electrodynamics of High-T_c Superconductors,'' IRE, Kharkov, Ukraine (May 2003) and ''Basic Studies and Novel Applications,'' Jena, Germany (June 2003).

6. APPENDIX. ORDER PARAMETER IN THE HOMOGENEOUS CURRENT STATE

In this Section we study the homogeneous current state in the bulk d-wave superconductor (see also Ref. 21). We note that the order parameter Δ_0 is a function of temperature T, superfluid velocity v_s, and the angle χ between the crys-

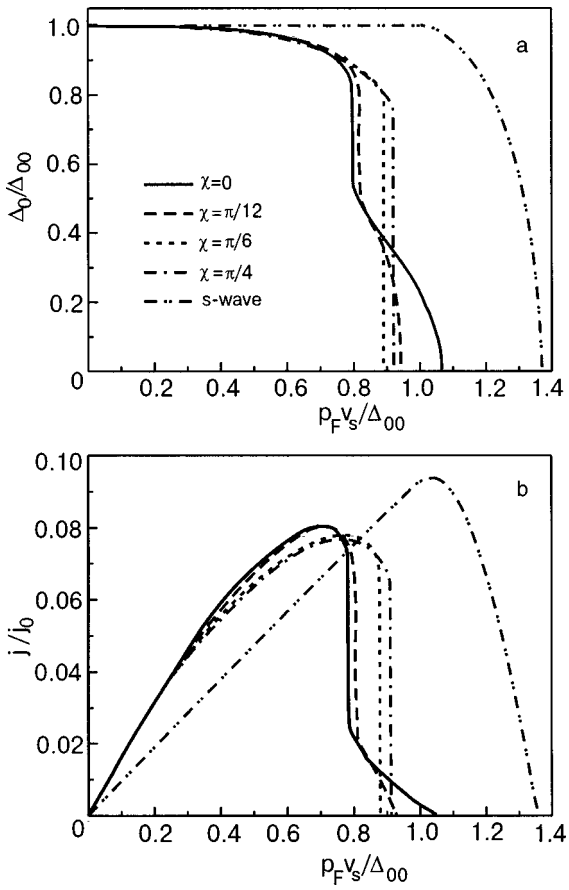

FIG. 5. Order parameter $\Delta_0(T, \mathbf{v}_s)$ (a) and current density (b) in a bulk d-wave superconductor versus superfluid velocity v_s for different angles χ between $\mathbf{v}_s$ and the **a** axis ($T = 0$).

tallographic axis a and the direction of the superfluid velocity $\mathbf{v}_s$. For that we must solve Eqs. (2) and (9) with g and f given by Eqs. (3) and (4):

$$\frac{1}{\lambda}=2T\sum_{\omega>0}\int_{-\pi/2}^{\pi/2}d\theta\,\mathrm{Re}\frac{\Delta^2(\theta)/\Delta_0^2}{\Omega},$$

$$\frac{\mathbf{j}}{j_0}=-\frac{T}{\pi T_c}\sum_{\omega>0}\int_{-\pi/2}^{\pi/2}d\theta\hat{\mathbf{v}}_F\,\mathrm{Im}\frac{\tilde{\omega}}{\Omega}.$$

Here $\lambda=N_0V_d$, $\tilde{\omega}=\omega_n+i\mathbf{p}_F\cdot\mathbf{v}_s$, $\Omega=\sqrt{\tilde{\omega}^2+\Delta^2}$, $\Delta(\theta)=\Delta_0(T,\mathbf{v}_s)\cos 2(\theta-\chi)$.

For $T=0$ (replacing $\pi T\Sigma_\omega$ by the integral $\int d\omega$) we obtain the equations for the order parameter Δ_0 and the current density j:

$$\ln\left(\frac{\Delta_{00}}{\Delta_0}\right)=\frac{2}{\pi}\int d\theta\left(\frac{\Delta(\theta)}{\Delta_0}\right)^2\ln\left(\left|\frac{\mathbf{v}_s\cdot\mathbf{p}_F}{\Delta(\theta)}\right|+\sqrt{\left(\frac{\mathbf{v}_s\cdot\mathbf{p}_F}{\Delta(\theta)}\right)^2-1}\right),\tag{23}$$

where $\Delta_{00}=\Delta_0(T=0,v_s=0)=\xi\omega_c\mathrm{e}^{-2/\lambda}$, $\xi=4\mathrm{e}^{-1/2}$, and

$$\frac{j}{j_0}=-\frac{1}{4\pi}\frac{v_sp_F}{T_c}+\frac{1}{2\pi^2}\int d\theta|\cos\theta|\sqrt{\left(\frac{\mathbf{v}_s\cdot\mathbf{p}_F}{T_c}\right)^2-\left(\frac{\Delta(\theta)}{T_c}\right)^2}.\tag{24}$$

In Eqs. (23) and (24) the integration is performed in the region where $\Delta(\theta)^2<(\mathbf{v}_s\cdot\mathbf{p}_F)^2$ for $\theta\in(-\pi/2,\pi/2)$.

In Figs. 5 we plot the order parameter $\Delta_0(T,\mathbf{v}_s)$ and the current density versus the superfluid velocity v_s for different angles χ at low temperature. For comparison we also plot the curves for the s-wave superconductor. A numerical analysis at low temperature shows that in spite of the strong anisotropy of the pairing potential, the order parameter Δ_0, the critical velocity v_s^{cr}, and the critical current j_c depend weakly on the angle χ between $\mathbf{v}_s$ and the crystallographic a axis (see Figs. 5 and in Ref. 21). Namely, the respective difference is maximal for $\chi=0$ and $\chi=\pi/4$ and does not exceed 0.1. For small values of the superfluid velocity, i.e., in the approximation linear in the parameter v_sp_F/T_c, both Δ_0 and j are independent of χ.

For a temperature close to $T_c=\beta\omega_c\mathrm{e}^{-2/\lambda}=0.47\Delta_{00}$, where $\beta=(2/\pi)e^C$, (C is the Euler constant), both the gap function Δ_0 and current density j are independent of the angle χ:

$$\Delta_0^2=\frac{32\pi^3}{21\zeta(3)}T_c^2\left(1-\frac{T}{T_c}\right)-\frac{4}{3}(p_Fv_s)^2,\tag{25}$$

$$\frac{j}{j_0}=-\frac{7\zeta(3)}{32\pi^3}\frac{\Delta_0^2}{T_c^2}\frac{p_Fv_s}{T_c}.\tag{26}$$

The temperature dependence of the critical velocity v_s^{cr} follows from Eq. (25): $p_Fv_s^{\mathrm{cr}}/T_c=\sqrt{8\pi^2/7\zeta(3)}\sqrt{1-T/T_c}$.

*E-mail: omelyanchouk@ilt.kharkov.ua

[1)]There is also a term with the factor $(p_fv_s/T_c)(\Delta_0^4/T_c^4)$, which is neglected here. This term results in equal shifts of j_S for $\varphi=\pm\pi/2$.

[1] S. Yip, Phys. Rev. B **52**, 3087 (1995).
[2] M. Matsumoto and H. Shiba, J. Phys. Soc. Jpn. **65**, 2194 (1996).
[3] A. Huck, A. van Otterlo, and M. Sigrist, Phys. Rev. B **56**, 14163 (1997).
[4] M. Sigrist, Prog. Theor. Phys. **99**, 899 (1998).
[5] T. Löfwander, V. S. Shumeiko, and G. Wendin, Phys. Rev. B **62**, R14653 (2000).
[6] S. Kashiwaya and Y. Tanaka, Rep. Prog. Phys. **63**, 1641 (2000).
[7] M. H. S. Amin, A. N. Omelyanchouk, and A. M. Zagoskin, Phys. Rev. B **63**, 212502 (2001); M. H. S. Amin, A. N. Omelyanchouk, S. N. Rashkeev, M. Coury, and A. M. Zagoskin, *ibid.* **318**, 162 (2002).
[8] E. Il'ichev *et al.*, Phys. Rev. Lett. **86**, 5369 (2001).
[9] L. B. Ioffe *et al.*, Nature (London) **398**, 679 (1999).
[10] A. Blais and A. M. Zagoskin, Phys. Rev. A **61**, 042308 (2000); A. M. Zagoskin, J. Phys.: Condens. Matter **9**, L419 (1997).
[11] M. H. S. Amin, A. Yu. Smirnov, and A. M. Zagoskin *et al.*, arXiv:cond-mat/0310224 (2003).
[12] Yu. A. Kolesnichenko, A. N. Omelyanchouk, and S. N. Shevchenko, Phys. Rev. B **67**, 172504 (2003).
[13] J. P. Heida, B. J. van Wees, T. M. Klapwijk, and G. Borghs, Phys. Rev. B **57**, R5618 (1998).
[14] V. Barzykin and A. M. Zagoskin, Superlattices Microstruct. **25**, 797 (1999).
[15] Urs Lederman, Alban L. Fauchere, and Gianni Blatter, Phys. Rev. B **59**, R9027 (1999).
[16] M. H. S. Amin, A. N. Omelyanchouk, and A. M. Zagoskin, Fiz. Nizk. Temp. **27**, 835 (2001) [Low Temp. Phys. **27**, 616 (2001)].
[17] A. Morpurgo, B. J. van Wees, and T. M. Klapwijk, Appl. Phys. Lett. **72**, 966 (1998).
[18] F. K. Wilhelm, G. Shön, and A. D. Zaikin, Phys. Rev. Lett. **81**, 1682 (1998).
[19] G. Eilenberger, Z. Phys. **214**, 195 (1968).
[20] I. O. Kulik and A. N. Omelyanchouk, Fiz. Nizk. Temp. **4**, 296 (1978) [Sov. J. Low Temp. Phys. **4**, 142 (1978)].
[21] J. Ferrer, M. A. Gonzalez-Alvarez, and J. Sanchez-Canizares, Superlattices Microstruct. **25**, 1125 (1999).

This article was published in English in the original Russian journal. Reproduced here with stylistic changes by AIP.

LOW-TEMPERATURE MAGNETISM

Magnetic phase diagram of the manganites $Bi_{1-x}Sr_xMnO_3$

O. S. Mantytskaya, I. O. Troyanchuk,* and A. N. Chobot

Institute of Solid State and Semiconductor Physics of the National Academy of Sciences of Belarus, ul. P. Brovki 17, Minsk 220072, Belarus

H. Szymczak

Institute of Physics of the Polish Academy of Sciences, 02-668 Warsaw, Poland
(Submitted December 9, 2002; revised November 6, 2003)
Fiz. Nizk. Temp. **30**, 295–303 (March 2004)

An experimental study of the crystal structure and the magnetic and elastic properties of the manganites $Bi_{1-x}Sr_xMnO_3$ is carried out. The following phase transformations are found: ferromagnet ($x<0.15$)–spin glass ($0.15\leqslant x\leqslant 0.25$)–charge-ordered antiferromagnet ($0.35 \leqslant x\leqslant 0.8$). The ferromagnetic state corresponds to ordering of the orbitals of the Mn^{3+} ions. It is assumed that the orbitally disordered phase is not realized in the $Bi_{1-x}Sr_xMnO_3$ system in the concentration interval $0.15\leqslant x\leqslant 0.35$. Samples with $0.25\leqslant x\leqslant 0.8$ undergo a first-order transition of the crystal structure, attributed to ordering of the Mn^{3+} and Mn^{4+} ions in the ratios 1:1 ($x\leqslant 0.6$) and 1:3 ($x\geqslant 0.7$). The antiferromagnetic charge-ordered and spin glass phases coexist in samples with $0.25<x<0.35$, possibly because of the martensitic character of the charge order–disorder phase transformation. A hypothetical magnetic phase diagram is constructed. © *2004 American Institute of Physics.* [DOI: 10.1063/1.1645181]

1. INTRODUCTION

$A_{1-x}B_xMnO_3$ oxides with the perovskite structure (B $=Ca^{2+}$, Sr^{2+}, Pb^{2+}, Ba^{2+}) are magnetic semiconductors in which a strong interrelationship between the magnetic and electrical properties is observed. These compounds are of particular interest in connection with the giant magnetoresistance effect observed in them at temperatures near the Curie point.[1]

Perovskites with the chemical formula $LnMnO_3$ (Ln $=$La, Y, rare-earth ion) are antiferromagnets with magnetic structure of the *A* type and, according to Ref. 2, are characterized by O' orthorhombic distortions of the unit cell ($c/\sqrt{2}<a<b$) due to ordering of the e_g orbitals of the Mn^{3+} ions. The ferromagnetism of manganites doped with the alkaline-earth ions Ca^{2+}, Sr^{2+}, Pb^{2+}, and Ba^{2+} is due to the positive exchange interaction between the ions $Mn^{4+}-Mn^{3+}$ (Refs. 2 and 3). According to the double exchange theory, the ferromagnetic properties of the manganites are due to real transitions of the charge carriers between manganese ions, i.e., to the appearance of heterovalent manganese ions. For example, substitution of the La^{3+} ion by Sr^{2+} in the system $La_{1-x}Sr_xMnO_3$ is accompanied by an antiferromagnet–ferromagnet transition at $x=0.12$ (Ref. 4). Magnetic measurements show that $La_{2/3}Sr_{1/3}MnO_3$ is a ferromagnet with the highest Curie temperature ($T_C=375$ K) among the orthomanganites with the perovskite structure.

The properties of $BiMnO_3$ give it a distinctive place among the $AMnO_3$ manganites. This compound is a ferromagnet with a temperature of the transition to the paramagnetic state of around 100 K.[5,6] The crystal structure is characterized by triclinic distortions. Substitution of the Bi^{3+} ion by Sr^{2+} in the $Bi_{1-x}Sr_xMnO_3$ system leads to a decrease of the spontaneous magnetization.[6] Although the conductivity increases gradually, this compound does not become metallic at concentrations up to $x=0.67$ (Ref. 7). Another extremely interesting property of bismuth manganite doped with strontium ions is the very high charge- ordering temperature T_{co} (around 550 K) observed in the compound $Bi_{0.5}Sr_{0.5}(Mn^{3+}_{0.5}Mn^{4+}_{0.5})O_3$ (Refs. 8 and 9).

Despite the differences in magnetic properties and crystal structure, bismuth manganite, like the rare-earth manganites, is an insulator. It has been hypothesized that the cause of the behavior described is a special type of orbital ordering, different from that in rare-earth manganites.[10] Recent structural studies[11] confirm that hypothesis.

The goal of the present study is to establish the mechanism of the concentration phase transformations, both ferromagnet–antiferromagnet and charge order–disorder, in the $Bi_{1-x}Sr_xMnO_3$ system.

2. EXPERIMENTAL TECHNIQUE

Solid solutions of the series $Bi_{1-x}Sr_xMnO_3$ ($0.2\leqslant x \leqslant 0.8$) were obtained by the usual ceramic method from stock consisting of oxides and carbonates with a purity of 99.99% or better. The initial components were mixed in the stoichiometric ratio. A preliminary annealing was done in air at 900 °C for 6 h. Synthesis was carried out in air at 1100–1250 °C for 2h. The synthesis temperature was increased uniformly with increasing strontium concentration. The samples were slowly cooled (100 °C per hour) in an oven. The temperature was maintained to a precision of

± 5 °C. The perovskites $BiMnO_3$ and $Bi_{0.9}Sr_{0.1}MnO_3$ were obtained under conditions of high pressure ($P=5$ GPa, $T=900$ °C).

The $Bi_{0.75}Sr_{0.25}MnO_3$ sample was reduced after synthesis. This was done by placing it in an evacuated ($P \sim 10^{-4}$ Pa) quartz ampoule together with a definite amount of metallic tantalum, which was used as an oxygen absorber. The quartz ampoule was held at 900 °C for 10 h and then cooled to room temperature at a rate of 100 degrees per hour.

An x-ray structural analysis on a DRON-3 diffractometer in CrK_α radiation showed that all of the components are single-phase perovskites. The angular position of the diffraction peaks was determined to an absolute error of $\pm 0.01°$. To improve the accuracy, the calculations were done using reflections lying above 60°. The unit cell parameters were determined to an accuracy of 0.001 Å or better. The specific magnetization was measured on a Foner vibrating sample magnetometer in fields up to 16 kOe with an accuracy of 10^{-2} G·cm^3/g or better. For studying the elastic properties we measured the temperature dependence of the resonance frequency in the excitation of mechanical vibrations in the sample, the square of the resonance velocity ν^2 being proportional to the Young's modulus. The studies were done on samples of cylindrical shape 50–55 mm long and 5 mm in diameter. The rate of change of the temperature was 2 °C per minute. The resonance frequency was determined to an accuracy of ± 1 Hz.

The electrical conductivity was determined by the standard four-probe method on samples with dimensions of $2 \times 2 \times 10$ mm with a relative error of 0.6%. The contacts were formed by the ultrasonic deposition of indium. During the investigations of the magnetic and electrical properties of the samples the temperature was maintained to a precision of ± 1 K.

3. RESULTS AND DISCUSSION

According to the results of an x-ray structural analysis, the samples with strontium concentrations $x=0.20$, 0.22, and 0.25 were characterized by a monoclinic unit cell. Compositions in the interval $0.3 \leqslant x \leqslant 0.8$ had a tetragonally distorted unit cell. It should be noted that the diffraction peaks were rather narrow, indicating a uniform chemical composition and a perfect crystal lattice. Synthesis under conditions of high pressure and quenching from 1000 °C had little effect on the unit cell parameters.

Table I gives the unit cell parameters of some of the solid solutions obtained. Analysis of the tabulated data shows that the degree of tetragonal distortion, reflected in the ratio c/a, reaches a maximum value at $x=0.5$. It is also characteristic that the parameter a remains practically unchanged as x increases from 0.35 to 0.5 and then decreases linearly with further increase of x to 0.75. The parameter c, on the contrary, decreases in the region $x=0.35-0.5$ and remains practically unchanged for $x=0.5-0.75$. The unit cell volume shows a gradual decrease with increasing strontium concentration.

Our sample of the compound $BiMnO_3$ has a Curie temperature $T_C=104$ K and a magnetic moment, estimated from the field dependence of the magnetization, of around $3.3\mu_B/Mn^{3+}$, in good agreement with published data.[5,6]

TABLE I. Unit cell parameters of the compounds for different strontium concentrations.

Composition, x	Symmetry	Parameters, Å	c/a	V, Å^3
0	Tr	$a=c=7.86$, $b=7.98$, $\alpha=91.20$, $\beta=90.35$		246.36
0.25	M	$a=3.894$, $b=3.925$ $c=3.992$, $\beta=90.47$		61.01
0.35	T	$a=3.926$, $c=3.856$	0.982	59.45
0.40	T	$a=3.927$, $c=3.839$	0.978	59.20
0.42	T	$a=3.914$, $c=3.803$	0.972	58.24
0.50	T	$a=3.909$, $c=3.794$	0.971	57.96
0.58	T	$a=3.901$, c=3.791	0.972	57.68
0.60	T	$a=3.882$, $c=3.795$	0.976	57.19
0.70	T	$a=3.869$, $c=3.791$	0.980	56.74
0.75	T	$a=3.866$, $c=3.793$	0.981	56.69
0.80	T	$a=3.855$, $c=3.813$	0.989	56.67

Note: Tr stands for triclinic, T for tetragonal, and M for monoclinic symmetry.

Small substitutions of Bi^{3+} by Sr^{2+} led to a sharp decrease in the strength of the ferromagnetic exchange interactions. The $Bi_{0.9}Sr_{0.1}MnO_3$ sample had $T_C=80$ K and a magnetic moment of around $2.3\mu_B/Mn^{3+}$. The magnetization does not reach saturation in fields up to 16 kOe. The magnetic properties of this solid solution contrast sharply with those of the rare-earth manganites $Ln_{1-x}Sr_xMnO_3$ (Ln=La, Pr, Nd, Sm, Eu), in which substitution of a small fraction (10%) of the Ln ions by Sr ions stabilizes the ferromagnetic state.[12]

Figure 1 shows the results of a study of the temperature dependence of the specific magnetization of solid solutions in the concentration interval $0.2 \leqslant x \leqslant 0.35$ during heating of the samples after zero-field cooling (ZFC) and after cooling in a rather weak field of 100 Oe (field cooling, FC). It should be noted that for all the samples the FC and ZFC curves diverge near 40 K. Above that temperature the curves practically coincide. The magnetic ordering temperature determined from the inflection point of the ZFC curve decreases monotonically with increasing strontium concentration. The magnetization in a field $H=15$ kOe at a temperature of 5 K is far from saturation (Fig. 2).

Figure 3 shows the magnetic properties of the sample with $x=0.25$ before and after reduction. For the stoichiometric $Bi_{0.75}Sr_{0.25}MnO_3$ an appreciable growth of the specific magnetization $M(T)$ in a field of 10 kOe is observed with decreasing temperature below 80 K (Fig. 3a). We attribute this to growth of the number of superparamagnetic clusters with a type of short-range magnetic order peculiar to $BiMnO_3$. The value of the specific magnetization of the reduced sample was strongly diminished. The curve of $M(T)$ in a field of 5 kOe in this case (Fig. 3b) has a pronounced kink, which can be linked to the antiferromagnetic ordering temperature, at around $T_N=150$ K. This indicates that some

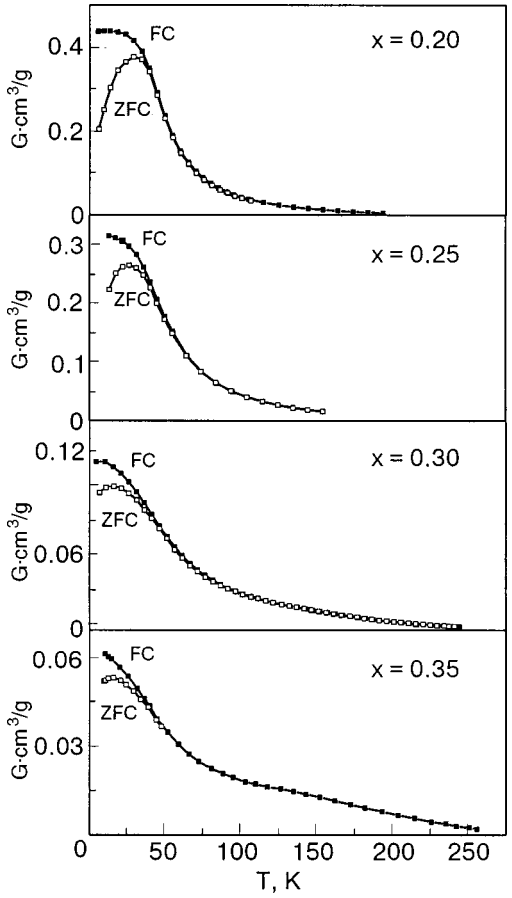

FIG. 1. ZFC and FC magnetization as functions of temperature for solid solutions with compositions $0.20 \leqslant x \leqslant 0.35$, measured in a field $H = 100$ Oe.

regions in the stoichiometric compounds with $x = 0.25$ are also antiferromagnetically ordered, with $T_N = 150$ K. It is known[13,14] that the antiferromagnetic component of the exchange interactions should increase with increasing concentration of oxygen vacancies, as is observed for the compound $Bi_{0.75}Sr_{0.25}MnO_{3-\gamma}$.

For stoichiometric samples with $0.35 \leqslant x \leqslant 0.6$ anomalous behavior of the specific magnetization was also observed near 150 K (Fig. 4). The clearest anomaly was ob-

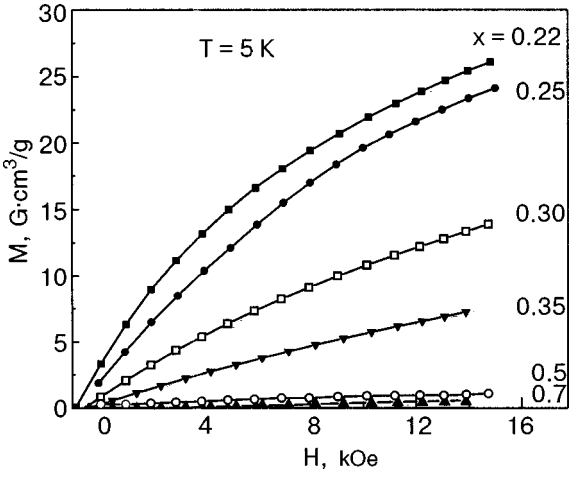

FIG. 2. Field curves of the specific magnetization for compounds with $0.22 \leqslant x \leqslant 0.7$ at $T = 5$ K.

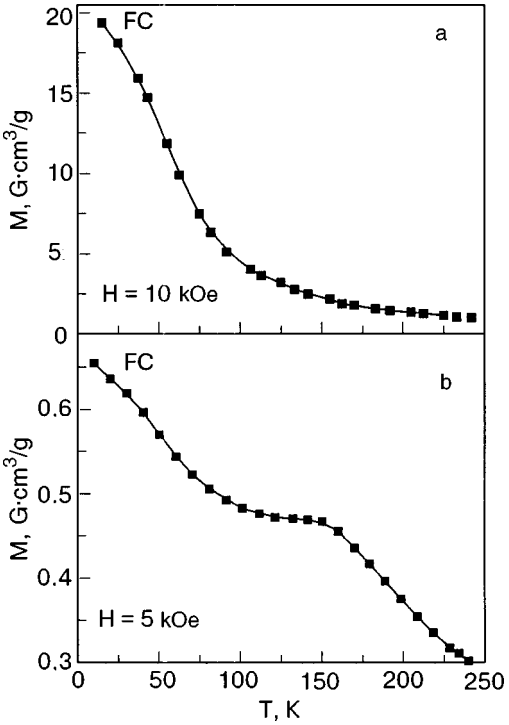

FIG. 3. Temperature dependence of the specific magnetization for a compound with $x = 0.25$ before (a) and after (b) the sample was reduced.

served for the compound with $x = 0.6$. It was also at 150 K that antiferromagnetic ordering was observed in $Bi_{0.5}Sr_{0.5}MnO_3$ in a neutron-diffraction study.[8] We therefore attribute the anomalous behavior of $M(T)$ near T_N to antiferromagnetic ordering. For compounds with $x = 0.35$, 0.42, and 0.5 the magnetic ordering temperatures are determined from magnetic measurements (Fig. 4) as the points of intersection of the approximating straight lines and are equal to 153, 150, and 140 K, respectively. The magnetic behavior was qualitatively different in the concentration interval $0.7 \leqslant x \leqslant 0.8$. The specific magnetization of compounds with $x = 0.75$ and 0.8 begins to increase as room temperature is approached. For technical reasons we could not measure the magnetization at temperatures above 380 K, but it is seen that the specific magnetization of the sample with $x = 0.75$ is maximum near $T_{co} = 380$ K (inset in Fig. 4d). The Néel point apparently lies below that temperature. We assume that $T_N = 260$ K, since a kink is observed in the $M(T)$ curve near that temperature. It should be noted that anomalous behavior of the specific magnetization due to magnetic ordering is expressed very weakly in the $Bi_{1-x}Sr_xMnO_3$ system, making it difficult to determine the Néel point. We assume that the true values of the magnetic ordering temperature may differ by 5–10 K from the values given in this paper. Precise determination of T_N will require neutron-diffraction measurements.

Additional information was obtained from a study of the elastic properties (Fig. 5). The $\nu^2(T)$ curve was found to have a minimum for all the samples in the concentration interval $0.25 \leqslant x \leqslant 0.75$. The anomalous behavior of the Young's modulus may be due to the presence of a structural phase transformation in the crystal. The temperature of this phase transformation decreases with increasing strontium content, from $T_{c0} = 600$ K ($x = 0.25$) to $T_{co} = 375$ K (x

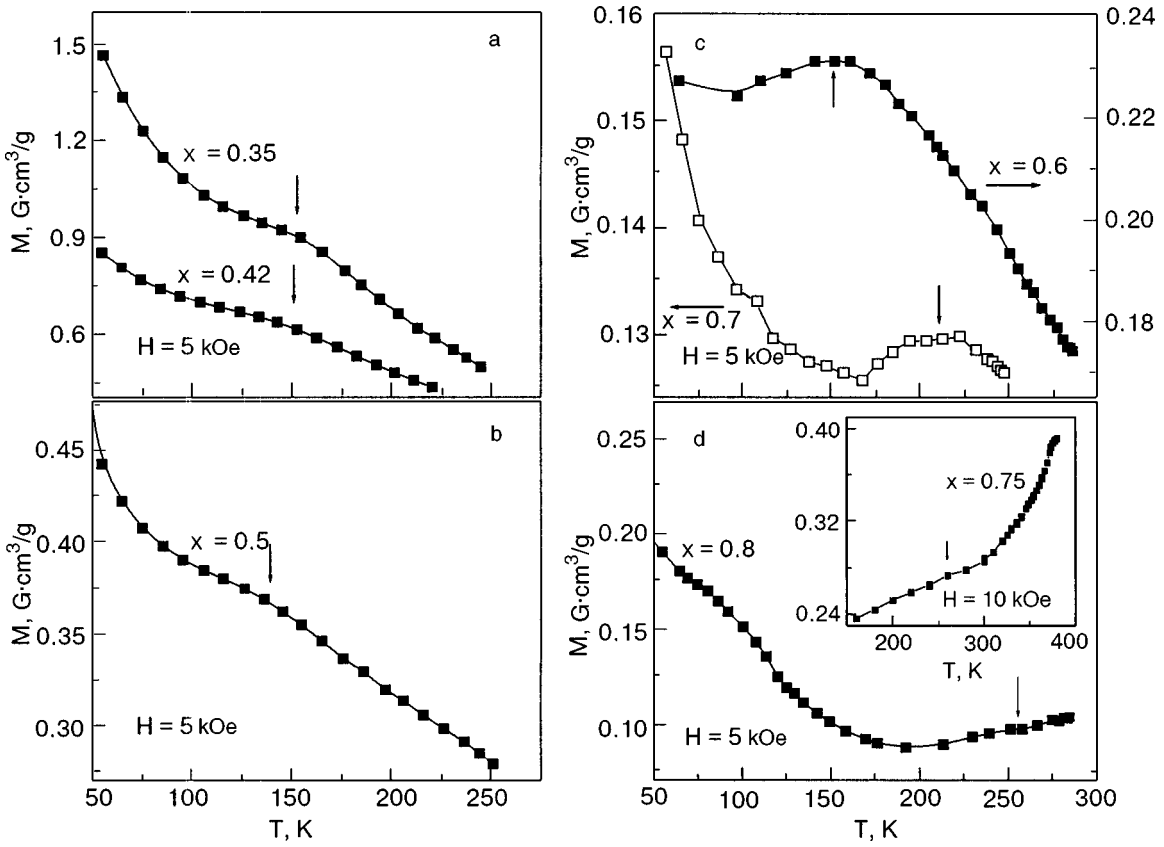

FIG. 4. Temperature dependence of the magnetization for samples with $x=0.35$, 0.42, 0.5, 0.6, 0.7, and 0.8 in a field $H=5$ kOe and for a sample with $x=0.75$ in a field $H=10$ kOe.

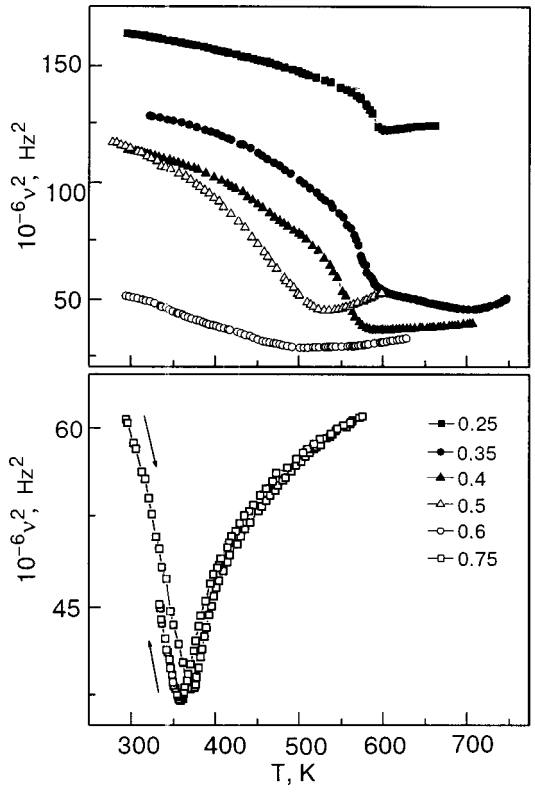

FIG. 5. Temperature dependence of the square of the resonance frequency for compounds with $x=0.25$, 0.35, 0.4, 0.5, 0.6, and 0.75.

=0.75). The temperature hysteresis near the structural transformation for the compound with $x=0.75$ is evidence of a first-order phase transition. In the region of the phase transformation the magnetization has a maximum (inset in Fig. 4d).

Measurements of the resistivity $\rho(T)$ of solid solutions of the system $Bi_{1-x}Sr_xMnO_3$ have revealed a semiconductor character of the conduction. Figure 6 shows the behavior of

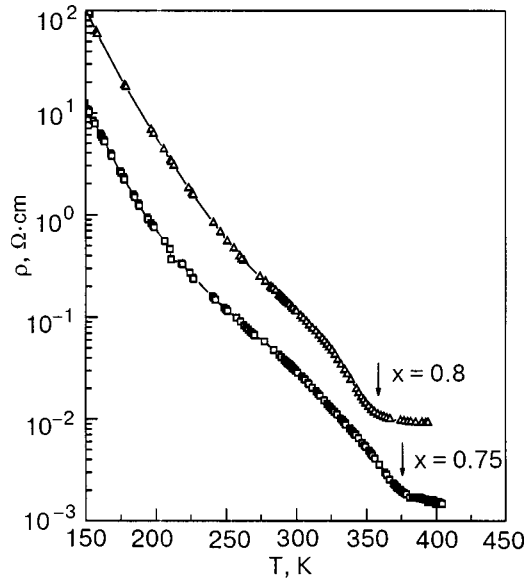

FIG. 6. Resistivity versus temperature for samples with $x=0.75$ and 0.08.

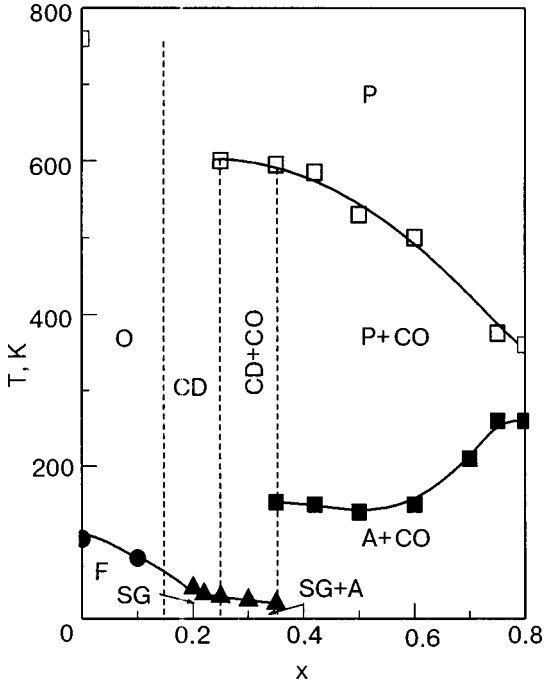

FIG. 7. Hypothetical magnetic phase diagram of the $Bi_{1-x}Sr_xMnO_3$ manganites: F is the ferromagnetic phase, O is an orbitally ordered phase, P is the paramagnetic phase, CO is the charge ordered phase, CD is the charge disordered phase, A is the antiferromagnetic phase, SG is a cluster spin glass. The critical temperatures are denoted by the following symbols: ●—T_C, ▲—freezing temperature of the magnetic moments of the clusters, ■—T_N, □—temperature of the structural phase transformation of the crystal.

the resistivity of the samples with $x=0.75$ and 0.8. For $Bi_{0.25}Sr_{0.75}MnO_3$ a change in the trend of $\rho(T)$ is observed near 375 K; this correlates with the behavior of the magnetization and Young's modulus. For $Bi_{0.2}Sr_{0.8}MnO_3$ analogous behavior of the resistivity occurs at 360 K. Above the transition temperature the conductivity remains practically unchanged with increasing temperature.

Figure 7 shows a hypothetical magnetic phase diagram of the $Bi_{1-x}Sr_xMnO_3$ system, constructed from the results of the present studies. The compound $BiMnO_3$ is a ferromagnetic insulator with $T_C=104$ K. Substitution of Bi^{3+} by Sr^{2+} led to a decrease of the Curie point and magnetic moment. The long-range ferromagnetic order is apparently destroyed near a critical concentration $x\approx0.15$ (the dashed line passing through the point $x=0.15$ on the phase diagram is the midpoint of the segment between the points $x=0.1$ and 0.2), at which the volumes of the ferromagnetic and antiferromagnetic phases become comparable. The system breaks up into clusters with different magnetic order. Competition between ferromagnetically and antiferromagnetically ordered clusters in the interaction gives rise to a state of the cluster spin glass type. In samples with a concentration of $0.35\leqslant x\leqslant0.6$ long-range antiferromagnetic order is realized below the Néel point. For the compound with $x=0.7$ the critical temperature T_N is near 210 K. The Néel points of the samples with $x=0.75$ and 0.8 are around 260 K, since the magnetization curves have a kink near that temperature (Fig. 4d). Thus in the case of antiferromagnetic compositions the magnetic ordering temperature is almost unchanging in the concentration interval from $x=0.35$ to 0.6 and then increases to 260 K, indicating a change in the type of antiferromagnetic ordering. The temperature of the structural transformation of the crystal, determined from studies of the elastic properties (Fig. 5) and measurements of the resistivity (Fig. 6), decreases smoothly with increasing strontium concentration in the interval from $x=0.25$ to 0.8.

Let us analyze the nature of the magnetic state in manganites undoped with alkaline-earth ions. Such compounds contain manganese ions only in the trivalent state. The antiferromagnetic structure of $LnMnO_3$ (Ln=La, Y, a rare-earth ion) can be explained on the basis of the Kanamori–Goodenough rule with allowance for the antiferrodistortive ordering of the orbitals of the d_{z^2} type.[15] For this type of ordering of the orbitals the exchange interactions in the ab plane are ferromagnetic, while those between planes are antiferromagnetic. In that case, half of the exchange bonds have a positive sign and the other half, negative. For $BiMnO_3$ the situation is different. Neutron- diffraction studies have revealed three different positions of the Mn^{3+} ions, with sharply different types of distortion of the MnO_6 octahedra.[11] Despite this difference, all of the Mn^{3+} ions were assigned a d_{z^2} orbital ground state, with different directions of the orbitals for each type of distorted octahedron. In this model two-thirds of the total number of exchange bonds are positive, and the resulting magnetic structure is ferromagnetic. However, it should be noted that, in our view, the neutron-diffraction data of Ref. 11 can be interpreted another way. According to our model, one-third of the manganese ions are found in the d_{z^2} state and two-thirds in the $d_{x^2-y^2}$ state; this corresponds to stretching of one-third of the MnO_6 octahedra and compression of the other two-thirds. In this case one expects that all of the exchange bonds will be ferromagnetic. In our view this model gives a better explanation of the experimental results of Ref. 11.

According to neutron-diffraction studies,[8] in a sample with $x=0.5$ a magnetic two-phase state consisting of antiferromagnetic structures of types A and CO is realized. The CO type of magnetic order corresponds to a charge-ordered phase, similar to that which is realized in manganites of the $Pr_{0.5}Ca_{0.5}MnO_3$ type.[16] The transition to the charge- disordered state is observed at 520 K, a very high temperature in comparison with $Ln_{0.5}Ca_{0.5}MnO_3$. Our results on the investigation of the elastic properties of the sample with $x=0.5$ show a critical temperature close to that obtained in Ref. 16. Therefore, we assume that the minimum on the $\nu^2(T)$ curve is due to a charge order–disorder phase transition. For compounds with $0.25\leqslant x\leqslant0.4$ one also observes anomalous behavior of the elastic properties at $T=500$–600 K, close to the temperature of the anomalous behavior of the sample with $x=0.5$. Therefore, it is natural to suppose that these anomalies are also due to a charge ordering effect. In the solid solutions $Pr_{1-x}Ca_xMnO_3$ (Ref. 17) the charge ordering of the 1:1 (Mn^{3+}/Mn^{4+}) type begins at $x=0.3$ and is completed at $x=0.7$. Apparently in the $Bi_{1-x}Sr_xMnO_3$ system the charge ordering begins at a lower level of doping. In principle this accords with the anomalously high charge ordering temperature (over 500 K). Another way the $Bi_{1-x}Sr_xMnO_3$ system differs from $Pr_{1-x}Ca_xMnO_3$ is that T_{co} decreases with increasing concentration of tetravalent manganese, whereas in the praseodymium–calcium series this temperature increases somewhat. Possibly this is due to

some role of the bismuth ions in the formation of the type of charge and orbital structure. Unlike the lanthanides, the bismuth ions actively participate in the chemical bonding, in which case the crystal structure can be strongly distorted owing to the anisotropy induced by the bismuth ions. Because of the presence of bismuth ions, the charge structures of $Bi_{0.5}Sr_{0.5}MnO_3$ and $Pr_{0.5}Ca_{0.5}MnO_3$ differ. In the praseodymium series the charge structure can be represented as an alternation of layers occupied by Mn^{3+} and Mn^{4+} ions, whereas in $Bi_{0.5}Sr_{0.5}MnO_3$ these layers have an every-other alternation.[18] In principle, in samples with a high concentration of bismuth ions there should be more layers with the trivalent manganese ions than layers with tetravalent manganese. Possibly the Mn^{3+} ions occupy the positions of the Mn^{4+} ions, but in that case the charge ordering temperature should decrease with decreasing Sr content. In the $Pr_{1-x}Ca_xMnO_3$ system the concentration transition from the ferromagnetic to the charge-ordered antiferromagnetic state occurs via a mixed two-phase state, as has been revealed by optical and electron-microscope studies.[19] We assume that a state consisting of a spin glass and a charge-ordered antiferromagnetic phase is also realized in the $Bi_{1-x}Sr_xMnO_3$ system at concentrations $0.25<x<0.35$. Indirect evidence of this may be seen in the experimental data on the elastic and magnetic properties. That is, the anomalies of the elastic properties (Fig. 5) can be linked with the charge ordering, and the anomaly in the magnetization curve of the reduced sample with $x=0.25$ at $T=150$ K (Fig. 3b) practically coincides with the antiferromagnetic ordering temperature of the stoichiometric compounds with $0.35\leqslant x\leqslant 0.6$.

In samples with $0.7\leqslant x\leqslant 0.8$ a change of type of the magnetic and charge ordering occurs. This agrees with the results on heavily doped compounds of the $Pr_{1-x}Sr_xMnO_3$ system.[20] For example, neutron diffraction studies have shown that the magnetic structure in $Pr_{0.15}Sr_{0.85}MnO_3$ is of the *C* type, which corresponds to charge ordering of Mn^{3+} and Mn^{4+} in the ratio 1:3. The Néel point and charge ordering temperature lie near room temperature. We assume that an analogous type of magnetic structure and charge ordering is realized in $Bi_{0.25}Sr_{0.75}MnO_3$ and $Bi_{0.2}Sr_{0.8}MnO_3$. The temperatures $T_{co}=375$ K for the compound with $x=0.75$ and $T_{co}=360$ K for $x=0.8$ can be ascribed to a charge order–disorder transition. It is difficult to determine the magnetic ordering temperature from the available data. However, based on the magnetic measurements (Fig. 4) one can assume that they are found near 260 K, where a kink was observed on the $M(T)$ polytherms.

Let us consider the nature of the exchange interactions in doped manganites containing tetravalent manganese ions. To explain the magnetic and electrical properties of ferromagnetic manganites the so-called double exchange interaction model was proposed in Ref. 21 and subsequently developed in more detail in Ref. 22. The double exchange is based on a real transition of an electron from the half-filled e_g orbitals of the Mn^{3+} ion to the unoccupied e_g orbital of Mn^{4+}. Such a transition is energetically favorable when the local spins *S* of nearest-neighbor Mn^{3+} and Mn^{4+} ions are parallel. Ferromagnetic ordering of the local spins increases the hopping probability of e_g electrons and promotes the appearance of metallic conduction. However, for high conductivity it is necessary to have a strong overlap of the $3d$ orbitals of the manganese and the $2p$ orbitals of the oxygen. It is assumed that this parameter is controlled by the Mn–O–Mn bond angle.[4,15] The larger the size of the lanthanide ion, the larger the Mn–O–Mn bond angle and $3d$ bandwidth and, accordingly, the higher the magnetic ordering temperature and conductivity. The Mn–O–Mn angles in manganite compounds with bismuth ions are rather large, as is attested to by studies of the crystal structure[11] and by the rather high Curie temperature of $BiMnO_3$. Consequently, in the case of an orbitally disordered phase one would expect that the ferromagnetic part of the exchange interactions will be dominant, in contradiction to our experiment. In addition, we did not observe a transition to metallic conduction upon doping of $BiMnO_3$ with Sr^{2+} ions. We therefore assume that an orbitally disordered phase is not realized in the $BiMnO_3$ system in the concentration interval $0.15\leqslant x\leqslant 0.25$, in contrast to the rare-earth manganites. The temperature of the orbital disordering in $BiMnO_3$ is apparently rather high—around 760 K. That is the temperature at which evolution of a latent heat of transformation has been observed.[23] Doping with Sr^{2+} ions leads to the appearance of the non-Jahn–Teller ions Mn^{4+}, and the temperature of the orbital ordering steadily decreases until another type of orbital state is realized. A state of the orbital glass type should correspond a definite magnetic state with a short- range type of magnetic order. We therefore assume that the spin-glass state in the system $Bi_{1-x}Sr_xMnO_3$ is realized as a result of a competition between ferromagnetic clusters with the type of magnetic order peculiar to $BiMnO_3$ and antiferromagnetic clusters in which the orbitals of the Mn^{3+} ions are frozen in a random direction. With increasing concentration of the Sr^{2+} ions a new type of antiferromagnetic clusters appears on account of the charge ordering.

Thus we can conclude that the magnetic properties of the $Bi_{1-x}Sr_xMnO_3$ system are intimately related to such phenomena as orbital and charge ordering. The role of these effects is apparently significantly larger than in other systems of manganites because of the high polarizability of the Bi^{3+} ion.

This study was supported by the Fund for Basic Research of the Republic of Belarus (Project F01-014) GPOFI ''Nanomaterials and Nanotechnologies'' (Task 3.3, nanomaterials and nanotechnologies).

*E-mail: troyan@ifttp.bas-net.by

[1] M. McCormack and S. Jin, Appl. Phys. Lett. **64**, 3045 (1994).
[2] J. B. Goodenought, Magnetism and the Chemical Bond, Interscience, New York (1963), Metallurgiya, Moscow (1968).
[3] P. G. De Gennes, Phys. Rev. **18**, 141 (1960).
[4] H. Kuwahara, Y. Tomioka, A. Asamitsu, Y. Moritomo, and Y. Tokura, Science **270**, 961 (1995).
[5] F. Sugawara, S. Iida, Y. Syono, and S. Akimoto, J. Phys. Soc. Jpn. **20**, 1529 (1965).
[6] I. O. Troyanchuk and V. N. Derkachenko, Fiz. Tverd. Tela (Leningrad) **32**, 2474 (1990) [Sov. Phys. Solid State **32**, 1436 (1990)].
[7] H. Chiba, T. Atou, and Y. Syono, J. Solid State Chem. **132**, 139 (1997).
[8] C. Frontera, J. L. Garcia-Munoz, A. Llobet, M. A. G. Aranda, C. Ritter, M. Respaud, and J. Vanacken, J. Phys.: Condens. Matter **13**, 1071 (2001).
[9] J. L. Garcia-Munoz, C. Frontera, M. A. G. Aranda, A. Llobet, and C. Ritter, Phys. Rev. B **63**, 064415 (2001).

[10] I. O. Troyanchuk, N. V. Kasper, O. S. Mantytskaya, and S. N. Pastushonok, Sov. Phys. JETP **78**, 212 (1994).
[11] T. Atou, H. Chiba, K. Ohoyama, Y. Yamaguchi, and Y. Syono, J. Solid State Chem. **145**, 639 (1999).
[12] I. O. Troyanchuk, N. V. Samsonenko, H. Szymczak, and A. Nabialek, J. Solid State Chem. **131**, 144 (1997).
[13] K. P. Poeppelmeier, M. E. Leonowicz, and J. M. Longo, J. Solid State Chem. **44**, 89 (1982).
[14] S. V. Trukhanov, N. V. Kasper, I. O. Troyanchuk *et al.*, J. Solid State Chem. **169**, 85 (2002).
[15] J. B. Goodenough, A. Wold, R. J. Arnott, and N. Menyuk, Phys. Rev. **124**, 373 (1961).
[16] Y. Tomioka, A. Asamistsu, H. Kuwahara, and Y. Moritomo, Phys. Rev. B **53**, R1689 (1996).
[17] C. Frontera, J. L. Garcia-Munoz, A. Llobet, J. S. Lord, and A. Planes, Phys. Rev. B **62**, 3381 (2000).
[18] M. Hervieu, A. Maignan, C. Martin, N. Nguyen, and B. Raveau, Chem. Mater. **13**, 1356 (2001).
[19] I. G. Deas, J. F. Mitchell, and P. Schiffer, Phys. Rev. B **63**, 172408 (2001).
[20] C. Martin, A. Maignan, M. Hervieu, B. Raveau, Z. Jirak, A. Kurbakov, V. Trounov, G. Andre, and F. Bouree, J. Magn. Magn. Mater. **205**, 184 (1999).
[21] C. Zener, Phys. Rev. **82**, 403 (1951).
[22] P. G. De Gennes, Phys. Rev. **118**, 141 (1960).
[23] H. Fagir, H. Chiba, M. Kikuchi, Y. Syono, M. Mansori, P. Satre, and A. Sebaoun, J. Solid State Chem. **142**, 113 (1999).

Translated by Steve Torstveit

ELECTRONIC PROPERTIES OF METALS AND ALLOYS

On the quantum oscillations of the sound attenuation coefficient in layered conductors

O. V. Kirichenko* and V. G. Peschansky

B. Verkin Institute for Low Temperature Physics and Engineering, National Academy of Sciences of Ukraine, pr. Lenina 47, Kharkov 61103, Ukraine

D. Krstovska

Faculty of Natural Sciences and Mathematics, Physical Institute, P.O. Box 162, 1000 Skopje, Republic of Macedonia

(Submitted August 1, 2003)
Fiz. Nizk. Temp. **30**, 304–308 (March 2004)

The attenuation of a transverse sound wave in a layered conductor with a quasi-two-dimensional dispersion relation of the charge carriers in a quantizing magnetic field is considered. The oscillatory dependence of the sound attenuation coefficient on the inverse magnetic field is analyzed, and the role of Joule losses in the absorption of energy from the sound wave by electrons is ascertained for different orientations of the magnetic field with respect to the plane of the layers. © *2004 American Institute of Physics.* [DOI: 10.1063/1.1645182]

The specifics of a quasi-two-dimensional dispersion relation of the charge carriers in a layered conductor are manifested in peculiar effects in the propagation of sound waves at low temperatures in a high magnetic field **H**, when the mean free time τ of the charge carriers is considerably longer than the period of gyration $2\pi/\Omega$ of an electron along a closed orbit in the magnetic field.

In a layered conductor a longitudinal sound wave is very weakly attenuated if the wave vector **k** and the vector **H** are directed along the normal to the layers. The high acoustic transparency of the conductor in such an experimental geometry is due to the fact that the Joule losses are insignificant, and the energy losses due to renormalization of the energy of the charge carriers (a deformation mechanism of absorption) are proportional to the square of the small quasi-two-dimensionality parameter η of the electron energy spectrum.[1,2] If there is even a small deviation of the magnetic field or wave vector from the normal to the layers the role of the Joule losses increases substantially.

Unlike the case of longitudinal sound, in the propagation of sound waves with the transverse polarization the Joule losses are substantial, over a wide range of magnetic field, for any orientation of the vectors **k** and **H** with respect to the layers.

If the temperature smearing T of the Fermi distribution function of the charge carriers is much less than the distance $\Delta\varepsilon=\hbar\Omega$ between the quantized Landau energy levels, then all of the thermodynamic and kinetic characteristics of the conductor, including the sound attenuation coefficient Γ (Refs. 3 and 4), oscillate with variation of $1/H$. The periods of these oscillations are determined by the areas of the extremal cross sections of the Fermi surface, and the amplitudes contain information about the effective cyclotron masses of the electrons on the extremal cross sections.

Let us consider the attenuation of a transverse sound wave in a layered conductor in a quantizing magnetic field in the case when

$$T \ll h\Omega \ll \eta\mu, \tag{1}$$

where μ is the chemical potential of the electrons.

For the sake of brevity in the calculations we take the dispersion relation of the charge carriers in the form

$$\varepsilon(\mathbf{p}) = \frac{p_x^2 + p_y^2}{2m} - \eta v_0 \frac{\hbar}{a} \cos\frac{ap_z}{\hbar}. \tag{2}$$

Here **p** and m are the quasimomentum and mass of the electron, $v_0=(2\varepsilon_F/m)^{1/2}$ is its characteristic velocity along the layers, a is the distance between layers, and the quasi-two-dimensionality parameter η can be less than unity.

Although the dependence of the energy of the charge carriers on their quasimomentum in organic layered conductors is more complicated, the use of a model dispersion relation of the form (2) permits a complete explanation of the dependence of the sound attenuation coefficient on the value of the magnetic field and the orientation of the vectors **k** and **H**. Generalization to the case of a quasi-two-dimensional spectrum of arbitrary form does not present any difficulty and leads only to a refinement of numerical factors of the order of unity in the expression for Γ.

A sound wave propagating in a conductor leads to renormalization of the charge carrier energy:[5]

$$\delta\varepsilon = \lambda_{ik}(\mathbf{p})u_{ik}. \tag{3}$$

Here u_{ik} is the strain tensor, and λ_{ik} are the components of the deformation potential tensor, taken with allowance for conservation of the number of charge carriers.

The quasi-two-dimensional character of the charge-carrier spectrum is reflected in anisotropy of the deformation potential. The deformation interaction of electrons with a sound wave is weakened for sound waves propagating along the normal to the layers or polarized along it. If the tensor components λ_{ik} with $i,k \neq z$ are of the order of magnitude of the Fermi energy, then the components of the deformation potential for which at least one of the indices is equal to z can be written in the form[6]

$$\lambda_{ik} = \eta \text{Ł}_{ik} \varepsilon_F \cos \frac{ap_z}{\hbar}, \tag{4}$$

where Ł_{ik} is a number of the order of unity.

Besides the deformation interaction with the sound wave, electrons also are acted on by the electromagnetic wave generated by the sound.[7,8] In a reference frame tied to the vibrating crystal lattice, the electric field of this wave has the form

$$\tilde{\mathbf{E}} = \mathbf{E} - \frac{i\omega}{c}[\mathbf{u}\times\mathbf{H}] + \frac{m\mathbf{u}\omega^2}{e}, \tag{5}$$

where ω is the frequency of the wave, $\mathbf{u}$ is the displacement vector of the sites of the crystal lattice, e is the charge of the electron, and c is the speed of light. The electric field $\mathbf{E}$ satisfies the Maxwell equations

$$\text{curl curl } \mathbf{E} = \frac{4\pi i\omega}{c^2}\mathbf{j} + \frac{\omega^2}{c^2}\mathbf{E} \tag{6}$$

and the condition of continuity of the electric current in the conductor:

$$\text{div } \mathbf{j} = 0. \tag{7}$$

In a magnetic field $\mathbf{H}=(0, H\sin\theta, H\cos\theta)$ deviating from the normal to the layers by an angle θ, the cross section of the Fermi surface on the plane $p_H \equiv \mathbf{p}\cdot\mathbf{H}/H = \text{const}$ are closed and do not contain points of self-intersection if

$$|\theta| < \text{arctg } 1/\eta\,. \tag{8}$$

In this case the electron energy levels can be found with the aid of the quasiclassical quantization condition

$$S(\varepsilon, p_H) = \frac{2\pi e\hbar H}{c}\left(n + \frac{1}{2}\right), \tag{9}$$

where $S(\varepsilon, p_H)$ is the area bounded by the electron trajectory. It is easily seen that in the case of the dispersion relation (2) the energy levels take the form

$$\varepsilon_n = \left(n+\frac{1}{2}\right)\hbar\Omega_0\cos\theta\sqrt{1+\eta\frac{v_0 am}{\hbar}\tan^2\theta\cos\zeta} - \eta\frac{v_0\hbar}{a}\cos\zeta - \eta^2\frac{mv_0^2\tan^2\theta\sin^2\zeta}{2[1+\eta(v_0 am/\hbar)\tan^2\theta\cos\zeta]}, \tag{10}$$

where $\zeta = ap_H/(\hbar\cos\theta)$, $\Omega_0 = eH/mc$.

At temperatures low compared to the Debye temperature the sound attenuation in a conducting crystal is determined mainly by the interaction of the acoustic wave with conduction electrons. In the quasi-classical approximation the sound energy absorption coefficient Γ can be written in the form[2]

$$\Gamma = \frac{2}{\rho u^2\omega^2 s}\frac{2eH}{c(2\pi\hbar)^2}\sum_n\int dp_H\left(-\frac{\partial f_0}{\partial\varepsilon_n}\right)\frac{\overline{|\psi|^2}}{\tau}. \tag{11}$$

Here ρ is the density of the crystal, s is the speed of sound, τ is the mean free time of the charge carriers, f_0 is the Fermi distribution function, and the overbar denotes averaging over the time of motion t of the electron along the quasiclassical closed orbit in the magnetic field. The function ψ, which takes into account the excitation of the electron system by the sound wave, can be written in the form

$$\psi = \int_{-\infty}^{t} dt' \,[e\mathbf{v}\cdot\tilde{\mathbf{E}} - i\omega\lambda_{ij}u_{ij}] \times \exp\{i\cdot\mathbf{k}\,[\mathbf{r}(t') - \mathbf{r}(t)] + \nu(t'-t)\}, \tag{12}$$

where $\nu = i\omega + 1/\tau$.

Let us consider a sound wave with a displacement vector $\mathbf{u}=(u,0,0)$, propagating in the direction normal to the layers. Using formulas (4), (11), and (12) and also the equations of motion for a charge in a magnetic field,

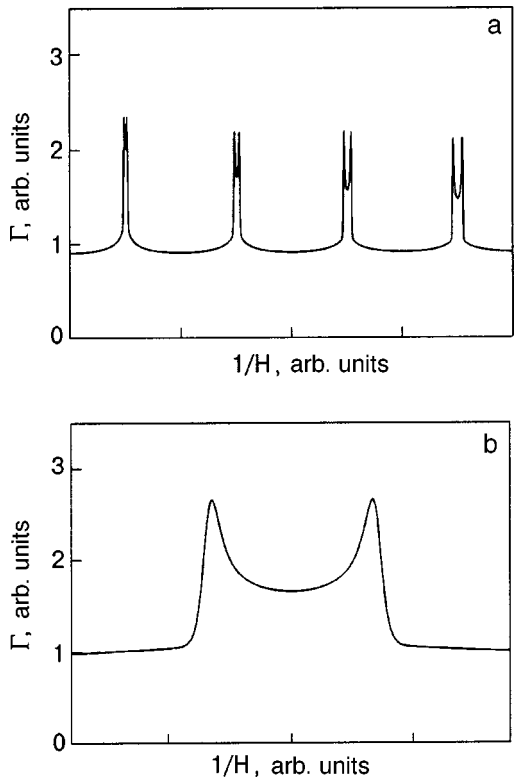

FIG. 1. The dependence of Γ on $1/H$ for $\theta=0$, $\eta=10^{-2}$, $\beta\gamma<1$ in arbitrary units. The figures have different horizontal scales.

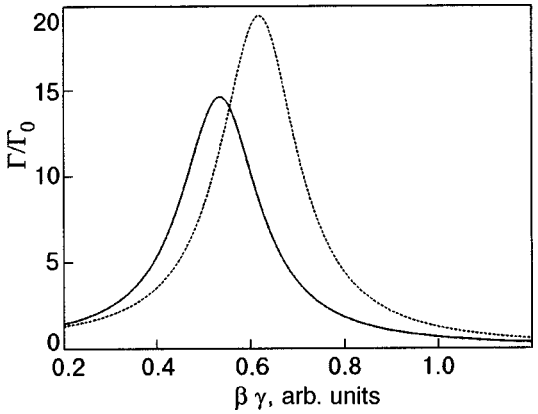

FIG. 2. Curves of Γ_{mon} for different values of the angle θ.

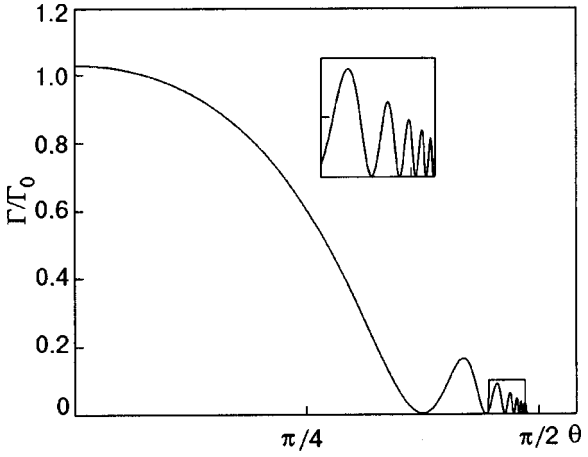

FIG. 3. Γ_{mon} versus angle θ for $\beta\gamma \gg 1$, in relative units.

$$\frac{\partial p_x}{\partial t} = \frac{eH}{c}(v_y \cos\theta - v_z \sin\theta),$$

$$\frac{\partial p_y}{\partial t} = -\frac{eH}{c} v_x \cos\theta, \quad \frac{\partial p_z}{\partial t} = \frac{eH}{c} v_x \sin\theta \frac{\partial p_z}{\partial t}, \tag{13}$$

one is readily convinced that in the region of sound frequencies in which the inequality $kl\eta \ll 1$ holds, the sound absorption coefficient can be written in the form

$$\Gamma = \frac{2}{\rho u^2 \omega^2 s} \frac{2eH\tau}{c(2\pi\hbar)^2} \sum_n \int dp_H \left(-\frac{\partial f_0}{\partial \varepsilon_n}\right) \times \left\{ \left[\eta k \omega u L_{xz} \varepsilon_F J_0\left(\frac{amv_0}{\hbar} \tan\theta\right) \cos\zeta \right]^2 + \frac{(e\gamma v_0)^2}{2\cos^2\theta} (|\tilde{E}_x|^2 + |\tilde{E}_y|^2) \right\}, \tag{14}$$

where J_0 is the Bessel function, and the parameter $\gamma = 1/(\Omega_0 \tau) \ll 1$.

With the use of Maxwell's equations (6), (7) it is not hard to find the electric field in the conductor if it is assumed that

$$\cos\theta \gg \gamma. \tag{15}$$

This condition, like inequality (8), excludes from consideration a small region of angles θ near $\theta = \pm\pi/2$ where the magnetic field is almost parallel to the layers.

In the leading approximation in the small parameter η the components of the electric field of the electromagnetic wave have the form

$$\tilde{E}_x = \frac{i\omega}{c} uH \cos^2\theta \frac{i\beta\gamma}{\cos^2\theta - (\beta\gamma)^2 - 2i\beta\gamma^2},$$

$$\tilde{E}_y = -\frac{i\omega}{c} uH \cos\theta \frac{\cos^2\theta - i\beta\gamma^2}{\cos^2\theta - (\beta\gamma)^2 - 2i\beta\gamma^2}, \tag{16}$$

where $\beta = (s\omega_p/c\omega)^2 \omega\tau$, and ω_p is the plasma frequency.

Using the Poisson summation formula and changing from integration over n to integration over energy with the aid of formula (10), we obtain the following expression for the oscillatory (in $1/H$) part of the sound energy absorption coefficient:

$$\Gamma_{\text{osc}} = \frac{\Gamma_0}{kl} \left(\frac{\hbar\Omega_0 \cos\theta}{\eta\mu}\right)^{\frac{1}{2}} \left[\left(\frac{(kl\eta)^2}{2}\right) L_{xz}^2 J_0^2\left(\frac{amv_0}{\hbar} \tan\theta\right) + F(\gamma,\theta) \right] \times \sum_N \frac{(-1)^N}{\sqrt{N}} \Psi(N\Lambda) \left[\cos\left(\frac{NcS_1}{2eH\hbar} - \pi/4\right) + \cos\left(\frac{NcS_2}{2eH\hbar} + \pi/4\right) \right]. \tag{17}$$

Here $\Gamma_0 = 2mN_c v_0 \omega/\rho s^2$, N_c is the electron density, $l = v_0\tau$, $\Phi(z) = z/\sinh z$, $\Lambda = 2\pi^2 T/\hbar\Omega_0 \cos\theta$, and the extremal values of the critical area of the Fermi surface on a plane $p_H = \text{const}$ have the form

$$S_{1,2} = \frac{2\pi m}{\cos\theta} \frac{\mu \pm \eta v_0 \hbar/a}{\sqrt{1 \mp \eta(amv_0/h)\tan^2\theta}}. \tag{18}$$

In a quasi-two-dimensional conductor these values do not differ strongly from each other, and the oscillations therefore have a double-peak (doublet) form (Fig. 1).

The terms containing the factor L_{xz} in formula (17) describe the absorption of energy from the sound wave due to renormalization of the electron spectrum in a vibrating lattice (deformation mechanism). The Joule losses are determined by the function $F(\gamma,\theta)$, which has the form

$$F(\gamma,\theta) = \cos^2\theta \frac{\cos^2\theta + \beta^2\gamma^2}{[\cos^2\theta - (\beta\gamma)^2]^2 + \beta^2\gamma^4}. \tag{19}$$

Analogous terms are also contained in the smoothly varying (with magnetic field) part of the absorption coefficient:

$$\Gamma_{\text{mon}}=\frac{\Gamma_0}{kl}\left[\frac{(kl\eta)^2}{2}L_{xz}^2 J_0^2\left(\frac{amv_0}{\hbar}\tan\theta\right)+F(\gamma,\theta)\right]. \quad (20)$$

The density of charge carriers in the organic conductors now under intensive study are comparable to the density of conduction electrons in ordinary metals, so that the parameter β can be much greater than unity. At a sufficiently high magnetic field ($\beta\gamma<\cos\theta$) the induction mechanism of sound-wave attenuation is the main one, and a peak should be observed on the absorption curve at $\beta\gamma=\cos\theta$ due to the excitation of a helicoidal wave in the conductor (Fig. 2). If $\beta\gamma$ is much greater than unity, then the Joule losses are small ($F(\gamma,\theta)=\cos^2\theta/\beta^2\gamma^2$) and there can be competition between the induction and deformation mechanisms of absorption of the sound energy by electrons. At sufficiently large angles of deviation of the magnetic field from the normal to the layers the coefficient Γ varies periodically with the angle θ. In the region where $(\beta\gamma)^{-1}\simeq kl\eta$ the amplitude of these oscillations is comparable to the monotonically varying (with angle) part of the absorption coefficient (Fig. 3).

The effects considered above, which are specific to quasi-two-dimensional conductivities, are completely observable in the region of ultrasonic frequencies $\omega\sim 10^8$ s^{-1} in magnetic fields of the order of tens of tesla.

*E-mail: kirichenko@ilt.kharkov.ua

[1] O. V. Kirichenko and V. G. Peschanskiĭ, Fiz. Nizk. Temp. **27**, 1323 (2001) [Low Temp. Phys. **27**, 978 (2001)].
[2] O. V. Kirichenko, V. G. Peschansky, O. Galbova, G. Ivanovski, and D. Krstovska, Fiz. Nizk. Temp. **29**, 812 (2003) [Low Temp. Phys. **29**, 609 (2003)].
[3] V. L. Gurevich, V. G. Skobov, and Yu. D. Firsov, Zh. Éksp. Teor. Fiz. **40**, 786 (1961) [Sov. Phys. JETP **13**, 552 (1961)].
[4] V. M. Gokhfel'd and S. S. Nedorezov, Zh. Éksp. Teor. Fiz. **61**, 2041 (1971) [Sov. Phys. JETP **34**, 1089 (1972)].
[5] A. I. Akhiezer, Zh. Éksp. Teor. Fiz. **8**, 1338 (1938).
[6] O. V. Kirichenko and V. G. Peschansky, Fiz. Nizk. Temp. **25**, 1119 (1999) [Low Temp. Phys. **25**, 837 (1999)].
[7] A. B. Pippard, Philos. Mag. **46**, 1104 (1955).
[8] A. I. Akhiezer, M. I. Kaganov, and G. Ia. Liubarskii, Zh. Éksp. Teor. Fiz. **32**, 837 (1957) [Sov. Phys. JETP **5**, 685 (1957)].

Translated by Steve Torstveit

Thermoelectric effects in layered conductors in magnetic field

O. Galbova, G. Ivanovski, and D. Krstovska

*Faculty of Natural Sciences and Mathematics, Physical Institute, P.O. Box 162, 1000 Skopje, Republic of Macedonia**

(Submitted August 7, 2003)
Fiz. Nizk. Temp. **30**, 309–311 (March 2004)

The magnetic-field dependence of the thermopower in layered conductors with a quasi-two-dimensional electron energy spectrum of arbitrary form is investigated theoretically. It is shown that the dependence of the thermopower on the magnitude and orientation of the magnetic field with respect to the layers contains detailed information about the velocity distribution of the charge carriers on the Fermi surface. © *2004 American Institute of Physics.*
[DOI: 10.1063/1.1645183]

Thermomagnetic phenomena in high magnetic fields **H** are extremely sensitive to the form of the electron energy spectrum of degenerate conductors.[1] At sufficiently low temperatures T, where the temperature smearing of the Fermi distribution function $f_0(\varepsilon)$ of the conduction electrons is much less than the distance between quantized energy levels $\Delta\varepsilon=\hbar\Omega$ and the charge carriers can complete many orbits with frequency Ω in the magnetic field during the mean free time τ, the amplitude of the quantum oscillations of the thermopower with variation of $1/H$, as a rule, significantly exceeds the part of the thermopower that varies smoothly with H. This allows this quantum oscillation effect to be used as the basis of an extremely accurate and reliable spectroscopic method of studying the Fermi surface (FS). However, even for $T>\hbar\Omega$, when it is not so important to take into account the quantization of the energy levels of the charge carriers, thermoelectric coefficients at high magnetic field ($\Omega\tau\gg1$) contain rather detailed information about the energy spectrum of the charge carriers.

Let us consider the thermoelectric phenomena in layered conductors with an energy spectrum of the conduction electrons of arbitrary form:

$$\varepsilon(p)=\sum_{n=0}^{\infty}\varepsilon_n(p_x,p_y)\cos\left\{\frac{anp_z}{\hbar}+\alpha_n(p_x,p_y)\right\};$$
$$\varepsilon_n(-p_x,-p_y)=\varepsilon_n(p_x,p_y);$$
$$\alpha_n(p_x,p_y)=-\alpha_n(-p_x,-p_y), \tag{1}$$

where a is the distance between layers, and $\hbar$ is Planck's constant.

We shall assume that the functions $\varepsilon_n(p_x,p_y)$ fall off with increasing index n, so that the velocity of the electrons along the normal to the layers is much less than the characteristic velocity v_F of the electrons along the layers:

$$v_z=\mathbf{v}\cdot\mathbf{n}<\eta v_F. \tag{2}$$

In a large family of organic conductors based on tetrathiafulvalene in magnetic fields of the order of several tens of tesla the Shubnikov–de Haas effect is observed at the most diverse orientations of the magnetic field with respect to the layers,[2–4] which attests to the fact that at least one sheet of the FS of these organic charge-transfer complexes has the form of a slightly corrugated cylinder. For the sake of brevity in the calculations we shall assume that the FS consists of only one slightly corrugated cylinder of arbitrary shape. The degree of corrugation of the FS is determined by the ratio of the conductivity in the directions parallel to and perpendicular to the layers in the absence of magnetic field; this ratio is proportional to the square of the quasi-two-dimensionality parameter η of the electron energy spectrum. In the organic layered conductors studied experimentally, η^2 is of the order of $10^{-3}-10^{-4}$, and in graphite it can reach a small value of the order of 10^{-5}.

By solving the kinetic equation for the charge-carrier distribution function at a fixed electrical current density **j** and temperature gradient ∇T one can find the electric field

$$E_i=\rho_{ik}j_k+\alpha_{ik}\frac{\partial T}{\partial x_k}. \tag{3}$$

Here ρ_{ik} is the resistivity tensor, which is the inverse of the conductivity tensor σ_{ik}, and

$$\alpha_{ik}=\frac{\pi^2}{3e}T\rho_{ij}\frac{\partial}{\partial\mu}\sigma^e_{jk}. \tag{4}$$

The tensor components σ^e_{jk} coincide with σ_{ik} if the momentum relaxation time τ_p^- in the latter is replaced by the energy relaxation time τ_e; μ is the chemical potential of the system of conduction electrons.

At sufficiently low temperatures T, much less than the Debye temperature T_D, viz., $T\ll T_D(l_k/k_0)^{1/3}$, where l_k and l_0 are the mean free paths of the charge carriers at room temperature and at $T=0$, respectively, and the charge carriers are scattered mainly by impurity atoms and crystal lattice defects. In this temperature region the times τ_p^- and τ_e are of the same order of magnitude. The condition of high magnetic field is attainable only at liquid helium temperatures, where the condition given above is clearly satisfied, and in what

follows we shall therefore not distinguish between the momentum and energy relaxation time of the electrons.

One of the interesting phenomena specific to a quasi-two-dimensional electron energy spectrum is the manifestation of oscillations of the magnetoresistance to a current transverse to the layers as a function of the angle θ between the magnetic field vector and the normal to the layers.[5,6] An anomalous oscillation effect should be expected when the temperature gradient is directed along the normal to the layers. In that case if the magnetic field $\mathbf{H}=(0,H\sin\theta,H\cos\theta)$ deviates substantially from the layers, then to a sufficient degree of accuracy the thermoelectric field is directed mainly along the z axis when $\Omega\tau\eta^2\ll 1$, so that

$$E_z=-\alpha_{zz}\frac{\partial T}{\partial z},\qquad \alpha_{zz}=\frac{\pi^2}{3e}T\frac{\partial}{\partial\mu}\ln\sigma_{zz}, \tag{5}$$

where the conductivity transverse to the layers, σ_{zz}, in the case $\gamma=1/\Omega\tau\ll 1$ has the form[7,8]

$$\sigma_{zz}=\frac{ae^2m^*\tau\cos\theta}{(2\pi\hbar)^4}\sum_{n=1}^{\infty}n^2I_n^2(\theta)+\eta^2\sigma_0(\eta^2\varphi_1+\gamma^2\varphi_2). \tag{6}$$

The functions $\varphi_i(\theta)$, which depend on the concrete form of the dispersion relation of the charge carriers, is of the order of unity, m^* is the cyclotron effective mass of the conduction electrons, and σ_0 is of the order of magnitude of the conductivity along the layers in the absence of magnetic field.

The dependence of σ_{zz} on the orientation θ of the magnetic field with respect to the layers has narrow peaks which for $\tan\theta\gg 1$ repeat with a period $\Delta(\tan\theta)=2\pi\hbar/naD_p$, where D_p is the diameter of the transverse cross section of the Fermi surface along the p_y axis. These minima are usually associated with the orientations of the vector $\mathbf{H}$ for which the integral

$$I_n(\theta)=\tilde{T}^{-1}\int_0^{\tilde{T}}dt\,\varepsilon_n(t)\cos(p_y(t)an\tan\theta/\hbar), \tag{7}$$

vanishes for $n=1$ (here $\tilde{T}=2\pi/\Omega$ is the period of the motion of the charge in the magnetic field).

The coefficients $I_n(\theta)$ falls off slowly with increasing n, and at those angles θ_c for which $I_1(\theta_c)=0$ a substantial role in the electrical conductivity and thermoelectric coefficient

$$\alpha_{zz}(\theta)=\frac{\pi^2}{3e}\frac{Ta}{\hbar v_\perp}\left\{F(\theta)+\tan\theta\frac{2\sum_{n=1}^{\infty}n^3I_nI_n'(\xi_n)}{\sum_{n=1}^{\infty}n^2I_n^2}\right\} \tag{8}$$

is played by the term with $n=2$. Here $v_\perp$ is the velocity of the conduction electrons along the y axis at the turning point on the electron orbit $\varepsilon=\text{const}$, $p_H=\text{const}$, and

$$\xi_n=\frac{aD_p}{2\hbar}n\tan\theta.$$

The terms with $n=1$ and $n=2$ do not vanish simultaneously, and from now on we will be considering only these two terms. Inclusion of the next terms in the sum over n will lead only to insignificant refinements in the dependence of the kinetic coefficients on $\tan\theta$. The function $F(\theta)$ is of the order of unity and for $\tan\theta\gg 1$ represents an insignificant background in the dependence of α_{zz} on $\tan\theta$.

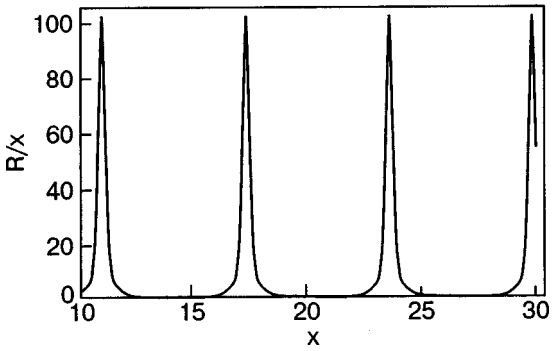

FIG. 1. Dependence on x of the normalized magnetoresistance transverse to the layers for $\lambda=10^{-2}$. The positions of the maxima of R/x are shifted from the values $x_k=3\pi/2+2\pi k$ by an amount 2λ.

For $\tan\theta\gg 1$ the integrand in formula (7) is a rapidly oscillating function, and the main contribution to the integral comes from small neighborhoods of the points of stationary phase, where $v_x=0$. There are at least two such points on the electron orbit: $v_x(t_1)=v_x(t_2)=0$. Then $\varepsilon_n(t_1)=\varepsilon_n(t_2)$, and, as a result, the asymptotic expression for $I_n(\theta)$ has the form

$$I_n(\theta)=2\varepsilon_n(t_1)\frac{|2\pi h|^{1/2}}{\tilde{T}\left|an\left\{\frac{\partial^2p_y(t_1)}{\partial t_1^2}\right\}\tan\theta\right|^{1/2}}\times\cos\left\{\frac{anD_p}{2h}\tan\theta-\frac{\pi}{4}\right\}, \tag{9}$$

and the thermoelectric coefficient $\alpha_{zz}(\theta)$ for $x=(aD_p/\hbar)\tan\theta\gg 1$ can be represented by the formula

$$\alpha_{zz}(\theta)=-\frac{\pi^2}{3e}\frac{T}{D_pv_\perp}\left\{F(\theta)+x\frac{\cos x+2\lambda\cos 2x}{1+\sin x-\lambda(1+\sin 2x)}\right\}, \tag{10}$$

where $\lambda=2\varepsilon_2^2(t_1)/\varepsilon_1^2(t_1)\ll 1$.

Figures 1 and 2 give the angular dependence of the mag-

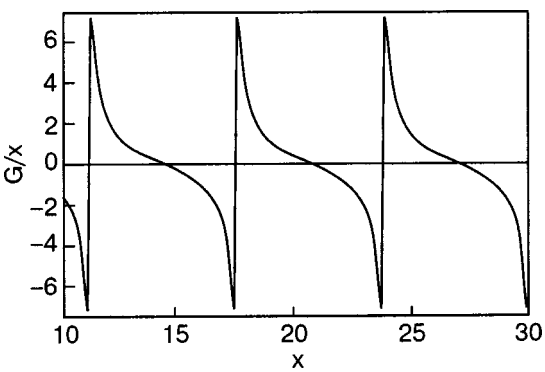

FIG. 2. Normalized thermopower at large x and $\lambda=10^{-2}$. The maxima of the thermopower are proportional to $1/2\lambda$ and are shifted from the position of the maximum values of R/x by an amount $\sqrt{2\lambda}$.

netoresistance and thermoelectric field for $\lambda = 10^{-2}$.

The thermopower goes to zero when the magnetoresistance is equal to its maximum values. The positions of the maxima deviate from the values $x_k = 3\pi/2 + 2\pi k$ (k is an integer) by a small amount λ, and the value of the thermoelectric coefficient at the extrema is inversely proportional to $\sqrt{\lambda}$.

Thus the experimental study of the thermopower in quasi-two-dimensional conductors permits one to determine the degree of diminution of the harmonics of the Fourier series expansion of the carrier energy as a function of the momentum projection transverse to the layers and to find their velocity distribution on the Fermi surface.

We thank V. G. Peschansky for fruitful discussions.

*E-mail: danica@iunona.pmf.ukim.edu.mk

[1] Yu. A. Bychkov, L. É. Gurevich, and G. M. Nedlin, Zh. Éksp. Teor. Fiz. **37**, 534 (1959) [Sov. Phys. JETP **10**, 377 (1960)].
[2] J. Wosnitza, *Fermi Surfaces of Low-Dimensional Organic Metals and Superconductors*, Springer Tracts in Modern Physics (1996), p. 165.
[3] M. V. Kartsovnik and V. N. Laukhin, J. Phys. (France) **6**, 1753 (1996).
[4] J. Singelton, ''Studies of quasi-two-dimensional organic conductors based on BEDT-TTF using high magnetic fields,'' Rep. Prog. Phys. **63**, 1111 (2000).
[5] M. V. Kartsovnik, V. N. Laukhin, V. I. Nizhankovskiĭ, and A. A. Ignat'ev, JETP Lett. **47**, 363 (1988).
[6] M. V. Kartsovnik, P. A. Kononovich, V. N. Laukhin, and I. F. Shchegolev, JETP Lett. **48**, 541 (1988).
[7] V. G. Peschansky, Phys. Rep. **288**, Nos. 1–6, 305 (1997).
[8] V. G. Peschanskiĭ, Zh. Éksp. Teor. Fiz. **121**, 1204 (2002) [JETP **94**, 1035 (2002)].

Translated by Steve Torstveit

QUANTUM EFFECTS IN SEMICONDUCTORS AND DIELECTRICS

Influence of mechanical stress and temperature on the photoluminescence in the low-temperature phase of C_{60} fullerite

A. Avdeenko,* V. Gorobchenko, P. Zinoviev, N. Silaeva, and V. Zoryanskiĭ

B. Verkin Institute for Low Temperature Physics and Engineering, National Academy of Sciences of Ukraine, pr. Lenina 47, Kharkov 61103, Ukraine

N. Gorbenko, A. Pugachev, and N. Churakova

Kharkov Polytechnical Institute National Engineering University, ul. Frunze 21, Kharkov 61002, Ukraine
(Submitted August 14, 2003)
Fiz. Nizk. Temp. **30**, 312–317 (March 2004)

The results of a study of the low-temperature (5–90 K) photoluminescence of thin films of C_{60} obtained by vacuum deposition on heated mica substrates are reported. The structure of the films is analyzed by the method of high-energy electron diffraction. The features of the luminescence of structural traps (X traps), which arise on account of mechanical stresses created by bending of C_{60} films of different structure on mica substrates, are investigated for the first time. The temperature behavior of the photoluminescence bands due to defects of this kind is investigated. The processes of trapping and transport of electronic excitations in the low-temperature phase of C_{60} are discussed. © *2004 American Institute of Physics.*
[DOI: 10.1063/1.1645184]

Spectral luminescence methods have been widely used for studying the relaxation and transport of excitons in C_{60} fullerite (see, e.g., the reviews[1,2] and the references cited therein) since the time of the discovery[3] and synthsis[4] of this compound, which is now a model for description of π-electron systems. The photophysical properties of excited states which reflect the symmetry of the C_{60} molecule and crystal are unique and therefore extraordinarily interesting, especially in view of the very promising applications of this material in photonics and optoelectronics.

Although the mechanisms giving rise to the low-temperature photoluminescence (PL) spectra of crystalline C_{60} have been rather scrupulously studied (see, e.g., the surveys[5,6] and the references therein), a number of unsolved problems remain in connection with the localization and transport of excitations, e.g., Jahn–Teller self-trapping of excitons[7] and the features of the resonance intermolecular interaction of C_{60} molecules found in excited states of even symmetry.[8,9]

Since the time of the pioneering work of Eremenko and Medvedev,[10] structural imperfections in crystals,[11] created mainly by mechanical stress, have been used with great success as a tool for studying excitonic processes in molecular crystals.[12–14]

In the present paper we report the first-ever results on the influence of mechanical stresses on the spectra of low-temperature photoluminescence of thin films of C_{60} fullerite of different structure on mica substrates and discuss the mechanisms of trapping and transport of singlet excitons.

We studied thin films of fullerite C_{60} obtained by evaporation of C_{60} single crystals of at least 99.9% purity onto mica substrates heated to different temperatures in a vacuum of around 10^{-3} Pa. A quartz oscillator was used to determine the thickness of the film and the rate of deposition. The structure of the films was monitored by electron-diffraction and electron-microscope methods.

The use of a mica substrate with a suitable choice of deposition regime makes it possible to obtain rather good crystalline films with no stacking faults.[15,16] Because of this, the low-temperature PL spectra of such films, which are investigated here for the first time, have qualities approaching those of single crystals[6] and can reveal effects due to the influence of mechanical stresses.

The photoluminescence of thin films of C_{60} fullerite was excited by a spectral line of a DRSh-1000 high-pressure mercury lamp. This line, at an energy of 2.84 eV, was selected by means of an SPM-2 monochromator with a spectral slit width of 10 nm. The PL was registered ''in reflection'' by an MDR-3 monochromator with a spectral slit width of 5.2 nm. The PL spectral were registered using a cooled FÉU-79 photomultiplier, with a spectral sensitivity curve of the type S-8 in the photon-counting mode. The PL spectral were corrected for the spectral sensitivity of the detection equipment. The integration and processing of the signal was done with the use of a personal computer. The temperature of the sample, which was found in gaseous helium, was regulated to a precision of 0.5 K or less over the temperature range from 5 to 90 K. Internal stresses were produced in the C_{60} film on mica by bending the substrate by different angles. The corresponding tensile stresses in the C_{60} film varied from 90 to 150 MPa (according to our calculations using the experimental values[17] of the low-temperature elastic constants) and the compressive stresses from 28 to 50 MPa, depending on the bending angle. To elucidate how the stresses created in the

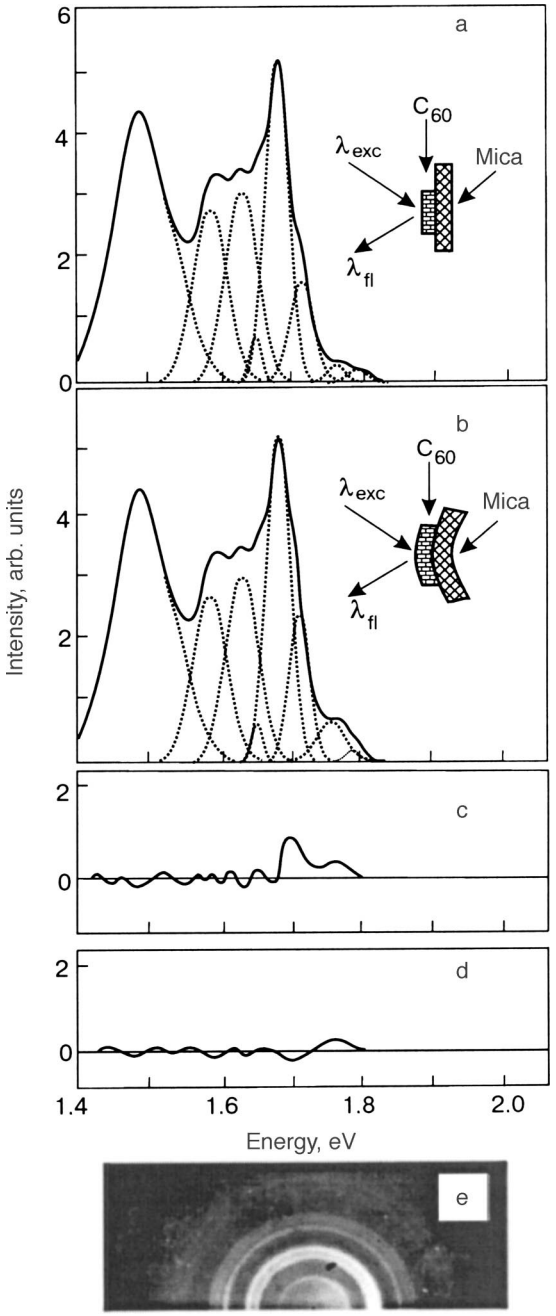

FIG. 1. Photoluminescence (PL) spectra of an oriented thin film of C_{60} fullerite 90 nm thick on a mica substrate at 5 K under photoexcitation with an energy of 2.84 eV; unstressed film (a); film with stress resulting from deformation of the substrate (b); the difference spectrum of the PL, obtained by subtracting I in panel "a" from I in panel "b": $I(b)-I(a)$ (c); the difference spectrum obtained by subtracting $I(a)$ from the PL spectrum of the film after the stress was removed (d); the pattern of high-energy electron microdiffraction on the crystal structure of the C_{60} film (e). The dotted lines in panels "a" and "b" correspond to a computer decomposition of the spectra into bands of Gaussian shape.

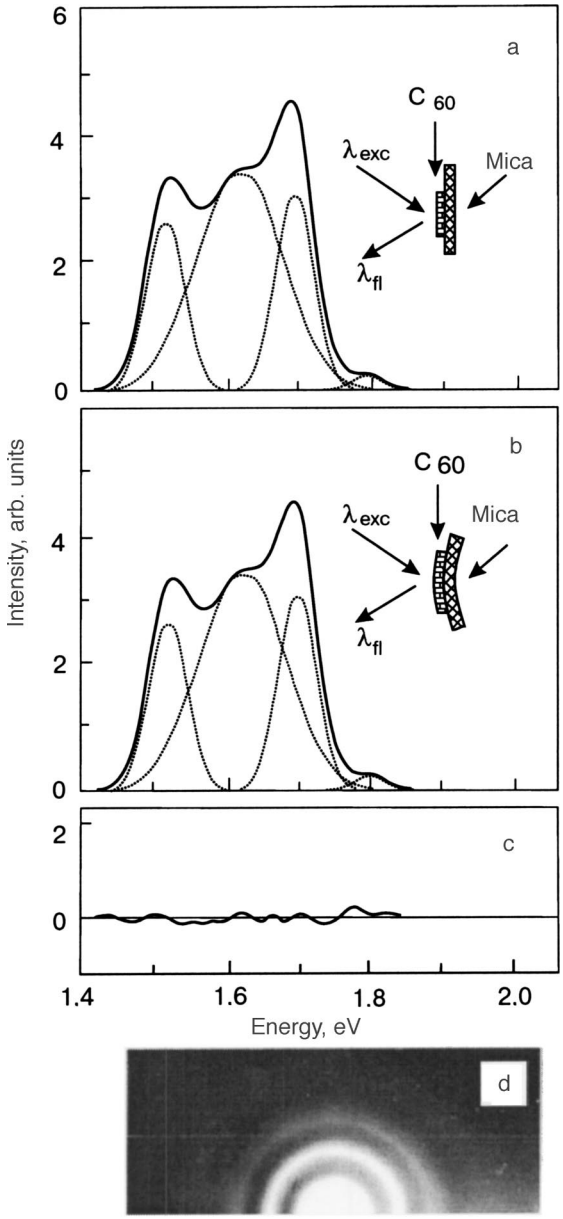

FIG. 2. PL spectra of a disoriented C_{60} thin film 60 nm thick on a mica substrate at a temperature of 5 K under photoexcitation at an energy of 2.84 eV: the unstressed film (a); the film containing stresses resulting from deformation of the substrate (b); the difference spectrum obtained by subtraction $I(b)-I(a)$ (c); the pattern of high-energy electron microdiffraction on the crystal structure of the C_{60} film (d). The dotted curves in panels "a" and "b" correspond to a computer decomposition of the spectra into bands of Gaussian shape.

film by bending it affect the PL spectra, we subtracted the initial spectra from the spectra obtained for the bent film. For this procedure the spectra were normalized to the integrated intensity by the method proposed in Ref. 18.

The influence of the mechanical stresses produced at maximum bending of the mica substrates on the low-temperature PL spectra of thin films of C_{60} fullerite with different structures is well seen in Figs. 1 and 2. Figure 2 shows the PL spectra for oriented films 90 nm thick obtained at a substrate temperature of 180 °C and a deposition rate of 0.1 nm/s. The films were continuous and had an fcc lattice with a period close to that of bulk fullerite. The microcrystals in those films were of the order of 30–40 nm in size. Figure 2 shows the luminescence spectrum for a disoriented film 60 nm thick obtained at a substrate temperature of 17 °C and a deposition rate of 0.1 nm/s. The mean size of the microcrystals in the latter films was around 5 nm. These two types of films, having different structures determining the specifics of the luminescence spectra, were chosen in light of our previous investigations.[19]

As can be seen in Fig. 1c, which shows the difference between the PL spectra (normalized by the method of Ref.

18) of the unstressed film (Fig. 1a) and bent film (Fig. 1b), bending of the film leads to changes in the luminescence spectrum, the changes being observed in the high-energy part of the luminescence of stress-induced structural defects which are apparently of a dislocation character.[20,21]

The main changes in the luminescence spectrum (Fig. 1c) are observed near 1.7, 1.76, and 1.79 eV. The behavior of the low-temperature PL band of the C_{60} crystal under applied pressure has been studied in some detail:[22] there is a band at 1.69 eV due to radiative transitions in the intrinsic, so-called ''dimer'' trap,[6] which is influenced rather strongly by pressure (the application of pressure leads to a long-wavelength shift, broadening, and changes in intensity of this band), and bands due to the luminescence of *X* traps, which are shifted little at low pressures. The task of the present study was to investigate the structural defects created upon bending of the substrate (*X* traps) as tests for the motion of excitons in films of different structure. The band at energy 1.76 eV has appeared in practically all of the studies of structural defects in C_{60} fullerite (see, e.g., Ref. 5), whereas the band at energy 1.79 eV is apparently peculiar to the films, since it is not observed in single crystals.

Figure 1d shows the difference between the normalized PL spectra of a film of C_{60} fullerite, taken prior to the bending of the substrate and after the substrate was straightened out. It is seen that the structural defects are partially ''healed'' after the mechanical stress is removed.

A completely different picture is observed for the disoriented, nanocrystallite film. As is seen in Fig. 2, in this case there is practically no luminescence of induced defects, apparently because the migration of electronic excitation energy is confined in the nanocrystals; this is the so-called exciton confinement.[19]

In order to discuss the possible mechanisms for the phenomena observed when C_{60} fullerite films of different structure are stressed, it is important to consider several factors that influence the processes of relaxation and migration of excitations in solid C_{60}.

It is known that the lowest-energy excited electronic states of the C_{60} molecule in the point group I_h are even, so that the luminescence from the first excited singlet state of symmetry T_{1g} is dipole-forbidden. The mechanisms responsible for the PL of individual molecules is determined mainly by the Herzberg–Teller vibronic interactions.[6,23]

In the C_{60} crystal, because the transition dipole moment for the lowest singlet state of the Frenkel exciton is zero, the resonance intermolecular interaction is small and is of a quadrupolar character, as was shown experimentally in Ref. 9. The exciton can also be localized by Jahn–Teller distortion of the C_{60} molecule upon photoexcitation, when the symmetry of the molecule changes from I_h to D_{5d} (Refs. 7 and 24). The structure of the PL spectra of Frenkel excitons is largely determined, as in the case of individual C_{60} molecules, by the Herzberg–Teller vibronic interaction mechanism.[6,20]

In spite of the weak intermolecular interactions, excitonic effects are manifested in the PL spectra not only in the form of luminescence of self-trapped Frenkel excitons[6,7,20] and charge-transfer excitons[25] but also in the luminescence of *X* traps, which are due to the presence of structural defects.[20,21] Delocalization of a neutral molecular excitation

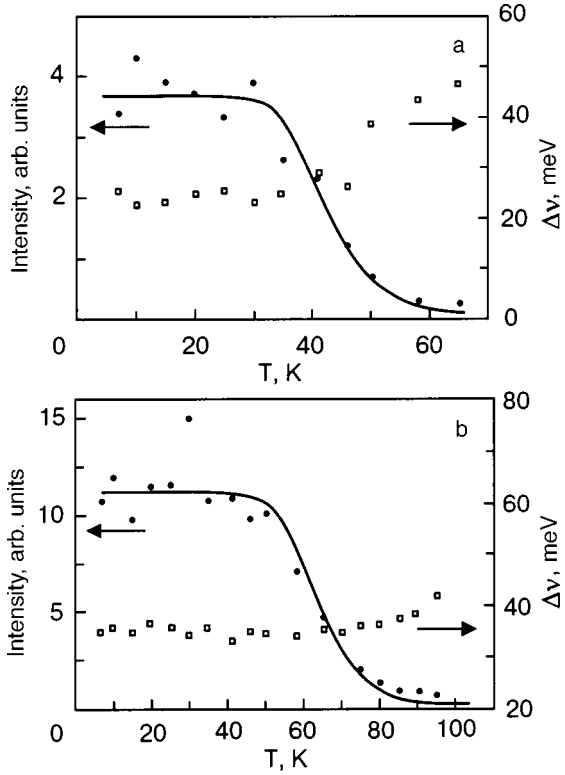

FIG. 3. Temperature dependence of the energy of the maxima of the PL bands of X_1 traps (a) and X_2 traps (b) with energies of 1.79 and 1.76 eV and the half-widths $\Delta\nu$ of these bands in oriented films 90 nm thick (see Fig. 1a). The experimental curves are approximated by using formula (1) with the following parameters: a) $\gamma=2.6\times10^4$, $E_a=0.04$ eV. b) $\gamma=8.0\times10^4$, $E_a=0.06$ eV.

can be promoted by the admixing to it of charge-transfer states,[26] even in the case when that excitation can be essentially immobile in the absence of charge transfer.[27]

It is this mobility of the excitations that brings about the luminescence of *X* traps in the most perfect single crystals[6] and oriented films[19] of C_{60} fullerite.

To determine the depth of the *X* traps relative to the bottom of the Frenkel exciton band, we measured the temperature dependence of the relative yield in the bands obtained by Gaussian decomposition of the PL of *X* traps in the region 5–90 K (Fig. 3). In the temperature interval 5–90 K we observed a steep falloff of the intensity of the luminescence of the X_1 and X_2 traps. Keeping in mind that the energy of self-trapping of singlet excitons in C_{60} fullerite is rather small[6] and assuming that the activational character of the temperature dependence of the intensity of the bands of the *X* traps in the luminescence spectrum should be indicative of localization of excitons at those traps,[22] we have estimated the activation energy for the emptying of the *X* traps, approximating this temperature dependence by the formula[20,28]

$$I(T)=I_0/[1+y\exp(-E_a/k_BT)], \tag{1}$$

where I is the intensity of the emission from an *X* trap at the given temperature, I_0 is the intensity of the emission from a trap at the lowest temperatures, γ is the ratio of the probabilities of radiative and nonradiative deactivation of the excited state of the trap, k_B is Boltzmann's constant, and E_a is the depth of the trap relative to the bottom of the free-exciton

band. The experimental results are presented in Fig. 3. The activation energy for the X_1 trap ($E_{max}=1.79$ eV) is 0.04 eV (at $\gamma=2.6\times10^4$), while that for the X_2 trap is 0.06 eV (at $\gamma=8.0\times10^4$). Using the values given above for the energy positions of the peaks of the X traps, one can determine the energy of the 0–0 excitonic transition under the assumptions adopted; it turns out to be 1.83 eV, which is in rather good agreement (within our experimental error) with the published data.[8,29]

Thus the stress-induced structural traps (the so-called X traps) are a test for the relaxation dynamics and transport of excitations in C_{60} fullerite films of different structure.

The authors thank V. V. Eremenko for steadfast interest and support of this study, and S. L. Gnatchenko and M. A. Strzhemechny for helpful discussions.

*E-mail: avdeenko@ilt.kharkov.ua

[1] J. Shinar, Z. V. Vardeny, and Z. H. Kafafi (eds.), *Optical and Electronic Properties of Fullerenes and Fullerene Based Materials*, Marcel Dekker, New York–Basel (2000).
[2] P. Rudolf, M. S. Golden, and P. A. Brühwiler, J. Electron Spectrosc. Relat. Phenom. **100**, 409 (1999).
[3] H. W. Kroto, J. R. Heath, S. C. O'Brien, R. F. Curl, and R. E. Smalley, Nature (London) **318**, 162 (1985).
[4] W. Krätschmar, L. D. Lamb, K. Festiropulous, and D. R. Huffman, Nature (London) **347**, 354 (1990).
[5] V. Capozzi, M. Santoro, G. Perna, G. Celentano, A. Minafra, and G. Casamassima, Eur. Phys. J.: Appl. Phys. **14**, 3 (2001).
[6] I. Akimoto and K. Kan'no, J. Phys. Soc. Jpn. **71**, 630 (2002).
[7] X. Sun, G. P. Zhang, Y. S. Ma, R. L. Fu, X. C. Shen, K. H. Lee, T. Y. Park, Th. F. George, and L. N. Pandey, Phys. Rev. B **53**, 15481 (1996).
[8] R. Eder, A.-M. Janner, and G. A. Sawatzky, Phys. Rev. B **53**, 12786 (1996).
[9] M. Knupfer, J. Fink, E. Zojer, G. Leising, and D. Fichou, Chem. Phys. Lett. **318**, 585 (2000).
[10] V. V. Eremenko and V. S. Medvedev, Fiz. Tverd. Tela (Leningrad) **2**, 1572 (1960) [Sov. Phys. Solid State **2**, 1426 (1961)].
[11] H. Bässler, Phys. Status Solidi B **107**, 9 (1981).
[12] S. Arnold, W. B. Whitten, and A. C. Damask, J. Chem. Phys. **53**, 2878 (1970).
[13] J. O. Williams, B. P. Clarke, J. M. Tomas, and M. J. Shawe, Chem. Phys. Lett. **38**, 41 (1976).
[14] A. Lisovenko, M. T. Shpak, and V. G. Antonyuk, Chem. Phys. Lett. **42**, 339 (1976).
[15] A. Richter, R. Ries, K. Szulzewsky, B. Pietsak, and R. Smith, Surf. Sci. **394**, 201 (1997).
[16] K. Yase, N. Ara-Kato, T. Hanada, H. Takiguchi, Y. Yoshida, G. Back, K. Abe, and N. Tanigaki, Thin Solid Films **331**, 131 (1998).
[17] N. P. Kobelev, R. K. Nikolaev, N. S. Sidorov, and Ya. M. Soĭfer, Fiz. Tverd. Tela (St. Petersburg) **44**, 415 (2002) [Phys. Solid State **44**, 429 (2002)].
[18] D. V. Dyachenko-Dekov, Yu. V. Iunin, A. N. Izotov, V. V. Kveder, R. K. Nikolaev, V. I. Orlov, Yu. A. Ossipyan, N. S. Sidorov, and E. A. Steinman, Phys. Status Solidi B **222**, 111 (2000).
[19] A. A. Avdeenko, V. V. Eremenko, P. V. Zinoviev, N. B. Silaeva, Yu. A. Tiunov, N. I. Gorbenko, A. T. Pugachev, and N. P. Churakova, Fiz. Nizk. Temp. **25**, 49 (1999) [Low Temp. Phys. **25**, 37 (1999)].
[20] W. Guss, J. Feldmann, E. O. Göbel, C. Taliani, H. Mohn, W. Muller, P. Haussler, and H.-H. ter Meer, Phys. Rev. Lett. **72**, 2644 (1994).
[21] M. Tachibana, K. Nishimura, K. Kikuchi, Y. Achiba, and K. Kojima, J. Lumin. **66–67**, 249 (1995).
[22] K. P. Meletov and V. D. Negrii, Phys. Status Solidi B **211**, 217 (1999).
[23] G. Herzberg, *Molecular Structure and Molecular Spectra. III. Electronic Spectra and Electronic Structure of Polyatomic Molecules*, Van Nostrand Reinhold, New York, (1966), MIR, Moscow (1969).
[24] X. L. R. Dauw, G. J. B. van den Berg, D. J. van den Heuvel, O. G. Poluektov, and E. J. J. Groenen, J. Chem. Phys. **112**, 7102 (2000).
[25] E. L. Shirley, L. X. Benedict, and S. G. Louie, Phys. Rev. B **54**, 10970 (1996).
[26] S. Kazaoui, N. Minami, Y. Tanabe, H. J. Byrne, A. Eilmes, and P. Petelenz, Phys. Rev. B **58**, 7689 (1998).
[27] P. Petelenz and V. H. Smith, Chem. Phys. Lett **181**, 430 (1981).
[28] K. Kaneto, K. Rikitake, T. Akiyama, and H. Hasegawa, Jpn. J. Appl. Phys. **36**, Pt. 1, 910 (1997).
[29] M. Suzuki, T. Iida, and K. Nasu, Phys. Rev. B **61**, 2188 (2000).

Translated by Steve Torstveit

LATTICE DYNAMICS

Phase transitions in the magnetoelastic crystals $CsDy_{1-x}Gd_x(MoO_4)_2$

G. A. Zvyagina,* V. D. Fil', Yu. N. Kharchenko, and N. M. Nesterenko

B. Verkin Institute for Low Temperature Physics and Engineering, National Academy of Sciences of Ukraine, pr. Lenina 47, Kharkov 61103, Ukraine

(Submitted July 10, 2003)
Fiz. Nizk. Temp. **30**, 318–331 (March 2004)

Based on the data of ultrasonic studies and on the temperature behavior of the absorption spectra, a study of the phase diagram of the crystals $CsDy_{1-x}Gd_x(MoO_4)_2$ is made and the structural distortions occurring as a result of the pseudo-Jahn–Teller effect are discussed. It is shown that in the presence of impurities there are several lines of phase transitions on the $x-T$ phase diagram. It is established that one of the phase transitions these found is essentially of a magnetoelastic origin. © *2004 American Institute of Physics.*
[DOI: 10.1063/1.1645185]

1. INTRODUCTION

The double molybdates of rare-earth elements, with the composition $MRe(MoO_4)_2$, where M is an alkali metal (K, Cs, Rb) and Re is a rare-earth element, are layered magnetic dielectric crystals characterized by the presence of low-temperature phase transitions. The layered crystal $CsDy(MoO_4)_2$ has a first-order structural phase transition (SPT), the nature of which is not yet completely clear, at a critical temperature $T_c \approx 40$ K. The SPT is accompanied by a downward jump of the ground state energy of the dysprosium ions and is therefore attributed to cooperative Jahn–Teller (JT) ordering.[1] The SPT is sensitive to the substitution of a small amount of the Dy^{3+} ions by ions of the non-JT rare-earth elements. According to the data of Ref. 2, doping of a sample with Gd^{3+} and Eu^{3+} ions leads to a sharp lowering of the phase transition temperature, and at $x > 0.05$ (x is the concentration of the rare-earth impurities) it vanishes completely. Starting with $x \geqslant 0.03$ a line of second-order phase transitions, with a relatively weak dependence of the critical temperature on concentration, splits off from the line of first-order phase transitions. However, studies[3] of the system $CsDy_{1-x}Gd_x(MoO_4)_2$ ($x = 0.01$, 0.04, 0.05, 0.1) have shown that the phase diagram is more complex than had been assumed previously.[2] Studies of the phase diagram continue to this day, although the experimental data obtained with the use of different methods are rather contradictory. In particular, studies of the specific heat of $CsDy(MoO_4)_2$ over a wide range of temperatures (40 K $< T <$ 330 K) have revealed that, besides the previously known first-order SPT ($T_c \approx 42$ K) there are a number of anomalies attesting to substantial restructurings of the energy spectrum of the crystal.[4] One of these, at $T_i \approx 59$ K, has been attributed to a transition to an incommensurate phase. For a crystal with 5% Gd^{3+} the temperature dependence of the specific heat does not contain the anomaly corresponding to the first-order SPT nor the anomaly near 60 K that is observed for undoped $CsDy(MoO_4)_2$. However, at $T_c \approx 30.5$ K one observes a weak peak in the specific heat, which was interpreted by the authors as a second-order SPT. A study of the Raman scattering spectra of $CsDy(MoO_4)_2$ and $CsDy_{0.93}Gd_{0.07}(MoO_4)_2$ has revealed the presence of a first-order SPT at $T_c \approx 50$ K in both crystals.[5] We note that none of the techniques listed permits one to observe the whole sequence of SPTs realized in the system $CsDy_{1-x}Gd_x(MoO_4)_2$. Furthermore, according to recent data[6] of an x-ray structural analysis of $CsDy(MoO_4)_2$, the crystal structure of this substance, at least at room temperature, is not orthorhombic, as had been assumed previously,[7] but monoclinic.

Because the nature of the SPTs in both $CsDy(MoO_4)_2$ and in the doped crystals and also the lattice symmetry in the corresponding phases still remains unsettled, we have continued the study of the $x-T$ phase diagram of the $CsDy_{1-x}Gd_x(MoO_4)_2$ system. In particular, to refine the phase diagram we have used samples with $x = 0.07$, in which phase transitions have been observed in the Raman scattering spectra at 50 and 30 K.[5]

Since one of the mechanisms proposed for the first-order SPT in $CsDy(MoO_4)_2$ is ordering of the cooperative JT type, which derives from the electron–phonon interaction, it is important to observe the behavior of the phonon (acoustic) subsystem while simultaneously tracking the changes in the electron spectrum of the JT ions. In the present paper we have therefore undertaken a comprehensive study of the system $CsDy_{1-x}Gd_x(MoO_4)_2$ by both an ultrasonic method and by optical spectroscopy.

Thus the goal of this study was to determine the types of the SPTs and to analyze the symmetry of the phases in doped crystals, to study the influence of magnetic field on the temperature of the SPT in doped crystals, and to discuss the possible mechanisms for the SPTs using the data of ultrasonic studies and optical spectroscopy.

2. SAMPLES AND EXPERIMENTAL TECHNIQUES

The $CsDy(MoO_4)_2$ and $CsGd(MoO_4)_2$ crystals contain characteristic layered and chainlike structures and, according to Ref. 7, are isostructural. At $T \approx 300$ K the cell parameters

of these crystals are close (for $CsDy(MoO_4)_2$ they are $a=9.51$ Å, $b=7.97$ Å, $c=5.05$ Å and for $CsGd(MoO_4)_2$, $a=9.52$ Å, $b=8.05$ Å, $c=5.07$ Å), and the ionic radii of the rare-earth elements are also close; it was therefore assumed that doping leads to an isostructural substitution of Dy^{3+} ions by Gd^{3+}. The crystals were grown by the method of spontaneous crystallization from a fluxed melt. The impurity concentration was assumed to be the same as the relative content of gadolinium in the stock and for the systems studied was $x=0$, 0.03, 0.04, 0.05, 0.07, 0.1, and 0.25.

The crystals were thin (≈ 1 mm) mica-like slabs having a perfect cleavage plane (**bc**). Besides the perfect cleavage plane there was also a less perfect cleavage plane (**ac**), the presence of which was easily established from the nonrandom orientation of the breakage lines.

The orientation of the samples was carried out at room temperature by x-ray ''photography of reflected rays'' with an accuracy of $\sim 2-3°$. According to the data of an experimental structural analysis,[6] the symmetry of the $CsDy_{1-x}Gd_x(MoO_4)_2$ crystals at $T\approx 300$ K is close to orthorhombic, but there are small monoclinic distortions. The deviation of the monoclinic angle from a right angle is small ($\approx 2°$) and comparable to the accuracy of orientation of the samples. This circumstance and also the presence of twins made it impossible to take the monoclinicity into account in preparing the samples for the acoustic experiments.

The samples had characteristic dimensions of $0.5\times 1\times 1$ mm. The faces parallel to the perfect cleavable plane (**bc**) were not subjected to mechanical processing. The other two faces, parallel to the (**ac**) and (**ab**) planes, were polished with dry sandpaper with a micron abrasive. The working faces of the samples were plane-parallel to a precision of 1 μm. The residual stresses arising after the mechanical polishing were relieved by annealing the samples at $T\approx 900$ K.

As compared to Ref. 3, the equipment used in the acoustic measurements was of a new generation.[8] This made it possible, first, to carry out high-accuracy ($\sim 1\%$) measurements of the absolute sound velocities rather than crude transit-time estimations. Second, the fact that the limiting resolving power is maintained over a practically unlimited dynamic range made it possible to register slight features in the behavior of the sound velocity against the background of very substantial variations in the relative measurements.

In the experiment we used a continuous temperature pulling at a rate of 10 K/h in the interval $2\text{ K}<T<60$ K. The temperature was measured by a carbon resistance thermometer. The thermometer was not in direct contact with the sample but was placed in a common volume which was thermally insulated and filled with a heat-transfer gas (He^4 at 1–10 torr). The temperature difference between the sample and thermometer did not exceed 0.5 K, and the resolution was 0.05 K or better. For the measurements of the relative variations of the sound velocity in an external magnetic field we used a superconducting solenoid with a maximum magnetic field of ≈ 3.5 T.

The absorption of light by Dy^{3+} ions in the $CsDy_{0.93}Gd_{0.07}(MoO_4)_2$ crystal was studied in the region of transitions between levels of the ground multiplet $^6H_{15/2}$ and the excited states $^6F_{3/2}$ and $^6F_{5/2}$ at temperatures of 2–70 K.

TABLE I. Absolute values of the sound velocities in $CsDy(MoO_4)_2$, measured at $T=77$ K.

Geometry (mn)	Sound velocity, 10^5 cm/s
aa	2.85
ab	0.7
ac	1.9
ba	0.9
bb	3.28
bc	1.89
ca	1.97
cb	1.9
cc	4.04

Note: Geometry (**mn**) means that in the experiment the sound wave vector **q** was parallel to the direction **m** in the crystal while the polarization vector **u** was parallel to the direction **n**; the measurement error was 1% except in the geometries (**ab**) and (**ba**), where it was $\sim 10\%$.

For the experiment we used an apparatus based on a DFS-12 dual monochromator. The spectra were recorded using a photomultiplier in the photon-counting mode.

3. EXPERIMENTAL RESULTS AND DISCUSSION

3.1. Ultrasound (experiment)

With the goal of elucidating the influence of impurities on the phonon subsystem of the crystal we did acoustic studies of $CsDy_{1-x}Gd_x(MoO_4)_2$ ($x=0$, 0.03, 0.04, 0.05, 0.07, 0.1, and 0.25). For correct comparison of the results of the acoustic and optical measurements we used the same samples with $x=0.07$ for which phase transitions had been observed at 50 K and at approximately 30 K by the Raman scattering method.[5]

Studies have shown that doping with gadolinium has practically no effect (within the experimental error) on the absolute values of the sound velocities in $CsDy_{1-x}Gd_x(MoO_4)_2$ crystals ($x=0$, 0.04, 0.1). The results of the measurements at $T=77$ K for the undoped crystal $CsDy(MoO_4)_2$, are presented in Table I. Here and below we use a shortened notation for the experimental geometry. For example, the geometry (**ab**) means that the sound wave vector **q** is parallel to the **a** direction, while the polarization **u**, i.e., the displacement of the particles in the sound wave, is in the **b** direction. The accuracy of the measurements was generally on the 1% level. The geometries (**ab**) and (**ba**) are exceptions. The very small sound velocity and the resulting large damping in those geometries do not permit the achievement of a single-mode measurement regime in them, and, as a result, rather large errors of an interference nature arise. That is the reason why the value of the sound velocity in the (**ab**) geometry in Ref. 3 is substantially different from that obtained in the present study.

Qualitatively the results reflect a certain degree of layering of the crystals due to the relatively low values of the sound velocities. This effect is especially noticeable in the

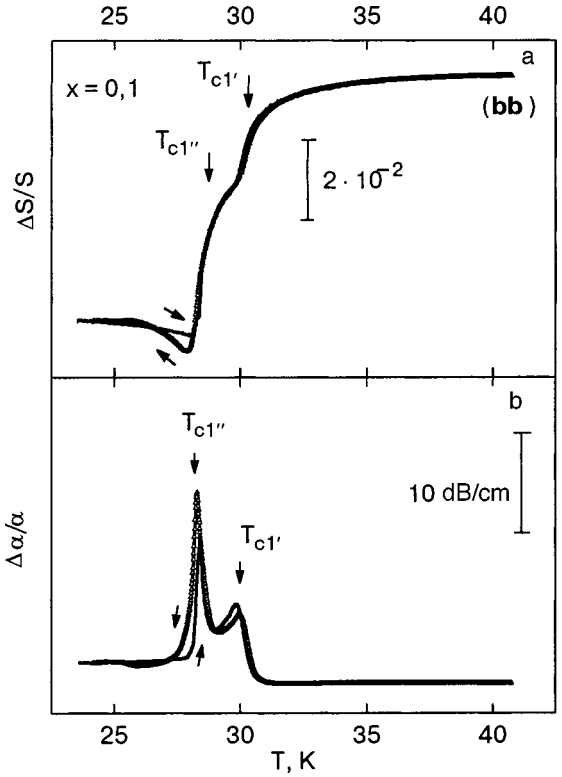

FIG. 1. Temperature dependence of the relative changes of the sound velocity ($\Delta S/S$) (a) and absorption ($\Delta\alpha/\alpha$) (b) in $CsDy_{1-x}Gd_x(MoO_4)_2$ for $\mathbf{q}\|\mathbf{b}$, $\mathbf{u}\|\mathbf{b}$.

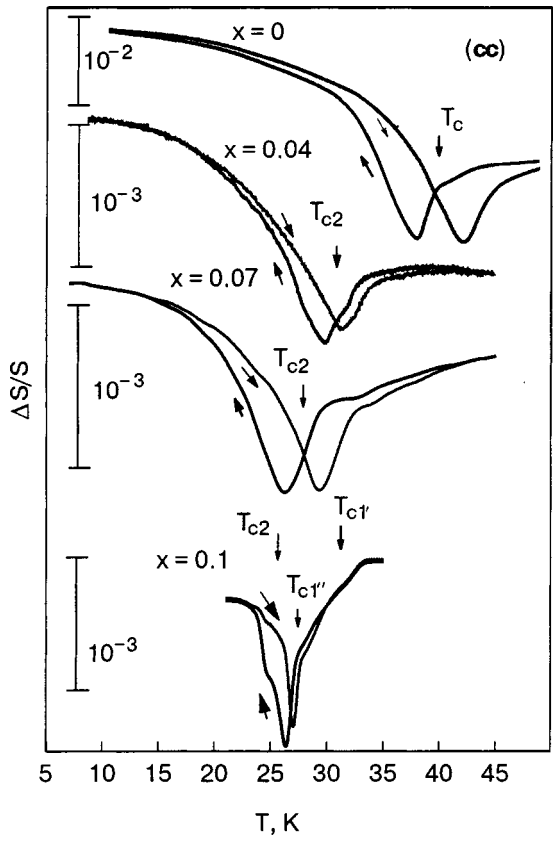

FIG. 2. Form of the temperature dependence of the relative changes in the sound velocity in $CsDy_{1-x}Gd_x(MoO_4)_2$ for $\mathbf{q}\|\mathbf{c}$, $\mathbf{u}\|\mathbf{c}$.

(**ab**) and (**ba**) geometries, when the vectors **q** and **u** are orthogonal to the cleavage planes. Some "nonreciprocity" of the results can be noted, i.e., the values of the transverse sound velocities measured in the geometries (**ac**) and (**ca**) are different, as are the values measured for (**ab**) and (**ba**). This, we believe, is due to the monoclinic distortions of the crystal structure.

The temperature behavior of the relative variations of the sound velocities measured in different geometries for the crystals $CsDy_{1-x}Gd_x(MoO_4)_2$ ($x=0$, 0.04, 0.07, 0.1) are presented in Figs. 1–5. As is seen in the figures, in the interval 20–40 K the behavior of both the longitudinal and transverse velocities has anomalies (jumps and kinks) which are characteristic of structural transformations. The typical anomalies for all the crystals (described in more detail below) can be associated to the critical temperatures $T_{c1'}$, $T_{c1''}$, and T_{c2}.

It is known[9] that a second-order structural phase transition is characterized by a jump in the temperature dependence of the longitudinal elastic moduli of the crystal and a kink (jump of the derivative) in the temperature dependence of the transverse moduli. As is seen in Figs. 1, 2, and 3, the temperature curves of the longitudinal velocities have jumps at the temperatures $T_{c1'}$ and $T_{c1''}$. For the velocity measured in the (**bb**) geometry the jumps $\Delta S/S$ are appreciable ($\sim 2\times10^{-2}$) and are accompanied by upsurges in the sound absorption at these same temperatures (see Fig. 1). For the other geometries the variation of the longitudinal velocities at $T_{c1'}$ and $T_{c1''}$ are much smaller in scale and are somewhat smeared in temperature (Fig. 2, $x=0.1$, and Fig. 3). Therefore the critical temperatures $T_{c1'}$ and $T_{c1''}$ are determined from the position of the maximal jumps in the temperature dependence of the longitudinal velocity (and of the related elastic moduli) measured in the (**bb**) geometry (Fig. 1).

The temperature curves of the transverse velocities have kinks at these same temperatures (Figs. 4 and 5). We note that the anomalies of both the longitudinal (jumps) and transverse (kinks) velocities near $T_{c1'}$ and $T_{c1''}$ have a qualitatively similar character that is typical of second-order phase transitions.

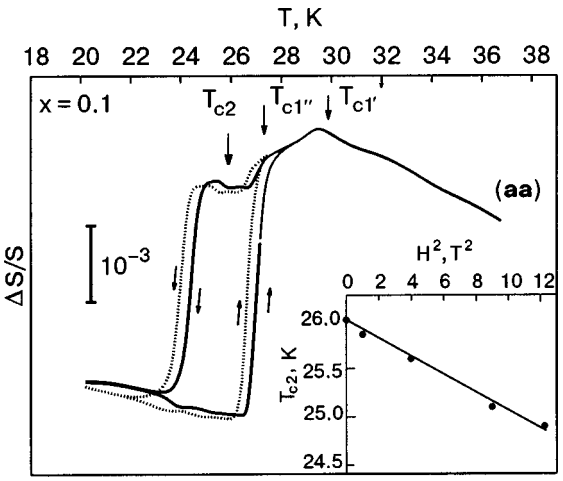

FIG. 3. Temperature dependence of the relative changes of the sound velocity in $CsDy_{1-x}Gd_x(MoO_4)_2$ for $\mathbf{q}\|\mathbf{a}$ and $\mathbf{u}\|\mathbf{a}$. The solid curve is in the absence of magnetic field, the dotted curve in an external magnetic field $H=3.5$ T applied along the **a** direction. The inset shows the dependence of the critical temperature T_{c2} on the square of the magnetic field strength.

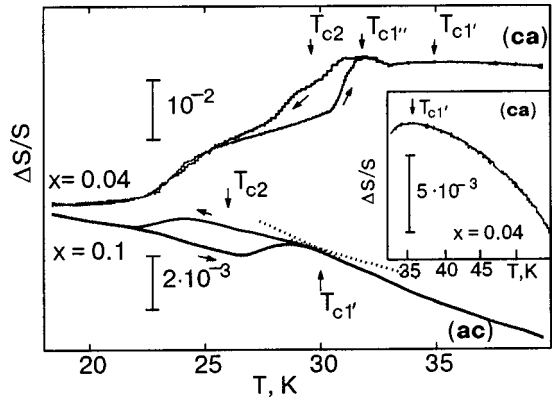

FIG. 4. Temperature dependence of the relative changes of the sound velocity in $CsDy_{1-x}Gd_x(MoO_4)_2$ for **q**∥**a**, **u**∥**c** and **q**∥**c**, **u**∥**a**. The inset shows the temperature dependence of the relative changes in the sound velocity (**q**∥**c**, **u**∥**ba**) in $CsDy_{0.96}Gd_{0.04}(MoO_4)_2$ in the temperature interval 30–55 K.

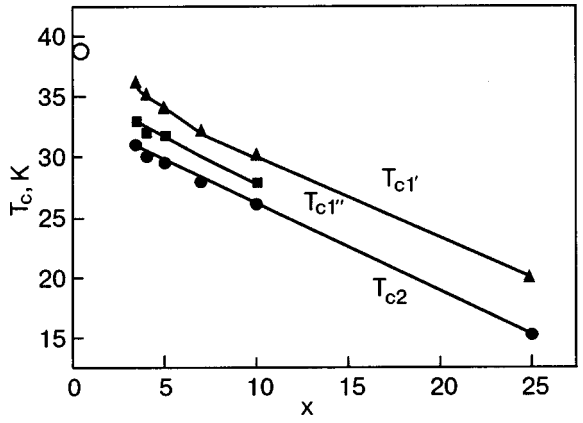

FIG. 6. Fragment of the $x-T$ phase diagram of $CsDy_{1-x}Gd_x(MoO_4)_2$ crystals (x is the concentration of the rare-earth impurity). Lines of second-order phase transitions (▲,■); line of first-order phase transitions (●); first-order phase transition in the crystal without impurities (○).

At lower temperatures, as follows from the data of Figs. 1–5, there is another SPT, at which distinct hysteresis loops are observed. The values of the jumps for the longitudinal and transverse velocities are approximately equal (of the order of 10^{-3}). The jumps of the longitudinal velocity measured in the (**aa**) geometry is localized in a narrow temperature interval (1.5 K), while for the other geometries the jumps have some temperature smearing. The significant temperature hysteresis accompanying the anomalies attests to the first-order nature of this SPT.

We determined experimentally the two values of the temperature at which the jumps of the longitudinal and transverse velocities are observed on cooling and heating. The value of the critical temperature T_{c2} indicated in the figures is the mean value between the temperatures of the jumps of the longitudinal velocity [(**aa**) geometry] on decreasing and increasing temperature. Let us mention some features of this first-order phase transition.

First, for the sound waves with **q**∥**b** one observes practically no anomalies, although a slight irreversibility is discernable in this case as well (Fig. 1). Second, the form of the anomaly near T_{c2} for longitudinal sound, measured in the (**cc**) geometry, is preserved for the crystals, including the crystal not containing impurities (Fig. 2), only the scale of the low-temperature shoulder on the $\Delta S/S(T)$ curve is changed. Furthermore, increasing the gadolinium content decreases the ''excess'' part of the left shoulder of the curve relative to the right. Taking into consideration that the sound anomalies are ''inherited'' in all the impurity-containing crystals, while the temperatures $T_{c1'}$, $T_{c1''}$, and T_{c2} depend on the concentration x, we have constructed the phase diagram of these crystals (Fig. 6).

One way of obtaining additional information about the nature of the SPTs is to study the influence of magnetic field on them. For these crystals we chose the geometry (**aa**), in which all of the phase transformations under discussion are rather clearly expressed (Fig. 3). It turned out that with increasing magnetic field H the critical temperature T_{c2} is shifted quadratically to lower values in proportion to H^2 (inset in Fig. 3). The critical temperature $T_{c1'}$ is practically independent of the value of the applied magnetic field. Interestingly, the anomaly of the longitudinal sound is sensitive to external magnetic field.

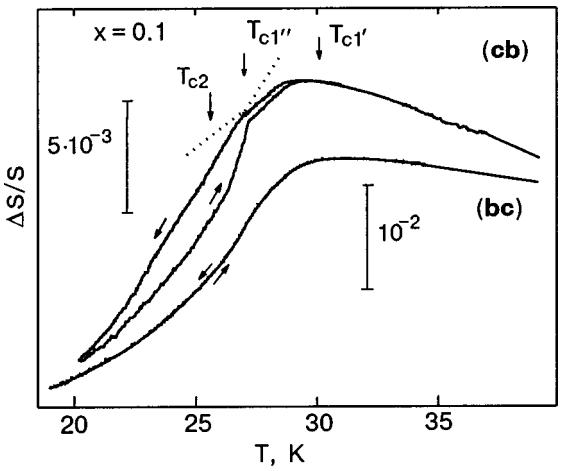

FIG. 5. Temperature dependence of the relative changes in the sound velocity in $CsDy_{1-x}Gd_x(MoO_4)_2$ for **q**∥**b**, **u**∥**c** and **q**∥**c**, **u**∥**b**.

3.2. Ultrasound (discussion)

The phase diagram of the crystals was constructed on the basis of the similarity of the sonic anomalies in the series of crystals with different impurity concentrations and the temperature dependence of the position of these anomalies. The upper and middle curves in Fig. 6 correspond to lines of SPTs with critical temperatures $T_{c1'}$ and $T_{c1''}$, respectively, and the lower curve to the line of transitions with critical temperatures T_{c2}. We assume that in the presence of a sufficient number of gadolinium ions the first-order phase transition in the $CsDy(MoO_4)_2$ crystal will be transformed into a sequence of three SPTs lying close in temperature. Such a phase diagram is possible if the phase transitions are characterized by interacting order parameters. Each of these order parameters depends on the impurity concentration. This determines the dependence (which is linear in the concentration region studied) of the critical temperatures of the SPTs on x. We stress that the order parameters interact differently with the electronic subsystem, their interaction being regulated by impurities of non-JT ions. The dependence of the sonic anomalies on the external magnetic field field near T_{c2} is a

direct indication that the nature of this SPT is largely determined by the magnetoelastic coupling. We also note that no dependence of the temperature $T_{c1'}$ on the magnetic field was seen, at least not at the available magnetic field strengths.

It has been established that the sonic anomalies in the doped crystals for different geometries are divided into three groups. One can therefore discuss them on the assumption that they are due to three different phase transitions lying close together in temperature. Let us discuss the nature of these phase transitions in view of the features of the sound propagation near the critical temperatures.

Since none of the transverse moduli exhibits noticeable softening near $T_{c1'}$ (Figs. 4 and 5), it follows from the phenomenological theory of SPTs[9] that the order parameter is not some linear combination of strain tensor components. Consequently, the phase transitions at $T_{c1'}$ should be classed by symmetry with the second-order improper ferroelastic transitions (there is no hysteresis around $T_{c1'}$). It is most natural to suppose that as a result of the SPT a loss of translational invariance occurs, accompanied by multiplication of the unit cell. In this case the order parameter η is of a scalar character.

Let us now discuss the behavior of the longitudinal moduli in the region of $T_{c1'}$ (Figs. 1–3). According to the general theory of second-order phase transitions,[9] jumps of the longitudinal modulus can be due to the existence of terms of the type $r\eta^2 C(u_{ik})$ in the expansion of the thermodynamic potential, where $C(u_{ik})$ is any linear combination of strain tensor components which is invariant with respect to all symmetry transformations of the symmetric phase, and r is the coupling coefficient. In any experimental geometry one always has the invariant u_{ii} (u_{ii} is the trace of the strain tensor), which is responsible for the jump of the bulk modulus of compression at the SPT and, accordingly, for the jump in the longitudinal sound velocities. The scale of these anomalies is determined by the common coefficient r, so that the anisotropy of the observed variations should be proportional to the ''bare'' sound velocities. However, it is seen from the data presented here that the change in sound velocity in the geometry (**bb**) (Fig. 1) is approximately two orders of magnitude larger than the analogous changes for the other geometries (Figs. 2 and 3). This means that, besides the invariant $r\eta^2 C(u_{ik})$ discussed already, the expansion of the thermodynamic potential has at least one other invariant $r_1\eta^2 u_{bb}$ with an anomalously large coupling coefficient r_1. According to the theory of elastic wave propagation in crystals,[10] the invariance of some diagonal component of the strain tensor (in our case u_{bb}) is an indication that that particular direction is a longitudinal normal, i.e., a direction in which ''pure'' acoustic modes propagate. The standard condition ensuring the existence of a longitudinal normal is that the wave normal coincides with an axis of symmetry (or is perpendicular to a plane of symmetry). Generally speaking, this condition is sufficient but not necessary, and a longitudinal normal can exist even for a propagation direction of a general kind,[10] but such a direction is hit upon in a largely accidental manner and can hardly be what we have here. This direction can be determined rigorously if one knows all the independent components of the tensor of elastic constants. However, our experiments do not permit us to obtain the completely set of tensor components.

Thus we assume that the **b** direction is an axis of symmetry in the system $CsDy_{1-x}Gd_x(MoO_4)_2$ near $T_{c1'}$, at least for an appreciable part of the crystal.

According to x-ray structural data,[6] the $CsDy(MoO_4)_2$ crystal at room temperature has a monoclinic lattice in which the twofold axis coincides with the **c** direction. In the temperature interval 70–48 K (48 K is the critical temperature of the first-order SPT) the structure is a mixture of twins of the monoclinic phase with orthorhombic inclusions between them. Below the SPT a new monoclinic phase is realized in the crystal, with a new monoclinic angle but with the same twofold axis as in the high-temperature monoclinic phase (the **c** direction). Unfortunately, there are no such data for the impurity-containing crystals. Nevertheless, it may be hoped that the evolution of these structures is analogous.

However, a consistent interpretation of the results of the acoustic experiments is possible only in case when the twofold axis of the monoclinic phase in the doped crystals coincides the **b** direction above $T_{c1'}$. The contradiction with the results of Ref. 6 can be resolved by assuming that the jumps of the sound velocity in the (**bb**) geometry observed by us are due to a structural transition in the orthorhombic inclusions.

Since the longitudinal and transverse velocities near the critical temperatures $T_{c1'}$ and $T_{c1''}$ experience similar anomalies, the phase transformation at $T_{c1''}$ probably occurs by an analogous scenario. Therefore, all the arguments set forth above as to the character of the SPT at $T_{c1'}$ also apply to the case of the SPT at $T_{c1''}$. The presence of two phase transitions of the same type with close values of the critical temperatures can be explained, e.g., by passage through two commensurate phases in the process of the structural reorganization of the crystal.

Let us now discuss the phase transition at T_{c2} using only the ultrasound data. Two possible scenarios for the SPT at T_{c2} can be suggested. The structural transformation is due either to a transition from one monoclinic phase to another with an accompanying jumplike change in the monoclinic angle (as was in fact indicated in Ref. 6) or to a jumplike transition to a monoclinic phase of the orthorhombic interlayers mentioned above. It can be assumed that the values of the diagonal components of the elastic constant tensor, which reflect the scale of the forces acting between atoms of the crystal lattice, change weakly at the phase transition. The changes in the sound velocities in any geometry of the experiment are due to both rotation of the principal axes of the tensor and to the appearance of new components in it (upon the transition from the orthorhombic to the monoclinic phase). Then, if the **b** axis remains a longitudinal normal at the SPT, analysis of the corresponding Christoffel equations shows that the velocities of the $\mathbf{q}\|\mathbf{b}$ acoustic modes that remain ''pure'' do not change. At the same time, for the other geometries ($\mathbf{q}\|\mathbf{a}$ or $\mathbf{q}\|\mathbf{c}$) the interference of the elastic constants should lead to jumplike changes of the sound velocity. Let us discuss further the features of the hysteresis loops of the velocity of longitudinal sound measured in the (**cc**) geometry (Fig. 2).

Despite the different width of the hysteresis loops for

crystals with different impurity concentrations, the anomalies at T_{c2} are similar for all the crystals. It is known that the width of the hysteresis loop at a first-order SPT depends on the particular nucleation processes for each sample.

Indeed, the value of the hysteresis is influenced by the complex domain structure in the vicinity of the temperature of the first-order SPT in the undoped samples, which is due to the significant lattice strains and also to the presence of twins in the low-temperature phase.[6] The features of the temperature dependence of the sound velocity measured in the (**cc**) geometry in the vicinity of $T_{c1'}$ and of $T_{c1''}$ are determined by the proximity to the fields of lability of the first-order phase transition at T_{c2}. Our experiments showed that for the other geometries the hysteresis loops are closed below $T_{c1''}$ for all concentrations. Therefore we assume that the sonic anomalies along the lines $T_{c1'}(x)$ and $T_{c1''}(x)$ the sonic anomalies are not accompanied by hysteresis, i.e., these are second-order phase transitions.

We note in conclusion that one of the shortcomings of Ref. 3 was the actual absence of a transition in going from the doped crystals to the undoped $CsDy(MoO_4)_2$. In Ref. 3 the structural transformation was determined only from the vanishing of acoustic contact, which is probably due to the significant jumps in the unit cell parameters of the crystals at the first-order SPT.[11] In the present study, by suitably choosing the experimental geometry and decreasing the area of acoustic contact we were able to record the shape of the anomalies in the sound velocity in the vicinity of the phase transitions both for crystals with a low impurity concentration and for the undoped $CsDy(MoO_4)_2$ (Fig. 2). Despite the change in scale of the effect and the increase in the width of the hysteresis loop, it is clear that the anomalies all have the same type of shape and that there are no additional features on the low-temperature wing of the temperature dependence.

The ultrasonic measurements give information only about the macroscopic changes in the system. The changes of the absorption spectra at the phase transitions permit one to assess the local distortions of the structure and carry additional information about the nature of the phase transitions, and that was our motivation for studying them.

3.3. Absorption spectra (experiment)

Figure 7 shows the changes in the absorption spectra of the crystal $CsDy_{0.93}Gd_{0.07}(MoO_4)_2$ in the temperature region 5–33 K in the energy interval 13200–13300 cm^{-1}. In that energy region the absorption of light in the free dysprosium ion occurs on account of electronic transitions from the levels of the ground term $^6H_{15/2}$ to the excited multiplet $^6F_{3/2}$. As we see, the absorption spectrum is modified as the temperature is raised.

At low temperatures the absorption spectrum of the doped crystal, like that of $CsDy(MoO_4)_2$, consists of an intense doublet with an interval of $\sim 8\ cm^{-1}$ between components and a weak satellite on the high-energy side (Figs. 7 and 8). As is seen in the figures, the spectra differ in the position of the doublet—in the $CsDy(MoO_4)_2$ crystal it is shifted by approximately 75 cm^{-1} to lower energy. In the impurity-containing crystal the band arising with decreasing temperature on the low-energy side is, like the main line, asymmetric and is apparently also a doublet (Fig. 7). In

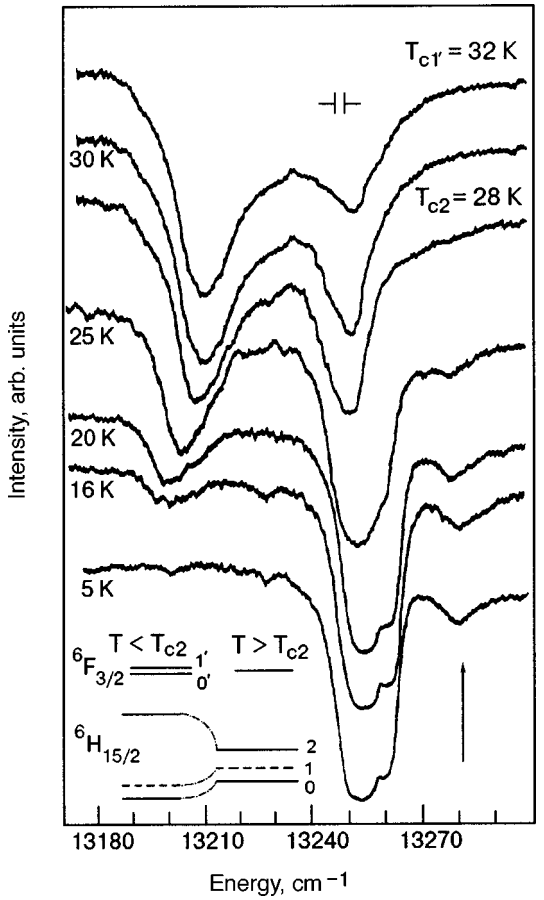

FIG. 7. Absorption spectra for different temperatures in $CsDy_{0.93}Gd_{0.07}(MoO_4)_2$, $\mathbf{E}\|\mathbf{b}$, the transition $^6H_{15/2}$–$^6F_{3/2}$. The inset shows the level scheme above and below T_{c2}.

$CsDy(MoO_4)_2$ the spectrum typical of the low-temperature phase changes with a jump near 42 K, and above that temperature it takes on the form of two well-resolved bands with an interval between them of 41 cm^{-1} (Ref. 12), as in the doped crystal near 28–30 K (Fig. 7). We note that in the crystal containing 7% Gd^{3+} this temperature is close to the value of T_{c2} determined from the ultrasonic measurements.

The spectrum of the doped crystal near 32 K has some slight changes from that at 30 K (Fig. 7): there is a change in the relative values of the intensities of the components of the spectrum for the two polarizations, while the energy interval between them remains unchanged. In the vicinity of 50 K there are no qualitative changes in the spectra which could indicate a phase transition.

Since the spectrum contains poorly resolved lines of different intensity, it was necessary to do a computer processing of the spectrum. The spectrum was modeled by a set of lines, the number of which was decided on the basis of additional considerations set forth below. Figure 9a shows the decomposition of the spectrum at 25 K, and Fig. 9b shows the temperature dependence of the components of the fine structure of the spectrum of the $CsDy_{0.93}Gd_{0.07}(MoO_4)_2$ crystal.

In the computer modeling it was assumed, first, that a doublet structure of the lines is present for the main band and the band that is rising. The spectrum was described by a superposition of lines having the characteristic shape for a damped oscillator, with temperature-dependent parameters:

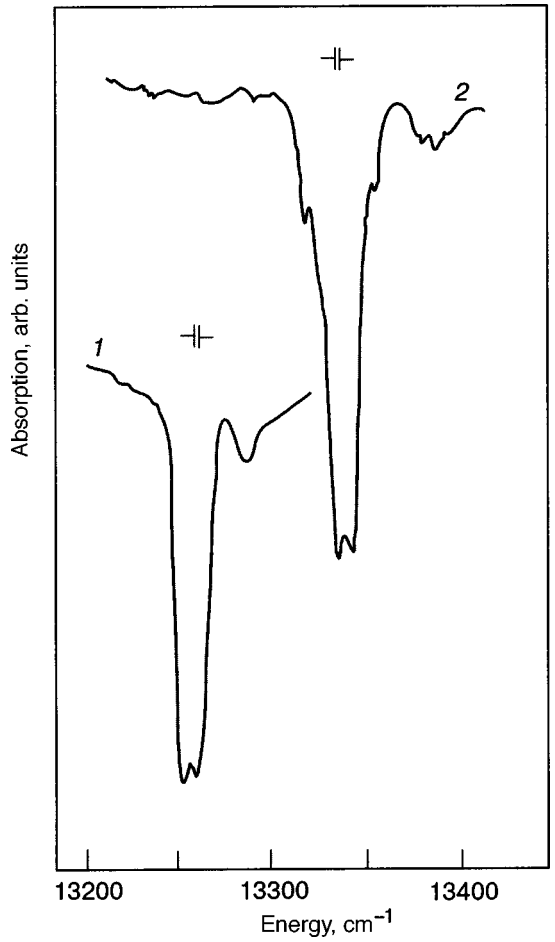

FIG. 8. Absorption spectra for the crystals $CsDy_{0.93}Gd_{0.07}(MoO_4)_2$ (*1*) and $CsDy(MoO_4)_2$ (*2*) at a temperature of 6 K; the $^6H_{15/2}-^6F_{3/2}$ transition, $\mathbf{E}\|\mathbf{b}$.

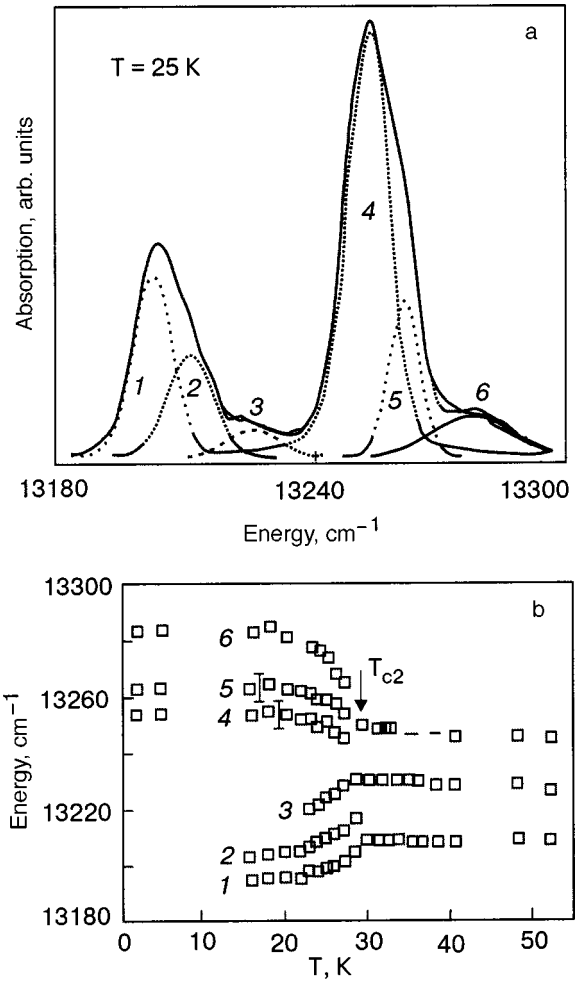

FIG. 9. Decomposition of the spectral profile at $T=25$ K, $\mathbf{E}\|\mathbf{b}$ (a); position of the maxima of the lines for the transition $^6H_{15/2}-^6F_{3/2}$ in the crystal $CsDy_{0.93}Gd_{0.07}(MoO_4)_2$ with changing temperature (results of a calculation) (b); the distribution of the intensity of the envelope of the spectrum has been logarithmized.

the intensity, half-width, and position of the maximum. The change in line shape has almost no effect on the position of the maxima of the spectral components in the temperature region where the maxima of the lines were rather well resolved.

Second, for $T>28$ K the high-frequency component of the spectrum has a half-width that does not exceed the half-width of an individual component of the doublet at $T<28$ K, and it is a single line. Therefore in the decomposition of the spectrum it was assumed that above that temperature either the doublet structure of the lines is absent or the second component has a low intensity.

Third, in the temperature region 20–28 K a weak line appears between the main and the rising doublets, leading to asymmetry of the adjacent line (Fig. 7). Therefore, to describe the spectrum formally we introduced one more component into consideration (line *3* in Fig. 9a). In addition, the modeling took into account a high-energy spectral component (line *6*), which was observed at low temperatures. Figure 9b shows the temperature dependence of the maxima of the lines, based on the modeling results.

To elucidate the nature of the low-temperature doublet we recorded the absorption spectrum corresponding to the transition to another excited level—the spectrum of the transition $^6H_{15/2}-^6F_{5/2}$ (Fig. 10). At low temperatures one would expect three lines for this transition. However, besides the three intense lines, the spectrum at 6 K contains weak narrow lines on the low-frequency side and weak broad lines on the high-frequency side. Increasing the temperature, as can be seen in Fig. 10, mainly affects the low-frequency wing of the saturated line: two satellites with intervals of approximately 50 and 20 cm^{-1} arise at $T=20$ K. Despite the complex character of the spectrum, one can conclude that the series of three intense lines corresponds to the transition from the ground level to an excited triplet, and these lines are single (Fig. 10). This last statement follows from the fact that the line with half-width 15 cm^{-1} cannot be the envelope of two bands split by 8 cm^{-1} (at a spectral resolution of 1.5–2 cm^{-1}). The spectra measured at low temperatures for the two polarizations $\mathbf{E}\|\mathbf{b}$ and $\mathbf{E}\|\mathbf{c}$ are similar and are shifted as a whole by 2 cm^{-1}.

On the temperature dependence of the position of the maxima of the lines (Fig. 9b) one can see that the temperature 28 K is distinguished by kinks in the plots of the energy position of the individual lines. Some of the lines are not observed at all above that temperature.

Thus it follows from the experimental results that the absorption spectrum of the doped crystal in the temperature region 5–32 K is qualitatively altered, and the jumplike changes, i.e., the vanishing of the doublets and the depolar-

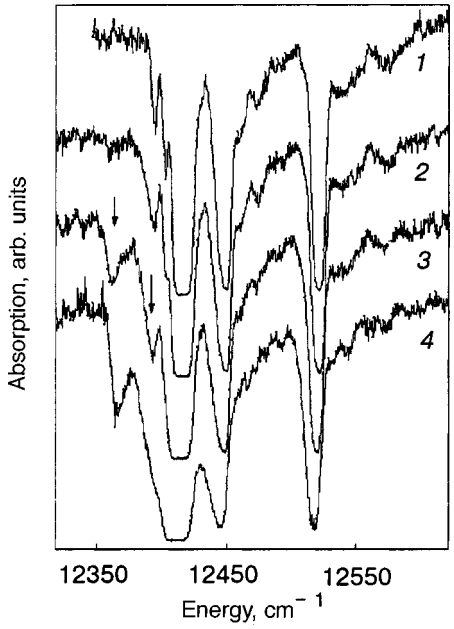

FIG. 10. Absorption spectrum in the $CsDy_{0.93}Gd_{0.07}(MoO_4)_2$ crystal at different temperatures T [K]: 6 (*1*), 15 (*2*), 20 (*3*), 25 (*4*); $\mathbf{E}\|\mathbf{b}$, the transition $^6H_{15/2}-^6F_{5/2}$. The spectral slit is 2 cm^{-1}.

ization of the lines, occur at temperatures of 28 and 32 K, which are close to the values of T_{c2} and $T_{c1'}$ obtained in the ultrasonic measurements on $CsDy_{0.93}Gd_{0.07}(MoO_4)_2$. The doublet structure of the spectrum is manifested for both the doped and ''pure'' crystals below the critical temperature T_{c2} (28 and 42 K, respectively). Above T_{c2} the spectra of the two crystals are practically indistinguishable.[12] Therefore, it can be assumed that the initial phase preceding the transitions at $T_{c1'}$ and T_{c2} is the same in both crystals. Decreasing the temperature from 28 to 5 K leads to a smooth increase in the energy interval between the ground level and (apparently) the second excited level by approximately 16 cm^{-1} and also to the rise of a line on the high-energy side (line *6* in Fig. 9a,b). Let us turn to a discussion of the results.

3.4. Absorption spectra (discussion)

In the double molybdates the dysprosium ions occupy positions without a center of inversion, and for that reason the intraconfigurational transitions of a dipole nature are allowed. The unit cell of $CsDy(MoO_4)_2$ at room temperature contains two dysprosium ions, and therefore the number of Davydov components is 2. In the phase preceding the SPT the number of components is doubled because the volume of the unit cell is doubled in comparison with the room-temperature phase. The odd (active in the absorption spectra) excitations are energetically distinct in the different polarizations. In determining the possible number of lines in the spectra one must also take into account the fact that the ground state of the term $^6H_{15/2}$ of the rare-earth ion is split by the low-symmetry crystalline field. The number of components is determined by the value of its total angular momentum $J=15/2$ and is equal to 8. In the excited states $^6F_{3/2}$ and $^6F_{5/2}$ the multiplicities of the Stark splitting are equal to 2 and 3. Hence one can determine the expected number of lines in the spectra at low temperatures, when the excited levels of the ground multiplet are not occupied. Let us discuss the energy level (band) scheme of the ground and excited multiplets of the dysprosium ions inferred from an analysis of the experimental spectra.

The doublet structure of the transition from the ground state $^6H_{15/2}$ to the excited state $^6F_{3/2}$ near helium temperatures may be due to both the presence of the Davydov components $0-0'$ and $0-1'$ of the transitions (Fig. 7) and to the energy inequivalence of the rare-earth centers, and to the splitting of the excited state $^6F_{3/2}$. We determined that in the series of transitions from the ground term $^6H_{15/2}$ to the components of the excited term $^6F_{5/2}$ the lines are single, and the Davydov (polarization) splitting does not exceed 2 cm^{-1}. This means that the doublet structure of the lines in the spectrum for the transition $^6H_{15/2}-^6F_{3/2}$ at temperatures below 28 K is determined by the splitting of the excited state $^6F_{3/2}$. Comparing the temperature evolution of the spectra for the transitions $^6H_{15/2}-^6F_{3/2}$ and $^6H_{15/2}-^6F_{5/2}$ (Figs. 7 and 10) and taking into account the appearance of new lines as a result of thermal population of the levels of the ground multiplet, we conclude that the first excited level of the ground state of the ground multiplet $^6H_{15/2}$ of the dysprosium ions lies at an energy near 20–23 cm^{-1}. The level scheme reconstructed from the spectra for the $^6H_{15/2}-^6F_{3/2}$ transitions is shown in Fig. 7.

We note the fact that the satellites arising for $^6H_{15/2}-^6F_{5/2}$ (denoted by arrows in Fig. 10) are observed only for one of the most intense lines. This means that the absorption processes going from the excited levels (bands) ($1-0'$ and $2-0'$ in our case; see the scheme) are, first, related to the intensity of the main transition and, second, are substantially weaker than the $0-0'$ and $0-1'$ transitions, respectively. This implies that the rise of the lines is due to two-frequency processes occurring at the boundary point of the band. Thus the single-ion approximation, which was used to describe our spectrum, is valid only on the assumption of small dispersion of the branches. The small Davydov splitting is a measure of this dispersion.

On the other hand, the appearance of doublet structure of the main lines for the transition $^6H_{15/2}-^6F_{3/2}$ is due to a phase transition and reflects the distortions of the crystalline field near the dysprosium ions. The position symmetry of the rare-earth ions can change at the phase transition on account of the doubling of the number of layers in the unit cell. However, doubling of the layers occurs already at 50 K,[5] and the 8 cm^{-1} splitting of the lines in the spectrum takes place only below 28 K. From this we conclude that at the SPT with critical temperature T_{c2} distortions probably arise in the $\{(Dy-Gd)(MoO_4)_2\}_\infty^-$ layer and, in our opinion, lead to the appearance of the doublet structure of the spectrum (Figs. 7 and 8) in the low-temperature phase.

Let us discuss further the possible lattice distortions in the undoped crystal, starting from a comparative analysis of the low-temperature spectra of the cesium crystals and the $KDy(MoO_4)_2$ crystal, which can be regarded as a layered polytype of them. Indeed, the unit cells of the initial phases of both $CsDy_{0.93}Gd_{0.07}(MoO_4)_2$ and $KDy(MoO_4)_2$ contain at least two $\{Dy(MoO_4)_2\}_{1\infty}^-$ layers.[5,13] The structure of the layer and the oxygen polyhedron surrounding the dysprosium ion are nearly the same in the two crystals. In the po-

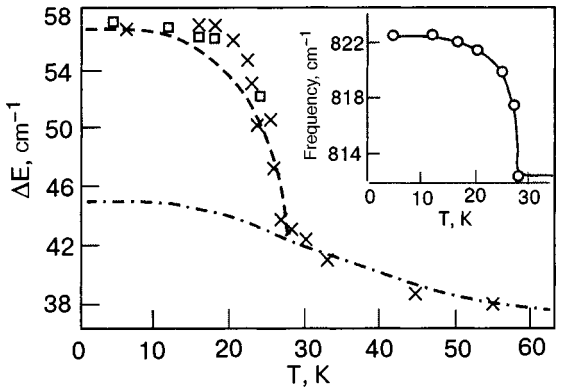

FIG. 11. Temperature dependence $\Delta E(T)$ determined from the absorption spectra (×) and Raman scattering spectra (□).[15] The inset shows the temperature dependence of the frequency of the $(MoO_4)_2$ deformation vibrations.[5] The dashed and dot-and-dash curves are the approximations by formulas (2) and (3).

tassium molybdate the dysprosium ions are shifted slightly along the smallest cell parameter, forming a zigzag chain along the intermediate cell parameter, in contrast to the cesium case.[6] In addition, the $(MoO_4)^{2-}$ tetrahedra in the potassium structure are rotated by a small angle α relative to the plane of symmetry, which is parallel to (**ab**).[13] Let us compare the absorption spectra of the potassium and cesium crystals in the low-temperature phases.

It is known[14] that in the $KDy(MoO_4)_2$ spectra for the transition ${}^6H_{15/2}-{}^6F_{3/2}$ at low temperatures the interval between components of the intense doublet corresponding to the transition from the ground state to the components of the excited state ${}^6F_{3/2}$ is $\sim 8\ cm^{-1}$, i.e., the same value as in the cesium crystals studied.

We assume that the distortion of the structure of the $CsDy_{0.93}Gd_{0.07}(MoO_4)_2$ crystal during the phase transformation leads to the same distortions of the local environment of the dysprosium ions as for the $KDy(MoO_4)_2$ structure, this coincidence being not only qualitative but quantitative as well (we are referring to the agreement of the value of the energy interval between components of the doublet, $8\ cm^{-1}$). Taking into consideration the results of Refs. 5 and 15, let us discuss the changes in the spectrum with temperature due to the smooth changes in the position of the lines with increasing temperature.

The temperature dependence of the energy interval 0–2 in the region 6–50 K, reconstructed using the data in Fig. 9b, is shown in Fig. 11. It is seen that with increasing temperature the value of the energy interval (splitting) decreases, and a kink appears on the temperature dependence at 28 K, i.e., near T_{c2}. The squares in Fig. 11 show the position of the low-frequency Raman-active excitation (with energy $58-42\ cm^{-1}$) that rises in the Raman scattering spectrum in the low-temperature phase.[15] This excitation is even with respect to inversion and apparently corresponds to the transition 0–2 between the ground and second excited levels of the ground multiplet (see the scheme in Fig. 7). The close values of the energy interval determined by the two methods (from the absorption and Raman-scattering spectra) indicate that the Davydov splitting of the even and odd components is small. We note that in the Raman scattering spectra in the low-temperature phase one observes an excitation with a frequency of $23-25\ cm^{-1}$, which according to the scheme in Fig. 7 corresponds to the 0–1 transition and, hence, to the position of the first excited level of the dysprosium ions.[15] Its position in the low-temperature phase varies with decreasing temperature in the same way as the position of the ground state, unlike the case of the high-frequency excitation.

The inset in Fig. 11 shows the temperature dependence of the frequency of the deformation vibrations of the $(MoO_4)^{2-}$ tetrahedra surrounding the Dy^{3+} ions (the frequency region $\sim 810\ cm^{-1}$).[5,15] It is seen that the temperature dependence of the energy interval between levels of the ground multiplet of the dysprosium ions is similar to the temperature dependence of the frequency of the deformation vibration of the $(MoO_4)^{2-}$ anions. This correlation is apparently due to the fact that the phase transition in the cesium crystal is accompanied by a rotation of the tetrahedral anions $(MoO_4)^{2-}$. The ordering of the distortions of the oxygen polyhedra surrounding the dysprosium ions is accompanied by an energy benefit in the electronic subsystem of the rare-earth ions, i.e., by ordering of the cooperative JT type.

Thus one can conclude that as a result of the ''freezing in'' of the vibrations, including rotations of the tetrahedral anions and displacement of the rare-earth ions along the **c** axis (the dysprosium ions have an analogous position in the potassium structure), the structure of the low-temperature phase of $CsDy_{0.93}Gd_{0.07}(MoO_4)_2$ is distorted. As a result of the phase transition the local symmetry of the JT centers is altered and an additional, temperature-dependent splitting arises between the fine-structure components of the spectrum of the Dy^{3+} ion; this splitting is discussed below.

The changes of the spectra with temperature can be described qualitatively in the framework of a model for a two-level spin system[16] (the Hamiltonian of which is analogous to the Hamiltonian of interacting effective spins 1/2 in a transverse magnetic field). In the mean field approximation this Hamiltonian has the form

$$\mathcal{H} = \mathcal{H}_1 + \mathcal{H}_2 = -(\lambda + \mu)\langle S^z\rangle \Sigma_n S^z(n) - \Delta/2 \Sigma_n S^x(n). \tag{1}$$

Here $\mathcal{H}_1$ describes the behavior of the pseudospin component $\langle S^z\rangle$ arising as a result of the change in symmetry, i.e., as a result of the interaction with the elastic subsystem. $\mathcal{H}_1$ is associated with the behavior of the interval 0–2 in the molecular field $(\lambda+\mu)$, where λ is a constant characterizing the interaction of the electronic subsystem with the elastic deformations, and $\mu = K\langle S^z\rangle^2$ characterizes the nonlinear coupling between the elastic and electronic subsystems. $\mathcal{H}_2$ determines the interaction of the S^x components of the pseudospin with the lattice, which gives rise to the initial splitting Δ in the spectrum and its temperature dependence without a change in symmetry.

The temperature behavior of the energy splitting $W(T)$ corresponding to the behavior of the interval 0–2 in $CsDy_{0.93}Gd_{0.07}(MoO_4)_2$ is associated to the behavior of $\langle S^z\rangle$ according to the formula[17]

$$W(T) = (\Delta^2 + (W(0)^2 - (\Delta^2)\langle S^z\rangle^2)^{1/2}. \tag{2}$$

The normalized value of $\langle S^z \rangle$ varies from 0 near T_{c2} to 1 at zero temperature, and $W(T)$, $W(0)$, and Δ are the splitting between the ground and excited levels at $T < T_{c1'}, T_{c2}$, at zero temperature, and at $T \gg T_{c2}$, respectively. Formula (2) takes into account the interaction of the pseudospin mode $\langle S^z \rangle$ with deformations of the A_g and B_g types. The latter alter the symmetry of the lattice and, accordingly, the local symmetry of the JT center. We note that in the case when the cell contains several inequivalent JT centers, the interaction of the deformation A_g with the pseudospin mode can also lead to a change in $\langle S^z \rangle$, on account of the rotation of the axes of the g-factor tensors of the individual JT centers. Taking into account the temperature dependence of the interval Δ above $T_{c2} \sim 28$ K, we approximate the temperature dependence of the splitting in the low-temperature region as

$$W_1(T) = (\Delta_1 + (W_1(0) - \Delta_1) \tanh W_1(T)/2kT, \qquad (3)$$

which is governed by the influence of the thermal contraction of the lattice on the position of the levels, i.e., the interaction of the pseudospin components $\langle S^z \rangle$ with the A_g deformation without allowance for the change in this interaction near the critical temperature. Here Δ_1, $W_1(T)$, and $W_1(0)$ are the values of the interval 0–2 at temperatures $T \gg T_{c1,c2}$, at lower temperatures T, and at zero temperature, respectively.

The solid curve in Fig. 11 corresponds to the temperature dependence of the experimentally measured interval between the ground and excited level in the absorption spectrum and can be described by a superposition of (2) and (3) for $\mu = 0$. It can be seen that there is agreement near $T_{c2} \sim 28$ K. At temperatures in the vicinity of 20 K the deviation exceeds the experimental error and is due to both the insufficiently correct application of the two-level model for the description of the temperature behavior of $W(T)$ and to the necessity of taking into account the interaction of the electronic states with the compressive (expansive) deformations, i.e., deformations of the A_g type, which change near the phase transition (their change reflects the behavior of the longitudinal moduli, Figs. 1 and 3). It is possible that the anomalous increase below 28 K of the longitudinal velocity measured in the (**cc**) geometry (Fig. 2) reflects this interaction. Furthermore, the phase transition at the temperatures T_{c2} is a first-order, close to second-order, SPT, and jumps can be observed in the spectra.

The analysis done for $\mu = 0$ formally describes a second-order phase transition. The first-order phase transition observed in the ultrasonic studies can be described in an analogous way, as was done in Ref. 18. For this it is sufficient to take into account the nonlinear coupling between the electronic and elastic subsystems. Taking such a coupling into account is equivalent to taking into account the interaction of the electronic subsystem with low-energy optical phonons.

Let us discuss one more component of the spectrum—the line *6* (Fig. 9b). As is seen in Fig. 7, the intensity of this line (indicated by an arrow) increases with decreasing temperature. The intervals between the high-frequency component *5* and this line *6* and between lines *3* and *5* (Fig. 9b) are the same, ~ 23 cm^{-1}. This interval corresponds approximately to the position of the first excited level of the ground state $^6H_{15/2}$ (see Fig. 7). In our opinion, the appearance of the satellite *6* is due to the simultaneous excitation of the transitions $0-0'$ at one rare-earth center and the 0–1 transitions at the second of a pair of interacting rare-earth centers (it is analogous to the appearance of pair processes in crystals with exchange-coupled pairs of magnetic ions).

We note that pair excitations can additionally be allowed in the dipole approximation at energetically inequivalent JT centers coupled by an elastic interaction (the analog of the exchange interaction). Such centers can exist for two reasons. First, because of the nonisomorphicity of the substitution of gadolinium ions by dysprosium in the initial lattice. Second, because of the appearance of energetically inequivalent centers arising on account of the doubling of the unit cell volume at the phase transition and on account of the lowering of the symmetry of the low-temperature phase in comparison with the system of the initial phase. Let us discuss the second of these possibilities.

We assume that the number of dysprosium ions N occupying a general position in the unit cell is twice as large as the order n of the factor group. This is possible if, e.g., multiplication of the unit cell volume occurs at a phase transition to a phase with a low lattice symmetry, viz., when the SPT from the orthorhombic phase with $Z = 4$ occurs to a monoclinic phase with $Z = 8$. Then, besides the Davydov components, which arise on account of the interaction between energetically equivalent rare-earth ions (they are related by symmetry elements of the factor group) there arise additional Davydov components due to ions not related by any symmetry elements with the first group of ions. It follows from our results that if inequivalent centers exist, then the energy difference between them is small and does not exceed $1-2$ cm^{-1} for the $0-0'$ transition.

Thus the following conclusions can be reached on the basis of an analysis of the absorption spectra. We attribute the changes observed in the spectra of $CsDy_{0.93}Gd_{0.07}(MoO_4)_2$ in the interval 28–10 K we attribute to the cooperative JT effect, the temperature of which corresponds to T_{c2}. It is assumed that analogous changes occur in the spectra of all the doped crystals, and they are due to phase transitions occurring near T_{c2}, i.e., along the corresponding lines of phase transitions on the $x-T$ diagram (Fig. 6). At the temperature $T_{c1'}$ only a redistribution of the intensities of the lines in the electronic spectra is noticed.

4. CONCLUSIONS

We have constructed the phase diagram of the system of crystals $CsDy_{1-x}Gd_x(MoO_4)_2$ for $x = 0$, 0.03, 0.04, 0.05, 0.07, 0.1, and 0.25, based on experimental data obtained by two independent methods. The first-order phase transition to the low-temperature phase in $CsDy(MoO_4)_2$ is modified in the doped crystals and is observed as a cascade of phase transitions lying close together. For crystals containing a gadolinium impurity with a concentration $x > 0.03$, two lines of second-order phase transitions and one line of first-order transitions are observed; the anomalies of the longitudinal and transverse sound velocities along these lines are different but they are similar in all the crystals. Such a phase diagram can arise in the case of a multicomponent order parameter. In a crystal without impurities the multicomponent nature of the

order parameter leads to a first-order phase transition because of the nonlinear interaction of the components.

It was established on the basis of ultrasound studies that the observed second-order phase transitions in $CsDy_{1-x}Gd_x(MoO_4)_2$ are improper ferroelastic transitions, as a result of which the unit cell increases in volume by an integer number of times, apparently along the **c** direction in the $\{Dy(MoO_4)_2\}_\infty^-$ layer. It was established that the low-temperature phase (below $T_{c1'}$ and $T_{c1''}$) cannot have higher than monoclinic symmetry. Since the initial phase (above $T_{c1'}$) already contains two $\{Dy(MoO_4)_2\}_\infty^-$ layers, in the low-temperature phase the number of inequivalent rare-earth JT centers is at least quadruple the number at room temperature. Thus the layered crystals studied are multicenter Jahn–Teller magnetoelastics.

The first-order phase transition at T_{c2} is accompanied by qualitatively similar anomalies in the behavior of longitudinal sound in both the ''pure'' and doped crystals. It was established from the absorption spectra that the phase transition at T_{c2} is satisfactorily described in the theory of the pseudo-JT effect. Therefore the response of the anomalies of the sound velocity measured in the (**aa**) geometry to a magnetic field up to 3.5 T is regular. On the other hand, no response of the anomalies of the sound velocity to a magnetic field was detected at the temperature $T_{c1'}$. There are grounds for assuming that at the phase transitions along the lines $T_{c1'}(x)$ the lattice distortions are of a different nature. In view of the results of the spectral studies, it is natural to suppose that near that temperature the Dy^{3+} ions are displaced along the **c** direction without substantial distortion of the electron shell.

In closing we wish to thank N. F. Kharchenko, V. I. Fomin, and A. A. Zvyagin for helpful discussions, Ya. I. Zagvozdina for help in the measurements, and V. S. Kurnosov for providing the programs for processing the spectra. Partial financial support for this study was provided under INTAS Grant 94-935.

*E-mail: zvyagina@ilt.kharkov.ua

[1] A. I. Zvyagin, S. D. El'chaninova, T. S. Stetsenko, L. N. Pelikh, and E. N. Khatsko, Fiz. Nizk. Temp. **1**, 79 (1975) [Sov. J. Low Temp. Phys. **1**, 39 (1975)].
[2] S. D. El'chaninova and A. I. Zvyagin, Fiz. Nizk. Temp. **4**, 1465 (1978) [Sov. J. Low Temp. Phys. **4**, 690 (1978)].
[3] G. A. Zvyagina, S. V. Zherlitsyn, V. D. Fil', and A. A. Gurskas, Ferroelectrics **110**, 35 (1990).
[4] É. E. Anders, I. V. Volchok, A. I. Zvyagin, V. B. Kokshenev, and S. V. Startsev, Izv. Akad. Nauk SSSR, Ser. Fiz. **50**, 369 (1986).
[5] V. I. Fomin, V. P. Gnezdilov, V. V. Eremenko, and N. M. Nesterenko, Fiz. Tverd. Tela (Leningrad) **31**, 266 (1989) [Sov. Phys. Solid State **31**, 871 (1989)].
[6] I. K. Bdikin, I. M. Shmyt'ko, and S. D. El'chaninova, Kristallografiya **39**, 27 (1994) [Crystallogr. Rep. **39**, 21 (1994)].
[7] V. A. Vinokurov and P. V. Klevtsov, Kristallografiya **17**, 127 (1972) [Sov. Phys. Crystallogr. **17**, 102 (1972)].
[8] E. A. Masalitin, V. D. Fil', K. R. Zhekov, A. N. Zholobenko, T. V. Ignatova, and Sung-Ik Lee, Fiz. Nizk. Temp. **29**, 93 (2003) [Low Temp. Phys. **29**, 72 (2003)].
[9] B. A. Strukov and A. P. Levanyuk, *Ferroelectric Phenomena in Crystals: Physical Foundations*, Springer-Verlag, Berlin–New York (1998); Nauka, Moscow (1983).
[10] F. I. Fedorov, *Theory of Elastic Waves in Crystals*, Plenum Press, New York (1968), Nauka, Moscow (1965).
[11] A. A. Gurskas, N. M. Nesterenko, V. P. Popov, and A. G. Sokolov, Izv. Akad. Nauk SSSR, Ser. Fiz. **53**, 1382 (1989).
[12] S. S. Gerashchenko, O. V. Miloslavskaya, Yu. N. Kharchenko, V. I. Kut'ko, and N. M. Nesterenko, J. Mol. Struct. **563–564**, 359 (2001).
[13] V. I. Spitsyn and V. K. Trunov, Dokl. Akad. Nauk SSSR **185**, 854 (1969) [*sic*].
[14] S. D. El'chaninova, V. P. Kuznetsov, E. E. Lakin, S. V. Matveev, O. D. Kolotiy, V. D. Zavrazhnova, T. V. Pakhmanina, and E. S. Perepelitsa, Ferroelectrics **175**, 85 (2000).
[15] Ya. I. Zagvozdina, N. M. Nesterenko, and Yu. N. Kharchenko, Ferroelectrics **239**, 197 (2000).
[16] N. Nesterenko, V. Gnezdilov, V. Fomin, Ya. Zagvozdina, and Yu. Kharchenko, in *Proceedings of the 18-th ICORS, August 25–30, 2002, Budapest, Hungary (2002)*.
[17] G. A. Gehring and K. A. Gehring, Rep. Prog. Phys. **38**, 1 (1975).
[18] G. A. Gehring, S. I. Swithenby, and M. R. Wells, Solid State Commun. **18**, 31 (1976).
[19] G. A. Zvyagina and A. A. Zvyagin, Fiz. Nizk. Temp. **26**, 482 (2000) [Low Temp. Phys. **26**, 354 (2000)].

Translated by Steve Torstveit

Oscillations of the elastic superstructure formed by a lattice of screw dislocations

A. M. Kosevich*

B. Verkin Institute for Low Temperature Physics and Engineering, National Academy of Sciences of Ukraine, pr. Lenina 47, Kharkov 61103, Ukraine

(Submitted July 18, 2003)
Fiz. Nizk. Temp. **30**, 332–339 (March 2004)

The equations of small oscillations of a dislocation lattice formed by a periodic system of parallel rectilinear screw dislocations are formulated. The stability of such a lattice is discussed, and it is shown that it brings about a corresponding spontaneous twisting of a crystalline sample. The long-wavelength collective oscillations of an isotropic elastic medium containing a dislocation lattice are described, among which are some which resemble plasma oscillations in a system of electric charges. The dispersion relations are obtained for five branches of oscillations, corresponding to the five degrees of freedom of the system under study (three degrees of freedom for displacements of the medium and two corresponding to bending oscillations of the dislocations). The possibility of observing the resonance frequency in the oscillation spectrum near the analog of the plasma frequency is pointed out. © *2004 American Institute of Physics.* [DOI: 10.1063/1.1645186]

1. INTRODUCTION

The physical properties of optical and acoustic superlattices have lately been attracting a heightened interest. By a superlattice we mean a macroscopic periodic structure created on the basis of an elastic or dielectric medium. A so-called 2D superlattice of this kind can be formed, e.g., by a set of rectilinear defects aligned into a periodic ''forest'' of parallel lines. The vortex lattices in type-II superconductors and in superfluid helium are realizations of superlattices of this sort (see, e.g., the reviews[1,2] and a recent paper[3] on the subject).

Although screw dislocations in a crystal are analogous to vortices, the dynamics and interaction of dislocations differ from those for vortices. Rectilinear screw dislocations interact like rectilinear electric charges, and one expects that oscillations of the plasma type, which are impossible in principle in a vortex lattice, will appear in the dynamics of the dislocation structures. Indeed, long-wavelength oscillations of a 2D dislocation structure called a dislocation wall has a dispersion relation typical for the plasma oscillations of a 2D electron gas.[4,5] Unfortunately, the plasma oscillations in a system of rectilinear dislocations were omitted from Ref. 6.

The term dislocation lattice will be understood to mean a system of parallel screw dislocations of the same sign, intersecting the plane perpendicular to them at the sites of a 2D lattice. The question naturally arises: What stabilizes such a lattice of mutually repulsive dislocations?

It seems to us that the key point in the formulation of the dynamical equations of the system of dislocations is to take into account correctly the dislocation flux density directly in the equations of the elastic field (in the presence of moving dislocations).[4,7] The proposed system of equations is reminiscent of the equations of the electromagnetic field in the presence of moving charges but is somewhat more complicated. The equations of motion of the ''charges,'' i.e., the screw dislocations, are taken in the simplest form—an elastic string model. The dynamical equations of the elastic field and the equations of motion of the dislocations comprise a complete system, permitting description of small oscillations of the dislocation lattice.

We study long-wavelength oscillations of the dislocation lattice, for which the wavelength of the oscillations is much greater than the lattice period. We obtain two independent branches of oscillations. One branch comprises coupled oscillations of the density of the dislocation lattice (compression–expansion waves) and transverse oscillations of the elastic medium (waves of rotation about a direction of the dislocation axes). Corresponding to two degrees of freedom, this branch is characterized by two dispersion relations. One of them pertains to the in-phase motion of the lattice and the medium and thus in the low-frequency limit has the form of an acoustic dispersion relation; the second pertains to antiphase motion of the lattice and the elastic medium, and therefore in the long-wavelength limit it has a gap, the frequency of which involves the plasma frequency of the dislocation lattice.

The other branch comprises coupled transverse oscillations of the dislocation lattice and oscillations of the elastic medium which have a component of the displacement velocity along the dislocation axes. The indicated motions have three collective degrees of freedom: transverse oscillations of the dislocation lattice in the plane perpendicular to the dislocation axes (the displacement of the dislocation lines occurs in that plane), and two degrees of freedom corresponding to expansion–compression waves of the elastic medium and waves of rotations in the elastic medium about axes lying in that plane. Accordingly, this branch of oscillations gives rise to three dispersion relations: two of them describe in-phase waves of oscillations of the dislocation lattice and elastic medium, and one describes antiphase oscillations.

A description of the analogous results obtained in the simple, so-called scalar model has been published in Ref. 8.

2. STABILITY OF THE DISLOCATION LATTICE

A screw dislocation parallel to the z axis creates a one-component, purely shear displacement field: the displacement vector $\mathbf{u}=(0,0,w)$ has only one nonzero component w, which depends on the coordinates x,y. If an isolated screw dislocation coincides with the z axis, then it creates an elastic field in which the value of w acquires a fixed increment upon passage around the axis:

$$w=\frac{b}{2\pi}\phi, \quad \phi=\arctan\frac{y}{x}, \tag{1}$$

where b is the Burgers vector of the dislocation, which is directed along the z axis: $\mathbf{b}=(0,0,b)$. The displacement field (1) is related to the stress

$$\sigma_{z\phi}^{0}=\frac{bG}{2\pi}\frac{1}{r}, \tag{2}$$

where $\sigma_{z\phi}$ is the $z\phi$ element of the stress tensor in cylindrical coordinates.

We assume that the system of parallel screw dislocations oriented along the z axis and intersecting the (x,y) plane at discrete, periodically arranged points form a 2D lattice, the unit cell of which has area S_0: $S=NS_0$, where S is the cross-sectional area of the sample in the (x,y) plane, and N is the total number of dislocations. The coordinates of these points in the equilibrium lattice are

$$\mathbf{x}(\mathbf{n})=\mathbf{R}_{\mathbf{n}}\equiv\sum_{\alpha}\mathbf{a}_{\alpha}n_{\alpha}, \quad \mathbf{n}=(n_1,n_2,0), \tag{3}$$

where $\mathbf{a}_{\alpha}$ ($\alpha=1,2$) are the basic translational vectors of the lattice ($a_{\alpha}\sim a$, where a is the distance between neighboring dislocations).

In organizing such a lattice of screw dislocations it should be kept in mind that screw dislocations of the same sign repel one another as like charges.[4] Therefore, such a lattice cannot be found in equilibrium without compensation of the repulsion of the dislocations. The vortex lattice in a superconductor is stabilized by the magnetic flux through the conductor. The vortex lattice in superfluid helium is stabilized by torque exerted by the vessel containing the helium. An analogous ''external field'' exists even in the case of a lattice of vortex dislocations in a sample free from external influences.

Consider a crystalline sample in the form of a cylinder of large radius R (in the limit $R\to\infty$). A large number of screw dislocations parallel to the axis of the cylinder form a 2D lattice with a unit cell area S_0 in the (x,y) plane. As we are primarily interested in the macroscopic (averaged) properties of the lattice, we assume that the dislocations are distributed continuously with a density $1/S_0$. Recall that a dislocation lying along the axis of the cylinder creates a stress field (2) around the axis. But because the stress field of the screw dislocations is similar to the electric field of linear charges or currents, the stresses at a distance r from the axis of the cylinder are created by all the dislocations intersecting an area $S=\pi r^2$ around the axis of the cylinder and are equal to the stresses around one dislocation lying along the axis of the cylinder ($x=y=0$) and carrying the total ''charge'' (Burgers vector bS/S_0) of all those dislocations:

$$\sigma_{z\phi}=\frac{S}{S_0}\sigma_{z\phi}^{0}=\frac{bG}{2S_0}r. \tag{4}$$

These stresses, first, create a force acting on a dislocation lying a distance r from the axis of the cylinder:

$$f_r=b\sigma_{z\phi}=\frac{b^2G}{2S_0}r. \tag{5}$$

Second, although the dislocation field (4) satisfies the boundary conditions $\sigma_{rr}=\sigma_{rz}=\sigma_{r\phi}=0$ on the free lateral surface of the sample, it creates the following moment of torque on the end of the cylinder:

$$M_z=\int r\sigma_{z\phi}dS=2\pi\int_0^R\sigma_{z\phi}r^2dr=\frac{\pi Gb}{4S_0}R^4. \tag{6}$$

Thus we see that the dislocation lattice creates stresses that generate nonzero torque M_z on the ends of the cylinder. If the ends of the cylinder are free, then the stress field (4) does not satisfy the boundary conditions on the ends (even if the latter are infinitely remote). Consequently, the true solution of the equations of equilibrium of the cylinder must include the additional stresses that compensate the torque M_z, i.e., that produce an average torque M_z on the ends of the cylinder.[9] These stresses (and the corresponding displacements) are easily obtained from the theory of the torsion of rods. It is known that in the torsion of a rod under the influence of a torque M_z a displacement vector u_{ϕ} arises which makes the angle of torsion uniform over the length of the rod:

$$\frac{d\theta}{dz}=\frac{\partial}{\partial z}\left(\frac{u_{\phi}}{r}\right)=\frac{1}{r}\frac{\partial u_{\phi}}{\partial z}=\frac{M_z}{C}, \tag{7}$$

where $C=(1/2)\pi GR^4$ is the torsional stiffness of the cylindrical rod.

Taking (6) and (7) into account, we easily write the distribution of the additional displacements and stresses in the cylinder:

$$u_{\phi}=-\frac{brz}{2S_0}, \qquad \sigma_{\phi}=-\frac{bG}{2S_0}r. \tag{8}$$

The stresses described by the second relation in (8) can be looked upon as a certain external field in relation to the dislocation lattice. Comparing (8) and (5), we see that the interaction force of a given dislocation with the remaining, continuously distributed dislocations is exactly compensated by these ''external stresses.'' This means that the expected repulsion of the discrete dislocations calculated according to formula (5) with the use of (2) is eliminated on average when the boundary conditions and symmetry of the problem with a continuous distribution of dislocations are taken into account. In other words, the equilibrium state of the dislocation lattice is stabilized by the twisting of the sample.

Since the average stresses created by the whole lattice are compensated, it is necessary to eliminate the average dislocation stresses from the force of interaction of each dislocation with the remaining dislocations in the lattice. Consequently, in the proposed scheme the lattice of screw dislo-

cations of the same sign is treated as if in the presence of a background of continuously distributed dislocations of the opposite sign.

3. DYNAMICAL EQUATIONS OF THE ELASTIC FIELD WITH SCREW DISLOCATIONS

The elastic field of the dislocations is determined, naturally, by their spatial distribution (the dislocation density tensor $\alpha_{ik}(\mathbf{x},t)$, $i,k=1,2,3$) and their fluxes (the Burgers-vector flux density tensor[4,7] $j_{ik}(\mathbf{x},t)$). In the general case the indicated densities are related by the analog of the continuity equation:

$$\frac{\partial \alpha_{ik}}{\partial t} + e_{ilm}\nabla_l j_{mk} = 0, \tag{9}$$

where e_{ikl} is an antisymmetric unit tensor of the third rank, and $\nabla_i = \partial/\partial x_i$. In the case of an individual dislocation intersecting the plane $z=\text{const}$ at a point $\mathbf{x}_0=(x_0,y_0)$ these densities are equal to

$$\alpha_{ik} = \tau_i b_k \delta(\mathbf{x}-\mathbf{x}_0), \quad \mathbf{x}=(x,y), \tag{10}$$

where τ is a unit vector tangential to the dislocation line, **b** is the Burgers vector of the dislocation, and

$$j_{ik} = e_{ilm}\tau_l V_m b_k \delta(\mathbf{x}-\mathbf{x}_0), \tag{11}$$

where **V** is the velocity vector of an element of the dislocation (in the case of rectilinear dislocations directed along the z axis, this vector has only two components: V_α, $\alpha=1,2$).

If the dislocations are distributed in a crystal, then it is impossible to introduce a displacement vector **w** of the medium as a single-valued function of the coordinates, and the deformation of the medium is described by a distortion tensor u_{ik} $(i=1,2,3)$.[4,7] The distortion tensor is the primary independent characteristic of the deformation of the medium (its symmetric part defines the strain tensor) and appears in the basic equation of the theory of elasticity of a crystal containing dislocations:

$$e_{ilm}\nabla_l u_{mk} = -\alpha_{ik}. \tag{12}$$

If the dislocations move, then Eq. (12) remains in force, but a vector **j** appears. The introduction of a dislocation flux density is a key point in the construction of the dynamic elastic field, since it determines one of the basic equations of the theory of moving dislocations:[4,7]

$$\frac{\partial u_{ik}}{\partial t} = \frac{\partial v_k}{\partial x_i} + j_{ik}, \quad i,k=1,2,3. \tag{13}$$

In the present case of screw dislocations lying along the z axis, the Burgers vector has only one nonzero component $b_z=b$, and therefore the index k in Eqs. (10) and (11) enters as a parameter, and it is convenient to introduce the vector notation for the flux density of the Burgers vector:

$$j_i = j_{iz}. \tag{14}$$

In addition, we take into consideration that in the problem of the oscillations of a dislocation lattice the velocity of the dislocation is a small quantity, and in the approximation linear in **V** the vector τ in the definition (11) can be assumed to be directed always parallel to the z axis (it is convenient to set $\tau_z=-1$). Then $j_z=0$, and

$$j_\alpha = b\varepsilon_{\alpha\beta}V_\beta \delta(\mathbf{x}-\mathbf{x}_0), \quad \alpha=1,2, \tag{15}$$

where the matrix $\varepsilon_{\alpha\beta}$ is equal to

$$\varepsilon_{\alpha\beta} = \begin{pmatrix} 0 & 1 \\ -1 & 0 \end{pmatrix}, \quad \alpha=1,2. \tag{16}$$

Then Eq. (13) takes the form

$$\frac{\partial u_{iz}}{\partial t} = \frac{\partial v_z}{\partial x_i} + j_i, \ i=1,2,3; \quad \frac{\partial u_{i\alpha}}{\partial t} = \frac{\partial v_\alpha}{\partial x_i}, \quad \alpha=1,2. \tag{17}$$

The dislocation flux density in the lattice is the sum of the quantities (15) over all the lattice:

$$j_\alpha = b\varepsilon_{\alpha\beta}\sum_{\mathbf{n}} V_\beta(\mathbf{n})\delta(\mathbf{x}-\mathbf{R}(\mathbf{n})). \tag{18}$$

In the problem of small oscillations of a lattice of screw dislocations relation (18) contains sufficient information for calculating the contribution of the moving dislocations to the time dependence of the elastic field. Indeed, the velocity of displacement of an element of the elastic medium, $\mathbf{v}(\mathbf{x},t)$, is the solution of the following equation, which is reconciled with the basic equation of the dynamic theory of elasticity and with Eq. (13):[4,7]

$$\rho\frac{\partial^2 v_i}{\partial t^2} - \lambda_{iklm}\nabla_k\nabla_l v_m = \lambda_{iklm}\nabla_k j_{lm}, \quad i=1,2,3, \tag{19}$$

where ρ is the density (mass per unit volume) of the substance, and λ_{iklm} is the elastic-constant tensor of the crystal.

However, Eq. (19) does not in any measure take into account the discreteness of the medium and the presence of the so-called Peierls relief. The latter is due to the obvious physical circumstance that even small displacements of a dislocation relative to the crystal lattice requires the performance of a definite amount of work, an additional force arises which is applied at the point of the dislocation and is proportional to the value of the relative displacement between the medium and dislocation. For us it is more convenient to introduce this force later in the discussion of the equation of motion of the dislocation. We now note that for a lattice of screw dislocations in an isotropic medium, Eq. (19) simplifies:

$$\frac{\partial^2 v_i}{\partial t^2} - c_t^2\Delta v_i - (c_l^2-c_t^2)\nabla_i \operatorname{div}\mathbf{v} = c_t^2(\nabla_z j_i + \nabla_\alpha j_\alpha \delta_{iz}), \quad i=1,2,3, \tag{20}$$

where c_t and c_l are the velocities of transverse and longitudinal sound, respectively. It is convenient to rewrite Eq. (20) in components:

$$\left(\frac{\partial^2}{\partial t^2} - c_t^2\Delta\right)v_z - (c_l^2 - c_t^2)\nabla_z \operatorname{div}\mathbf{v} = c_t^2\nabla_\alpha j_\alpha, \tag{21}$$

$$\left(\frac{\partial^2}{\partial t^2} - c_t^2\Delta\right)v_\alpha - (c_l^2 - c_t^2)\nabla_\alpha \operatorname{div}\mathbf{v} = c_t^2\nabla_z j_\alpha, \quad \alpha = 1, 2. \tag{22}$$

Since the Green tensor for the dynamical equation of the theory of elasticity of an isotropic medium is known in explicit form, Eqs. (20)–(22) allow us to express the velocity of displacement of the elements of the medium directly in terms of the spatial derivatives of the dislocation flux density.

4. DYNAMICS OF THE DISLOCATION LATTICE

Thus, if the distribution of dislocation fluxes is known, then we have equations describing the dynamic elastic fields in the sample. In order to close this system it is necessary to write equations determining the velocities of the dislocations, i.e., equations of motion of dislocations under the influence of the elastic fields. The simplest form of such an equation is the equation of vibrations of an elastic string. Let $\mathbf{U}(\mathbf{n},z,t)$ be the displacement vector of an element of the nth dislocation $\mathbf{U}(U_1,U_2,0)$, the time dependence of which determines the velocity of the dislocation: $\mathbf{V}_\alpha = \partial U_\alpha/\partial t$, $\alpha = 1,2$. Then the aforementioned equation has the form (we omit the index specifying the number of the dislocation)[4,7]

$$m\frac{\partial^2 U_\alpha}{\partial t^2} = \eta\frac{\partial^2 U_\alpha}{\partial z^2} + f_\alpha + S_\alpha. \tag{23}$$

Here m is the effective mass per unit length of the dislocation. The main part of the effective mass in the so-called logarithmic approximation is the field mass (the inertial mass of the elastic field created by the dislocation):

$$m_* = \frac{\rho b^2}{4\pi}\ln\left(\frac{R_{\text{curl}}}{r_0}\right), \tag{24}$$

where R_{curl} is either the radius of curvature of the dislocation line or the wavelength of the bending vibrations, and r_0 is the interatomic distance. However, the true mass of a unit length of the dislocation exceeds that value, since the restructuring in the core of a moving dislocation entails the motion of a portion of the atoms in the vicinity of the axis of the dislocation at distances of the order of r_0 from it. The order of magnitude of the mass of the atoms inside a tube of radius $r_0 \sim b$ per unit length of the dislocation can be estimated as $\rho r_0^2 \sim \rho b^2$. Comparing this estimate with (24) and remembering that this mass must be added to (24), one will understand that the effective mass per unit length of a dislocation $m > m_*$.

Further, η is the linear tension of the screw dislocation, created by the elastic interaction of a given element of the dislocation with the other parts of the same dislocation:

$$\eta = \frac{\rho c_t^2 b^2}{4\pi}\ln\left(\frac{R_{\text{curl}}}{r_0}\right). \tag{25}$$

The corresponding force determines the self-effect of the curved dislocation; it is due to the self-energy of an individual dislocation loop.

The force $\mathbf{f}$ describes the elastic interaction of a given dislocation with the remaining continuously distributed dislocations; it is given by

$$f_\alpha = b\varepsilon_{\alpha\beta}\sigma_\beta = bG\varepsilon_{\alpha\beta}(u_{\beta z} + u_{z\beta}), \tag{26}$$

where σ_β, $u_{\beta z}$, and $u_{z\beta}$ are the stresses and distortions after subtraction of the elastic fields of the uniformly and continuously distributed dislocations linked with the elastic medium.

Finally, $\mathbf{S}$ is the force due to the discreteness of the lattice, including dissipative forces. As we are interested in the dispersion relation for small oscillations, we neglect the latter and take the force $\mathbf{S}$ in the form

$$\mathbf{S} = -m\omega_0^2\mathbf{U}, \tag{27}$$

where ω_0 is the oscillation frequency of the dislocation structure in a valley of the Peierls relief.

However, it should be kept in mind that $\mathbf{U}$ is, of course, the displacement of the dislocation with respect to the medium, i.e., that part of the displacement of an element of the medium which is responsible for the plastic deformation.[7] It can be written as $\mathbf{U} = \mathbf{u}_g - \mathbf{u}$, where $\mathbf{u}_g$ is the geometric displacement of the medium at the point where the element of the dislocation line is located, and $\mathbf{u}$ is the elastic displacement of an element of the medium, giving rise to an elastic distortion $u_{ij} = \nabla_i u_k$.

Force (27) derives from the additional energy arising on account of the aforementioned work of displacement of the dislocation relative to the medium, which is conveniently written in the form

$$\delta E = \frac{1}{2}m\omega_0^2\sum_{\mathbf{n}}\int dz\,\mathbf{U}^2(\mathbf{x},z). \tag{28}$$

It is clear that the energy (28) also gives rise to a force density $f_i^D = -\partial E/\partial u_i$ acting on volume elements of the medium at the places where the dislocations that have been displaced from their equilibrium positions are located. It is given by

$$\mathbf{f}^D = m\omega_0^2\sum_{\mathbf{n}}\mathbf{U}(\boldsymbol{n},z)\delta(\mathbf{x} - \mathbf{R}(\mathbf{n})). \tag{29}$$

The force density (29) should be included in the main equation of motion of the elastic medium, and its time derivative

$$\frac{\partial f_i^D}{\partial t} = m\omega_0^2\sum_{\mathbf{n}}V_i(\mathbf{n},z)\delta(\mathbf{x} - \mathbf{R}(\mathbf{n})) \tag{30}$$

should be added (after being divided by ρ) to the right-hand side of Eq. (20).

Having the equations of motion of the dislocations (23) and the equations of the elastic field, either in the form (20) or in the form (21), (22), supplemented by the force density (29), one can study the collective oscillations of the dislocation lattice and elastic medium.

5. LONG-WAVELENGTH COLLECTIVE OSCILLATIONS

Let us investigate the long-wavelength oscillations of the dislocation lattice, assuming that the wavelength of the oscillations is much greater than the lattice period a ($ak \ll 1$). In this approximation the distribution of the disloca-

tions can be assumed continuous, characterized by its density $n(\mathbf{x},t)$. In equilibrium $n=n_0$, where $n_0=1/S_0=\text{const}$. The lattice dynamics is determined mainly by the average dislocation flux density **j**, which in the linear approximation has the nonzero components

$$j_\alpha(\mathbf{x},t)=bn_0\varepsilon_{\alpha\beta}V_\beta(\mathbf{x},t),\quad \alpha=1,2, \tag{31}$$

where **V** is the average velocity of the dislocations. The velocity **V** must be determined by the equation of motion of the dislocation (23). As we are interested in effects of a purely field origin, we neglect the effect of the Peierls relief, i.e., we set $\omega_0=0$. We rewrite the equation of motion (23) using (26) and (27):

$$\frac{\partial V_\alpha}{\partial t}-s^2\frac{\partial^2 U_\alpha}{\partial z^2}=\frac{bG}{m}\varepsilon_{\alpha\beta}(u_{\beta z}+u_{z\beta}), \tag{32}$$

where s is the velocity of the dislocation bending wave ($s^2=\eta/m$). Recalling the remarks made in regard to the effective mass per unit length of the dislocation, we assume $s<c_t$.

We differentiate Eq. (32) with respect to time and use Eq. (13) and also expression (31). After elementary calculations we obtain

$$\frac{\partial^2 V_\alpha}{\partial t^2}+\omega_{pl}^2V_\alpha-s^2\frac{\partial^2 V_\alpha}{\partial z^2}=\frac{bG}{m}\varepsilon_{\alpha\beta}\left(\frac{\partial v_z}{\partial x_\beta}+\frac{\partial v_\beta}{\partial z}\right), \tag{33}$$

where we have introduced the notation

$$\omega_{pl}^2=\frac{b^2Gn_0}{m}. \tag{34}$$

The frequency ω_{pl} is the analog of the plasma frequency.

We reconcile the notation in (33) with Eqs. (21) and (22), for which purpose we introduce the average two-dimensional flux density of dislocation lines

$$\mathbf{J}=bn_0\mathbf{V}. \tag{35}$$

Then in place of (33) we write

$$\frac{\partial^2 J_\alpha}{\partial t^2}+\omega_{pl}^2J_\alpha-s^2\frac{\partial^2 J_\alpha}{\partial z^2}=\omega_{pl}^2\varepsilon_{\alpha\beta}v_{z\beta}, \tag{36}$$

where we have used the notation

$$v_{ik}=\nabla_i v_k+\nabla_k v_i,\quad i,k=1,2,3.$$

It is easy to see that the equations relating the functions $P=\operatorname{div}\mathbf{J}\equiv\nabla_\alpha J_\alpha$ and $(\operatorname{curl}\mathbf{v})_z$ separate out from the rest of the dynamical equations and form an autonomous pair:

$$\left(\frac{\partial^2}{\partial t^2}+\omega_{pl}^2-s^2\frac{\partial^2}{\partial z^2}\right)P=\omega_{pl}^2\nabla_z(\operatorname{curl}\mathbf{v})_z, \tag{37}$$

$$\left(\frac{\partial^2}{\partial t^2}-c_t^2\Delta\right)(\operatorname{curl}\mathbf{v})_z=c_t^2\nabla_z(\operatorname{curl}\mathbf{j})_z\equiv-c_t^2\nabla_z P. \tag{38}$$

For collective oscillations of the type $\exp(i\mathbf{k}\cdot\mathbf{x}-i\omega t)$, Eqs. (37) and (38) determine a branch of oscillations with an anisotropic dispersion relation, which we shall write in the implicit form

$$(\omega^2-c_t^2k^2)(\omega^2-\omega_{pl}^2-s^2k_z^2)=\omega_{pl}^2(c_tk_z)^2. \tag{39}$$

The quadratic equation (39) has two roots, which give a simple dependence of the frequency on the wave vector in the long-wavelength limit ($ck\ll\omega_{pl}$).

1. An anisotropic dispersion relation of the low-frequency oscillations of the acoustic type:

$$\omega^2=\sin^2\theta(c_tk)^2\equiv c_t^2(k_x^2+k_y^2), \tag{40}$$

where θ is the angle between the wave vector and the z axis ($k_z=k\cos\theta$). If the dispersion relation is continued into the region of large wave vectors, then one can see that with increasing k this relation approaches the curve of $\omega^2=s^2k_z^2$.

2. An anisotropic dispersion relation with a gap (high-frequency oscillations):

$$\omega^2=\omega_{pl}^2+\cos^2\theta(c_t^2+s^2)k^2\equiv\omega_{pl}^2+(c_t^2+s^2)k_z^2. \tag{41}$$

Let us again trace the dispersion curve of the branch in the region of large wave vectors. With increasing k this curve approaches $\omega^2=c_t^2k^2$. It is seen that both dispersion relations are indeed highly anisotropic.

Thus one branch of collective oscillations corresponds to coupled oscillations of the transverse components of the elastic field $(\operatorname{curl}\mathbf{v})_z$ and the longitudinal expansion–compression oscillations of the dislocation lattice (P). Of course, the plasma frequency is incorporated in the characteristic of those oscillations. In a wave propagating in the (x,y) plane, the fields $\operatorname{curl}\mathbf{v}(x,y,t)$ and $P(x,y,t)$ become independent and oscillate with the dispersion relations

$$\omega^2=c_t^2(k_x^2+k_y^2),\quad \omega=\omega_{pl}.$$

The transverse oscillations of the lattice are related to the oscillations of the vector variable $\mathbf{R}=\operatorname{curl}\mathbf{J}$ and with the longitudinal oscillations of the elastic field ($\operatorname{div}\mathbf{v}$) and that part of the transverse oscillations of the elastic field which is included in the coordinate dependence of the velocity component v_z, i.e., in the components $(\operatorname{curl}\mathbf{v})_\alpha$, $\alpha=1,2$. This branch of oscillations is described by Eq. (21) and by the following obvious pair of equations:

$$\left(\frac{\partial^2}{\partial t^2}-c_l^2\Delta\right)\operatorname{div}\mathbf{v}=2c_t^2\nabla_z\operatorname{div}\mathbf{j}=2c_t^2\nabla_z R_z, \tag{42}$$

$$\left(\frac{\partial^2}{\partial t^2}+\omega_{pl}^2-s^2\frac{\partial^2}{\partial z^2}\right)R_z=-\omega_{pl}^2\left[\nabla_z\operatorname{div}\mathbf{v}+\left(\frac{\partial^2}{\partial x_\alpha^2}-\frac{\partial^2}{\partial z^2}\right)v_z\right]. \tag{43}$$

The solution of equations (21), (42), and (43) in the form of harmonic plane waves leads in an obvious way to the following dispersion relation, which is of third order with

respect to ω^2:

$$(\omega^2 - c_l^2 k^2)(\omega^2 - c_t^2 k^2)(\omega^2 - \omega_{pl}^2 - s^2 k_z^2) = \omega_{pl}^2 c_t^2 \times [(\omega^2 - c_l^2 k^2)(k_x^2 + k_y^2 - k_z^2) + 2k_z^2(\omega^2 - c_t^2 k^2)] + 2\omega_{pl}^2 (c_t k_z)^2 (c_l^2 - c_t^2)(k_x^2 + k_y^2 - k_z^2). \quad (44)$$

Although this is a rather awkward equation, its roots are easily analyzed in the long-wavelength limit, when one can drop terms higher than quadratic in the expansion of the frequency in powers of k. The high-frequency branch begins with the expansion

$$\omega^2 = \omega_{pl}^2 + (s^2 \cos^2\theta + c_t^2)k^2 \quad (45)$$

and with increasing k it approaches a dependence $\omega^2 = c_l^2 k^2$. It is characteristic that the curve of Eq. (45) lies above the curve of Eq. (41); this means that the indicated curves do not intersect as k increases.

In the low-frequency region two branches of the acoustic spectrum arise, $\omega_{1,2} = c_{1,2}k$, the sound velocities in which are the roots of the quadratic equation

$$(c^2 - c_l^2)(c^2 - c_t^2) = c_t^2 (c_l^2 \cos^2 2\theta + c_t^2 \sin^2 2\theta - c^2). \quad (46)$$

In the high-frequency limit one of the last two branches approaches the dispersion relation for transverse sound, while the second takes the form of the dispersion relation

$$\omega = sk\cos\theta \equiv s k_z .$$

In discussing the behavior of the dispersion relations at large values of the wave vector, one must be careful to analyze both the high-frequency and low-frequency branches. The point is that the dispersion relations obtained are valid for $\lambda \gg a$ (or $ak \ll 1$). At large k a periodic dependence of the dispersion relation of the lattice on the quasi-wave vector is manifested, with the period $\mathbf{G}$ of the reciprocal lattice: $\omega(\mathbf{k}) = \omega(\mathbf{k}+\mathbf{G})$, where $G = 2\pi/a$. Therefore the dispersion relations obtained are actually valid in all small neighborhoods of any reciprocal lattice vector $\mathbf{g}$, i.e., for $a|\mathbf{k}-\mathbf{g}| \ll 1$. The fictitious continuation of the curves of the lower branch for $k \sim \pi/a$, and also the inevitably arising intersection of the curves of the upper branch at $k = ((p+1)/2) \times (\pi/a)$, $p = 1,2,3,\ldots$ can be described only on the basis of the dynamical equations of the discrete dislocation lattice. But this is the subject of a separate study.

On the basis of the long-wavelength treatment it is impossible to say whether there is a band of forbidden frequencies between the upper and lower branches (a gap in the spectrum). However, it can be stated that in the frequency spectrum there is a limiting frequency $\omega_{\rm pl}$ marking the lower edge of the upper branch of oscillations, which clearly can be manifested in the resonance acoustic properties of a crystal containing a dislocation lattice. An important distinguishing feature of this frequency is the dependence of its position on the density of dislocations in the lattice (on the value of the lattice period). The experimental observation of this property of the limiting resonance frequency would be direct confirmation of the presence of plasmonlike collective oscillations in the dislocation lattice.

The author thanks Oksana Charkina for assistance with the organization of this article, Vasiliy Natsik for helpful comments, and Ali Najafi and Ramin Golestanian for providing a manuscript of their paper, which called the problem considered here to the author's attention.

*E-mail: kosevich@ilt.kharkov.ua

[1] G. Blatter, M. V. Feigel'man, V. B. Geshkenbein, A. I. Larkin, and V. M. Vinokur, Rev. Mod. Phys. **66**, 1125 (1994).
[2] E. H. Brandt, Rep. Prog. Phys. **58**, 1465 (1995).
[3] A. Yu. Galkin and B. A. Ivanov, Phys. Rev. Lett. **83**, 3053 (1999).
[4] A. M. Kosevich, *Dislocations in the Theory of Elasticity* [in Russian], Naukova Dumka, Kiev (1978); A. M. Kosevich, "Crystal dislocations and the theory of elasticity," in *Dislocations in Solids*, Vol. 1, edited by F. R. N. Nabarro, North-Holland, Amsterdam (1979), p. 31.
[5] A. M. Kosevich and M. L. Polyakov, Fiz. Tverd. Tela (Leningrad) **21**, 2941 (1979) [Sov. Phys. Solid State **21**, 1694 (1979)].
[6] V. V. Nikolaev, A. N. Orlov, and G. G. Taluts, Fiz. Met. Metalloved. **23**, 424 (1967).
[7] A. M. Kosevich, *Theory of the Crystal Lattice (The Physical Mechanics of Crystals)* [in Russian], Kharkov, Vishcha Shkola (1988); A. M. Kossevich, *The Crystal Lattice. Phonons, Solitons, Dislocations*, Wiley-VCH, Berlin (1999).
[8] A. M. Kosevich, Fiz. Nizk. Temp. **29**, 930 (2003) [Low Temp. Phys. **29**, 697 (2003)].
[9] J. D. Eshelby, "Boundary problems," in *Dislocations in Solids*, Vol. 1, edited by F. R. N. Nabarro, North-Holland, Amsterdam (1979), p. 167.

Translated by Steve Torstveit

LOW-TEMPERATURE PHYSICS OF PLASTICITY AND STRENGTH

Creep of beta-tin single crystals at subkelvin temperatures

V. D. Natsik,* V. P. Soldatov, L. G. Ivanchenko, and G. I. Kirichenko

B. Verkin Institute for Low Temperature Physics and Engineering, National Academy of Sciences of Ukraine, pr. Lenina 47, Kharkov 61103, Ukraine

(Submitted August 18, 2003)
Fiz. Nizk. Temp. **30**, 340–350 (March 2004)

The creep of β-Sn single crystals oriented for slip in the $(100)\langle 010\rangle$ system is investigated in the temperature range 0.45–4.2 K. A transient creep, decaying in time by a logarithmic law, is registered both above and below 1 K. The temperature dependence of the coefficient of logarithmic creep is studied in detail, and the existence of two qualitatively different regions of its behavior is established: in the interval 4.2–1.2 K the coefficient increases linearly with decreasing temperature, while below 1 K the creep acquires an athermal character and the coefficient remains constant. It is shown that the regularities observed in the experiment are in accord with the idea that the kinetics of creep in pure β-Sn is governed by the motion of dislocations in the Peierls potential relief by a mechanism of nucleation of kink pairs on the dislocation lines. This process entails the overcoming of a small effective potential barrier of the order of 0.001 eV: in the temperature region $T<1$ K the nucleation of kink pairs occurs by a quantum tunneling effect, and the creep is of a purely quantum character; at higher temperatures the leading role is played by thermal fluctuations, and the deformation kinetics corresponds to the classical ideas of thermally activated creep. Empirical estimates are obtained for the density of mobile dislocations and the work hardening coefficient. © *2004 American Institute of Physics.* [DOI: 10.1063/1.1645187]

INTRODUCTION

For many years in the physics of plasticity and strength of crystalline materials there has been particular interest in the so-called low-temperature anomaly—the substantial weakening or complete absence of temperature dependence of the plastic flow of crystals below a certain threshold temperature.[1] A clear manifestation of this anomaly was first registered in a study of the low-temperature creep of metallic crystals at temperatures in the liquid helium region.[2–5] Prior to the discovery of this anomaly it had generally been thought that the low-temperature creep of crystals is due to the thermally activated motion of dislocations. In the modern theories of low-temperature plasticity the possibility for creep to exist under deep cooling conditions, when the intensity of the thermal motion of the atoms is extremely low, is considered to be a manifestation of the quantum properties of the carriers of the plastic deformation (i.e., dislocations) and the influence of those properties on their mobility.[6–8]

Depending on the type of barriers that must be overcome by the dislocations, the manifestation of quantum effects in the kinetics of plastic deformation can be observed over a rather wide interval of low temperatures—$(10^{-2}-10^{-1})T_D$ (T_D is the Debye temperature).[8,9] However, the experimental data of greatest interest for studying the quantum mechanisms of plasticity are those obtained in the region of extremely low temperatures (below 1 K), where the influence of thermal activation on the mobility of dislocations is extremely weak and their quantum properties are manifested in pure form. However, at the present time such data are quite rare: the existence of creep at temperatures below 1 K has as yet been established only in two studies, which were done on single crystals of β-CuZn[10] and Zn.[11] For this reason it is necessary to add substantially to the list of crystals for which the plasticity has been studied at ultralow temperatures, to obtain new experimental data on the manifestations of athermal effects in that region, and to establish their connection with the quantum mechanisms of plastic deformation.

The goal of the present study was to investigate the kinetics of creep of single crystals of pure β-Sn in the temperature range 0.5–4.2 K. Tin belongs to the group of tetragonal body-centered crystals which have a large set of diverse slip and twinning systems. We had previously established that the low-temperature plastic deformation of β-Sn single crystals of high purity, oriented for predominant slip in the system $(100)\langle 010\rangle$, is governed by the motion of dislocations in the Peierls relief.[12] Unlike other crystals of the Peierls type (the bcc metals, ionic and alkali halide crystals, semiconductors), single crystals of pure β-Sn have a unique ability to maintain a high plasticity down to very low temperatures, which makes them ideal objects for studying the motion of dislocations in the Peierls relief over a wide range of low temperatures, including the subkelvin region.

According to the data of Refs. 13 and 14, the yield point of pure β-Sn single crystals, measured at a constant rate of tensile strain (active deformation), ceases to depend on temperature below a temperature of the order of 1 K, i.e., the characteristic signs of quantum plasticity appear. In Ref. 14 such behavior was explained by a transition from the ther-

mally activated creep of dislocations in the Peierls relief to a tunneling of the dislocations through the potential barriers of that relief. A comparison of the results obtained under conditions of active loading and creep, and also an exploration of the correlation between those results, is the second goal of the present study.

Finally, still another important circumstance is that the dislocation creep of β-Sn single crystal at very low strain rates (10^{-6}–10^{-5} s^{-1}) at temperatures of the order of 1 K and below reduces to a sequence of elementary correlated rearrangements of the atomic structure—the tunnel nucleation of kink pairs on the dislocation lines. Such processes are accompanied by the overcoming of very small effective potential barriers of the order of 10^{-3} eV,[15] and are one of the concrete examples of the manifestation of so-called macroscopic quantum tunneling effects (see Ref. 14 for more details on this). Effects of this type are discussed and investigated in the physics of weak superconductivity, in the physics of low-temperature lattice and magnetic phase transformations, etc. Therefore the study of athermal (quantum) creep of β-Sn in the subkelvin temperature region opens up new opportunities for studying one of the topical problems of the modern quantum physics of solids.

1. EXPERIMENTAL TECHNIQUES

The single-crystal samples were grown from 99.9995% pure stock in batches of 10 from a single seed by a modified Bridgman method.[16] They had a double-lobed shape (in the jaws of the testing machine) with a working part of rectangular cross section $25\times5\times1.5$ mm. The longitudinal axis of the samples was in a $\langle110\rangle$ direction, which is the most favorable for slip in the $(100)\langle010\rangle$ system.

Experiments were carried out in the temperature interval 0.45–4.2 K on an apparatus described in Ref. 11. The use of liquid ^{4}He as a coolant made it possible to achieve temperatures of 1.8–4.2 K, while temperatures in the range 0.45–2 K were obtained in a ^{3}He dilution refrigerator. The temperature was measured by a GaAs semiconductor thermometer and, in parallel, from the saturated vapor pressure of ^{3}He or ^{4}He. The relative error in the temperature measurements was not over 10^{-2}.

The samples for study were placed inside a superconducting solenoid and strained under tension in the regime of creep in the normal state, for which a longitudinal magnetic field $H>H_c=309$ G was produced in the solenoid, destroying the superconductivity of β-Sn at $T<T_c=3.7$ K.

The flow stress on the sample was increased in small steps of $\Delta\tau=0.2$–0.4 MPa (see Fig. 1). The elongation of the sample corresponding to each increment of stress was measured by an inductive strain gauge whose output signal was fed to a Shch302 digital voltmeter and then sent to a computer and displayed on the monitor. The accuracy of the measurements of the relative strain of the sample was 5×10^{-5} at a time constant of the measuring system of around 0.15 s. Before the yield point τ_0 was reached (for $\Sigma\Delta\tau<\tau_0$) the strain increments corresponding to the increments of the applied load led to elastic straining of the sample, and the curves $\Delta\varepsilon(t)$ corresponding to them had the characteristic Γ-shaped form. After the yield point was reached (for $\Sigma\Delta\tau>\tau_0$) the $\Delta\varepsilon(t)$ curves exhibited a pronounced stage of plastic flow with a decaying velocity (transient creep). Series of such curves obtained at different temperatures were processed and analyzed to ascertain the influence of the total strain of the sample and its temperature on the behavior of the main kinetic parameters of the low-temperature creep.

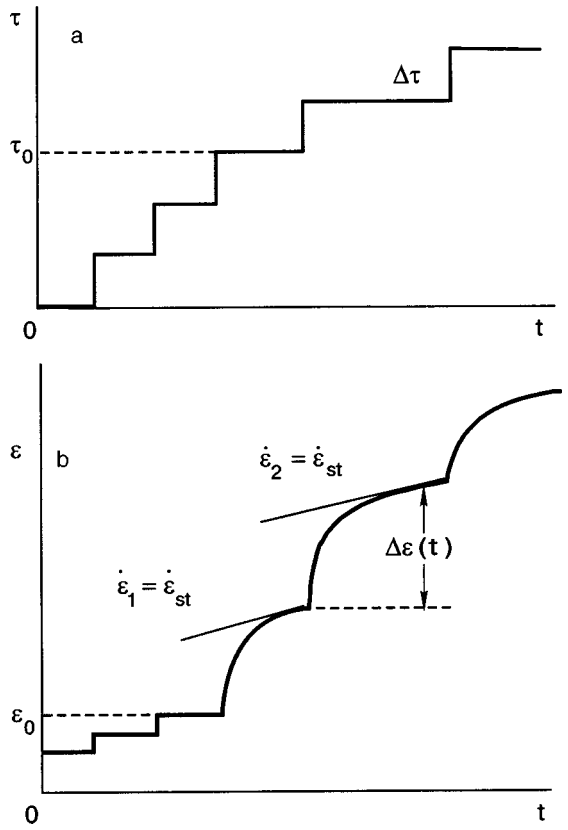

FIG. 1. Diagram of the stepped loading (a) and strain (b) of samples in the creep regime: τ is the applied stress, ε is the relative strain, $\Delta\varepsilon(t)$ is the time-dependent strain increment within an individual creep curve.

Let us mention some of the fine points of the methods used which play an important role in the conducting of the experiments. First, each increment of external load on the sample was added at approximately the same values of the creep rate immediately prior, $\dot\varepsilon_{st}\simeq10^{-5}$ s^{-1} (Fig. 1b). This made for approximately the same starting level of effective stress for all the creep curves recorded.

Second, the samples prepared for testing at $T<1.8$ K were prestrained by 3–4% at a temperature of 1.8 K, and then the temperature was lowered to the desired temperature and the loading was continued. This measure was taken because at $T<1.4$ K an incremental loading near the yield point often causes a sharp, hard-to-control, and very large strain increment ($\Delta\varepsilon\sim6$–7%), while at higher temperatures the uncontrollable strain jumps do not occur. This ''instability'' of the creep is due to the fact that samples of pure β-Sn under straining in the slip system $(100)\langle010\rangle$ at extremely low temperatures have an easy-slip stage with a very low hardening coefficient and, in individual cases, even a yield point. Thanks to the prestraining procedure we were able to obtain smooth creep curves all the way down to 0.45 K. For some samples the jumplike strain growth was absent even near the yield point, making it possible to obtain information about the parameters under study even at low degrees of total strain.

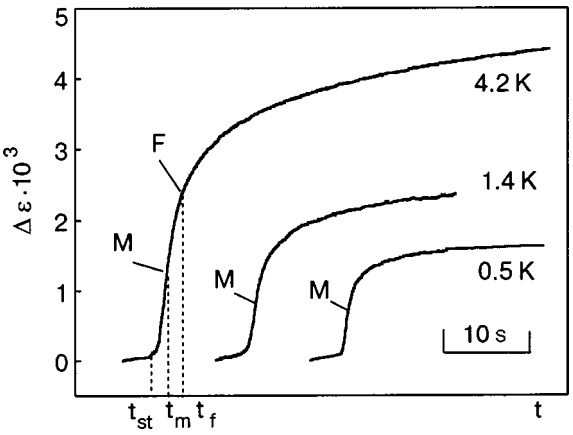

FIG. 2. Characteristic shape of the experimental creep curves for β-Sn single crystals in the normal state; the curves correspond to the same degree of total strain of the samples, $\varepsilon \simeq 0.07$. Notation: t_{st} is the time at which the load increment is applied, the point M on the creep curves corresponds to the time t_m at which the maximum creep rate is reached, and F corresponds to the time t_f of the start of the fluctuation regime.

2. EXPERIMENTAL RESULTS

2.1. Time dependence of the creep

Figure 2 shows "machine" curves of the creep $\Delta\varepsilon(t)$ of β-Sn single crystals at several different temperatures in the interval 0.5–4.2 K for a fixed value of the total strain of the sample, $\varepsilon = 0.07$. For clarity the curves have been shifted relative to one another along the time axis. It is seen that after an incremental loading $\Delta\tau$ at the time t_{st} all the curves start with brief stages of accelerated creep, and after the maximum strain rate is attained (this time is denoted by t_m) the creep process goes over to a damped regime. It is assumed that in the time interval $t_m - t_{st}$ a new regime of dislocation motion is established in the crystal, caused by the increment of flow stress. In this study we have not devoted much attention the fragments of the creep curves corresponding to the accelerated strain. A detailed discussion of that stage is given in Ref. 17.

The subsequent processing and analysis of the creep curves $\Delta\varepsilon(t)$ recorded in the experiments was done with allowance for the following arguments. It has long been established[1,18] that the decaying (transient) creep of crystalline materials under conditions of low temperatures is most often described by a logarithmic time dependence

$$\Delta\varepsilon(t) = \alpha \ln(\beta t + 1), \tag{1}$$

where α and β are parameters whose values depend on temperature and on the structural characteristics of the samples. The logarithmic character of the transient creep of β-Sn at low temperatures 1.6–78 K was confirmed in our previous study.[19] However, we later showed[15,17] that situations are possible in which the time dependence of the decaying creep has a more complicated character: in a number of cases the logarithmic stage of the creep is preceded by a brief exponential stage. This staged nature is due to the possibility of realizing two regimes of dislocation motion during the creep process: a logarithmic stage corresponds to a fluctuation (thermally activated or tunneling) regimes, while the exponential stage corresponds to a dynamic (above-barrier) regime. In this paper we will be interested primarily in the possibility of realizing the fluctuational motion of dislocations at subkelvin temperatures and in establishing the elementary physical mechanisms that govern such motion. Therefore, in processing the experimentally recorded creep curves the main problem is to separate out and analyze the logarithmic stage.

The solution of the problem described can be obtained by constructing "machine" curves of the creep $\Delta\varepsilon(t)$ in the coordinates $\ln\dot{\varepsilon}$–$\Delta\varepsilon$, where $\dot{\varepsilon} = d[\Delta\varepsilon(t)]/dt$. It is easy to see that the logarithmic dependence (1) is equivalent to the relation

$$\ln\dot{\varepsilon} = \ln\dot{\varepsilon}(t_f) - \alpha^{-1}[\Delta\varepsilon - \Delta\varepsilon(t_f)]. \tag{2}$$

Here t_f is the time at which the transient creep starts to take on a logarithmic (fluctuational) character, and $\dot{\varepsilon}(t_f) = \alpha\beta$ is the starting rate of logarithmic creep. Figure 3 shows the creep curves in the coordinates $\ln\dot{\varepsilon}$–$\Delta\varepsilon$ corresponding to the "machine" curves $\Delta\varepsilon(t)$ in Fig. 2. It is seen in Fig. 3 that when one goes from the temperature of liquid ^{4}He (Fig. 3a) to the subkelvin region (Fig. 3c) the character of the time dependence of the decay of the creep remains qualitatively the same: the creep curves for $t > t_m$ consist of two stages, the second of which is described rather well by relation (2).

Figure 3 can be used to determine the value of the creep deformation $\Delta\varepsilon(t_f)$ at which the creep starts to take on a fluctuational character at a fixed value of the temperature, and by juxtaposing Fig. 3 with Fig. 2 one can determine the values of the times t_f at which that stage begins. The results of such a separation of the logarithmic stages of the "machine" curves of the creep at different temperatures of the experiment but at a fixed value of the total strain of the sample are shown in Fig. 4a. By determining the geometric parameters of the straight lines that approximate the given stage of creep in Fig. 3, one can obtain numerical values of the parameters α and β of the fluctuation creep at different temperatures (Table I). The tabulated data allow one to construct fragments of the "machine" curves of the creep for times $t > t_f$ in a form which illustrates explicitly the logarithmic character of that stage (Fig. 4b).

For working out a physical interpretation of the transient creep the parameter α is the more informative, and therefore one of the important intermediate problems in the study is to obtain the experimental dependence of that parameter on the temperature T, degree of strain ε, flow stress τ, etc. To establish the relationship of α with each of these parameters separately, the corresponding creep curves must be obtained at fixed values of all the other parameters that influence the behavior of α.

2.2. Dependence of the coefficient of logarithmic creep on the strain and temperature

In this paper we are primarily interested in the temperature dependence $\alpha(T)$. To determine it we first obtained the curves of the strain dependence of this parameter at fixed values of the temperature, $\alpha(\varepsilon)_T$, on the basis of which we determined the temperature dependence of the coefficient $\alpha(T)_\varepsilon$ corresponding to a specified value of the prestrain ε.

The character of the dependence of the parameter α on the strain and temperature is shown in Fig. 5. We note that the values of $\alpha(\varepsilon, T)$ given in Fig. 5 were obtained in a

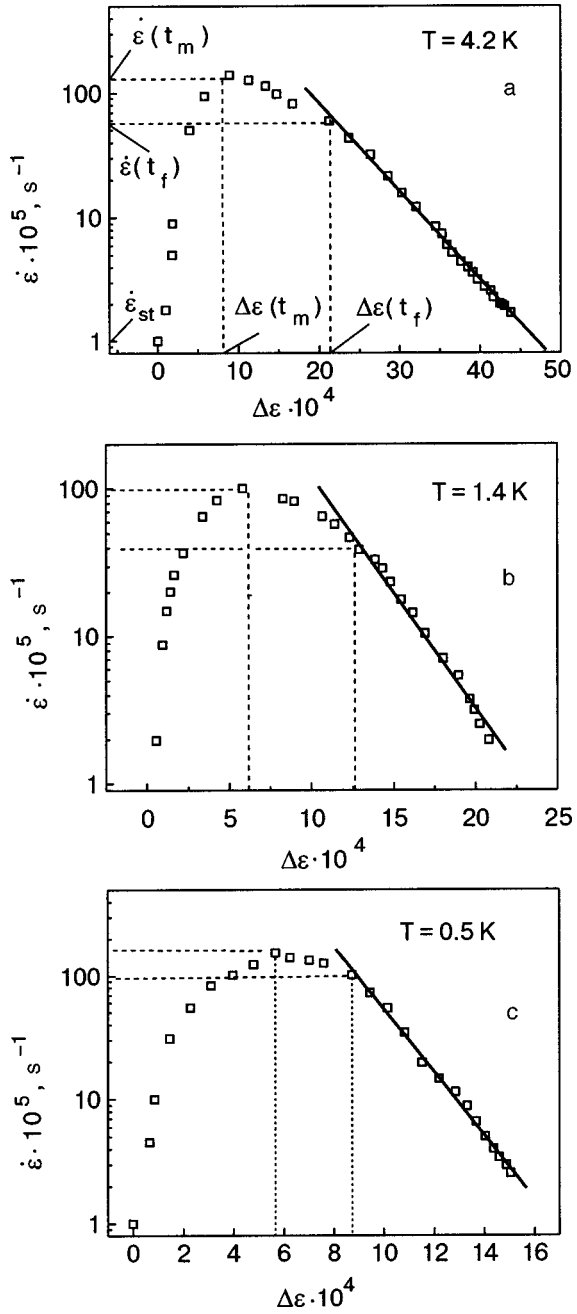

FIG. 3. Creep curves from Fig. 2 in the coordinates $\ln \dot{\varepsilon}$–$\Delta\varepsilon$ at different temperatures.

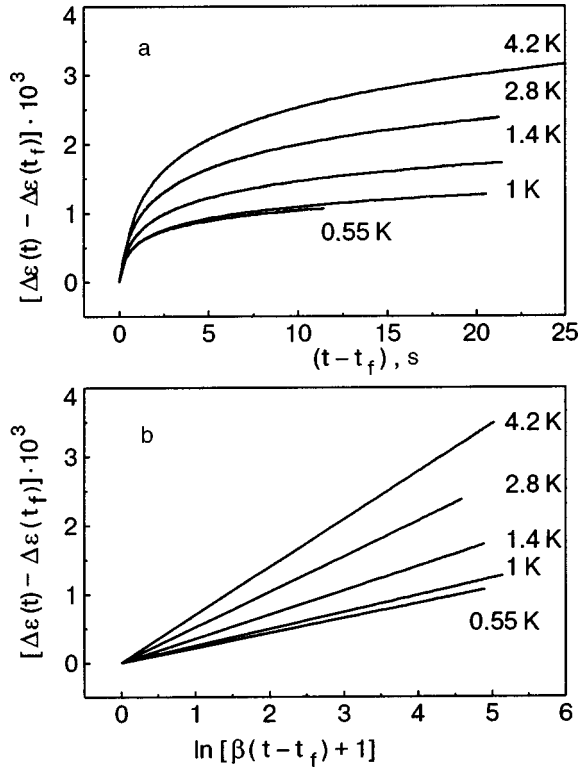

FIG. 4. Time dependence of the increment of creep deformation for the fluctuation stage in direct (a) and semilogarithmic (b) coordinates.

processing of the creep curves initiated by approximately equal increments of the flow stress $\Delta\tau \sim 0.2$–0.4 MPa upon the attainment of approximately equal starting values of the creep rate $\dot{\varepsilon}_{st} \simeq 10^{-5}$ s^{-1}. It is seen in Fig. 5 that with decreasing temperature the character of the strain dependence $\alpha(\varepsilon)_T$ changes. The $\alpha(\varepsilon)_T$ curves obtained at $T > 1.2$ K are characterized by a rather sharp decrease of α with strain at low degrees of strain (up to 5%) and then this dependence become weaker and sometimes even vanishes completely (Fig. 5a). In the temperature interval 0.5–1.2 K the value of the coefficient α is insensitive to temperature, and at 0.5 K it is also insensitive to the degree of strain (Fig. 5b).

The set of $\alpha(\varepsilon)_T$ curves can be used to obtain the temperature dependence of the coefficient $\alpha(T)_\varepsilon$ for fixed degrees of strain. The corresponding values of α needed for constructing these curves can be determined from the points of intersection of the curves in Fig. 5 with the straight lines $\varepsilon = \text{const}$. The $\alpha(T)_\varepsilon$ curve for $\varepsilon = 0.07$ is shown in Fig. 6a. The most important detail of this curve is the threshold temperature T_g separating the region with a pronounced temperature sensitivity of the coefficient α and the region of athermal behavior. In the first region the coefficient α decreases linearly with decreasing temperature, approaching zero when the $\alpha(T)$ curve is extrapolated to 0 K, while in the second region it remains constant at all temperatures. For the value of the relative strain chosen here, $\varepsilon = 0.07$, the threshold temperature lies in the region 1.2–1.5 K, and complete athermality sets in around 1 K. The temperature dependence of the coefficient α has a similar character for the other cross sections of the $\alpha(\varepsilon)_T$ curves, both to the right and left of the value $\varepsilon = 0.07$. This means that with increasing strain the type of barrier governing the motion of dislocations in the active slip system of β-Sn remains unchanged, and consequently so does the type of dislocation process that determines the character of the temperature dependence of the coefficient α.

TABLE I. Values of the parameters of logarithmic creep of β-Sn single crystals at different temperatures for a total strain of the samples $\varepsilon = 0.07$.

T, K	$\alpha \cdot 10^4$	β, s^{-1}
4.2	8.0	1.35
2.8	4.5	3.7
1.4	3.5	5.45
0.8	2.4	5.60
0.55	2.0	9.35

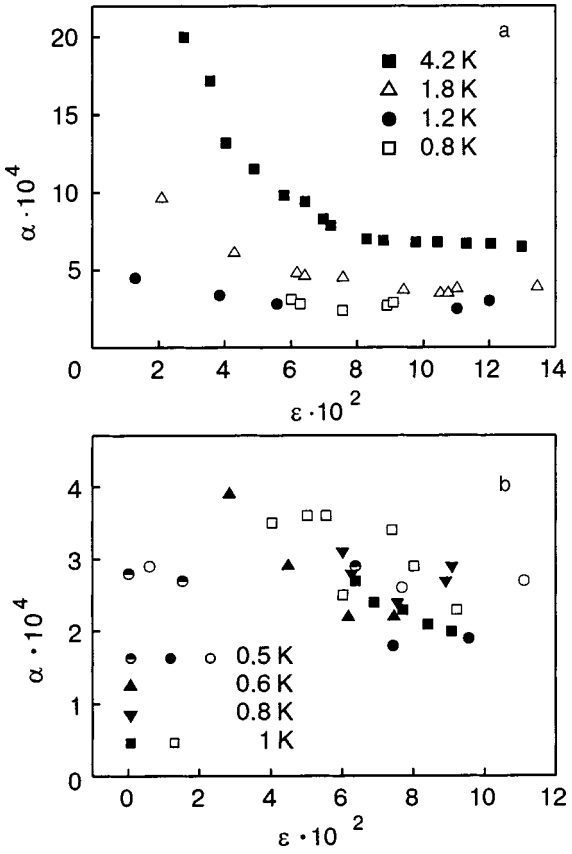

FIG. 5. Dependence of the coefficient α on the value of the plastic deformation ε at temperatures from 0.8 to 4.2 K (a) and from 0.5 to 1 K (b). The different symbols at the same temperature correspond to the data for different samples.

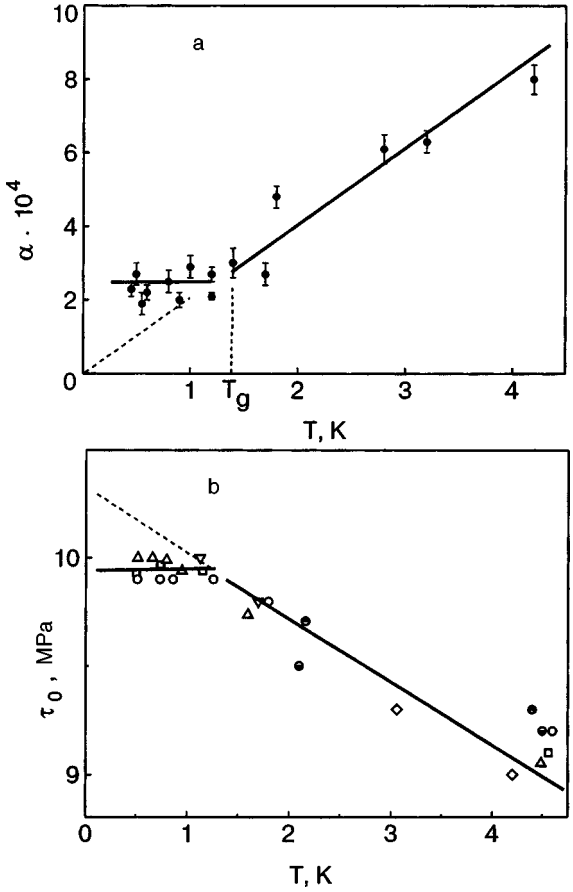

FIG. 6. Temperature dependence of the plasticity parameters of pure β-Sn: the coefficient of logarithmic creep α at a value of the total strain $\varepsilon \simeq 0.07$ (a) and the critical shear stress τ_0 for deformation of the samples at a constant rate $\dot{\varepsilon} = 7 \times 10^{-5}$ s^{-1} (Ref. 15) (b). T_g is the boundary temperature between the regions of quantum ($T < T_g$) and thermally activated ($T > T_g$) plasticity.

3. DISCUSSION OF THE RESULTS

Let us first mention the most important qualitative result of our investigation: the experimental observation of transient creep in β-Sn at subkelvin temperatures and the recording of fragments of the creep curves having a fluctuational nature. This, together with the results of Refs. 10 and 11, means that the classical ideas of creep, i.e., that it is a thermally activated process and so the creep of a decaying nature should vanish for $T \to 0$ K,[18] must be applied judiciously at extremely low temperatures.

As we mentioned in the Introduction, pure β-Sn single crystals oriented for predominant slip in the $(100)\langle 010\rangle$ system belong to the class of metals with a high Peierls potential relief. The plastic deformation of such crystals occurs owing to processes of nucleation, dynamic expansion, and annihilation of kink pairs on dislocations. The kink mechanism brings about a displacement of dislocations from one trough of the Peierls relief to another under the influence of an effective stress τ^*. At comparatively low values of the effective stress $\tau^* = \tau - \tau_i(\varepsilon) < \tau_P$ (τ is the external stress applied to the crystal, τ_i is the internal stress, and τ_P is the Peierls stress) and at low temperatures the nucleation of kinks is brought about by thermal or quantum fluctuations. In that case the fluctuation regime of dislocation motion is realized, and the damping of the creep occurs on account of work hardening, i.e., growth of the internal stresses. For $\tau^* > \tau_P$ the motion of dislocations becomes above-barrier, the plastic deformation acquires a dynamic character, and the damping of the creep occurs as a result of a decrease of the density of fast dislocations. A theory of the staged transient creep due to the regimes of dislocation motion named above was constructed in Ref. 15. In the present paper we will be interested in the possibility of existence, the regularities, and the mechanisms of fluctuation creep at temperatures of the order of 1 K.

According to Ref. 15, the transient creep rate $\dot{\varepsilon}(t)$, which is determined by the motion of a macroscopic flux of dislocations of density ρ in the Peierls relief, is described by the expression

$$\dot{\varepsilon}(t) = \dot{\varepsilon}_0 \exp\left[\frac{E(\tau^*)}{2kT^*(\delta_\tau, T, B)}\right], \tag{3}$$

$$E(\tau^*) = H_c \delta_\tau^{5/4}, \quad \delta_\tau = \left(1 - \frac{\tau^*}{\tau_P}\right),$$

$$\dot{\varepsilon}_0 = \rho (a^2 b \nu_0 v_k)^{1/2}.$$

Here a and b are, respectively, the period of the Peierls relief and the value of the Burgers vector of the dislocations, ν_0 is the characteristic vibrational frequency of the dislocation in a valley of the Peierls relief, v_k is the velocity of a dislocation kink along the dislocation line, H_c is the characteristic energy of the critical pair inflection, and T^* is the effective temperature characterizing the intensity of the quantum mo-

tion of a dislocation string in the Peierls relief at $T \ll \Theta_P$ (the quantum limit) and the intensity of its thermal motion at $T \gg \Theta_P$ (the classical limit). The following asymptotic expressions are valid for the effective temperature T^*:

$$T^*(\delta_\tau, T, B) \simeq s_0(\Theta_P \delta_\tau^{1/4} - \Theta_B), \quad T \ll \Theta_P; \tag{4}$$

$$T^*(\delta_\tau, T, B) \simeq T\left(1 + \frac{s_1}{Q_0 \delta_\tau} \ln \frac{\Theta_S}{T}\right) - \frac{s_1 \Theta_B}{Q_0 \delta_\tau}, \quad T \geqslant \Theta_P. \tag{5}$$

In writing formulas (4) and (5) we have used the following notation: Θ_P and Θ_B are, respectively, the characteristic temperatures associated with the zero-point vibrations of a dislocation in a Peierls valley and with the damping of such vibrations by the electron viscosity B, $Q_0 = H_c / k\Theta_P$ is the quasiclassicality parameter for the tunnel nucleation of a kink pair, Θ_S is the characteristic temperature of a free dislocation string, and s_0 and s_1 are numerical parameters. The empirical values of the parameters of the Peierls relief and dislocations in the β-Sn slip system under consideration, which are needed in expressions (3)–(5), were obtained in Ref. 14 on the basis of a study of active deformation and have the following values:

$\tau_P = 1.2 \times 10^7$ Pa, $H_c = 2 \times 10^{-20}$ J, $\nu_0 \simeq 5 \times 10^{11}$ s^{-1},

$B_n = 2 \times 10^{-5}$ Pa·s, $Q_0 = 5 \times 10^2$, $\Theta_P = 3.3$ K,

$\Theta_B = 0.4$K, $\Theta_S = 100$ K, $a = 3.2 \times 10^{-10}$ m,

$b = 5.8 \times 10^{-10}$ m, $s_0 = 0.9$, $s_1 = 5.4$.

We note that $\Theta_B \ll \Theta_P$, and therefore the correction to the effective temperature in formulas (4) and (5) due to the electron drag on dislocations is rather small and can be neglected in a description of the creep only in the normal state or only in the superconducting state of the metal. At the same time, this correction largely determines the effect of the superconducting transition on the plasticity of a metal and must be taken into account in a description of that effect.[14,15]

From formulas (3)–(5) one can obtain the following relations linking the effective stress τ^* and the creep rate $\dot{\varepsilon}$ in the quantum and classical limits:

$$\delta_\tau = \frac{2 s_0}{Q_0} \ln \frac{\dot{\varepsilon}_0}{\dot{\varepsilon}}, \quad T \ll \Theta_P; \tag{6}$$

$$\delta_\tau^{5/4} = \frac{2T}{Q_0 \Theta_P} \ln \frac{\dot{\varepsilon}_0}{\dot{\varepsilon}}, \quad T \gg \Theta_P. \tag{7}$$

In the theory of low-temperature transient creep it is usually assumed that within the confines of an individual creep curve a linear hardening law is obeyed: $\Delta \tau_i(t) = \kappa \Delta \varepsilon(t)$, where $\kappa = \kappa(\varepsilon)$ is the hardening coefficient corresponding to the total strain ε prior to the start of the individual creep curve. Under such an assumption the use of Eq. (3) for describing the creep kinetics leads to a logarithmic time dependence (1) in which the coefficient α is described by the one of the following expressions:[15]

in the classical limit $T \gg \Theta_P$

$$\alpha = \frac{8 \tau_P}{5 \kappa Q_0} \left(\frac{T}{\Theta_P}\right) \delta_{\tau f}^{-1/4}; \tag{8}$$

in the quantum limit $T \ll \Theta_P$

$$\alpha = \frac{2 s_0 \tau_P}{\kappa Q_0}. \tag{9}$$

In formula (8) the symbol $\delta_{\tau f}$ denotes the value of δ_τ at the time t_f corresponding to the start of the fluctuation stage on the creep curve.

Thus the theory[15] predicts the existence of two temperature regions with characteristic behavior of the coefficient α in each. The first of these, the ''high-temperature'' classical region, is characterized by a dominant role of thermal fluctuations in the overcoming of the barriers of the Peierls relief by the dislocations and an approximately linear temperature dependence of the coefficient α. The second region corresponds to the quantum limit, where the plastic deformation comes about through the tunneling motion of dislocations through the Peierls barrier and the coefficient α is insensitive to temperature. Comparing the $\alpha(T)_\varepsilon$ curve obtained on the basis of the experimental data (Fig. 6) with formulas (8) and (9), we come to the conclusion that the theory and experiment are in qualitative agreement.

The transition region on the temperature dependence of the curve $\alpha(T)$ and the boundary temperature T_g separating the region of thermally activated and quantum creep merit special discussion. According to the estimate obtained in Ref. 14, this temperature has a value of the order of

$$T_g \simeq \Theta_P \delta_{\tau f}^{1/4}. \tag{10}$$

Consequently, the location of the transition region on the temperature axis is determined not only by the characteristic temperature Θ_P, which is a fundamental quantum parameter of the crystal,[14] but also by the parameter $\delta_{\tau f}$, the value of which depends on the value $\tau^*(t_f)$ of the effective stress at the start of the logarithmic stage of the creep curve. Since τ^* is determined by the relationship between the flow stress τ applied to the crystal and the characteristic value of the internal stresses $\tau_i(\varepsilon)$, the boundary temperature T_g, strictly speaking, depends to some degree on random factors that vary in the course of an experiment. At the same time, that dependence is rather weak by virtue of of the small value of the exponent in formula (10). After estimating a value $T_g \simeq 1.3$ K on the basis of the experimental data on $\alpha(T)_\varepsilon$ (Fig. 6a), one can estimate the value of the parameter $\delta_{\tau f}$ for that particular experiment as

$$\delta_{\tau f} \simeq (T_g / \Theta_P)^4 \simeq 0.025.$$

According to formula (6), the following relation holds at the time t_f corresponding to the start of the logarithmic stage of quantum creep:

$$\dot{\varepsilon}_0 = \dot{\varepsilon}(t_f) \exp\left(\frac{Q_0 \delta_{\tau f}}{2 s_0}\right). \tag{11}$$

The empirical estimate $\delta_{\tau f} \simeq 0.025$ and the estimate $\dot{\varepsilon}(t_f) = 4 \times 10^{-4}$ s^{-1} from Fig. 3 allows one to obtain an empirical estimate of the parameter $\dot{\varepsilon}_0$ for that particular experiment: $\dot{\varepsilon}_0 = 0.5$ s^{-1}. This value is obtained on the basis of an analysis of the creep of samples prestrained to $\varepsilon = 0.07$. It is several orders of magnitude smaller than the value $\dot{\varepsilon}_0 \simeq 10^4$ s^{-1} found previously[14] in an analysis of the yield point under conditions of active tensile deformation at a rate of $\dot{\varepsilon} = 7 \times 10^{-5}$ s^{-1} for a different series of samples.

Starting from the expression for $\dot{\varepsilon}_0$ [see formula (3)] one can conclude that this difference is due to a difference of several orders of magnitude in the density ρ of mobile dislocations, which govern the plastic flow of the crystals in both of these cases. Using the results of Refs. 14 and 15, we obtain the estimates $\nu_0 \simeq 5\times 10^{11}$ s^{-1} and $v_k \simeq 3\times 10^2$ m/s.[1)] The value $\dot{\varepsilon}_0 \simeq 0.5$ s^{-1} found above corresponds to a density of mobile dislocations, which govern the quantum creep in the given experiment, of the order of $\rho \simeq 5\times 10^6$ m^{-2}.

Another important kinetic characteristic of the fluctuation creep process is the work hardening coefficient $\kappa(\varepsilon)$. An empirical estimate of this parameter for temperatures of the order of 1 K can be obtained using formula (9) and the average value of the coefficient $\alpha \simeq 2.4\times 10^{-4}$ in the quantum creep region for $\varepsilon = 0.07$ (see Figs. 5 and 6a): $\kappa(\varepsilon = 0.07; T < 1.3\ \text{K}) \simeq 1.8\times 10^8$ Pa. This value is close to the estimate $\kappa(\varepsilon = 0.07; T = 1.6\ \text{K}) \simeq 1.6\times 10^8$ Pa in Ref. 15 from the macroscopic strain diagram of β-Sn at $T = 1.6$ K in the normal state, but it is smaller by a factor of two than the value determined from analysis of the creep curves in the superconducting state.

We note that the conclusion that the work hardening rates of superconducting metals strained in the normal and superconducting states are different was reached previously in an analysis of active deformation processes.[20,21] This effect does not have an unambiguous physical interpretation, and it seems to us that additional useful information that would shed light on its physical nature can be obtained by studying the transient creep of such metals in the normal and superconducting states. A study of this effect on samples of β-Sn will be the subject of a separate paper.

It was shown above that measurements of the coefficient α in the quantum creep region and the use of formula (9) allow one to obtain the value of the work hardening coefficient directly if the values of the Peierls stress τ_P and the quasiclassicality parameter Q_0 are known for the crystal under study. However, in the region of thermally activated creep such a possibility does not exist. In that region one can find the experimental values of α at different temperatures (Fig. 6a). Then, by measuring the slope of the straight line on the plot of $\alpha(T)_\varepsilon$ for $T > T_g$ and using formula (9), one can obtain an empirical estimate of the product $\kappa\delta_{\tau f}^{1/4}$. Consequently, to determine the values of the force parameter $\delta_{\tau f}$ it is necessary to make independent measurements of the hardening coefficient κ. From the macroscopic strain diagram recorded during active deformation of pure β-Sn single crystals at $T = 4.2$ K[14] we find the value $\kappa(\varepsilon = 0.07; T = 4.2\ \text{K}) \simeq 1.2\times 10^8$ Pa. A value of a similar magnitude was obtained in Ref. 15 by the creep method at a temperature of 3.2 K. Using the given value of κ and the data of Fig. 6a, we obtain the estimate $\delta_{\tau f} \simeq 0.078$, which corresponds to conditions of thermally activated creep at $\varepsilon = 0.07$ and $T = 4.2$ K.

According to formula (6), at the time corresponding to the start of thermally activated creep the following relation holds:

$$\dot{\varepsilon}_0 = \dot{\varepsilon}(t_f)\exp\left(\frac{Q_0\Theta_P\delta_{\tau f}^{5/4}}{2T}\right). \tag{12}$$

The estimates obtained above, $\delta_{\tau f} \simeq 0.078$ and $\dot{\varepsilon}(t_f) \simeq 7\times 10^{-4}$ s^{-1} (Fig. 3c) allow one to estimate the parameters $\dot{\varepsilon}_0$ and ρ for the conditions of the experiment at $\varepsilon = 0.07$ and $T = 4.2$ K:

$$\dot{\varepsilon}_0 \simeq 2\ \text{s}^{-1},\quad \rho \simeq 2\times 10^7\ \text{m}^{-2}.$$

Another important question for the physics of low-temperature creep is the value of the effective potential barrier $E(\tau^*)$ governing the mobility of dislocations and the rate of plastic deformation [see formula (3)]. The value of this barrier $E(\tau^*) = H_c\delta_\tau^{5/4}$ is determined by both a fundamental parameter of the crystal, H_c, and by the force factor $\delta_\tau = \delta_{\tau f}$, which depends on the conditions of the experiment and the state of the defect structure of the sample in the particular experimental situation. For the experiment described in this paper at a total strain value of $\varepsilon = 0.07$ we obtain the following estimates:

in the quantum region at $T < 1.3$ K

$$E(\tau_f^*) \simeq 2\times 10^{-22}\ \text{J} \simeq 1.2\times 10^{-3}\ \text{eV};$$

in the classical region at $T = 4.2$ K

$$E(\tau_f^*) \simeq 8\times 10^{-22}\ \text{J} \simeq 5\times 10^{-3}\ \text{eV}.$$

The analysis in this Section suggests that the athermal creep observed in pure β-Sn single crystals at $T \leqslant 1$ K is due to the tunneling motion of dislocations in the Peierls relief. The elementary process governing such creep is the tunneling penetration of small parts of the dislocation line through an individual barrier of the Peierls relief, i.e., the nucleation of kink pairs. The nucleation of a kink pair entails the overcoming of the effective potential barrier $E(\tau^*)$. The quantum character of that process is due to the very small value of the barrier, of the order of 10^{-3} eV, and the low intensity of thermal fluctuations under conditions of extremely low temperatures. However, already at liquid helium temperature 4.2 K the creep at approximately the same rates is accompanied by the overcoming of a potential barrier several times larger, and the elementary process takes on a thermally activated character.

An analogous conclusion as to the quantum nature of the plastic deformation of β-Sn in the given temperature interval was reached in Ref. 14. Figure 6b shows the temperature dependence of the critical cleavage stress $\tau_0(T)$ of β-Sn single crystals in the interval 4.2–0.5 K from Ref. 14, obtained under conditions of a constant tensile strain rate (the regime of active deformation). It is easy to see that this temperature dependence repeats the characteristic features of the $\alpha(T)$ curve. This indicates that one can study the regularities and mechanisms of plastic flow in crystals under conditions of deep cooling by different methods of mechanical testing. At the same time, it should be kept in mind that the exact values of a number of parameters characterizing the plastic flow depend substantially on the particular conditions of an experiment, and their empirical estimates can have a significant scatter: for example, the force parameter δ_τ, the value of the effective barrier $E(\tau^*)$, the boundary temperature T_g of quantum plasticity, the density of mobile dislocations ρ, and the work hardening coefficient κ.

CONCLUSIONS

(1) The creep of single-crystal samples of pure β-Sn oriented to favor slip in the $(100)\langle 010\rangle$ system has been studied in the temperature range 0.45–4.2 K. The crystals were deformed by uniaxial extension in the normal state in an above-critical longitudinal magnetic field produced by a superconducting solenoid.

(2) Transient creep decaying in time by a logarithmic law was registered at all temperatures in the investigated range.

(3) The dependence of the coefficient of logarithmic creep on the degree of prestrain of the crystal and on the temperature of the samples was obtained. The existence of two temperature regions with different sensitivity of that coefficient to temperature was established. In the first of these, the ''high-temperature'' region ($1.5\ \mathrm{K} < T < 4.2\ \mathrm{K}$) the coefficient decreases linearly with decreasing temperature; below 1 K the creep takes on an athermal character, and at $0.45\ \mathrm{K} < T < 1\ \mathrm{K}$ the coefficient remains constant.

(4) A detailed analysis of the experimental results was carried out in the framework of the modern theory of low-temperature creep. The regularities established in the experiment are in accord with the idea that the low-temperature creep of β-Sn is governed by the motion of dislocations in the Peierls potential relief. The elementary process of such motion is the nucleation of kink pairs on the dislocation lines; this nucleation entails the overcoming of a small effective potential barrier of the order of 10^{-3} eV.

(5) In the temperature region $T \leqslant 1$ K the nucleation of kink pairs occurs by quantum-mechanical tunneling, and the creep is of a purely quantum nature, while at higher temperatures these processes take on a thermally activated character.

This study was carried out under the target program of the OFA of the National Academy of Sciences of Ukraine, Topic 1.4.10.1.8.

*E-mail: natsik@ilt.kharkov.ua

[1)] In Ref. 15 the value of v_k was mistakenly overestimated by about an order of magnitude.

[1] V. I. Startsev, V. Ya. Il'ichev, and V. V. Pustovalov, *Plasticity and Strength of Metals and Alloys at Low Temperatures* [in Russian], Metallurgiya, Moscow (1975).
[2] W. Meisner, M. Polany, and E. Shmid, Z. Phys. B **66**, 477 (1930).
[3] I. M. Glen, Philos. Mag. **1**, 400 (1956).
[4] A. G. Arco and J. Weertman, J. Met. **17**, 676 (1969).
[5] V. D. Natsik, A. I. Osetskii, V. P. Soldatov, and V. I. Startsev, Phys. Status Solidi B **55**, 99 (1972).
[6] N. F. Mott, Philos. Mag. **1**, 568 (1956).
[7] B. V. Petukhov and V. L. Pokrovskiĭ, Pis'ma Zh. Éksp. Teor. Fiz. **15, vyp. 1**, 63 (1972)].
[8] V. D. Natsik, Fiz. Nizk. Temp. **5**, 400 (1979) [Sov. J. Low Temp. Phys. **5**, 191 (1979)].
[9] V. D. Natsik and H.-J. Kaufman, Phys. Status Solidi A **65**, 571 (1981).
[10] S. Takeuchi, T. Hashimoto, and K. Maeda, Cryst. Res. Technol. **19**, 341 (1984).
[11] M. M. Kalugin, V. D. Natsik, V. P. Soldatov, and I. A. Shepel', Fiz. Nizk. Temp. **19**, 713 (1993) [Low Temp. Phys. **19**, 512 (1993)].
[12] G. I. Kirichenko, V. D. Natsik, and V. P. Soldatov, Fiz. Met. Metalloved. **63**, 386 (1987).
[13] G. I. Kirichenko, V. V. Pustovalov, V. P. Soldatov, and S.É. Shumilin, Fiz. Nizk. Temp. **11**, 1206 (1985) [Sov. J. Low Temp. Phys. **11**, 666 (1985)].
[14] V. D. Natsik, G. I. Kirichenko, V. V. Pustovalov, V. P. Soldatov, and S.E. Shumilin, Fiz. Nizk. Temp. **22**, 965 (1996) [Low Temp. Phys. **22**, 740 (1996)].
[15] V. D. Natsik, V. P. Soldatov, G. I. Kirichenko, and L. G. Ivanchenko, Fiz. Nizk. Temp. **29**, 451 (2003) [Low Temp. Phys. **29**, 340 (2003)].
[16] Yu. G. Kazarov, in *Condensed Matter Physics* [in Russian], Kharkov (1973), issue 11, p. 100.
[17] V. P. Soldatov, V. D. Natsik, and G. I. Kirichenko, Fiz. Nizk. Temp. **27**, 1421 (2001) [Low Temp. Phys. **27**, 1048 (2001)].
[18] F. Garofalo, *Fundamentals of Creep and Creep-Rupture in Metals*, MacMillan, New York (1965), Metallurgiya, Moscow (1968).
[19] G. I. Kirichenko and V. P. Soldatov, Fiz. Met. Metalloved. **54**, 560 (1982).
[20] V. V. Pustovalov, I. N. Kusmenko, N. V. Isaev, V. S. Fomenko, and S.E. Shumilin Fiz. Nizk. Temp. **30**, 109 (2004) [Low Temp. Phys. **30**, 82 (2004)].
[21] I. N. Kuz'menko, Author's Abstract of Candidate's Dissertation [in Russian], FTINT AN USSR, Kharkov (1984).

Translated by Steve Torstveit